# Ultracold Atoms in One Dimension: From Two to Many

**Dissertation**

**zur Erlangung des Doktorgrades**

**des Department Physik**

**der Universität Hamburg**

vorgelegt von

Ioannis Brouzos

aus Athen

Hamburg

2012

| | |
|---|---|
| Gutachter der Dissertation: | Prof. Dr. P. Schmelcher<br>Prof. Dr. H. Moritz |
| Gutachter der Disputation: | Prof. Dr. P. Schmelcher<br>Prof. Dr. M. Potthoff |
| Drittgutachter für die Auszeichnung: | Prof. Dr. B. Esry |
| Datum der Disputation: | 18 December 2012 |
| Vorsitzender des Prüfungsausschusses: | Prof. Dr. G. Huber |
| Vorsitzender des Promotionsausschusses: | Prof. Dr. P. Hauschildt |
| Dekan der Fakultät für Mathematik,<br>Informatik und Naturwissenschaften: | Prof. Dr. H. Graener |

To my family

## Zusammenfassung

**Ultrakalte Atome in einer Dimension: von zwei hin zu vielen Teilchen.** In dieser Dissertation werden ultrakalte bosonische und fermionische Systeme in Hinblick auf ihre stationären sowie dynamischen Eigenschaften in eindimensionalen harmonischen Fallen und endlichen Gittern untersucht. Alle physikalischen Systeme werden im Rahmen dieser Arbeit mit einem "Bottom-up-Ansatz" behandelt, ausgehend von dem zugrunde liegenden Zwei-Körper-Problem. Die dem hier entwickelten "correlated-pair wavefunction" Ansatz zugrunde liegende Idee verwendet die exakte Lösung des entsprechenden Zwei-Körper-Problems für die Konstruktion der korrelierten Vielteilchenwellenfunktion. Für Bosonen und Fermionen in der harmonischen Falle beschreibt der "correlated-pair wavefunction"-Ansatz sehr gut den Übergang von schwacher zur starker Wechelwirkung. Außerdem werden bosonische Systeme mit zeitlich getriebener Wechselwirkung in Hinblick auf resonante Anregungsdynamik untersucht, wobei für deren Analyse die Eigenschaften des Zwei-Körper-Spektrums und des entsprechenden Vielteilchenspektrums benutzt werden. Endliche Gitter mit kommensurabeler und inkommensurabeler Füllung werden mit Schwerpunkt auf "on-site" Effekten, welche aus starken Wechselwirkungen jenseits der Gültigkeit des "Single-Band-Ansatzes" resultieren, studiert. Die "correlated-pair wavefunction" wird auf Gitterfallen verallgemeinert, um solche Effekte behandeln zu können. Der "Interband"-Tunnelmechanismus tritt in endlichen Gittern auf, weil Resonanzen im Vielteilchenspektrum bei bestimmter Wechselwirkungstärke den "Self-Trapping"-Mechanismus überwinden. Mit Hilfe der analytischen Funktionen werden Eigenschaften von Observablen berechnet und mit numerischen Ergebnissen der etablierten Berechnungsmethoden Multi-Configurational Time-Dependent Hartree und Quantum Monte Carlo verglichen. Experimentellen Daten gemessen nach deterministischen Präperation von wenigen Fermionen in einer Falle stimmen sehr gut mit den Ergebnisse dieser theoretischen Arbeit überein.



## Abstract

**Ultracold atoms in one dimension: from two to many.** In this thesis ultracold bosonic and fermionic systems are studied with respect to their stationary and dynamical properties in one-dimensional harmonic traps and finite lattices. All physical systems explored within this work, are treated with a bottom-up approach, inspired from the underlying two-body problem. This perspective is at the most illustrated from the correlated-pair wavefunction, an Ansatz proposed here to describe the crossover from weak to strong interactions for bosons and fermions trapped in a one-dimensional harmonic potential. The underlying idea of the Ansatz is to employ the exact solution of the corresponding two-body system for the construction of a many-body correlated function. Moreover, bosonic systems under driven interaction strengths are studied with respect to resonant excitation dynamics, using for the analysis the properties of the two-body spectrum and the corresponding many-body ones. Furthermore finite lattices loaded with commensurate and incommensurate filling are investigated, with a focus on on-site effects induced from strong interactions beyond the validity regime of standard single-band approaches. A generalization of the correlated-pair wavefunction to lattice potentials is performed to cover these effects. Interband tunneling dynamics in finite lattices occur due to resonances in the many-body spectrum at certain typically strong interaction strengths breaking the self-trapping mechanism. The properties of the observables resulting from the analytical functions proposed here are compared with corresponding ones calculated by established computational methods: Multi-Configurational Time-Dependent Hartree and Quantum Monte Carlo. Recent experimental data obtained after deterministic preparation of few-fermion ensembles in a trap are in very good agreement with theoretical calculations performed in this work.

# Contents

# Introduction

> Das Zurückfahren der bunten Vielfalt auf das Allgemeine und Einfache, oder sagen wir im Sinne deiner Griechen: des 'Vielen' auf das 'Eine', ist, was wir mit 'Verstehen' bezeichnen.
>
> The ascription of the colorful Multiplicity and Variety to the General and Simple, or to say it in the sense of the Greeks: from the 'Many' to the 'One', is what we mean by 'understanding'.
>
> Wolfgang Pauli to Werner Heisenberg in Heisenberg's 'Der Teil und das Ganze, Gespräche im Umkreis der Atomphysik'

**Prologue** Democritus[1] introduced the idea of elementary units of matter, the atoms, their Greek name meaning that they are non further separable or divisible, i.e., they have no internal structure, and constitute all visible and non-visible physis. These archetypical physical systems have become in modern times a fascinating object of research for several generations of scientists, the most prominent contributors being the inventors of quantum mechanics in the beginning of the last century. The current notion of the word 'atom', has been elaborated and deviated from the initial idea of Democritus. Atoms are nowadays considered as relatively complex objects with internal structure while the classical hard-sphere picture has been irreversibly revolutionized by the probabilistic theory of quantum mechanics. However, the core idea of Democritus is more than alive and still occupies the thinking of the scientists who aim to shed light in the complex structure of the physical Cosmos from two perspectives: his claim for the existence of elementary constituents of matter which is underlying the whole field of particle physics, and his more general viewpoint to analyze complex structures and phenomena by a bottom-up approach. The philosophical implications of the latter thinking line, maybe called atomism, reductionism or materialistic structuralism, are only on the periphery of the present thesis. However, the basic theme of this work is to uncover the structure and quantum properties of interacting many-atom systems or in terms of Democritus to search for the 'atom' or 'basic entity' underlying many-body phenomena. The bottom-line idea is that for correlated systems interacting with pairwise forces the role of the 'basic entity' is played not by single atoms but by an interacting pair of atoms already correlated and with a rich behavior which is then projected to the many-body system in various ways. The objective is therefore redirected from the single atoms to the relation between them, particularly the pairwise interaction embedded in the two-body properties.

**Experimental Breakthrough** Although atomic physics researchers attributed very complicated properties to the underlying entities of nature, the degree of understanding has been such that state-of-the-art experiments have achieved an unprecedented control of many-body

[1] Democritus ($\Delta\eta\mu o\kappa\rho\acute{\iota}\tau o\varsigma$) was one of the great thinkers belonging to the philosophical tradition which appeared in the Minor Asia together with his teacher Leucippus.

ensembles of atoms [1, 2, 3]. Light beams and optical devices together with magnetic and electric fields are part of a very powerful experimental toolbox which enables the controlled manipulation of the atoms, freezing them down to nano-Kelvin temperatures [1], creating at will trapping potentials with certain dimensionality [4] and profile [2] and tuning even their collisional properties based on the so-called Feshbach resonances [5]. Certainly the most impressive achievement of this development was the realization of the Bose-Einstein condensate (BEC) in 1995 [6] with dilute gases 70 years after the initial prediction of Bose and Einstein that a degenerate quantum gas of bosons[2] occupies a single macroscopic state if it is cooled under a critical temperature. This breakthrough has initiated a lot of theoretical studies while more than a hundred labs with a cold atom apparatus exist nowadays around the world. A second wave of the experimental revolution emerged with the introduction of optical lattices [2], where many-body models mainly inspired from solid-state physics could be realized and studied with a large degree of controllability over the physical parameters and measurement accuracy with access to several observables. Exploration of phase transitions [7] and other important physical phenomena, is nowadays performed in an artificial system much larger, clearer and more transparent than the solid state equivalent while the idea of quantum simulators[3] has found its favorable environment in cold atom experiments.

This fascinating progress in the experiments goes hand in hand with theoretical investigations. Theoreticians are inspired from the enormous advances in experiment, and mainly from the fact that systems and models which were thought as rough simplifications of the complex natural reality can be nowadays designed almost at will in the labs. It is impossible to report even shortly in the frame of this introduction on the whole progress in the field, but review articles and textbooks [1, 2, 3, 5, 4, 8, 9] cover a lot of the different aspects of the past and current research. The rest of this introduction is mostly devoted to experimental and theoretical works which are conceptually or with respect to the content closely related to the present thesis, while more specific reference to certain works is left for the introduction of the corresponding chapters and sections.

**Thesis framework drawn by seminal theory works** The framework of this thesis can be ideally sketched with reference to five seminal theoretical works [10, 11, 12, 13, 14], three of which [10, 11, 12] have been done in the early 60's long before the experimentalists managed to turn them from ideal theoretical over-simplified models into lab-reality. The most common theoretical approach to study BEC physics is the Gross-Pitaevskii equation (GPE) [1, 10], a mean field treatment of cold bosonic many-body systems, relying on the fact that most atoms of the ensemble at temperatures below the critical BEC transition occupy a single orbital. This condensate-wavefunction or condensate mean field (ignoring thermal and quantum fluctuations) describes the BEC in a Hartree-product approximation built up from single-particle condensate-functions for each boson. The many-body system is then replaced by a one-body problem of a non-linear Schrödinger equation with an external 'mean field' accounting for the explicit interaction with the other atoms. This treatment and its extensions including Bogoliubov theory for elementary excitations and the Thomas-Fermi approximation for strong interactions ignoring the kinetic energy may be considered as over-simplifying. Nevertheless, they have been proven very powerful to explain phenomena of superfluid or non-linear nature like collective

[2]Nature provides exclusively only two categories of identical quantum particles, classified from there exchange symmetry: bosons are able to occupy the same state, since a permutation of two leaves the wavefunction which describes them unchanged (Bose-Einstein statistics) and fermions which are antisymmetric with respect to this exchange (Fermi-Dirac statistics), and as a result occupy different states (Pauli exclusion principle).

[3]'Quantum simulators' are thought as natural quantum computers which simulate physical models beyond the efficiency of standard computers. This is the first application of the idea of 'quantum computers' which is a broader research field aiming to use quantum physics effects to perform data operations.

oscillations [15], solitons [16], vortices [17], dynamics of Josephson junctions in double wells [18, 8], and provide a reliable theoretical approach for most experiments with a large number of bosons (of the order of a thousand to a million)[4].

There is though at least one weak point of this approach, which particularly manifests in one dimensional (1D) systems which are the focus of this thesis. When the interparticle interaction is very strong and the correlations between the atoms induce fragmentation, i.e., occupation of higher orbitals apart from the condensate mean-field, the GPE treatment is not adequate to describe the observable behaviour. In 1D systems strongly interacting ensembles exhibit spectacular features [4], the most prominent paradigm being the so-called fermionization of infinitely repulsive bosons which can be mapped to identical non-interacting fermions (Bose-Fermi map) as Girardeau has shown in his ground-breaking work in 1960 [11]. Intuitively one may understand this behaviour as an effective Pauli principle induced by the infinite repulsion prohibiting the coincidence of two or more bosons. Experimentally the realization of the so-called Tonks-Girardeau (TG) gas [19] and its excited state counterpart for infinitely attractive forces (usually called super-repulsive) the super TG gas [20] became possible with the construction of quasi-1D tubes by strong transversal confinement. These experiments and the theoretical work of Girardeau fired up the interest in 1D systems exhibiting ultra-strong interaction effects [4].

In the intermediate interaction regime between the two extremes (infinitely strong repulsion-TG and weakly interacting GPE) there is relatively less understanding and tools that can be employed. Yet 1D systems are preferred by theoreticians [4] since certain model Hamiltonians are integrable and usually approached via the so-called Bethe Ansatz[5][21]. One of these models is the Lieb-Liniger gas of bosons interacting via a contact potential in the continuum (absence of trap). The system has been analytically solved both for the ground and the excited states in the seminal paper of Lieb and Liniger in the early 60's [12], the solution holding for all interaction strengths from very weak to infinite repulsion (TG gas). This benchmark result has been further used to approach trapped systems via the local density approximation [22]. A main part of the present work is devoted to the approach of the crossover from weak to strong interactions for trapped bosonic and fermionic ensembles, thus following the path that Lieb and Liniger first opened and reaching the limit that Girardeau has drawn.

Trapped systems are essential in the research of cold atoms, among other reasons because the experiments always load the ensemble in a trap [1, 2]. Especially those experiments that aim to reach the 1D regime [4] use very strong laser fields in the transversal directions and a smoother parabolic potential in the longitudinal [19, 20]. In his seminal work Olshanii [13] has shown that these quasi-1D geometries affect the scattering properties of the atoms, introducing the so-called confinement induced resonances. The whole description boils down to an 1D effective interaction parameter (or scattering length) tunable from zero to infinity via confinement induced or Feshbach resonances. This effective description of the pairwise interactions will be taken for granted allover this thesis which does not aim at elaborating on collision properties (see relevant reviews [5]). Besides, from the viewpoint of many-body physics the scattering problem is considered as an input parameter, and not as a real many-body system but (like the GPE) as an effective one-body problem in the center-of mass frame. However there exist a lot

[4]Explanation of technical terms: Superfluid: a fluid with zero viscosity analogous to superconductor which has zero electrical resistance. Collective oscillations: collective motion of the condensate in the trap induced by a small initial perturbation of the trap due to the Bogoliubov elementary excitations. Solitons: exact solutions of the GPE in the non-linear regime, which propagate as waves in a fixed form without dispersion. Vortex: Rotating spiral motion of a fluid. Josephson junctions: superconductors (in this case superfluids coupled by a weak link. Note: In this introduction, technical terms and field jargon has been avoided as much as possible, and when this is not possible small explanations are given in the text or in footnotes.

[5]Other standard approaches like the Luttinger-liquid or bosonisation approach will not be discussed here, there are excellent reviews from Giamarchi and coworkers [4]

of important works for few-atom collisions [5, 9], also extending to the Efimov states [23].

There is nevertheless a two-body system which is of central interest for the present work: the system of two interacting atoms in the harmonic trap which is explicitly solvable with respect to the relative motion for one, two and three dimensions in isotropic traps. The analytical solution performed by Busch. et. al [14] is used here for the 1D case as a building stone for the bottom-up description of the many-body problem. Essentially one of the most important proposals of the present thesis, the correlated-pair wavefunction (CPWF) to describe the ground state of a trapped many-body system is based on the two-body functions which represent the analytical solutions of the two-atom problem in the trap. In addition the energy spectrum and other properties of the two-atom system constitute a basic inspiration and analysis tool of this thesis.

**Thesis structure** Posturing the present thesis in this context, we emphasize that the many-body problems in 1D are approached here beyond the simplified one-body picture of mean-field treatments (GPE). The scattering properties (also effectively one-body) are used only as an input. Our approach here builds rather upon the single pair behaviour of two correlated atoms aiming to an explicit many-body description inspired from the Lieb-Liniger approach of the crossover from weak to strong interactions and the Bose-Fermi map for the limiting case of the TG gas. These three integrable systems in 1D [11, 12, 14], are the focus of the Chapter 1 of this thesis, which contains the main ideas of the corresponding works always seen from a 'two-to-many' perspective which underlies this work.

Chapter 2 is devoted to 1D bosonic systems in the harmonic trap the most natural and fundamental trapping potential which first appeared in 1D as well as higher dimensional experiments [1, 6, 15, 19, 24]. In the first part (Chapter 2.1) we introduce the main proposal of this thesis, the CPWF Ansatz [25] which is inspired from the two-body solution [14] aiming to describe analytically the crossover from weak to strong interactions of the many-body energies and densities. The accuracy of this Ansatz is tested with numerically exact calculations, and is shown to be qualitatively and quantitatively in agreement with related results obtained by numerical [26, 27, 28, 29] or approximate methods [22].

In a second step (Chapter 2.2), we set out from the stationary energy spectrum of the two- and many- body case to analyze excitation dynamics of a few-boson ensemble with a driven interaction strength in the harmonic trap [30]. Driven systems[6][8] are in general more complicated with exciting effects related also to quantum chaos in open quantum systems [31]. We build here again a bottom-up approach elaborating first on the two-boson case performing additionally a Floquet analysis[7] to explain the resonances which appear. This system has connections to recent experimental [32, 33] and theoretical works [34] with driven interaction, but also in general with non-equilibrium dynamics of driven cold atom systems [8, 35, 36, 37, 38] and collective oscillation properties [15, 24].

Since stationary, dynamical and driven few-body systems are investigated in this thesis, we have chosen as appropriate method for the numerical calculations the Multi-configurational Time-dependent Hartree (MCTDH) [39] which is shortly described in the Appendix A and has been already tested in several cases for calculating stationary states and tunneling dynamics of few bosons [29, 40, 41]. The present thesis extends also the use of MCTDH to driven cold-atom systems (Chapter 2.2) and fermions (Chapter 4) while for ground states of larger ensembles we have used the established Quantum Monte Carlo (QMC) method [27] also reported in the

[6]By driven we mean that a control parameter is externally modulated with time. In our case the modulation is periodic.

[7]Floquet method is a standard tool in quantum chaos studies [31] mapping an periodically oscillating system to an effectively stationary one and will be analyzed in Chapter 2.2.

Appendix A. The mathematical Appendix B reviews some special functions which are important for this thesis, especially concerning the construction principles of the CPWF.

In Chapter 3, bosonic systems are loaded to finite lattice potentials, with different filling factors to investigate stationary properties (Chapter 3.1) [42] and tunneling dynamics (Chapter 3.1) [43]. After the (harmonic) trapping and colling, optical lattices have become in the last ten years an indispensable tool of almost every cold atom experiment [2] and are usually approached by a tight-binding model with a coupling (tunneling) term between the lattice sites and an on-site interaction, a so-called (Bose or Fermi) Hubbard model [44]. The effective physics induced from such models are very rich especially concerning phase transitions [2] and dynamics [8]. The most prominent example is the Mott-insulator (with the atoms localized in each well) to a superfluid transition realized in optical lattices in 2002 [7] and giving a great boost in similar experiments and theoretical works [2]. In 1D lattices there are phenomena which are still not covered by this standard single-band approach of the Bose-Hubbard model [45, 46, 47], and which are the focus of this thesis. We consider several observables and show the interplay between commensurability and correlations [42] exploring different filling factors with integer or rational number of atoms per site with increasing interaction strength in finite lattices [42]. We also propose an analytical approach [48] based on a harmonic approximation for each cite for the localized (Wannier) functions, which we will not keep in a Gaussian shape (like in the standard approach) but modify them according to the CPWF which is based on the exact function of the two-atom case in a single site. This allows us to capture on-site effects that appear close to fermionization such as broadening of the on-site profiles in the densities and the appearance of additional peaks.

Based again on the analysis of the spectrum for a triple well system, we extend our study in the second part of this Chapter 3.2 to tunneling dynamics [43]. Tunneling is a basic counter intuitive quantum phenomenon studied extensively in double wells and finite lattices [18, 49, 50, 40] loaded with cold atoms showing impressive effects like Josephson oscillations [18], self-trapping due to the non-linearity [49] or correlated repulsively bound pair tunneling [50]. In 1D previous studies have explored the transition from correlated tunneling to single-particle tunneling at the TG limit [40] or effects beyond Bose-Hubbard and GPE [51, 52]. In this thesis, based on a bottom up approach on resonances of generalized number states extending effectively to several bands of the lattice energy spectrum, we analyze the interband dynamics [43] which appear for certain relatively strong interaction strengths breaking the self-trapping mean-field mechanism.

In the last Chapter 4 of this thesis the focus turns from bosonic to fermionic systems [3], and particularly a few-body two-component Fermi mixture in the harmonic trap [53]. Degenerate Fermi gases have been prepared in low temperatures [54] a few years after BEC, but are nowadays in the forefront of the research for novel phases [3] and fundamental aspects of magnetism [55] and superconductivity. In Chapter 4.1 we perform a generalization of the CPWF (proposed in Chapter 2.1) for fermi-mixtures in a 1D parabolic trap and test its accuracy for several population imbalances, varying the repulsive interaction strength. We explore the physics of an impurity in a fermi sea[8] connected to polaronic physics which is the focus of recent experiments and theoretical investigations [56, 57, 58, 59]. Cases of partial imbalance of population between the two fermionic components of the mixture, but also the balanced case are also covered.

One of the most exciting aspects of cold-atom physics is that experiments –however impossible it may seem– are sometimes possible to realize and detect very abstract and simple theoretical models, such that the theoretical treatment can be directly tested. A great motivation and inspiration for extending our study to fermionic systems, has been given from

[8]Impurity is an atom of different internal state which is distinguishable from the others which constitute the surrounding fermi sea of identical non-interacting fermions

the beautiful experiments performed from the group of Selim Jochim in Heidelberg. In these experiments they are able to deterministically prepare a certain number of fermions with controlled imbalance of population between the two components in a quasi-1D trap [60]. As first application they have studied the two-body case [61] and experimentally verified the seminal theoretical results [14, 62] which are also the basis of the present thesis. Extending recently their studies by building up a Fermi sea atom by atom around an impurity, they measured the energy and their results are available for comparison with our theoretical treatment in the very last part of this thesis (Chapter 4.2) [63] . The question that arises by this bottom-up approach is 'how many atoms are necessary to reach the infinite (polaronic physics)?' or to put it simpler 'how many is many?'[9].

Understanding the 'many' from the 'one' or better from 'a correlated single pair of atoms' is the bottom line of the present thesis which is summarized –for the certain systems examined in this work– in the concluding remarks (Chapter 5). Yet a lot of questions and new research ideas arise from the results that are shown here which experiment and theory are setting out to approach, with an unpredictable but certainly exciting feature.

[9]Philip W. Anderson's famous article 'More is Different' [64] fired up lively and passionate discussions about emergent phenomena providing the scientific research and philosophical thinking with indispensable oxygen.

# Chapter 1

# Integrable 1D many-body models

There are two basic arguments that speak against one-dimensional 1D systems and one for them. Opponents would say that 1D models are not realistic because the real world comprises higher dimensions. Furthermore 1D systems are not spectacular, and usually boring. We have already seen the counter-argument to the first position. In cold atom physics, creating quasi-1D systems with a high accuracy is absolutely possible and realistic experimentally, via strong confinement of the transversal degrees of freedom [19, 20, 24]. For the second argument, there could be many opinions, but from the perspective of many-body physics it is probably enough to say that on a line and only on a line, the two opposite types of identical particles the bosons and the fermions come close via the Bose-Fermi map [11]. Alone this connection between the systems with different statistics should be motivating enough to study 1D systems. The most important argument though, supporting 1D physics is that we can actually solve exactly in a closed form a lot of models, among them also the hard-core bosons which can be mapped to identical (non-interacting) fermions. This constitutes an oasis for theoreticians because apart from the textbook basic single-particle models (free space with periodic or hard-wall boundary conditions, harmonic trap, infinite lattice) they can also solve their many-body extension. This is not to be underestimated in view of the large complexity that many-body systems usually are attributed with.

The first decisive step for the exact solution of 1D systems was done right after the burst of the quantum theory revolution, in 1931 by Hans Bethe [21]. He proposed an Ansatz named after him, for solving the Heisenberg model for antiferromagnetism. The Bethe-Ansatz has been proven to be the absolute tool for exact solutions of fundamental 1D models like the Ising, the Hubbard and the Heisenberg model. In the 1960's Elliott Lieb and Werner Liniger solved via the Bethe Ansatz the uniform Bose gas in 1D [12]. The latter is the simplest and most fundamental Hamiltonian for bosonic systems in 1D, so it certainly deserves a rather short but detailed enough description in this thesis. It is consisted of just the kinetic energy and an interaction modeled by a Dirac $\delta$ function with a strength $g$

$$H = -\frac{1}{2}\sum_{i=1}^{N}\frac{\partial^2}{\partial x_i^2} + g\sum_{i<j}\delta(x_i - x_j) \tag{1.1}$$

The Lieb-Liniger (LL) parameter $\gamma = \frac{g}{n_{1D}}$ where $n_{1D} = N/L$ is the density of a system of $N$ bosons and length $L$ is a dimensionless measure of the interaction strength. An interesting difference from the 3D case is that for larger density the effective interaction becomes lower [1, 4, 13]. Rather than just reproducing the seminal paper of Lieb and Liniger [12], we will describe the solution from the viewpoint of this thesis: from two to many, or from a single pair to the case of arbitrary number of bosons. The same will be done for the extreme case of

infinitely strong repulsion between 1D hard core bosons which has been shown also in 1960 by Marvin Girardeau [11] to be soluble under a mapping to identical fermions. The aforementioned lattice models (Ising, Hubbard, Heisenberg) although extremely important are not on the focus of the present thesis[1].

This chapter is organized as follows: First we state and prove the theorem of Girardeau for the relation between hard-core bosons and fermions in general. Then we take the uniform case for two bosons infinitely repulsive which we generalize to an arbitrary atom number, thereby examining the Tonks-Girardeau (TG) limit of the LL model. Then we consider arbitrary interaction strength first for two atoms and then extend to the Bethe-Ansatz solution of the Lieb-Liniger model. In the last section we describe the solution of a trapped system of two atoms [14] which is essential for the whole theoretical approach of this thesis.

## 1.1 Tonks-Girardeau gas

It is well known that fermions are the constituents of matter and have the property to avoid being at the same state or at the same place (if they are identical). This so-called Pauli exclusion principle can be thought as a repulsive force or Fermi-pressure that actually prevents the world from collapse. Formally it means that the total wavefunction $\Psi_F(x_1, ..., x_N)$ describing a system system of $N$ fermions vanishes it the case at least two of them meet each other $\Psi_F(x_1, ..., x_i = x_j, ..., x_N) = 0$. If we now consider a system of bosons that experience an infinite repulsion every time they meet each other $x_i = x_j$ (or they overcome a certain hard-core sphere distance $|x_i - x_j| < R$), it is probably intuitive to think that they will resemble fermions at least in that $\Psi_B(x_1, ..., x_i = x_j, ..., x_N) = 0 = \Psi_F(x_1, ..., x_i = x_j, ..., x_N)$. This is the essential feature that allows us to map infinitely repulsive hard core bosons to non-interacting identical fermions and thereby provide an exact solution of this strongly interacting highly correlated system in terms of a non-interacting one. If we know the single-particle solutions of the external potential $\phi_n$ and we are able to construct the fermionic wavefunction by the Slatter Determinant $\Psi_F(x_1, ..., x_N) = \det[\phi_n(x_i)]$ and then impose the correct symmetry for the bosons. The formal statement and proof of this useful theorem that establishes a beautiful and on the first place non-expected relationship between 1D bosons and fermions is given next.

### 1.1.1 Bose-fermi map theorem

For any given 1D system without interaction, if $\Psi_F$ is the fermionic solution of the Schrödinger equation then

$$\Psi_B = A\Psi_F \qquad A := \prod_{i<j} \mathrm{sgn}(x_i - x_j) \tag{1.2}$$

has bosonic permutation symmetry and satisfies the Schrödinger equation with hard-core boundary conditions ($g \to \infty$)

$$\Psi_B|_{x_i=x_j} = 0, i < j. \tag{1.3}$$

Therefore with the use of products of signum functions (see also Appendix B) multiplying the fermionic function we can establish the right symmetry for the bosons. One can think of $A$ as a symmetrization operator which takes the values $\pm$ depending on the ordering of the particle coordinates on the line. If one does a permutation of between two coordinates $x_i \leftrightarrow x_j$ the sign of A changes. This is true for all odd permutations while the opposite happens for even ones. One can now simply see that $\Psi_B = A\Psi_F$ has the correct bosonic symmetry. If one

[1]The Bose-Hubbard model which is fundamental for 1D lattices will be shortly described and used as an analysis tool in the corresponding Chapter 3.1.

applies the permutation on it, the fermionic function takes a minus sign $\Psi_F \to -\Psi_F$ but this is healed by the operator A which also changes sign $A \to -A$ so that the combination remains the same $\Psi_B \to \Psi_B$. On the first place the operator $A$ seems to introduce a discontinuity to the function since the signum function is discontinuous at zero. It actually makes the function piecewise-defined in the different domains of ordering of the particle coordinates. Still the hard-core boundary condition Eq. 1.3 assures the continuity of the wavefunction at the turning points. Therefore we have the three properties that we need: (i) the function $\Psi_B$ is continuous inside each domain and at the boundaries, (ii) it is solution at each domain (since $\Psi_F$ is) and satisfies the boundary condition and (iii) it has bosonic symmetry.

The Bose-Fermi map applies to every stationary state (ground or excited). Especially for the ground state the simplification goes further since there are no other nodes (zeros) in both the bosonic and fermionic wavefunctions apart from those introduced by the hard-core boundary condition or the Pauli principle respectively. Therefore since the fermionic function $\Psi_F$ has the same sign as $A$ everywhere the product $A\Psi_F$ reduces to

$$\Psi_B = |\Psi_F|. \tag{1.4}$$

Another property of this map is extremely useful: Since $A^2 = 0$, all local quantities (as well as the energy) derived from the density $|\Psi_B|^2$ are exactly the same for hard-core bosons and identical fermions . This is not true for non-local properties like the momentum distribution. We are interested in observables like the local densities i.e. diagonal kernels of the reduced density matrices, which are the appropriate tools for analyzing a many body state $|\Psi\rangle$. The one-body density $\rho(x) \equiv \langle x|\hat{\rho}_1|x\rangle$, diagonal kernel of the one-body density operator $\hat{\rho}_1 \equiv \mathrm{tr}_{2,...,N}|\Psi\rangle\langle\Psi|$ is calculated by the integral:

$$\rho(x) = \int_{-\infty}^{\infty} ... \int_{-\infty}^{\infty} |\Psi|^2 dx_2 ... dx_N \tag{1.5}$$

with $\Psi(x_1, ..., x_N)$ normalized so that also $\int \rho(x)dx = 1$, tracing out all other degrees of freedom except for one. The two-body density $\rho_2(x_1, x_2) \equiv \langle x_1 x_2|\hat{\rho}_2|x_1 x_2\rangle$ diagonal kernel of the two-body density operator $\hat{\rho}_2 \equiv \mathrm{tr}_{3,...,N}|\Psi\rangle\langle\Psi|$ given by the integral:

$$\rho_2(x_1, x_2) \equiv \int_{-\infty}^{\infty} ... \int_{-\infty}^{\infty} |\Psi|^2 dx_3 ... dx_N \tag{1.6}$$

from which we obtain a two-body pair-correlation function[2]. These two functions illustrate the basic properties of a correlated system in a one- and two-body level, and will be shown in several cases discussed in the following Chapters.

In the infinitely repulsive TG limit they are equal to the fermionic ones:

$$\rho(x) = \sum_{n=0}^{N-1} |\phi_n(x)|^2 \tag{1.7}$$

and

$$\begin{array}{ll} \rho_2(x_1, x_2) = & \dfrac{1}{N(N-1)} \\ \sum_{0 \le n < n' \le N-1} & |\varphi_n(x_1)\varphi_{n'}(x_2) - \varphi_n(x_2)\varphi_{n'}(x_1)|^2. \end{array} \tag{1.8}$$

The ground state energy in the fermionization limit is also given by the fermionic expression $E_{\mathrm{TG}}(N) = \sum_{n=0}^{N-1} E_n$ summing up all single-particle state energies $E_n$ up to the Fermi edge (the state that the last fermion occupies).

[2]We will use the terms 'two-body' and 'pair-correlation' equivalently in the text.

One can derive also an extension of the Bose-Fermi map to mixtures (Bose-Bose or Bose-Fermi) or spinor systems [65]. Although this idea can be applied in very different contexts and systems, it is important to underline that it refers exclusively to 1D. For higher dimensions the division into domains fails, since for example two atoms may have the same position at $x_i = x_j$ but different in transversal direction, or the same radial distance and different angular part. There is therefore something special in 1D which makes possible such a beautiful effect, the relation between the basic statistical features of identical particles in nature.

### 1.1.2 Tonks gas limit of the Lieb-Liniger model

The immediate application of the Bose-Fermi map, would be the 1D uniform Bose gas – the LL model Eq. 1.1 in the case $\gamma, g \to \infty$. The fermionic function is build up from the eigenstates of the kinetic energy operator, i.e., the plane waves of the form $e^{ikx}$. We have $\Psi_F \propto \det[e^{ik_j x_l}]$ where det denotes the Slatter Determinant. According to Girardeau's theorem [11] Eq. 1.2 we then obtain for the wavefunction of the bosonic system:

$$\Psi_B = A\Psi_F \propto \det[e^{ik_j x_l}] \prod_{s<t} \mathrm{sgn}(x_t - x_s). \tag{1.9}$$

The gas is thought to be uniform in a space of length $L$ with periodic boundary conditions $\Psi(x_1, ..., x_j = 0, ..., x_N) = \Psi(x_1, ..., x_j = L, ..., x_N)$ for all particles (for hard-wall boundaries see [66]). This results to a condition for the $k$-vectors:

$$k_j = \frac{2\pi}{L}\left(n_j - \frac{N+1}{2}\right) \tag{1.10}$$

with $n_j$ an arbitrary integer. To obtain the ground state one should minimize the energy which is the same as the fermionic: $E = \frac{1}{2}\sum_j^N k_j^2$. This is done by choosing the $k$-vectors with the smallest magnitude, that is $n_j = j = 1, 2, ..., N$. For the basic case of two atoms this means $k_1 = -k_2 = \pi/L$ which results to the function:

$$\Psi_{TG-LL}(x_1, x_2) = \frac{\sqrt{2}}{L} \sin\left(\frac{\pi|x_1 - x_2|}{L}\right) \tag{1.11}$$

Let us immediately write down also the corresponding $N$-body ground state in terms of products of pair functions (which is a reformulation of this particular Slatter determinant):

$$\Psi_{TG-LL}(x_1, ..., x_N) = \frac{2^{N(N-1)/2}}{\sqrt{N!L^N}} \prod_{i<j} \sin\left(\frac{\pi|x_i - x_j|}{L}\right) = |\Psi_F| \tag{1.12}$$

It is obvious that these two last exact results for the single pair and the $N$-body problem of the Tonks gas have a strong relation. The pair-function, from which the $N$-body (product) state (Eq. 1.12) is built up, is exactly the one corresponding to the exact solution of the two-body case Eq. 1.11. This is particularly interesting from the viewpoint of this thesis since it has a strong similarity to the Ansatz proposed also for the case of the parabolically trapped system (see Chapter 2.1). This type of functions were first introduced by Jastrow [67] to solve problems with short-range interactions in nuclear physics where the density is much higher and the correlation factor is of short range. An other important point here is that both functions vanish at the manifolds where two atoms meet each other $\mathcal{M}_{ij} = \{(x_1, ...x_i, ..., x_j, ..., x_N) \in \mathbb{R}^N | x_i = x_j\}$. This is exactly the necessary condition that a fermionic or a TG wavefunction should meet. We illustrate this by plotting in Fig. 1.1.2 (a) the two-body case Eq. 1.11 as a function of the relative motion coordinate $\frac{x_1 - x_2}{L}$. The blue line corresponds to the TG limit of the two-atom case for

the LL-gas where the function vanishes at $x_1 = x_2$. Note also that the states $\Psi_{TG-LL}(x_1, x_2)$ and $\Psi_{TG-LL}(x_1, ..., x_N)$ are symmetric with respect to the exchange (or permutation) $x_1 \leftrightarrow x_2$ or in general $x_i \leftrightarrow x_j$ due to the absolute value in the corresponding Eqns. 1.11 and 1.12. The absolute value accounts in this product form of the ground state for the symmetrization operator $A$ (see previous section and Appendix B).

Since the periodic boundary conditions correspond to a rather artificial and exotic system of atoms confined on a ring, Lieb and Liniger rather preferred the thermodynamic limit where $N \to \infty$, $L \to \infty$ with a constant density $n_{1D} = N/L$. In this limit every sum over $j$ of a quantity $G(k_j)$ can be replaced by an integral over $k$:

$$\sum_j^N G(k_j) \to \frac{L}{2\pi} \int_{-k_0}^{+k_0} G(k) dk \quad \text{with} \quad k_0 = \pi n_{1D} = \pi N/L \tag{1.13}$$

from which one can compute several thermodynamic quantities (energy per atom, chemical potential and pressure):

$$\frac{E}{N} = \frac{k_0^2}{6} \quad \mu = \frac{\partial E}{\partial N}|_L = \frac{k_0^2}{2} \quad p = -\frac{\partial E}{\partial L}|_N = \frac{2E}{L} \tag{1.14}$$

These are all exactly the same as for fermions. But other properties like momentum distribution are related to the statistics of the identical particles as we have already mentioned.

### 1.1.3 Tonks gas limit of the harmonic trap

The most natural and fundamental extension of the LL model is the 1D Bose-gas trapped in a parabolic potential. It is well known that the harmonic trap is the most fundamental model for all traps since it represents a system next to the equilibrium point, and we are lucky that the corresponding single-particle quantum problem is analytically soluble via the Hermite polynomials. It is important to mention that a trapped system is also experimentally more realistic since the free untrapped case is just an idealization. Knowing the single-particle states of the Hamiltonian $H = -\frac{\partial^2}{\partial^2 x} + \frac{1}{2}x^2$, we can again express the fermionic function in terms of a determinant and the bosonic via the Bose-Fermi map. For two bosons the ground state looks exactly like the corresponding fermionic Slatter determinant (consisted of the ground and first excited state of the harmonic trap Hamiltonian):

$$\Psi_{TG-HT}(x_1, x_2) = \frac{1}{\sqrt{\pi}} e^{-\frac{x_1^2}{2} - \frac{x_2^2}{2}} |x_1 - x_2| \tag{1.15}$$

with the difference that we take again an absolute value due to the permutation symmetry.

The corresponding case of $N$ atoms if one again writes the Slatter determinant in a product form reads [68]:

$$\Psi_{TG-HT}(x_1, ..., x_N) = \frac{2^{N(N-1)/4}}{\sqrt{N! \prod_{n=0}^{N-1} n! \sqrt{\pi}}} \exp\left(-\sum_{i=1}^{N} \frac{x_i^2}{2}\right) \prod_{i<j}^{P} |x_i - x_j| \tag{1.16}$$

It is obvious again that these functions vanish at the collision points of any pair, and that the two-body part of the $N$-body case is a product of functions of the distance between two atoms $|x_i - x_j|$ which is a direct generalization of the two-body case. The exact solution for this limit is an essential tool for the Ansatz proposed in this thesis for arbitrary strength of the interaction in the 1D harmonic trap (Chapter 2.2).

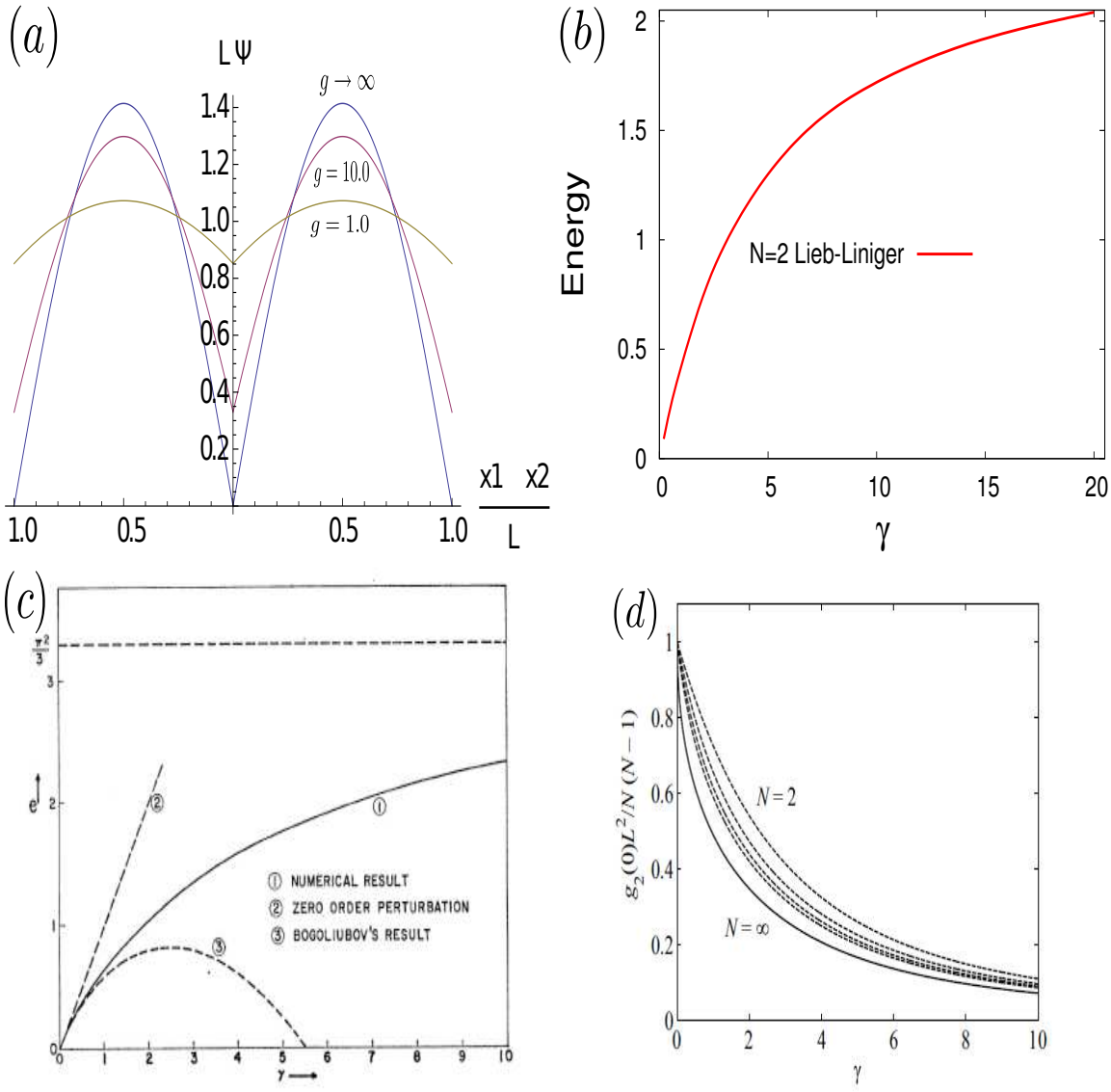


Figure 1.1: (a) Wavefunction for the relative motion for two atoms in the homogeneous 1D LL-gas for different interaction strengths. (b) Energy as a function of the interaction LL-parameter $\gamma$ for the same case. (c) Different approaches shown in [12] on the energy as a function of $\gamma$ for the thermodynamic limit. (d) The two-body correlation function at zero distance as a function of $\gamma$ for different number of atoms (from Pethick and Smith pg. 476 [1])

## 1.2 Lieb-Liniger model

Keeping in mind the extreme case of infinite interactions (TG gas) we turn now again to arbitrary coupling strengths firstly for the LL model [12] which is solved via the Bethe Ansatz [21]. The most important difference with the case of infinite repulsion is that the boundary condition due to the interaction does not have the simple form of Eq. 1.3 which is just a vanishing of the wavefunction at the meeting points analog to Pauli exclusion principle. Since the interaction strength $g$ is here finite the bosons still have some probability to be at the same spot. However the delta-like interaction potential of the LL-model (Eq. 1.1) introduces a discontinuity to the first derivative at the meeting points which is proportional to the strength of the interaction.

### 1.2.1 Lieb-Liniger for a single pair

Let us first consider the case of two bosons. It is always possible (when the particles are identical and the Hamiltonian quadratic) to separate into center of mass $R = \frac{x_1+x_2}{2}$ and relative coordinate $r = x_1 - x_2$. In this center of mass frame (CMF) we can rewrite the kinetic energy terms of the two-body Hamiltonian as $-\frac{\partial^2}{2\partial x_1^2} - \frac{\partial^2}{2\partial x_2^2} = -\frac{\partial^2}{4\partial R^2} - \frac{\partial^2}{\partial r^2}$. One can now reduce the problem to the relative motion since the center of mass is decoupled and does not experience any interaction. The lowest energy state corresponds to zero momentum in the center of mass motion.

The differential equation for the relative motion reads:

$$-\Psi''(r) + g\delta(r)\Psi(r) = E\Psi(r) \tag{1.17}$$

Integrating this in a small interval $r \in [-\epsilon, +\epsilon]$ around $r = 0$ and taking the limit $\epsilon \to 0$ we obtain:

$$\Psi'(0^+) - \Psi'(0^-) = g\Psi(0) \tag{1.18}$$

Considering that the function should be symmetric due to the bosonic nature $\Psi(r) = \Psi(-r)$ one may write more compactly:

$$2\Psi'(0) = g\Psi(0) \tag{1.19}$$

This general form of condition is known under the name Bethe condition, and is widely used in 1D systems where a delta function induces a discontinuity in the derivative. Let us perform also a slightly different derivation which will enhance the understanding of the argumentation in the many-body case (Chapter 2.1). We assume that the wavefunction should contain the absolute value of the relative motion coordinate i.e. the distance $\Psi(|r|)$ (as it will be proven to be the case). Then the operation of the relative motion Hamiltonian on this wavefunction can be written as:

$$\left[-\frac{d^2}{dr^2} + g\delta(|r|)\right]\Psi(|r|) = -\frac{d^2\Psi(|r|)}{d|r|^2} + \delta(|r|)\left[g - 2\frac{d}{d|r|}\right]\Psi(|r|) \tag{1.20}$$

using relations explained in the mathematical appendix B (Eq. B.1, B.2). Then the quantity multiplying the delta function should vanish when $|r| \to 0$ which results again to the Bethe condition. The other part of the equation (here just the kinetic term of the second derivative) indicates the specific functions $\Psi(|r|)$ that should be used (in this case the plane waves).

One can also rewrite the Bethe condition back to the original coordinate system:

$$\frac{1}{2}\left(\frac{\partial}{\partial x_1} - \frac{\partial}{\partial x_2}\right)\Psi|_{x_1=x_2+\epsilon} - \frac{1}{2}\left(\frac{\partial}{\partial x_1} - \frac{\partial}{\partial x_2}\right)\Psi|_{x_1=x_2-\epsilon} = g\Psi|_{x_1=x_2} \tag{1.21}$$

Taking into account the symmetry of the wavefunction the latter becomes:

$$\left(\frac{\partial}{\partial x_1} - \frac{\partial}{\partial x_2}\right)\Psi|_{x_1=x_2+\epsilon} = g\Psi|_{x_1=x_2} \tag{1.22}$$

The space attributed to the Bethe condition shows the importance it has on the solution of 1D problems, its main contribution being to assure that the two-body nature of collisions is correctly taken into account.

To proceed on the solution of the LL model for two atoms, we can now consider first in the fundamental domain $0 \leq x_1 \leq x_2 \leq L$ where we make the Ansatz of Bethe form[3]:

$$\Psi(x_1, x_2) = Ae^{ik_1x_1}e^{ik_2x_2} + Be^{ik_2x_1}e^{ik_1x_2} \tag{1.23}$$

The boundary condition Eq. 1.22 gives then

$$\frac{B}{A} = \frac{k_2 - k_1 + ig}{k_2 - k_1 - ig} \tag{1.24}$$

For real $k_2 - k_1 \Rightarrow |B| = |A|$ and for $g \to \infty \Rightarrow B = -A \Rightarrow \Psi(x_1, x_1) = 0$ which reproduces the result for the TG gas Eq. 1.11 obtained previously by means of the Bose-Fermi map.

Because of the symmetry $\Psi(x_1, x_2) = \Psi(x_2, x_1)$ for the full space we have:

$$\begin{aligned}\Psi(x_1, x_2) \propto (k_2 - k_1 - ig\mathrm{sgn}(x_2 - x_1))e^{ik_1x_1}e^{ik_2x_2} \\ -(k_1 - k_2 - ig\mathrm{sgn}(x_2 - x_1))e^{ik_2x_1}e^{ik_1x_2}\end{aligned}$$

From the periodic boundary condition for the first atom $\Psi(0, x_2) = \Psi(L, x_2)$ we obtain:

$$e^{ik_1L} = e^{-ik_2L} = \frac{k_1 - k_2 + ig}{k_1 - k_2 - ig} \tag{1.25}$$

and the periodic boundary condition for the second particle $\Psi(x_1, 0) = \Psi(x_1, L)$ is automatically satisfied due to the symmetry.

The total momentum is given by $P = (k_1 + k_2) = \frac{2\pi\nu}{L}$ from Eq. (1.25) where $\nu$ is an integer. The ground state has total momentum zero, therefore $k_1 = -k_2 = k$.

Combining the above we obtain the form of the ground state for two-atom Lieb-Liniger model for arbitrary interaction strength $g$:

$$\Psi_{LL}(x_1, x_2) = \frac{1}{L}\left[\frac{2kL}{kL + \sin(kL)}\right]\cos\left[k\left(|x_1 - x_2| - \frac{L}{2}\right)\right] \tag{1.26}$$

where $k \in [0, \pi/L]$ for the ground state as g increases according to the boundary condition:

$$g = 2k\tan(kL/2) \quad \text{or} \quad \gamma = kL\tan(kL/2). \tag{1.27}$$

which results from the Bethe condition Eq. 1.22 using the function of Eq. 1.26. We plot this function for different values of the interaction $\gamma$ in Fig. 1.1.2 (a). One realizes that with increasing $g$ (or $\gamma$) the probability to find the two atoms at the same spot reduces subsequently and reaches zero in the TG limit where the function takes the form obtained previously Eq. 1.11.

[3]One may consider again the problem only in the relative coordinates making an Ansatz of the form $\Psi(|r|) = A\sin(k|x|) + B\cos(k|x|)$ which probably more easily leads to the same result. We prefer though here to present the Bethe Ansatz form since it connects easier to the many-body case in the next section.

The energy for two atoms is $\gamma$-dependent it is monotonically increasing and reaches a finite value as $\gamma \to \infty$ :

$$E = k^2 = \frac{N}{2} n_{1D}^2 e(\gamma) \tag{1.28}$$

with $e(\gamma) = (kL)^2/4$ where $k$ depends on $\gamma$ due to the boundary condition Eq. 1.27. This function is plotted in Fig. 1.1.2 (b). For small $\gamma \ll 1$ we have $(kL)^2 \approx 2\gamma \Rightarrow e(\gamma) \approx \gamma/2$. For large $\gamma \gg 1$ we have $kL \approx \pi(1 - 2/\gamma) \Rightarrow e(\gamma) \approx \pi^2/4 - \pi^2/\gamma$. The energy per atom at fermionization $\gamma \to \infty$ is therefore $E_{\gamma\to\infty}/N = \frac{\pi^2 n_{1D}^2}{8}$ which is not very far from the estimation for the thermodynamic limit Eq. 1.14. This is an additional indication important for the present thesis (except those of the functional form that we have seen) that the two-body and the many-body case have a very close connection,

### 1.2.2 Lieb-Liniger for N bosons

In the general case of $N$-body LL model with arbitrary interaction strength we will just state the solution without proof, and show again the analogies with the two body case. The Bethe Ansatz reads:

$$\Psi(x_1, ..., x_N) = \mathcal{N} \sum_P (-1)^{[P]} e^{i \sum_n^N k_{P_n} x_n} \prod_{j>l} [k_{P_j} - k_{P_l} - ig\mathrm{sgn}(x_j - x_l)] \tag{1.29}$$

The sum runs over all permutations $k_1, k_2, ..., k_N$, while $[P]$ is the parity of the permutation. For one particular pair of atoms out of the ensemble this function looks very much like that of a single pair in the two atom case Eq. (1.26):

$$\Psi(x_1, x_2) \propto (k_l - k_j - ig\mathrm{sgn}(x_2 - x_1)) e^{ik_j x_1} e^{ik_l x_2} \tag{1.30}$$

$$-(k_j - k_l - ig\mathrm{sgn}(x_2 - x_1)) e^{ik_j x_1} e^{ik_l x_2}. \tag{1.31}$$

The periodic boundary condition is also analogous to the two-body one Eq. 1.27 :

$$e^{ik_j L} = \prod_{l \neq j} \frac{k_j - k_l + ig}{k_j - k_l - ig} \text{ for } j = 1, 2, ..., N. \tag{1.32}$$

For $g \to \infty$ these conditions reduce to those of the TG gas $e^{ik_j L} = (-1)^{N-1}$. By taking the logarithm the boundary condition for the $k$-vectors becomes

$$k_j L + \sum_l^N \theta(k_j - k_l) = 2\pi \left( n_j - \frac{N+1}{2} \right) \tag{1.33}$$

with $\theta(k) = i\ln\left(\frac{ig+k}{ig-k}\right) = 2\mathrm{arctan}(k/c)$. These conditions for $g \to \infty$ are identical to those of the TG gas Eq. 1.10 where for the ground state one should choose $n_j = 1, 2, ..., N$.

Unfortunately we do not have here a simple expression for the energy. Even for the thermodynamic limit it is rather a set of integral equations that defines $e(\gamma)$ in Eq. 1.28. More illustrative and having very similar behaviour to the two-body case is Fig. 1.1.2 (c). For large $\gamma \gg 1$ we have $e(\gamma) \approx \frac{\pi^2}{3} - \frac{4\pi^2}{3\gamma}$ which differs only by 4/3 times the result for two bosons (another indication of the connection between the two cases) and for $\gamma \to \infty$ reaches the value $\pi^2/3$. For the opposite limit $\gamma \to 0$ it has a linear increase $e(\gamma) \approx \gamma$. From $e(\gamma)$ one can calculate several thermodynamic quantities as before.

A very interesting fact is that the derivative of the energy with respect to the interaction parameter is connected via the so-called Hellmann-Feynman theorem [1] to the pair-correlation function at zero distance [$g_2(0) = \rho_2(x_1 = x_2)$]:

$$g_2(0) = n_{1D}^2 \frac{de(\gamma)}{d\gamma} \tag{1.34}$$

One may understand this intuitively since the change of the energy is related to the overlap of the atoms which is mainly prominent on the diagonal of the two-body density $x_1 = x_2$. This relation derived in Pethick and Smith pg. 475-476 has been illustrated in Fig. 1.1.2 (d) taken from this book, for few atoms $N = 2, 3, 4, 5$ and also for the thermodynamic $N \to \infty$ limit. Physically this simple calculation (given the $e(\gamma)$ relation) confirms the intuition that for low interaction parameter the overlap of the atoms is maximum, while it tends to zero in the TG limit ($\gamma \to \infty$) where the effective Pauli principle prevents the atoms from being at the same place. There is a very interesting aspect of this figure which we would like to underline, namely that the behaviour of the curves already for $N = 2$ but also for a few-body ensemble of $N = 5$ is very close to that of the thermodynamic limit ($N \to \infty$). This is an inspiring feature connecting the two- few- and many-body physics in 1D, a first sign that these systems are closely related, as the present thesis indicates in several other cases (trapped bosonic in Chapter 2.1, 3.1 and fermionic systems 4.1). It is also instructive that this happens already on the level of the energy and related to the two-body properties.

## 1.3 A single pair in the harmonic trap

The system of two atoms in the harmonic trap interacting with a regularized contact potential, seems so fundamental that one would expect a very old paper would have approached it. However the problem was first solved analytically by Thomas Busch et. al. in 1998 [14]. The solution explained in this seminal work is general and applies to all dimensionalities from an isotropic 3D parabolic trap, to 2D harmonic potential and finally the case on which we focus here i.e. the pure 1D harmonic trap. Since the latter case is of great importance for the present thesis constituting the building block and the basis for the construction and analysis of many-body states and dynamics, it will be presented next following a different pathway from the original (mainly 3D) paper, which will enhance the understanding of the many-body CPWF Ansatz (Chapters 2.1, 4.1).

In 1D the full Hamiltonian for two-atom problem in a harmonic trap of frequency $\omega_\parallel$ in the general case reads:

$$H = -\frac{\hbar^2\partial^2}{2m_1\partial x_1^2} - \frac{\hbar^2\partial^2}{2m_2\partial x_2^2} + \frac{1}{2}m_1\omega_\parallel 2x_1^2 + \frac{1}{2}m_2\omega_\parallel^2 x_1^2 + g_{1D}\delta(x_1 - x_2) \tag{1.35}$$

We have written down here the most general Hamiltonian but in this thesis only atoms of one atomic species therefore having equal mass $m_1 = m_2 = m$ will be concerned. Among other reasons because the above Hamiltonian only for the latter case decouples to the center-of-mass and relative motion as we will see next.

We choose this point to introduce the interaction strength parameter $g_{1D}$ which was derived the same year as the two-atom paper of Busch et. al by Maxim Olshanii in his seminal paper on confinement induced resonances[4][13]. . Olshanii derived the relation of this parameter to

[4]The two papers are from many scientists working on collision properties seen as complementary the former concentrating on the eigenstates of the closed and the latter on the universal properties of scattering in confined geometries

1. the 3D s-wave scattering length $a_{3D}$ which characterizes the collision properties in 3D for a given magnetic field and tuned by the Feshbach resonances [5] and should be smaller than the average interparticle distance.

2. the effective length of the trapping potential in the transversal direction $a_\perp \equiv \sqrt{\frac{\hbar}{m\omega_\perp}}$ which controls the dimensionality and in general for a quasi 1D system should be at least ten times larger than the corresponding one of the longitudinal trap $a_\parallel \equiv \sqrt{\frac{\hbar}{m\omega_\parallel}}$.

Given these conditions the effective 1D scattering length reads:

$$a_{1D} = -\frac{a_\perp}{a_{3D}}\left(1 - \frac{|\zeta(1/2)|a_{3D}}{\sqrt{2}a_\perp}\right) \tag{1.36}$$

where $\zeta(1/2) = 1.4603$ is the Riemann zeta function, while the interaction parameter we are interested here reads

$$g_{1D} = -\frac{2\hbar^2}{ma_{1D}} = \frac{2\hbar^2 a_{3D}}{ma_\perp^2}\left(1 - \frac{|\zeta(1/2)|a_{3D}}{\sqrt{2}a_\perp}\right)^{-1} \tag{1.37}$$

First observation here is that the effective interaction strength in 1D $g_{1D}$ is inverse analog to the effective 1D scattering length $a_{1D}$ which is different from the standard analogous behaviour in the 3D case. The tuning of this interaction parameter can be done in two ways as this relation shows: (i) by tuning the $a_{3D}$ via Feshbach resonances or (ii) by changing the transversal confinement length taking care to maintain the condition for being in the quasi-1D regime. We will consider this interaction parameter as tunable at will from weak to strong couplings, since this represents also the current status of the state-of-the-art experiments [20, 61, 24]. We perform now a rescaling of the Hamiltonian such that lengths and energies are scaled by $a_\parallel$ and $\hbar\omega_\parallel$ respectively.

$$H = -\frac{\partial^2}{2\partial x_1^2} - \frac{\partial^2}{2\partial x_2^2} + \frac{1}{2}x_1^2 + \frac{1}{2}x_1^2 + g\delta(x_1 - x_2) \tag{1.38}$$

with only one remaining free parameter $g = \frac{g_{1D}}{\hbar\omega_\parallel a_\parallel}$. This Hamiltonian and its many body equivalent will be studied next and in Chapters 2.1 and 4.1 for bosons and two-component fermions respectively with increasing repulsive interaction strength $g \in [0, \infty)$[5].

### 1.3.1 The exact solution in 1D

One may solve the above Hamiltonian in an equivalent way as we did for the Lieb-Liniger model in the continuum. One important feature of quadratic potentials in general is that they can be separated into center-of-mass and relative coordinates $H = H_{CM} + H_r$. The center of mass equation of motion here is another harmonic trap since $H_{CM} = -\frac{\partial^2}{4\partial R^2} + R^2$ (with effective mass $M_{CM} = N = 2$) with known solution for all eigenstates [eg. the ground state reads $\Psi_{CM} = \frac{1}{\sqrt{\pi}}\exp(-R^2/2)$]. Therefore the main effort concentrates on the relative motion part which in the case of two atoms in the trap reads:

$$H_r = -\frac{d^2}{dr^2} + \frac{1}{4}r^2 + g\delta(r) \tag{1.39}$$

This Hamiltonian is the same as that from the two-atom LL model, except from the second term coming from the trapping potential. The Ansatz used for the LL model with plane waves being

[5]Essentially this is also the parameter $g$ that appears in the LL model EQ. 1.1 if one is to realize it with cold atoms in quasi-1D traps.

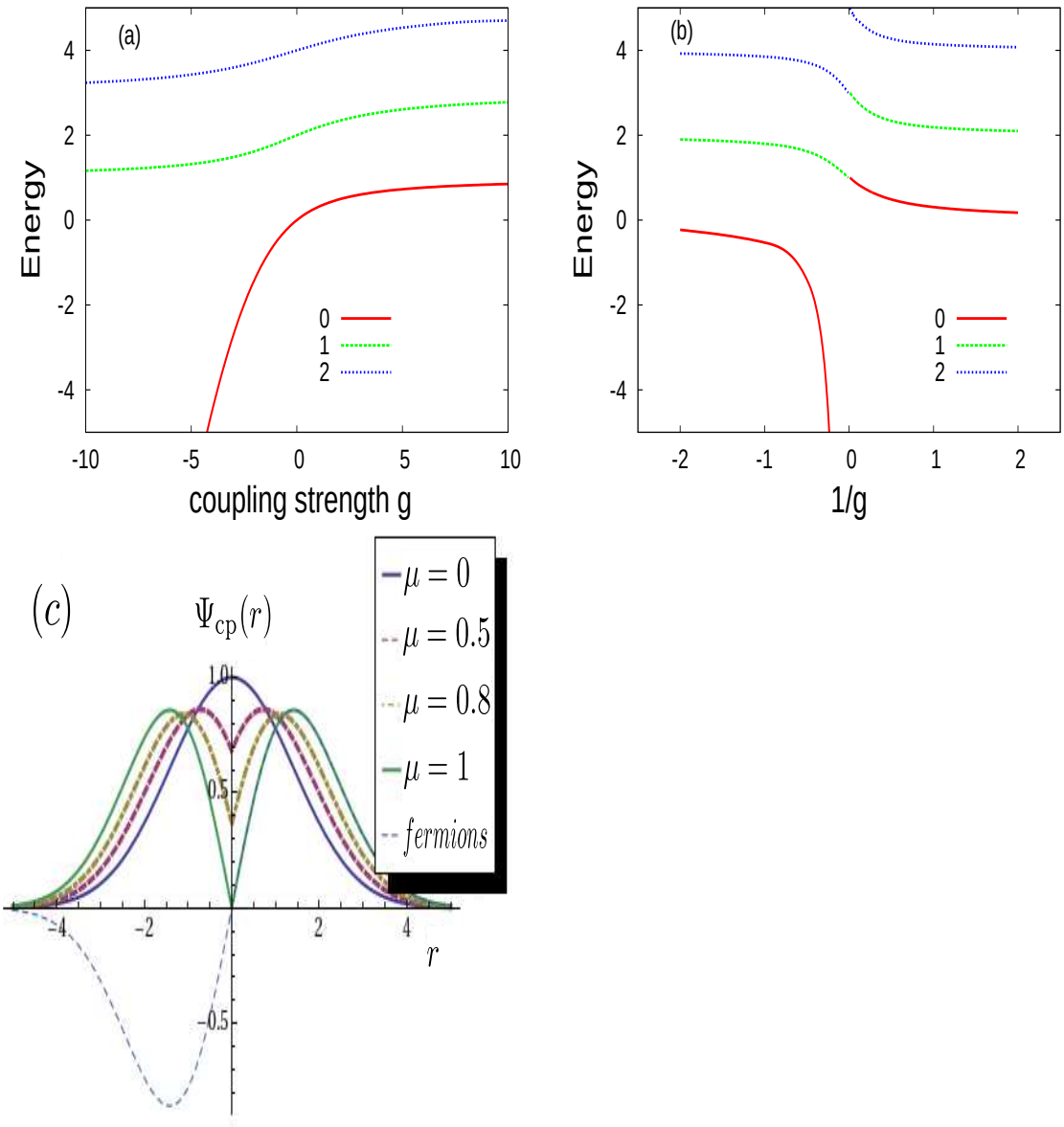


Figure 1.2: (a) Lower energy spectrum as a function of the interaction strength $g$ for the two-atom case in the harmonic trap [14]. (b) The same versus $1/g$. (c) The wavefunction of the relative motion for the same case, shown for different interaction strengths from zero to infinity corresponding to different parameters $\mu \in 0, 1$ and comparison of $\mu = 1$ with the fermionic antisymmetric function.

the eigenfunctions for the equation without the interactions (the mere kinetic energy operator in that case) should be here replaced by the corresponding one for the differential equation related to the trap. This equation

$$\left(\frac{d^2}{dr^2} - \frac{1}{4}r^2\right) D_\mu(r) = \left(\mu + \frac{1}{2}\right) D_\mu(r) \tag{1.40}$$

is called Weber equation and we show in the mathematical Appendix B that the solutions which we are interested in here are given by the so-called Parabolic Cylinder Functions (PCF) $D_\mu(r)$. For real $\mu$ and $r$ these functions diverge as $r \to -\infty$ but are well defined and converge to zero for $r \to +\infty$. This does not cause a problem, since due to the bosonic symmetry we need a function that is permutationally symmetric therefore we use the absolute value [or distance between the atoms $D(|-r|) = D(|r|)$] as we had also in the LL case. We remain therefore only with a well defined function of $|r|$ with one parameter, the effective quantum number $\mu$ that should be determined. The parameter $\mu$ determines also the energy $\varepsilon(\mu) = \mu + 1/2$ for the relative motion (see Eq. 1.40), which is here not necessarily a half integer like in the single-particle harmonic oscillator problem but can take every real value. To determine $\mu$ we impose the condition at the contact point coming from the interaction or else the Bethe condition exactly like in the case of the LL model (see Eq. 1.19):

$$2\frac{dD_\mu(r)}{dr}(0) = gD_\mu(0) \tag{1.41}$$

with the difference that here should be applied to the corresponding functions (PCF). Note that the presence of the trapping potential does not change the boundary condition: it vanishes in the 'integral around zero' (see Eq. 1.18) derivation, and it does not have a $\delta$ function contribution in the 'Hamiltonian operation' (see Eq. 1.20) derivation. From known formulas for the values of the (PCF) derivative Eq. B.22 and function Eq. B.21 at zero (see mathematical Appendix B) one obtains:

$$g = -\frac{2^{\frac{3}{2}}\Gamma\left(\frac{1-\mu}{2}\right)}{\Gamma\left(\frac{-\mu}{2}\right)} \tag{1.42}$$

This transcendental equation can be solved with respect to $\mu$ in order to define eigenenergies. In the repulsive interaction side for a certain $g$ there is one solution for every interval between two subsequent integers. To give a picture of the solution for the eigenenergies as a function of the interaction strength we plot in Fig. 1.3.1 (a), (b) the lowest part of the spectrum. For weak interactions $g < 1$ one can approximate the energy of the relative motion by

$$\varepsilon(g) = 2n + \frac{1}{2} + \frac{g}{\sqrt{2\pi}}\binom{n-\frac{1}{2}}{n} + O(g^2) \tag{1.43}$$

which is a small perturbation compared to the non-interacting levels $e(0) = 2n$[6]. On the other hand for strong coupling strength as $g \to \infty$ each state approaches the next (or previous in the attractive side) odd level $e(g \to \pm\infty) = 2n \pm 1$. At this 'fermionization' limit the ground state takes the form we already shown in Eq. 1.15, since the relative motion has the profile of the first Hermite polynomial $\Psi_r(|r|) = e^{-r^2/4}|r|$ (see also in the Mathematical Appendix B Eq. B.26). In Fig. 1.3.1 (c) we show the profile of the ground state of the relative motion for several interaction strengths $g$. We observe that the function acquires a cusp at $r = 0$ for $g > 0$ [or $\mu > 0$ from Eq. (1.19)] which goes to zero as $g \to \infty$ ($\mu \to 1$), retrieving the fermionic state but with bosonic symmetry. This behaviour of the two atoms avoiding each other at

[6]Note that only even states are relevant for the relative motion also due to the bosonic symmetry.

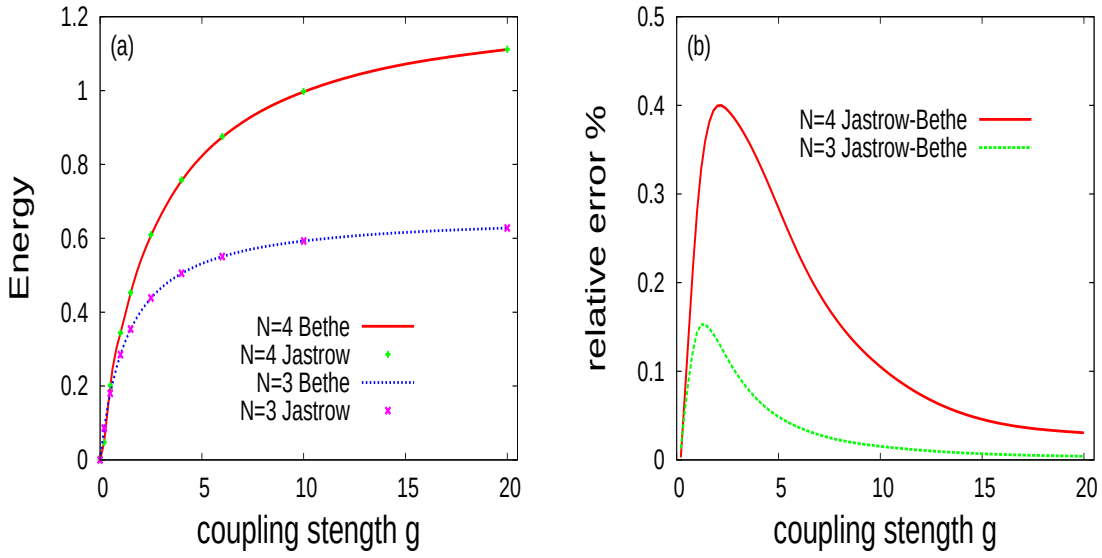


Figure 1.3: (a) The energy for $N = 3, 4$ atoms obtained by a Jastrow and a Bethe Ansatz in the homogeneous LL-case as a function of the interaction strength $g$. (b) The relative error that of the Jastrow Ansatz compared to the Bethe Ansatz (exact solution of the LL gas).

the contact points, which is enforced by the Bethe condition, is essential for the treatment of larger ensembles of atoms, and has been also seen in the case of the LL model. The PCF here has slightly different behaviour close to $r = 0$ and certainly vanishes like $\psi(r) \propto e^{-r^2/4|r|^\mu}$ as $r \to \pm\infty$ in contrast to the periodic nature of the LL Bethe Ansatz and the trigonometric function appearing in the corresponding two.body case Eq. 1.26 (see in comparison Fig. 1.1.2). Let us make also some comments on the attractive side which is not on the focus of this thesis. The lower state falls to a molecular behaviour with strong binding as $g \to -\infty$. The first excited state though corresponds to the so-called super-repulsive side since effectively the repulsion is even stronger than for the TG gas, and the energy increases further from the fermionization limit: this is the two-body analog of the super-TG gas. Better this is demonstrated in Fig. 1.3.1 (b) where the spectrum is plotted with respect to the inverse interaction parameter $1/g$ (which is analog to the effective 1D scattering length): we observe that the red line of the repulsive side is continued by the green line on the other side of infinite attractive interactions. Some times this is also called the attractive and repulsive side of the (Feshbach) resonance, the resonant position being at the point where $g$ diverges.

The discussion of this two-body case and the exact solution are very essential for this thesis particularly for the next Chapter 2. Interestingly the 3D and 2D solutions [14] also share a similar functional form and energy behaviour like the 1D case, a fact that gives hope to an extension of our proposals presented in the next Chapters to higher dimensions. More specific investigations on correlation properties of this two-body system [69] as well as quasi-1D corrections for anisotropic traps [62] are also worth mentioning.

### 1.3.2 From two to many: an interlude

In the previous sections of this chapter we presented in a pedagogical way from the 'two to many' perspective basic theoretical models and their solutions. We have seen that there are certain connections between the function for the two-body problem and those for the corresponding many body, as well as a two-body condition (Bethe condition) which appears all over since

it reflects the nature of the interaction: two-body contact ($\delta$-like) potential. Looking for a gap in this systematic study, there is absence of an analytical treatment for the case of the many-body trapped system for arbitrary interaction strength, since the system which lacks an exact solution. There exist though the solutions of the two body system (PCF) [14] and the many body TG-gas (Eq. 1.16 at the infinite interaction limit. The next Chapter 2.1 (as well as Chapter 4.1 for fermions) are devoted to this system and the basic proposal of this thesis: the many-body CPWF to describe the crossover from weak to strong interactions in the trap.

The term 'correlated-pair' indicates that the two-body solution in the trap presented above [14] is the 'building stone' upon which we construct our many-body Ansatz. The main problem is (compared to the LL case and the corresponding plane waves) that the two-body solution in terms of PCF's is not separable to a sum. Therefore the natural choice to construct a many-body function in this case is to take a product of pair-functions, a technique that is usually attributed to Jastrow [67], and even constitutes the main idea of the Laughlin wavefunction Ansatz for the explanation of the anomalous quantum Hall effect [70]. A Jastrow-type Ansatz will be also our choice for an explicit many-body wavefunction in the next Chapter 2.1.

We underline here that the Jastrow-type of Ansatz is different from the Bethe Ansatz in that it contains no sums. In this sense it is also simpler to write down the explicit wavefunction and in a sense more intuitive for the understanding of the many-body behaviour since it is totally based on the two-body one. The usual Jastrow Ansatz that is used for example in Quantum Monte Carlo studies (see Appendix A) as a variational or guiding function [27, 71] is inspired from the two-body solution of the LL-model containing the trigonometric function Eq. 1.26. Our choice for the trap is to use instead the corresponding two-body function from Busch et. al [14].

There is however a nice point to be made here within the LL model, comparing a Jastrow and a Bethe Ansatz. As we have seen the non-interacting but also the infinite repulsive case (TG gas) Eq. 1.12 the Bethe Ansatz and the Jastrow form are the same as can been shown from the exact solution of Girardeau [65]. Therefore one may use also in between (for intermediate interaction strengths) a Jastrow type Ansatz of the form:

$$\Psi_{LL-Jastrow}(x_1, x_2, ..., x_N) = C \prod \Psi_{LL}(|x_i - x_j|) \tag{1.44}$$

where $C$ is a normalization constant and $\Psi_{LL}(|x_i - x_j|)$ the two-body function in Eq. 1.26. In Fig. 1.3.2 (a) we compare energy obtained by the two Ansatzes, i.e. Bethe and Jastrow for few atoms (3 and 4) as an example. It is striking that is an impressive agreement for arbitrary interaction strengths, and as expected coincidence for zero and infinite interactions. In Fig. 1.3.2 (b) we show the relative error of the Jastrow Ansatz compared to the Bethe exact solution of the problem. The largest deviation is in the regime of intermediate interaction strengths, which implies that the correlations in that case are a bit different than those that the product form of the Jastrow Ansatz induces. A comparison like this will be done for the case of the harmonic trap in the next Chapter 2.1[7]although in that case the exact solution does not exist and therefore we have to resort to numerical methods for calculating the exact ground state and comparing it to our Jastrow-type Ansatz (the CPWF based on the two-body solution of the harmonic trap case). There is though a very important common feature of the LL-model and the trapped system, namely that the limiting cases of zero and infinite repulsion can be written in a form of a Jastrow-function (see Eq. 1.16 and 1.9) [71].

Although the above considerations clarify the most important part of the 'two to many' perspective of this thesis, the issue is not limited only to construction of ground states but concerns also the understanding of more complex phenomena of many-body physics. For example

[7]A Jastrow-type CPWF Ansatz is also extended to finite lattice potentials in Chapter 3.1 and to harmonically trapped two-component fermions in Chapter 4.1.

our analysis on driven interaction systems and on tunneling dynamics is dependent on the two- and more general few-body spectrum which underline corresponding resonant mechanisms (see Chapter 2.2, 3.2). In general one could say that the questions that arise from the study of few-body systems always reflect those for the many-body equivalent (or even the thermodynamic limit of infinitely many atoms), and what we can learn from the study of the 'few' may help us to understand better the 'many'. One other very important question which this thesis partially touches is the crossover between many-body and few-body physics, eg. one may ask what number of atoms is enough or necessary to reproduce the behaviour in the thermodynamic limit, or to put it in a simpler form the question 'how many is many?'. With these thoughts and questions in mind we set out to examine specific physical systems in 1D in the next Chapters.

# Chapter 2

# Bosons in a harmonic trap

In this chapter and for the most part of this thesis (except the last Chapter 4) we exclusively discuss bosonic systems. In particular here we are interested in the prototypical trap which represents the whole class of traps with a minimum: the harmonic (or parabolic) trap. Cold bosons in parabolic traps is the fundamental system of ultracold atom research, appearing in many experimental and theoretical works [1, 15, 24, 14, 26, 27, 28, 29]. The aim of this Chapter is to approach two particular physical problems: the ground state properties in a 1D harmonic trap along the crossover from weak to strong interactions (Chapter 2.1) and the excitation dynamics induced by a driven interaction strength (Chapter 2.2). Both problems are tackled via a bottom-up approach starting from the two-body case and generalizing to the many-body system. For the ground-state properties we introduce in Chapter 2.1 an Ansatz based on the functions which describe the two-body solution, the CPWF, the main proposal of this thesis. In the second part (Chapter 2.2) the interaction strength is not set to a specific value as in stationary problems but is rather periodically driven and induces correlated dynamics of the wave packet in the harmonic trap. The analysis builds upon the two-body stationary and Floquet energy spectrum, and concerns resonant excitation dynamics and acceleration processes.

## 2.1 Correlated-pair wavefunction (CPWF)

The standard way to approach the ground state properties of a 1D trapped system in the literature is to start from the homogeneous space solution of the LL-model (see Chapter 1) and perform a local-density approximation [22] which in fact transforms thermodynamical quantities like the chemical potential in order to take into account the trapping potential. Our approach here via the CPWF is different since it initiates not from the homogeneous but the trapped two-body system, and constructs an explicitly correlated many-body wavefunction in the form of Jastrow-Ansatz (see also Chapter 1). The power of this Ansatz is based on the fact that it captures correctly the behaviour at the contact points, while it also reproduces the exactly known limits at zero and infinite interactions (TG limit).

In the existing relevant literature the TG limit in the trap is investigated with respect to the stationary but also dynamical properties [68, 72, 73]. The crossover to this limit from 3D to 1D [27, 74, 75] as well as the different regimes of correlations, coherence and quantum degeneracy properties [76, 77, 22, 78] were investigated. On the side of numerical investigations, Quantum Monte Carlo[1]studies covered not only the 1D case but also the transition from high to low dimensional systems [27] while the evolution of the energies, the densities and other observables as a function of the interaction strength was studied in [26, 29, 28, 79]

[1]Quantum Monte Carlo method based in random walks is probably the most prominent approach for ground

Our approach here takes a detour from approximate and numerical methods. We will develop an analytical many-body wavefunction to accurately describe the crossover of a 1D bosonic system from weak to strong interactions in a harmonic trap. The explicit wavefunction, which is based on the exact two-body states [14] (see Chapter 1), consists of symmetric multiple products of the corresponding parabolic cylinder functions (see also Appendix B), and respects the analytically known limits of zero and infinite repulsion for arbitrary number of atoms (see Chapter 1). For intermediate interaction strengths we demonstrate, that the energies, as well as the reduced densities of first and second order, calculated from the CPWF are in excellent agreement with large scale numerical calculations. The construction principles, accuracy test and descriptive power of this Ansatz will be presented next.

### 2.1.1 System-Hamiltonian

The 1D N-body Hamiltonian in the harmonic trap reads:

$$H = -\frac{1}{2}\sum_{i=1}^{N}\frac{\partial^2}{\partial x_i^2} + \sum_{i=1}^{N}\frac{x_i^2}{2} + g\sum_{i<j}\delta(x_i - x_j) \tag{2.1}$$

where the contact interaction of atoms located at $x_i$, $i = 1, ..., N$, is represented by the Dirac $\delta$-function, and lengths and energies are scaled by $a_\parallel$ and $\hbar\omega_\parallel$ respectively (see also Chapter 1). We study this system with respect to the single remaining parameter $g$ which can change from zero to infinity (attractive i.e. negative values are not considered here).

Not only the two-body case (see Chapter 1) but also the N-body Hamiltonian has an important property that we employ here: the separability into center-of-mass and relative motion $H = H_{CM} + H_r$, where $H_{CM} \equiv \frac{P^2}{2N} + \frac{NR^2}{2}$ describes a harmonic oscillator in the center-of-mass coordinates $R = \frac{1}{N}\sum_{i=1}^{N} x_i$ and $P = -i\sum_{i=1}^{N}\frac{\partial}{\partial x_i}$. In the following, we exclusively address the relative motion problem which is non-trivially coupled in the general case. For example the corresponding Hamiltonian $H_r$ written in lab coordinates:

$$H_r = -\frac{1}{2N}\sum_{i<j}^{P}\left(\frac{\partial}{\partial x_i} - \frac{\partial}{\partial x_j}\right)^2 + \frac{1}{2N}\sum_{i<j}^{P} r_{ij}^2 + \sum_{i<j}^{P} g\delta(r_{ij}), \tag{2.2}$$

mixes different degrees of freedom in a non-trivial non-separable way.

### 2.1.2 Ansatz

The correlated-pair wavefunction (CPWF) developed here is inspired by the idea that the pairwise contact interaction may be adequately addressed in the many-body system, if the discontinuity of the derivative that it causes is imposed on each pair of atoms in the ensemble, in a similar way as for a single pair. Essentially the so-called Bethe condition which has been extensively discussed in the previous Chapter 1 can be also applied here for the specific form of Jastrow-like Ansatz we propose. The CPWF for the relative motion is formed as a pairwise product expansion of functions based on the two-body solutions, thereby respecting the two exactly solvable limits of zero and infinite interaction strength for an arbitrary number of atoms.

state properties and is explained in Appendix A. Other approaches are exact diagonalisation, density matrix renormalization group, and MCTDH which is the basic tool for this thesis.

**Postulates for the CPWF**

Specifically, our construction principle is composed of the following three postulates:

(i) The CPWF for the relative motion of $N$ atoms is a product of parabolic cylinder functions (PCF) $D_\mu$ [80] of the distance $r_{ij} = |x_i - x_j|$ of each pair:

$$\Psi_{\rm cp} = C \prod_{i<j}^{P} D_\mu(\beta r_{ij}), \tag{2.3}$$

where $P = \frac{N(N-1)}{2}$ is the number of distinct pairs and the parameters $\beta$ and $\mu$, to be determined next, are the same for every pair since we deal with identical particles, while the absolute value enforces bosonic permutation symmetry as we have seen also in the case of the LL model- especially the two-body and TG limits (see Eqs. 1.9, 1.26). The normalization constant $C$ will, without loss of generality, be omitted in the following.

(ii) The boundary (or Bethe) contact condition $2\beta D'_{ij}(0) = gD_{ij}(0)$ (see also Chapter 1), where $D'_{ij} = \frac{\partial D_{ij}}{\partial(\beta r_{ij})}$ and $D_{ij} = D_\mu(\beta r_{ij})$, is imposed for each pair in the ensemble at $r_{ij} = 0$, and determines $\mu$ for a certain value of the interaction strength $g$. With the known expressions for the PCF $D_\mu(x=0) = \frac{2^{\frac{\mu}{2}}\sqrt{\pi}}{\Gamma\left(\frac{1-\mu}{2}\right)}$ and $\frac{\partial D_\mu}{\partial x}(x=0) = -\frac{2^{\frac{\mu+1}{2}}\sqrt{\pi}}{\Gamma\left(-\frac{\mu}{2}\right)}$ [80] (see Mathematical Appendix B), the resulting transcendental equation

$$\frac{g}{\beta} = -\frac{2^{\frac{3}{2}}\Gamma\left(\frac{1-\mu}{2}\right)}{\Gamma\left(\frac{-\mu}{2}\right)} \tag{2.4}$$

is solved for $\mu$, selecting the solution in the interval $\mu \in [0,1]$ which corresponds to the ground state. The origin of this boundary condition will be discussed below. One may already note that this is pretty much the same relation (except from the parameter $\beta$ which appears here) as the one derived for the two-body case in Ref. [14] stated also in Eq. 1.42 of Chapter 1. This reflects already the two body nature of the Ansatz which builds upon the two-body function and the Bethe two-body boundary condition.

(iii) For

$$\beta = \sqrt{\frac{2}{N}}, \tag{2.5}$$

$\Psi_{\rm cp}$ reproduces the exact analytically known solutions in the limits $g = 0$ and $g \to \infty$, for any $N$. In these limits, $\mu$ equals 0 and 1 respectively and in both cases (as well as for every integer $\mu$) $D_\mu(x) = e^{-\frac{x^2}{4}}\mathrm{He}_\mu(x)$ where $\mathrm{He}_\mu(x)$ are the modified Hermite polynomials (see Mathematical Appendix B). Therefore the total wavefunction $\Psi = \Psi_R\Psi_r$ with $\Psi_R = C_R e^{-\frac{NR^2}{2}}$ and $\Psi_r = \Psi_{\rm cp}$ reproduces

$$\Psi_{g=0} = C_0 \exp\left(-\sum_{i=1}^{N}\frac{x_i^2}{2}\right) \tag{2.6}$$

for the non interacting and

$$\Psi_{g\to\infty} = C_\infty \exp\left(-\sum_{i=1}^{N}\frac{x_i^2}{2}\right)\prod_{i<j}^{P}|x_i - x_j| \tag{2.7}$$

for the infinitely strong interaction limit, which we also stated in Chapter 1 Eq. 1.16, discussing the TG case in the trap [68]. The latter coincides with the (fermionic) determinant, written in form of pairs, and with implemented bosonic symmetry. For this particular choice of $\beta$ the CPWF is also exact for arbitrary $g$ in the case of $N = 2$, but $\beta$ can be generally treated as a variational parameter for given values of $g$ and $N$.

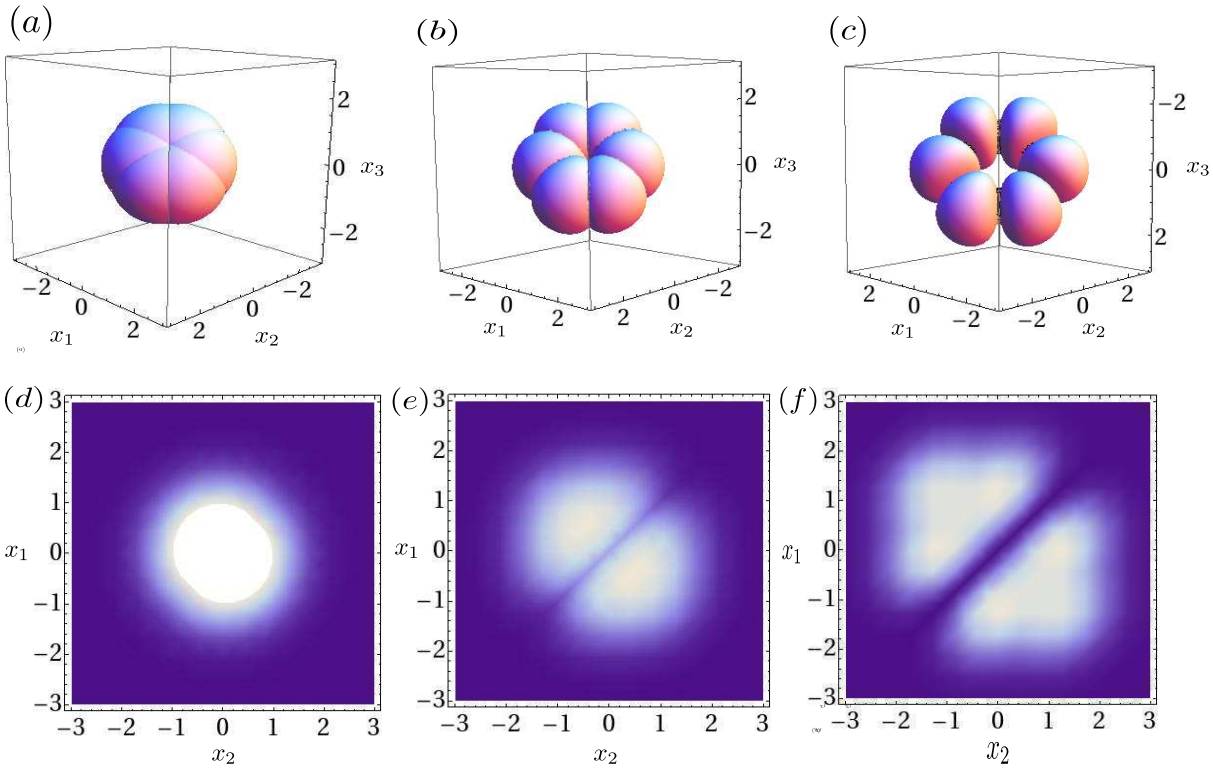


Figure 2.1: Contour plots of the density distribution $|\Psi(x_1, x_2, x_3)|^2 = 0.01$ for $N = 3$ using $\Psi_r = \Psi_{cp}$ with (a) $\mu = 0.2$, (b) $\mu = 0.5$ (c) $\mu = 0.8$. (d) The two-body correlation function (density) for (d) $g = 0.2$, (e) $g = 2.0$, (f) $g = 20.0$.

**Discussion**

Postulate (i) addressing the construction of a many-body wavefunction via a product of functions of the relative distance appears also in other treatments in similar form like Jastrow-Ansatzes [67]. Nevertheless, the particular choice of the PCF as a building block proves to be, as we will show, a very efficient approach for the present problem, owing its inspiration to the two-body exact solution by Busch et al. [14]. Key features of our approach are postulates (ii) and (iii) determining the properties of the PCF, thereby ensuring that $\Psi_{\rm cp}$ reproduces the two analytical limits of zero and infinite coupling for any $N$. It also constitutes the exact solution at arbitrary interaction strength for $N = 2$ (with $\beta = 1$) [14] which possesses a high degree of generality: it holds for bosons or fermions in one-, two- and three-dimensional harmonic traps and arbitrarily strong attractive or repulsive contact interactions, including ground and excited states of the relative motion (see also Chapter 1). This readily implies that if our CPWF with the former two-body solution as a building block is sufficiently accurate for the 1D repulsive bosonic case, a similar Ansatz could be envisaged for other setups.

To illuminate the imposed boundary condition in postulate (ii), as well as why the CPWF is exact for two atoms, we investigate the action of the relative motion Hamiltonian operator (Eq. 2.2) on the CPWF $\Psi_{\rm cp}$. Introducing the notation $\phi^{kl,mn,\ldots} = \prod_{i<j(ij\neq kl,mn,\ldots)} D_\mu(\beta r_{ij})$ and $\chi_{lm} = 1 - 2\delta_{lm}$, we obtain:

$$H_r\Psi_{\rm cp} = \sum_{i<j}^{P}\delta(r_{ij})\left(-2\beta D'_{ij}+gD_{ij}\right)\phi^{ij} \quad (2.8)$$

$$- \beta^2\sum_{i<j}^{P}\left(D''_{ij}-\frac{(\beta r_{ij})^2}{4}D_{ij}\right)\phi^{ij}$$

$$+\frac{2-N\beta^4}{4N}\sum_{i<j}^{P} r_{ij}^2 D_{ij}\ \phi^{ij}+\beta^2\sum_{k,l,m,n} D'_{kl}D'_{mn}\chi_{lm}\phi^{kl,mn},$$

where $\sum_{k,l,m,n}$ sums over non-repeated terms with $k\neq l\neq m\neq n$ using also relations explained in the mathematical Appendix B. The first sum in Eq. (2.8), containing the $\delta$-interaction for each pair, vanishes at $r_{ij}=0$ by imposing the boundary conditions $2\beta D'_{ij}(0)=gD_{ij}(0)$. This provides the behaviour at the two-body contact point arising from the discontinuity of $D'_{ij}$ for each pair, which we have also seen in the LL-model and two-body case in the harmonic trap (see Chapter 1, especially the derivation of the Bethe condition for the two-body LL model Eq. 1.20). Thus, the pair contact manifolds $\mathcal{M}_{ij}=\{(x_1,...x_i,...,x_j,...,x_N)\in\mathbb{R}^N|x_i=x_j\}$ (two-atom collisions) of dimensionality $N-1$ are taken into account, while higher order contact (three-atom collisions etc.) represent lower dimensional manifolds. The second sum in Eq. (2.8) is given by the Weber equation [80]: $D''(x)-\frac{x^2}{4}D(x)=-(\mu+\frac{1}{2})D(x)$ (see Mathematical Appendix B) which also appears in the two-body case (see Chapter 1 Eq. 1.40). As we have seen there the PCFs are the general solutions of this equations, which is an essential feature of the CPWF Ansatz and the contribution to the energy is $P(\mu+\frac{1}{2})$. For $N=2$ ($\beta=1$, $P=1$) the last two terms in Eq. (2.8) vanish and therefore $\Psi_{\rm cp}$ with the corresponding boundary condition is the exact solution with energy of relative motion $\epsilon_r=\mu+\frac{1}{2}$ (see also Chapter 1). For $N>2$ the last two sums in Eq. (2.8) do not vanish and provide additional contributions to the energy. Essentially the last terms constitute also the actual problem, of the non-separable highly-coupled Hamiltonian of the relative motion. Still the CPWF Ansatz succeeds in simplifying the rest of the terms in the way we have shown.

Before comparing our analytical approach with corresponding numerical results, we illustrate in Fig. 2.1 the spatial distribution of three atoms according to the CPWF. Similar to the two-body case (see Chapter 1 and Fig 1.3.1 where a cusp appears with increasing interaction at the collision point $r=0$, for three atoms the contour plots demonstrate, for increasing interaction strength, depletion of the probability density along the collision manifolds $\mathcal{M}_{ij}$. The conceptually important physical insight offered by our CPWF approach is that it captures the correlation properties in the vicinity of collision surfaces, i.e., the tendency of the atoms to repel and thus avoid each other. The latter is also demonstrated by the correlation hole which appears with increasing interaction on the diagonal ($x_1=x_2$) of the two-body density [see Fig. 2.1]. Furthermore the two body density is a broadened compared to the Gaussian shape at zero interaction. These important effects induced by the interaction are captured from our analytical approach, and are in accordance with numerical results in previous works [29].

### 2.1.3 Accuracy of the Ansatz

The Ansatz we proposed above is not the exact solution of the problem, but is a free of variational parameters approach to the ground state which is designed from first principles, i.e. the postulates we presented above. Surprisingly though such a theoretical idea is characterized apart from qualitative features that we have already seen (such as the depletion on the collision manifolds, and the two-body nature of the approach) by a very good quantitative agreement

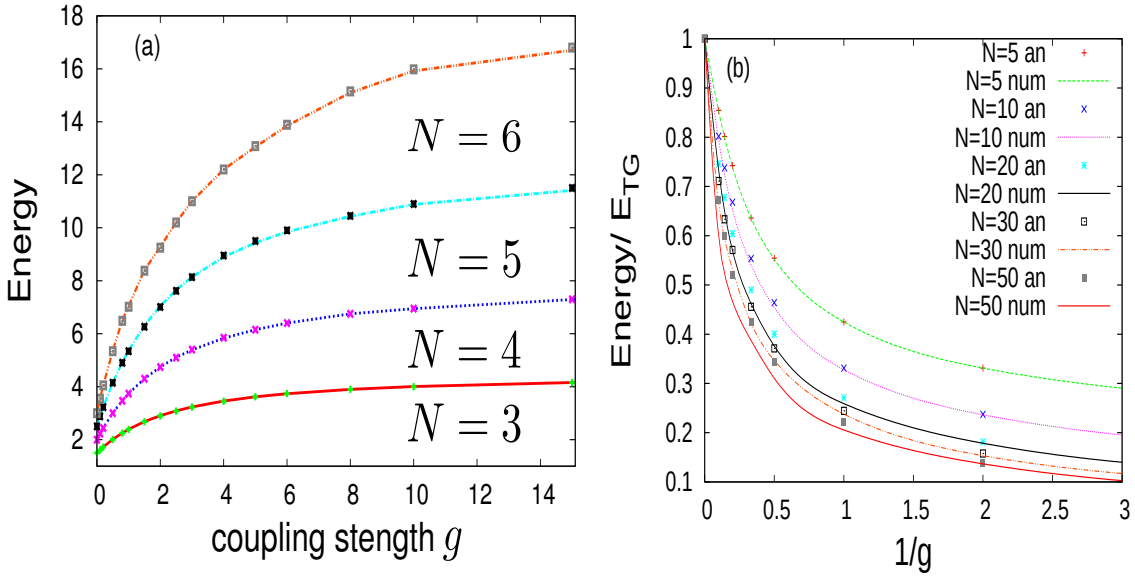


Figure 2.2: (a) Ground state energies as a function of the interaction strength for few bosons in the trap comparing results obtained by MCTDH and by the CPWF Ansatz. (b) Energies divided by the corresponding value of the TG limit as a function of the inverse interaction strength comparing DMC with CPWF calculations for many-body ensembles.

with calculations from numerically exact methods at least for a few atoms, as we will show next. We consider two very important observables the (ground state) energy and the (one body) density. We have already seen that an integration should be performed concerning the last terms of Eq. 2.8 to obtain the energy of the Ansatz. This has been done here for few atoms with integration routines in Mathematica. The one-body density together with the energy probably the most direct observable to probe experimentally eg. via absorption imaging which essentially scatters light on the atoms and the shadow produced due to the diffraction of the light from the atomic cloud is the fingerprint of the cloud density [1, 2].

There are several numerical approaches to the 1D problem which are limited in terms of the particle number they can handle for a given accuracy: Exact diagonalisation [26], Quantum Monte Carlo [27], and MCTDH [29] have been employed. We have compared the properties of the CPWF with numerical results from the MCTDH method for few atoms (up to 6) and with Quantum Monte Carlo for larger number of atoms. Both methods are explained in the methodological Appendix A[2].

### The few body case- MCTDH comparison

Let us start with the few body-case and the ground state energy. In Fig. 2.2 (a) we observe an excellent agreement between the energy calculated using $\Psi_{cp}$ and the numerical results as a function of $g$ for up to six atoms. The relative error is typically up to the order of $10^{-2}$ for the most difficult regime of intermediate values of $g$ (the curves also agree with Refs [26] and [29]). For very weak and very strong interactions (the latter being a challenging regime for numerical methods [29]) the CPWF gives highly reliable results being close to the exact

[2]For the MCTDH approach we assured high numerical accuracy with a dense grid, small width of the Gaussian extrapolation of the $\delta$-function and large basis sets. We have even employed an exact diagonalisation method to crosscheck the results of MCTDH, with the two numerically exact methods agreeing very well of the order of $10^{-3}$ relative accuracy in most cases (see also [26, 29]) and practically coincide to what concerns us here.

solution with $\beta = \sqrt{\frac{2}{N}}$, while for intermediate values of $g$ (corresponding to $\mu \approx 0.5$) stronger deviations are expected, especially as $N$ increases. Although we aim to a fully free-of-parameter explicit wavefunction approach, we note here that this deviations can nonetheless be cured very efficiently when the parameter $\beta$ is treated variationally leading to an agreement of $10^{-3}$ (has been checked with Mathematica calculations).

Concerning the actual behaviour of the energy curves there is a very similar smooth crossover for any number of bosons, which also resembles the functional form of the two-body case (see Chapter 1), a fact that was an important inspiration and motivation for the construction of the CPWF. According to standard 1D theory [13, 76, 22] the TG limit is approached either for large interactions $g \to \infty$ as confirmed here, but also for small number of atoms $N$. Therefore few-body 1D systems enter more easily the TG regime, which is an important motivation for studying them separately from many-body systems. In terms of the effective Lieb-Liniger parameter $\gamma \propto \frac{g}{N}$ (see also Chapter 1) the TG limit is approached for $\gamma \gg 1$ which corresponds to the two aforementioned cases [12, 22]. In accordance to this behaviour, the energy we calculate for a given $g$, lies closer to the Girardeau prediction $E_N^{TG} = \frac{N^2}{2}$ for smaller $N$. For instance at $g = 2.0$, $\frac{E_N}{E_N^{TG}} \approx 0.74, 0.64, 0.59, 0.56, 0.51$ for $N = 2, ..., 6$.

**The many body case- QMC comparison**

As we have demonstrated, few-body systems are preferable to study the transition to the TG state, and have also more pronounced effects in the densities as we will see in the next section. Yet concerning the accuracy of the two-body based CPWF Ansatz it is important to be checked for larger number of atoms. The MCTDH method (or the exact diagonalisation) we have used up to this point is not adequate for this purpose since many degrees of freedom strongly correlated exceed the efficiency of truncated-basis based methods (see also Appendix A on Computational methods). We resort therefore (among other options like Density-matrix renormalization group method [28], or extensions of MCTDH for bosons-MCTDHB [147] to the Quantum Monte Carlo (QMC) method described shortly in the Appendix A. Monte-Carlo simulations in configuration space have been using trial functions of Jastrow-type as an initial guess and as guiding functions for the diffusion [27]. In the Appendix A, the great importance of a good choice of an initial guess for the Variational Monte Carlo (VMC) but also of as a guiding (appearing in the quantum force as a function that 'guides' the walkers to positions where it is for physical reasons more possible for the atoms to be placed) for the Diffusion Monte Carlo (DMC) algorithms has been underlined. The typical trial-guiding function that are commonly used [27] are of the form of Bijl-Jastrow functions, with a single-particle part (SPP) which accounts for the form of the external potential and an interaction part (IP) which accounts for the collision. For a 1D harmonic trap the standard form reads:

$$\Psi_T = \underbrace{\prod_i e^{-\beta x_i^2/2}}_{\psi_{SPP}} \underbrace{\prod_{i<j} \cos\left[k\left(|x_{ij}| - \frac{L}{2}\right)\right]}_{\psi_{IP}} \tag{2.9}$$

The form of the SPP corresponds obviously to the ground state of a single-particle in a harmonic trap (setting also the presumably variational parameter $\beta = 1$). For the IP the standard Bijl-Jastrow type of functions are used, and an interesting remark is that the form $\cos\left[k\left(|x_{ij}| - \frac{L}{2}\right)\right]$ is actually the solution of the two-atom LL gas [12] (Eq. 1.26) of length $L$ with $k$ determined from the Bethe condition at the contact point $x_{ij} = 0$ [discontinuity of the derivative Eq. 1.19,Eq 1.27] (see also Chapter 1)[3]. For long range interparticle distances $|x_{ij}| > L$ one takes a constant

[3]This form of Jastrow Ansatz (Eq. 1.44) we compared also for the homogeneous case in the last section of Chapter 1, with the corresponding exact solution, i.e. the Bethe Ansatz.

value for the IP. Notice that this approach contains one variational parameter $L$ (if we consider $\beta$ fixed) which should be optimized since here there are no periodic boundary conditions as in the LL case.

The CPWF can be also used for Monte-Carlo simulations since it has the form of a Bijl-Jastrow function, but with a different approach for the two-body part than the standard trigonometric functions used in Eq. 2.9. Seen from this perspective the CPWF can be rewritten replacing the IP with the hypergeometric functions $U\left(-\frac{\mu}{2},\frac{1}{2},\frac{x_{ij}^2}{2}\right)$ (see Appendix B Eq. B.12), which apart from an exponential term (which combines with the center of mass motion), coincide with the Parabolic Cylinder functions which are the analytical solution of the relative motion of two atoms in a trap (see Chapter 1). Our proposal then for the trial function in the harmonic trap reads:

$$\Psi_T = \prod_i e^{-\beta x_i^2/2} \prod_{i<j} U\left(-\frac{\nu}{2},\frac{1}{2},\frac{r_{ij}^2}{2}\right) \tag{2.10}$$

and has no variational parameter in the IP since $\nu$ is given from the Bethe condition Eq. 1.42, while the one in the SPP can be fixed to $\beta = 1$ according to the ground state of the Hamiltonian of the harmonic oscillator (Eq. 2.1 with $g = 0$. The latter makes sure that the function simultaneously correct for the Tonks gas limit $g \to \infty$ with $\nu = 1$ [$U\left(-\frac{1}{2},\frac{1}{2},\frac{r_{ij}^2}{2}\right) = r_{ij} = |x_i - x_j|$ see Appendix B] (see also Chapter 1).

A remark on the two approaches is in order here: the functional form of the standard approach Eq. 2.9 can come very close to the one proposed here Eq. 2.3, since it contains a variational parameter $L$ which when optimized one obtains a functional form for the IP close to the hypergeometric functions. The advantage of the proposed approach is that it can be used without any free parameter. Still one can insert one variational parameter in the last argument of the hypergeometric function and use it variationally too, while the exponential in the SPP contains also a possible variational parameter $\beta$[4]. Nevertheless, our aim is rather to propose a trial function that can describe correctly the behaviour without free parameters. Since both approaches are employing in some sense the two-atom solution in the continuum (Eq. 2.9) and in the trap (Eq. 2.10), they offer a physical picture which generalizes the two-body problem to the many-body one.

Let us now discuss the results for the energy of the ground state as a function of the interaction strength $g$ for larger atom numbers (compared to those calculated with MCTDH), which are obtained using in VMC and DMC as initial guess and guiding function our Ansatz (Eq. 2.10). The CPWF is used without any free parameter and VMC is just used to estimate the energy of this Ansatz. Even inserting one variational parameter does not change the results a lot, therefore we concentrate on the parameter-free version of our Ansatz. The DMC is performed to calculate the numerically exact value of the energy (after equilibration) since it overcomes by the random process of walkers' redistribution the obstacle of a certain functional form which appears in the VMC (see Appendix A on Computational Methods). The particle numbers vary from 5-50 atoms which are typical population of each 1D tube in the corresponding experiments [20]. In Fig. 2.2 (b) the ground state energy of the interacting many-body system divided by the energy corresponding to the Tonks-Girardeau limit (which is equal to that of the corresponding system of identical fermions $E(g \to \infty) = N^2/2$ -see also Chapter 1) as a

[4]Note here that the writing of the CPWF in the initial form Eq. 2.3, connects the exponential of the relative motion and the hypergeometric function with one and the same parameter $\beta$. In the form of Eq. 2.10 the function containing two body terms is disconnected from the exponential behaviour and therefore one may use two independent free parameters. Equivalently in the original form one may insert additionally a variational parameter in the exponential of the center of mass motion.

function of the inverse of the interaction strength $1/g$ (which is proportional to the effective 1D scattering length $a_{1D} \propto -1/g$ [13]- see also Chapter 1). The uppermost curve (corresponding to the DMC calculation of the energy) and points (corresponding to the energy calculated from the CPWF with VMC Eq. 2.10 ) for $N = 5$ atoms confirm the results obtained before with MCTDH and Mathematica showing that our Ansatz works very accurately for few atoms. Still up to 10 atoms the qualitative and also quantitative agreement is very good (up to 2% error), especially for very weak $g \to 0$ and very strong interactions close to the resonance (TG limit) $g \to \infty$. In the intermediate interaction regime there are larger and larger deviations of the energy computed by the Ansatz as we see for 20, 30 and 50 atoms. Still the agreement remains good for strong and weak interaction strengths, and the qualitative behaviour throughout the crossover from non-interacting to fermionization is captured from the Ansatz.

We have seen therefore that the few-body cases (up to 10 atoms) are covered very well from this two-body based Ansatz, the CPWF, while the agreement for larger number of particles is mainly qualitative allover and very good close to the exactly known limits. Therefore this study rises the question of the kind of transition 'from two to few' and 'from few to many' in a very particular way[5]. An extension of this study may consider different forms of the two-body function and compare them, insert variational parameters, or parameters which can be determined imposing certain conditions or postulates, or understanding more deeply the nature of the short-range and long range behaviour (exponential and Bethe condition), or even extend this study to other problems with eg. different kind of interaction, mixtures, fermions, other types of potential. The two latter cases have been tried and are reported in the next two Chapters 3.1, 4.1. The above postulated CPWF is thus thought as a first approach on this direction providing already very interesting insight in this simple system of trapped interacting bosons.

### 2.1.4 Densities and remarks

#### One-body densities

Except from the energy the CPWF can be also compared with numerical results for other observables like densities. We have seen already the two-body density profiles in Fig. 2.1 which are very similar to that of numerical studies eg. [29], but such plots are difficult to compare. Therefore we show in Figs. 2.3 (b–d) curves depicting the profile of the one-body density $\rho(x)$ for various interaction strengths. In most of the cases the CPWF as stated in Eq. 2.3 is shown to capture very well not only qualitatively, but also quantitatively, the properties of the crossover from weak to strong correlations. As a result of increasing repulsion between the bosons, $\rho(x)$ flattens and forms an $N$-peak structure (including $x < 0$) close to fermionization, effects already shown in numerical studies [26, 27, 29] captured here from out analytical Ansatz. For intermediate $g = 2.0$, the deviation between the CPWF and numerical results is somewhat larger if $\beta$ is fixed to $\sqrt{\frac{2}{N}}$, but can be reduced substantially by treating $\beta$ variationally. For this case, we have also plotted the Thomas Fermi (TF) curve (in our scaling)

$$\rho(x)^{TF} = \frac{1}{N}\left(\frac{18N^2}{64g}\right)^{1/3}\left(1 - \frac{x^2}{R_{TF}^2}\right) \tag{2.11}$$

with $R_{TF} = \left(\frac{3}{2}Ng\right)^{1/3}$ [22]. The TF regime which results from the GPE equation if one neglects the kinetic energy therefore results to a simple inverted parabola profile of the density Eq. 2.11. The TF approximation is predicted to be valid for $\gamma \ll 1$, corresponding to a low interaction of

[5] One may connect this to the classical philosophical enigma known as sorites paradox: how many sand corns do we need to form a heap?

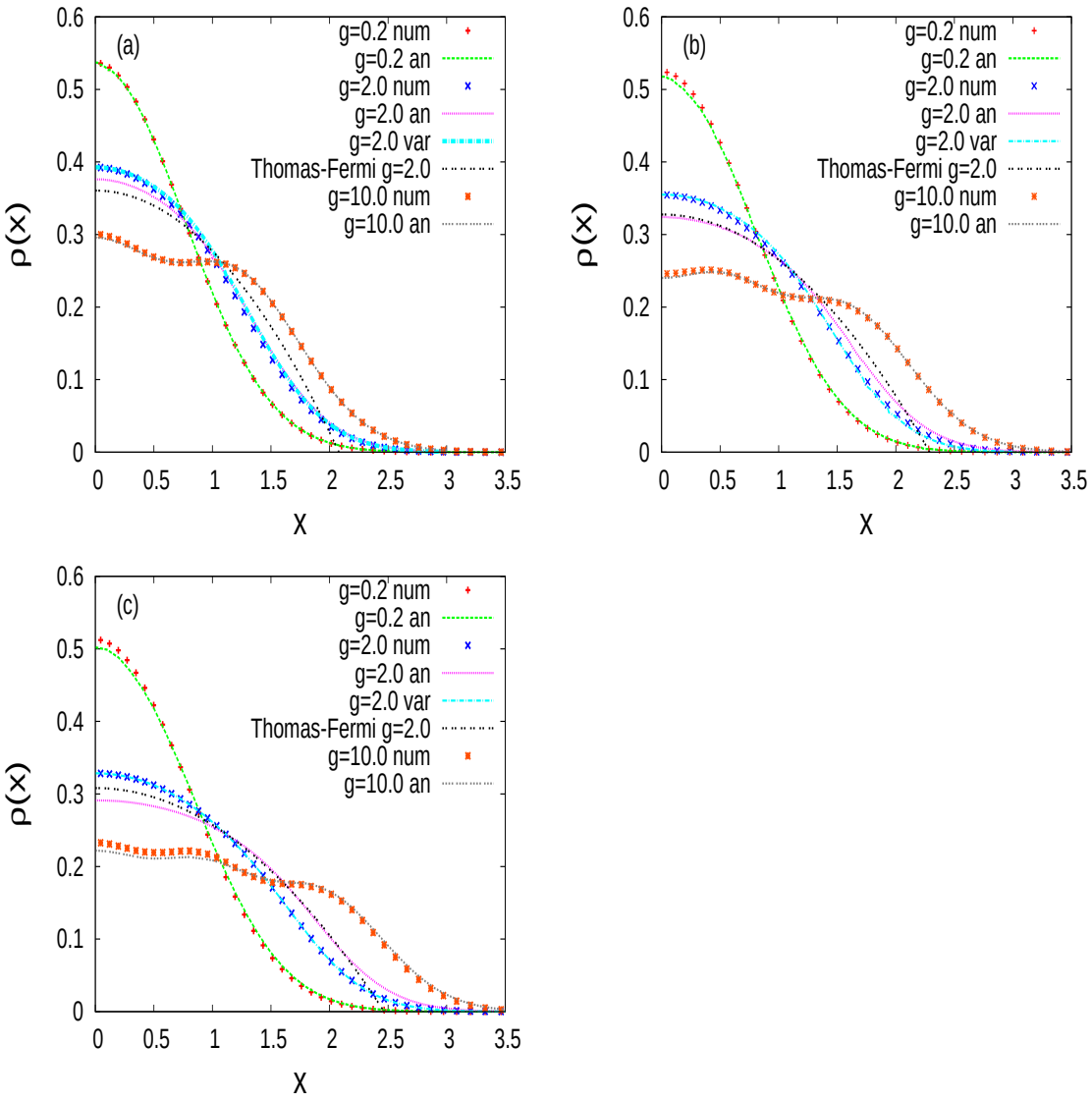


Figure 2.3: One-body density profiles $\rho(x)$ for (b) $N = 3$ (c) $N = 4$ and (d) $N = 5$ atoms obtained by MCTDH and CPWF for different coupling strengths $g$. For intermediate interactions $g = 2.0$ the Thomas-Fermi profile

the order of $g \approx 1$ for the presently used small $N$ (for very weaker or stronger interaction cases the TF profile deviates more from the exact [22]). We may note here that in the usual mean field treatment of BECs (in 3D) the TF approximation is considered as very strongly interacting. In 1D physics we have seen though that the TG regime is the true infinite repulsion limit. Nevertheless from the perspective of 'interaction energy', i.e. part of the energy of the system that is attributed to interaction, the TG regime can be considered as 'non-interacting' since in principle only kinetic energy of 'identical fermions' contributes according to the Bose-Fermi map. On the other hand the TF regime remains the 'strongly interacting' case in the sense that the interaction effects are very important. This may give also an insight to the maximum deviation of the CPWF from numerical results exactly for this intermediate interactions. We see that for fixed $g = 2.0$, the TF profile becomes more accurate for larger $N$ except from the edge tail which is due to quantum pressure missing in the TF approximation[6]. . The predictions concerning the Tonks gas (density profile and corresponding radius) in [22, 78, 68] are of course precisely reproduced here since for any $N$, CPWF is the exact solution in this case.

One may extend this study to other observables especially non-local ones, like the one-body density matrix, the momentum distribution, the dynamical structure factor, and higher order correlation functions. The choice here was to show simple observables like the energy and the density which demonstrate many important effects of 1D physics in the trap, and are intuitive to understand and relatively easy to measure.

**First conclusive remarks**

The many-body wavefunction presented in this section for the problem of zero-range repulsively interacting bosons with arbitrary coupling strength in a 1D harmonic trap, has been inspired by the exact analytical solution of the two-body case. We have shown that taking a product expansion of pair wavefunctions similar to the two-body solution, leads to an impressive agreement with extensive numerical calculations for any value of the coupling strength, while it reproduces the analytically solvable cases of zero and infinite interaction. Therefore the construction principle of our approach may be applicable to other setups, e.g. in higher dimensions or excited states, where the building block –the two-particle function– can be represented by an analytical expression similar to the exact solution of the relative motion for the two-body problem, and some limiting cases of the relevant parameters (here e.g. zero and infinite interaction strength) are either exactly or approximately known. Improvements of our approach may be possible (e.g. by taking into account variationally optimized parameters or lower dimensional spaces where three or more atoms meet), and it is an excellent starting point for variational calculations (performed also here), for Quantum Monte-Carlo methods as an appropriate guiding function of Jastrow type, or for exploring the limits of mean-field treatments. Along with an accurate description of a highly correlated many-body problem, we believe that this approach offers valuable physical insight into the correlation properties at collision manifolds, which is conceptually useful in the theoretical treatment of many-body problems.

## 2.2 Driven interactions

We have seen in the previous section how the correlation properties of the ground state change when the interaction strength increases. In this section we investigate the dynamical behaviour for an oscillating interaction strength, beyond stationary properties but using them as an analysis tool [30]. The driving of the interatomic coupling induces excitations of the relative mo-

[6] Also the prediction for $R_{TF} \propto N^{\frac{1}{3}}$ is confirmed by our results since the TF effective radius is reproduced if we consider $\rho(R_{TF}) \approx 5\%\rho(0)$ as negligible density

tion exclusively with specific and controllable contributions of momentarily excited many-body states. Mechanisms for selective excitation to few-body analogues of collective modes and acceleration occur in the vicinity of resonances. We study via the few-body spectrum and a Floquet analysis the excitation mechanisms, and the corresponding impact of the driving frequency and strength as well as the initial correlation of the bosonic state. The whole analysis is based on the fundamental case of two atoms which is analyzed in detail and forms a key ingredient for the bottom-up understanding of cases with higher atom numbers, thereby examining finite-size corrections to macroscopic collective modes of oscillation. In this way the 'from two to many' perspective which forms the bottom line of this thesis, is extended to the driven dynamical behaviour.

Before proceeding on the presentation of the results, a short report on progress of time-dependent driven systems in the context of cold atoms is essential. Time-dependent driving is usually applied to external traps, providing inspiring effects such as the dynamical control of tunneling [35, 36], dynamical localization [37], photon-assisted tunneling [38] via a periodic driving of the lattices or the excitation of collective oscillations in a harmonic trap [24] . However, investigations considering a time-dependent scattering length, usually referred to as 'Feshbach resonance management' [34] for the mean-field situation, have inspired a lot of research on control of solitons [81] or modulational instabilities [82]. Experimental investigations in this direction have been performed recently [32, 33]. Collective excitations via harmonic time-modulation of the scattering length have been proposed and analyzed in Refs. [83, 84] and experimentally achieved in Ref. [33]. The main advantage of the driving of the scattering length compared to other driving modes applied on the external potential for examining collective excitations [15, 24], is that other species or non-condensed fractions are hardly affected (only indirectly due to mean-field coupling or particle exchange terms) by the driving of the interaction of one-species [33]. Apart from the harmonic trap, a two mode system with time-varying interaction has been studied with Floquet theory, leading to many-body coherent destruction of tunneling and localization [85].

On the other hand, beyond the mean-field regime, there are relatively few works dealing with the time-dependent modulation of the scattering length, addressing mainly the experimental results on the formation of molecules [32] from a few-body perspective [86, 87]. While these works concentrate mainly on the attractive part of the two-body spectrum and on the corresponding bound state, our work focuses exclusively on repulsive interactions. As illustrated in Ref. [86] in a harmonic trap the coupling of an excited two-body state to the molecular ground state is very efficient since nearby states are out of resonance, and possess a relatively small coupling to the initial state. For the repulsive case as we will demonstrate, the relevant few-body states reflect the equidistant spectrum of the harmonic trap and therefore lead to a more complex dynamics involving several instantaneous configurations. A recent publication [88] explored the integrability of the system, via a similar model with time-modulated interaction thereby calculating the dynamical structure factor.

Very interesting theoretical studies have been done with the so-called scaling approach [89, 90], where time-dependent parameters controlling eg. the width of the many body function are inserted and the Schrödinger equation is then mapped to differential equations for these parameters, eg. the so-called Ermakov equation which relates to the rescaling of the width according to the driving of the trapping frequency. One reason that we chose to study time-dependent interaction in the harmonic trap, is that the scaling approach has been proven very powerful for the understanding of other kinds of driving like the breathing of the trap frequency. In the course of the research the author has investigated numerically such a driven system with the main findings concerning the change of the width of the wavefunction being in complete accordance with the predictions of the scaling approach. Therefore we concentrate next on the

time-dependent driving of the interaction strength and our bottom-up approach of many-body dynamics.

This part is organized as follows: Firstly we introduce our model of driven interaction strength, and subsequently focus is on the case of two atoms thereby examining the mechanisms of controlable collective excitations to specific states and the influence of parameter changes on them. We investigate next the acceleration mechanism via multiple excitations and calculate the Floquet spectrum of this case illustrating the underlying mechanism for the appearance of the resonances. An extension of this study to higher atom numbers is performed in the last part concentrating on the analogue of the breathing mode for collective oscillations and finite size corrections.

### 2.2.1 Modeling the time-dependent interaction

There are two parameters in Eq. 1.37 that can be tuned to attain a time-dependent interaction strength:

1. the scattering length $a_0$ via a change of the strength of e.g. a magnetic field $B$ approaching to or departing from a Feshbach resonance –Feshbach resonance management [34]– as $a_0 = a_{bg}(1 - \frac{\Delta B}{B-B_0})$ where $\Delta B$ and $B_0$ are the width and the position of the resonance, respectively, and $a_{bg}$ is the background scattering and

2. the transversal length $a_\perp$ by modifying the relevant laser parameters, taking into account the quasi-1D restrictions posed above (see Chapter 1 and [33]).

The 1Dl $N$-body Hamiltonian studied here is exactly the same as in the previous section Eq. 4.1 but with a time-dependent coupling $g(t)$. Initially, the atoms are prepared in the ground state of the harmonic trap with an interaction strength $g_0$. We will then explore the excitation dynamics for a periodic driving of the repulsive interaction strength of the form:

$$g(t) = g_0 + \Delta g \sin^2(\omega t) \tag{2.12}$$

where $\Delta g$ is the amplitude of the driving and $\omega$ the driving frequency. The impact of each of these three parameters of the driving law $(g_0, \Delta g, \omega)$ will be examined. The reason for the specific choice $\sin^2(\omega t)$ for the driving is our focus on repulsive interactions (as in the previous section), i.e., $g$ should stay positive for $g_0 \leq 0$. Since $\sin^2(\omega) = \frac{1-\cos(2\omega)}{2}$, the above driving law comprises a periodic oscillation with frequency $2\omega$. Investigating purely attractive interactions as done in Ref. [86] or alternating between attractive and repulsive interactions such as in Refs. [87, 32, 34] represent interesting but different situations.

### 2.2.2 Two-body problem and instantaneous eigenspectrum

In Chapter 1 we have seen that in the special case of two atoms the relative motion ($r = x_1 - x_2$) reduces to an effective one-body problem Eq. 1.39 with the driven contact interaction affecting only the relative motion, leaving unaffected the center of mass. Therefore we focus on the relative motion, which in the time-dependent case actually represents a one-particle problem with a harmonic trap and a delta barrier with oscillating height placed in the center. With the transformation $r = \sqrt{2}x$, $g(t) = \sqrt{2}g'(t)$ we obtain the standard form of the harmonic oscillator Hamiltonian

$$H_r = \frac{p_x^2}{2} + \frac{x^2}{2} + g'(t)\delta(x). \tag{2.13}$$

$H_r$ defines an analytically solvable eigenvalue equation as we have seen in the first Chapter 1 [14] in the case of a time-independent parameter $g$. We will discuss the resulting relative

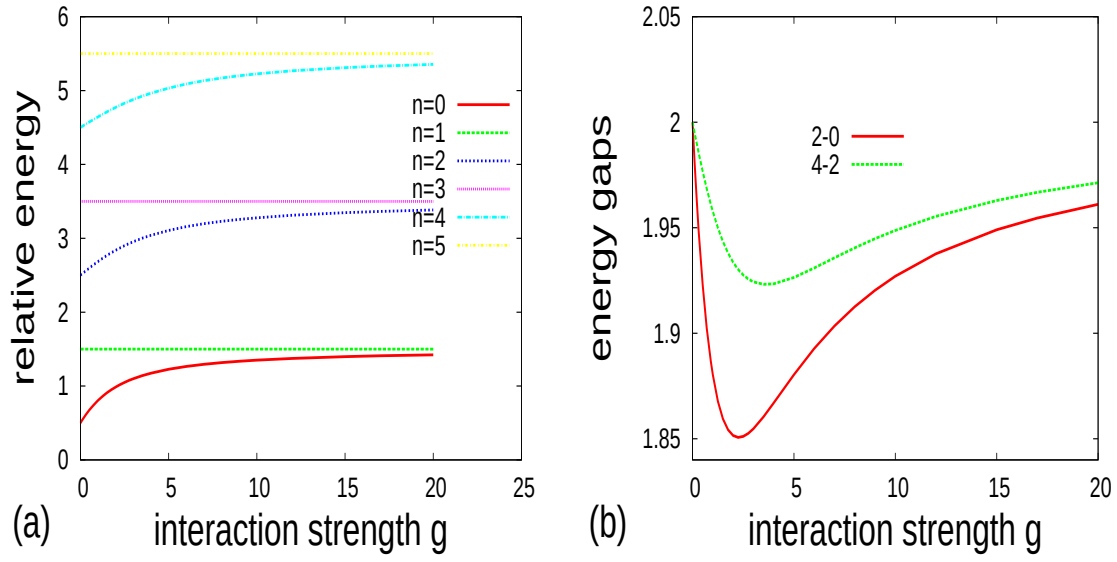


Figure 2.4: (a) The three lowest eigenenergies of the symmetric (0,2,4) and antisymmetric (1,3,5) eigenstates of the relative motion for two atoms with increasing interaction strength $g$. (b) The energy difference between the eigenstates of the relative motion $\epsilon_2 - \epsilon_0$ and $\epsilon_4 - \epsilon_2$ with increasing $g$.

motion spectrum in more detail as it is very important for the understanding of the excitation dynamics of the relative motion. The solutions cover in general the complete interval $g \in [0, \infty)$ and we will refer to them as the instantaneous eigenstates $\phi_n$, where $n = 0, 1, 2...$ are the energy levels for a certain time instant $t_{ref}$. In spite of the existence of these stationary solutions the driven time-dependent problem possesses no closed analytical solution, although a study via the evolution of the coefficients in an expansion with respect to the corresponding instantaneous eigenstates is natural [86, 87].

In Fig. 2.4(a) we show the lowest lying eigenenergies for $H_r$ for repulsive interaction strengths (the full range was presented in Chapter 1 Fig. 1.3.1). For $g = 0$ the eigenspectrum of $H_r$ is the harmonic oscillator single-particle spectrum with the equidistant eigenenergies $\epsilon_n = n + 1/2$. As $g$ increases the odd levels are unaffected by $\delta(x)$ since they possess a node at the coordinate origin. Each even level approaches energetically the next upper odd level forming a doublet spectrum, characteristic for double-well potentials (see also [29]). In the limit where the 'barrier height' is infinite $g \to \infty$ the even levels become degenerate with the odd ones a complementary picture for the TG limit $g \to \infty$. More important for the present study is the energy difference between two even levels with increasing interaction strength shown in Fig. 2.4(b). In fact, since the initial preparation is in the ground state which corresponds to an even state of the relative motion, the dynamics can only lead to a population of other even states, and the corresponding energy distance is crucial for the time-evolution. For the two limits of zero interaction and the Tonks-Girardeau gas ($g \to \infty$) the gap between two even parity levels is $|\epsilon_n - \epsilon_{n-2}|_{g=0\,,\,g\to\infty} = 2$. Starting from $g = 0$ and increasing $g$ this value slightly decreases [see Fig. 2.4(b)], since the states with larger quantum number $n$ possess a lower probability density at $x = 0$ and are therefore less affected by the contact interaction. The slope at $g = 0$ reads:

$$\left.\frac{d\epsilon_n}{dg}\right|_{g=0} = \langle\phi_n|\delta(x)|\phi_n\rangle = |\phi_n(0)|^2 = \frac{\pi}{n!\Gamma^2\left(\frac{1-n}{2}\right)} \tag{2.14}$$

The response to a minor increase of $g$ therefore depends on the value of the harmonic oscillator eigenstates at $x = 0$ which decreases with $n$ [see Fig. 2.4(a)]. Therefore at the onset of the

interactions the successive even states tend to approach each other energetically. Fig. 2.4(b) shows the effect of an increasing coupling strength $g$ on the distance between the first two even levels $\epsilon_0$ and $\epsilon_2$ (red line). The most rapid change of this energy gap is near $g = 0$ with a minimum value $\epsilon_2 - \epsilon_0 \approx 1.85$ at $g^* \approx 2.2$ and it approaches asymptotically the value 2 for $g \to \infty$. The slope $\frac{d\epsilon(g)}{dg}$ is decreasing as $g$ increases [see Fig. 2.4(a)] and from some value of $g$ on, the energy gap starts to increase again and asymptotically approaches the value of the non-interacting system. Additionally, since $\frac{d\epsilon_n}{dg}$ decreases with increasing $n$ the deviation from the value 2 for $\epsilon_2 - \epsilon_0$ shown in Fig. 4.1(b) (red line) is the largest possible such deviation between two successive (even) states. This is exemplarily shown in the same figure by the distance between the next pair of successive states $e_2$ and $e_4$ (green line). It is obvious that the energy gap $\epsilon_4 - \epsilon_2$ is always larger than the $\epsilon_2 - \epsilon_0$ gap, and this holds analogously also for gaps between higher lying neighboring states.

The above discussed features of the energy spectrum and the corresponding gaps, possess a crucial impact on the dynamics which we will discuss later. As $g(t)$ changes with time according to Eq. (2.12) different regions of $g$-values in Fig. 2.4 are probed according to the choice of the parameters $g_0$ and $\Delta g$. We might already foresee e.g. that a driving around small $g$-values possesses a greater impact than for a driving for larger $g$-values, since the corresponding slope is larger, subsequently leading to larger energy variations. The equidistance of the spectrum close to the two extreme limits, as well the decrease of the gaps at small to intermediate values of $g$ will also be of great importance concerning a possible resonant behaviour.

### 2.2.3 Resonant controllable excitation

The wave packet of the relative motion at $t = 0$ corresponds to the ground state of $H_r$ in Eq. (2.13) with $g(0) = g_0$. This an even state and since parity is conserved during the time evolution only even parity states can be occupied, which relates to the bosonic permutation symmetry. In this work we are interested mainly in two quantities:

- the population of momentarily eigenstates $\phi_n$ at a certain time $p_n(t_{ref}) = |\langle\phi_n(t_{ref})|\psi(t_{ref})\rangle|^2$, where $\psi(t)$ is the wavefunction of the relative motion. We use $t_{ref} = \frac{2\pi k}{\omega}$ $(k \in \mathbb{N}_0)$ without loss of generality.

- the time evolution of the energy $\epsilon(t)$. We refer only to the relative energy since the center of mass is completely untouched by the change of $g$.

We start our investigation in the regime of small driving amplitudes where the excitation dynamics is to a larger extent controllable. The main role in this regime is played by the driving frequency. If this frequency is much lower than the gap between two even states ($\omega << 1$) then we are in the adiabatic regime and the evolution involves only the momentarily ground state $\phi_0$ (with $p_0 > 0.99$). Approaching the first resonance $\omega = 1$ from below induces an excitation to the state $\phi_2$ of the relative motion. This is shown for a typical case in Fig. 2.5 (a) where $g_0 = 0$, $\Delta g = 0.05$ and $\omega = 0.99$. We see that the ground state looses population while the second excited state gains. The next even level $\phi_4$ remains almost unpopulated. For the particular case though where $g_0 = 0$ (and correspondingly for $g_0 \to \infty$) since the eigenspectrum is initially completely equidistant, an excitation to the next level $\phi_4$ is not prohibited corresponding to a two step process. Therefore we see in Fig 2.5 (b) that a bit closer to the resonance ($\omega = 0.997$) the $n = 4$ level gains population after the $n = 2$ level does so. This is also in general the case for larger amplitudes $\Delta g > 0.5$ where multiple excitations are enhanced as we will see later on. Therefore, while the system departs – in this case completely – from the ground state, the first collective excitation to state $n = 2$ is necessarily combined with a transfer of population to the next level and therefore a controllable excitation exclusively to the second

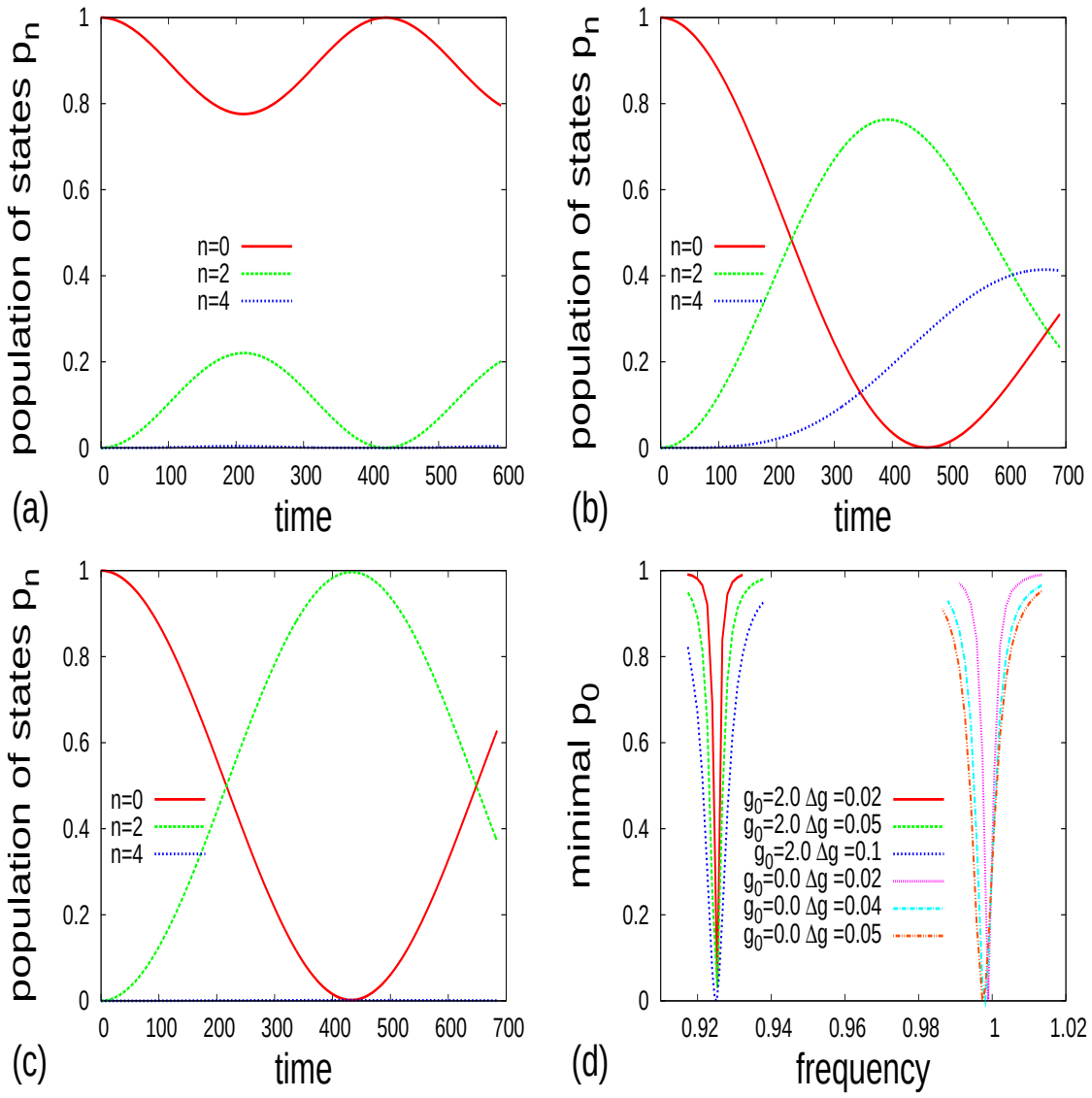


Figure 2.5: Population of instantaneous eigenstates with time variation, for (a) $g_0 = 0.0$, $\Delta g = 0.05$, $\omega = 0.99$, (b) $g_0 = 0.0$, $\Delta g = 0.05$, $\omega = 0.997$, (c) $g_0 = 2.0$, $\Delta g = 0.1$, $\omega = 0.925$. Profile of the resonances via the minimal occupation of the ground state with varying driving frequency. Several cases are shown for different values of $g_0$ and $\Delta g$.

level (complete depopulation of ground state and complete population of the second excited level) is not possible here. It becomes though possible if the initial interaction is stronger. For instance for $g_0 = 2.0$, $\Delta g = 0.1$ we see in Fig. 2.5 (c) a complete transfer of population to the first excited level. Therefore, the non-harmonicity in the spectrum due to the initial correlations is helpful from the point of view of a controllable state excitation and preparation. Let us note that for a controlable creation of such states, one should choose a small amplitude $\Delta g < 0.5$, since larger amplitudes lead easily to multiple occupation of excited states due to the close to equidistant spectrum. Additionally the driving frequency should be carefully tuned to be close to the corresponding energy spacing of the spectrum with $g(0) = g_0$. For this case $\omega = 0.925$ –somewhat lower than the resonant frequency for the non-interacting $g_0 = 0$ situation– we have a decreased gap in the energy spectrum [see Fig. 2.5 (b)].

As an overview of the resonances in this regime we present in Fig. 2.5 (d) the minimal occupancy of the instantaneous ground state $p_0$ as a function of the driving frequency for several small amplitudes of the driving. We observe that far from resonance the minimal $p_0 \approx 1$, so there is hardly any excitation as expected. The frequency where the ground state becomes at a certain time completely unoccupied corresponds to the resonance. The resonant frequency is slightly shifted to lower values for a larger amplitude of the driving which is attributed to the decrease of the energy gap in the spectrum [see Fig. 2.5 (b)], as $\Delta g$ covers larger regions of $g$ (for $g_0 = 0$). We also observe that for $g_0 = 2.0$ the resonant frequency is shifted to much lower values than for $g_0 = 0$, approximately corresponding to the energy gap of the levels at $g = 2.0$ ($\omega = \frac{\epsilon_2 - \epsilon_0}{2} \approx 0.925$). For this case though, small changes in the driving amplitude do not shift significantly the position of the resonance, since the energy spacing in the vicinity of this value of $g_0$ does not change substantially [see Fig. 2.4 (b)]. However, the most important difference of the two cases for different initial coupling strength $g_0$ is the fact that the case $g_0 = 0$ leads easily to multiple excitation of higher states since the energy gaps are all close to the same value corresponding to the same resonant frequency, while for larger $g_0$ the energy spacing is not equidistant and therefore a complete controlable transfer to a certain state is possible.

A comment on the robustness of the initial state preparation is in order here. Apart from being easily excitable to different instantaneous states, the initially non-interacting ensemble is in general more sensitive to the driving of the interaction. Even far from resonance the evolution of this initial state ($g_0 = 0$), leads to a change in energy of the order of 10% while for stronger and particular intermediate interactions as well as close to the fermionization regime $g_0 = 20.0$ it is ten orders of magnitude lower. This is understandable if one inspects the slopes of the energy curves in Fig 2.4 (a), which are much larger for small values of $g$. This could be a signature for the detection of a highly correlated ensembles like the Tonks Girardeau gas, i.e., by studying their response to changes of the interaction strength.

Not only an excitation to the first excited state of the relative motion is possible, but also to other excited states if the resonant frequency is chosen correspondingly as we can see in Fig. 2.6 (a). As expected the resonance width though decreases for transitions to higher states. The effect of the initial $g_0$ and of the amplitude $\Delta g$ is similar to the previous case.

For larger amplitudes the controllability of the excitation process reduces, as many states are subsequently excited, and simultaneously taking part in a complex time evolution. A typical example is presented in Fig. 2.6 (b). Still the frequency plays the dominant role and only close to resonances the evolution leads to highly excited states of the spectrum. Mechanisms of acceleration appear then which we will discuss in the following section. We would like to note here that a large $\Delta g$, offer the possibility of 'multi-photon excitations'. In this case even for low frequencies which are an integer ratio of the principle resonant frequency, excitations become possible.

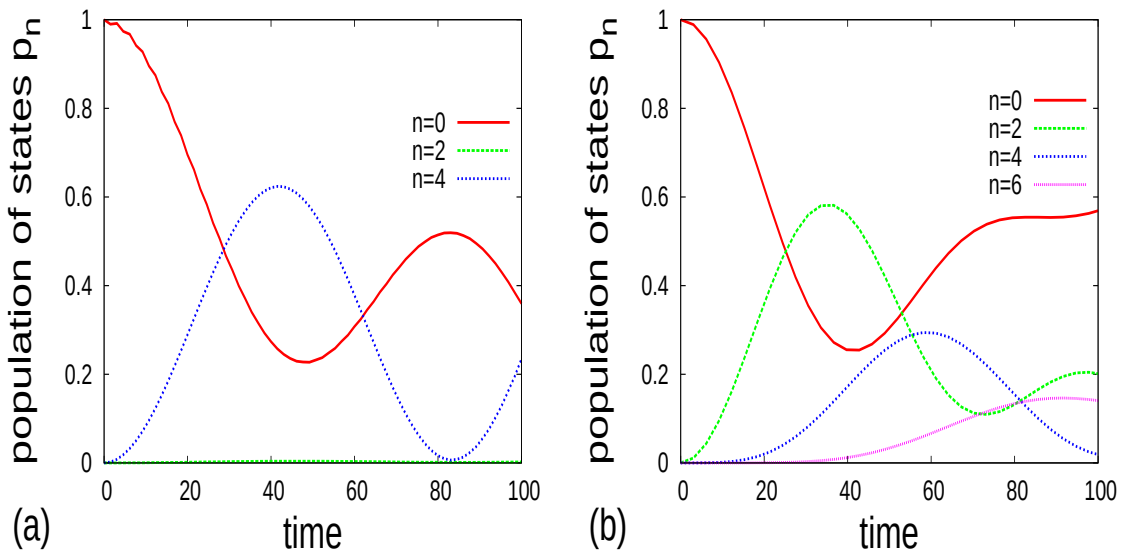


Figure 2.6: Occupation of the adiabatic eigenstates of the Hamiltonian for $g_0 = 0$, $\Delta g = 0.5$ close to the second and the first resonance (a) $\omega = 1.98$ (b) $\omega = 0.998$

### 2.2.4 Multiple excitation and Floquet analysis

We will now more thoroughly examine the case of strong driving, which makes it possible, as we will show, to accelerate the atoms, i.e., to increase the mean value of the energy with time. The process of multiple excitations as we have seen, is possible close to resonances, since the spectrum is approximately equidistant. Especially a larger value of $\Delta g$ leads to a covering of wider areas of the energy gaps, and therefore the comparatively small differences between the gaps effectively drain away. Through this multiple excitation process, the system never returns completely to the ground state, and indeed occupies gradually increasingly higher lying states. This excitation process induces an increase of the energy to very high values as long as the gaps to higher excited states are in the resonance window.

We present in Fig. 2.7 the time evolution of the expectation value of the energy, close to the first resonance for $\Delta g = 20.0$. For values of the frequency sufficiently far from resonance, a repopulation of the ground state in the course of the time can be observed, while a multi-mode behavior is encountered due to an excitation of several states. Approaching the resonance, the instantaneous ground state is never repopulated significantly, on the opposite, higher states of the spectrum are subsequently populated in the same manner as shown in Fig. 2.6 (b). This leads to an acceleration, i.e., energy gain of the atoms. Our finite time simulations indicate that this energy gain approaches a saturation to very high values of the energy for strong but finite $\Delta g$.

#### Floquet quasienergies

Let us analyze this resonant mechanism from the perspective of Floquet theory which has been developed for time-periodic Hamiltonians. The Ansatz of the Floquet theory for the time-dependent wave packet reads:

$$\psi_k(r,t) = e^{iq_k t} \sum_n u_n^k(r) e^{in\omega t} \tag{2.15}$$

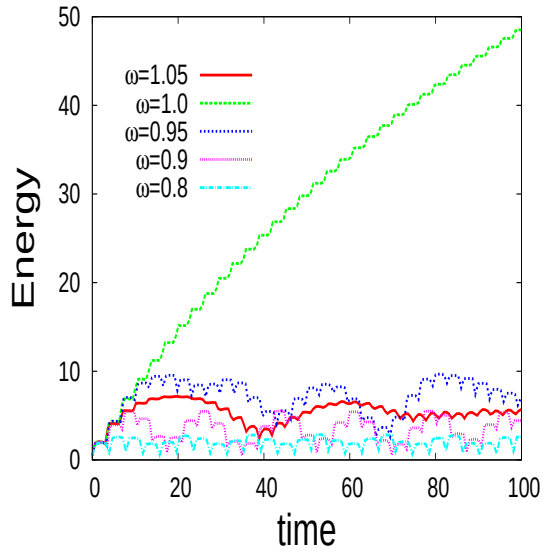


Figure 2.7: Time evolution of the expectation value of the energy for $\Delta g = 20.0$, $g_0 = 0$ and several frequencies close to resonance. Acceleration shown close at the resonant frequency

where $u^k(r,t) = \sum_n u_n^k(r)e^{in\omega t}$ are the so-called Floquet eigenstates or quasi-energy states, which are time periodic functions expanded here into a Fourier series and $q_k$ are the quasienergies. Introducing this Ansatz into the Schrödinger equation for the Hamiltonian in Eq. (2.13) we find:

$$\begin{aligned} q_k u_n^k(r) &= \left[n\omega + (-\tfrac{d^2}{dr^2} + \tfrac{1}{4}r^2) + (g_0 + \tfrac{1}{2}\Delta g)\delta(r)\right] u_n^k(r) \\ &\quad -\tfrac{1}{4}\delta(r)\Delta g(u_{n-2}^k(r) + u_{n+2}^k(r)) \end{aligned} \tag{2.16}$$

The r.h.s. of this equation is the Floquet Hamiltonian which has diagonal, i.e., proportional to $u_n^k$, and off-diagonal terms coupling the different modes $u_{n-2}^k$, $u_{n+2}^k$. To find $u_n^k$ and eigenvalues $q_k$ one should solve this eigenvalue problem by diagonalizing the corresponding Hamiltonian. The harmonic oscillator $f_m(r)$ basis is very convenient to express the Floquet Hamiltonian in our particular problem, not only because of the harmonic part of the potential which has as matrix elements the harmonic oscillator eigenvalues but also because the matrix elements of $\delta(r)$ are of the form $\int dr f_m(r)\delta(r)f_{m'}(r) = f_m(0)f_{m'}(0)$. An alternative method equally well-suited for our problem is to write the Floquet eigenvectors in terms of parabolic cylinder functions [80] $D(\nu, x)$ which are the solutions of the underlying stationary problem [14] (see Chapter 1). In this representation we have

$$u_n^k(r) = c_n^k D_n^k(-(q_k + n\omega), r) \tag{2.17}$$

and we use again the important properties Eq. B.21 and B.22. By integrating Eq. (2.16) using these relations we obtain a recursive system of algebraic equations for the coefficients $c_n$. Demanding that this system possesses solutions we obtain the values of quasienergies $q_k$. We have used both methods to derive the eigenspectrum of the Floquet Hamiltonian for our problem and confirmed the agreement crosschecking the results and thereby the numerical convergence.

We show in Fig. 2.8 (a) the eigenspectrum of the Floquet Hamiltonian, i.e., the Floquet quasi-energies with increasing driving frequency $\omega$ for a typical case $g_0 = 0.0$ and $\Delta g = 1.0$. In the dense spectrum of quasi-energies we encounter points of accumulation when the frequency is at resonant values ($\omega = 1, 2, 3...$). At these points, many Floquet quasi-energies take a value close to the harmonic oscillator eigenenergies ($0.5, 1.5, 2.5...$), and form Floquet bands. The

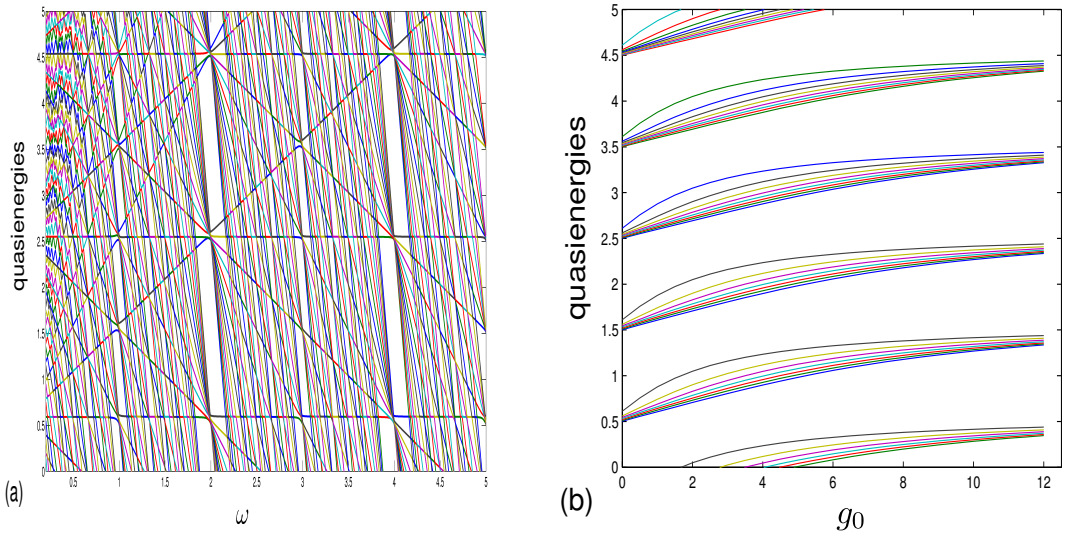


Figure 2.8: Floquet eigenspectrum for (a) increasing driving frequency $\omega$ with $g_0 = 0.5$ $\Delta g = 0.5$, (b) increasing initial interaction strength $g_0$ for the resonant frequency $\omega = 1$ and $\Delta g = 0.5$

even-frequency resonances ($\omega = 2, 4, 6...$) correspond to accumulation points with an energy gap 2, i.e. at the quasi-energy values $0.5, 2.5, 4.5, ....$

Let us now show how these results obtained for the Floquet Hamiltonian are connected with the quantum acceleration processes for quantum resonances. In dynamical systems a pure point Floquet spectrum is associated with localized behavior and the energy remains bounded at all times, while singularly continuous components are responsible for diffusive behavior and growth of the energy (see Ref. [[91]] and references therein). At the resonant driving frequencies as we have seen above the quasi-energies are accumulating and approach particular values forming close to continuous areas. This property of the spectrum leads to the acceleration and energy gain.

Besides, in Fig. 2.8 (b) we see that with increasing $g_0$ and for the resonant frequency $\omega = 1$ the eigenenergies of the Floquet spectrum deviate from each other, and only come close again as we approach the fermionization limit in the next upper level. This deviation from the accumulation points makes the evolution less diffusive for intermediate interactions, and corresponds to the picture of the instantaneous spectrum, where the energy gaps for intermediate values of $g$ become less equidistant, prohibiting multiple excitation.

### 2.2.5 Larger atom numbers and finite size effects

The extensive analysis of the two-body case above, is very useful for a bottom-up understanding of the effects occurring for higher atom numbers. The main reason for this are the properties of the many body spectrum of the harmonic oscillator including the delta-type interaction. We present in Fig. 2.9 the energetically low lying part of the spectrum for three and four atoms with increasing interaction strength [see also Ref. [29]]. We observe that all states show a quite similar evolution and thus the energy gaps between them do not deviate significantly (crossings or anti-crossings do not occur). Also important is that most of the states correspond to excitations of the center of mass, which are not relevant to our study. For example the first excited state and one of the two states of the second excited band which behave exactly like the ground state, correspond to the ground state of the relative motion and to the first and second

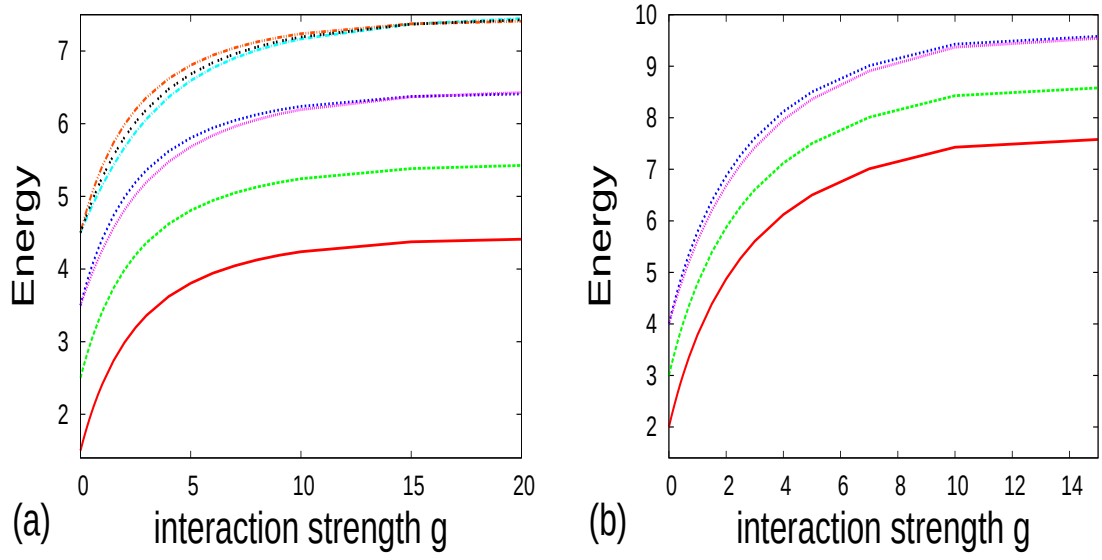


Figure 2.9: The lowest eigenenergies with increasing interaction $g$ for (a) three and (b) four bosons.

excitation of the center of mass motion, respectively.

The time-dependent variation of the interaction strength which affects only the relative motion offers the possibility of a controllable excitation to specific states also for higher atom numbers, since states like those mentioned above which correspond to excitations of the center of mass do not contribute to the time evolution and are therefore avoided. We demonstrate this in Fig. 2.10 (a) for the case of three atoms and an initial value $g_0 = 2.0$ in the intermediate regime, where an excitation predominantly to the lower state (corresponding to an excitation of the relative motion) of the second excited band of eigenstates is performed [see Fig. 2.9(a)]. We denote here by the numbers $0, 2, 4$ the energetically ordered states which correspond to a respective excitation of the many body relative motion. The resonant frequency for excitation from state 0 to state 2 will be referred as the principle resonance in the following.

The above signifies that higher number of particles allow for a similar control of their dynamics as in the case for two atoms which is mainly due to the similarities of their underlying energy spectrum. One important difference here is that for equal parameters, systems with larger atom numbers experience a stronger impact of the driving than those with a lower atom number. This can be seen from the the maximum loss of population of the instantaneous ground state with time in Fig. 2.10 (b) in a non-resonant case which gets larger with an increasing number of particles. An explanation for this atom number related effect is the response of the ground state energy to the variation of $g$:

$$\frac{dE}{dg}\Big|_{g=0} = \frac{N(N-1)}{2} \int |\phi_0(x)|^4 dx, \tag{2.18}$$

where we see that the slope of the total energy at $g = 0$ increases quadratically with the particle number. Therefore a variation of $g$ possesses a greater impact for higher atom numbers.

Another important observation concerning the size of the system is the position of the principle resonance in the regime of intermediate interactions. We have seen already that for e.g. $g_0 = 2.0$ the resonant frequency is lower than for very weakly or strongly interacting initial states. This frequency becomes even lower as the number of particles increase which is based on the decreasing energetical spacing in the corresponding many-body spectra with increasing

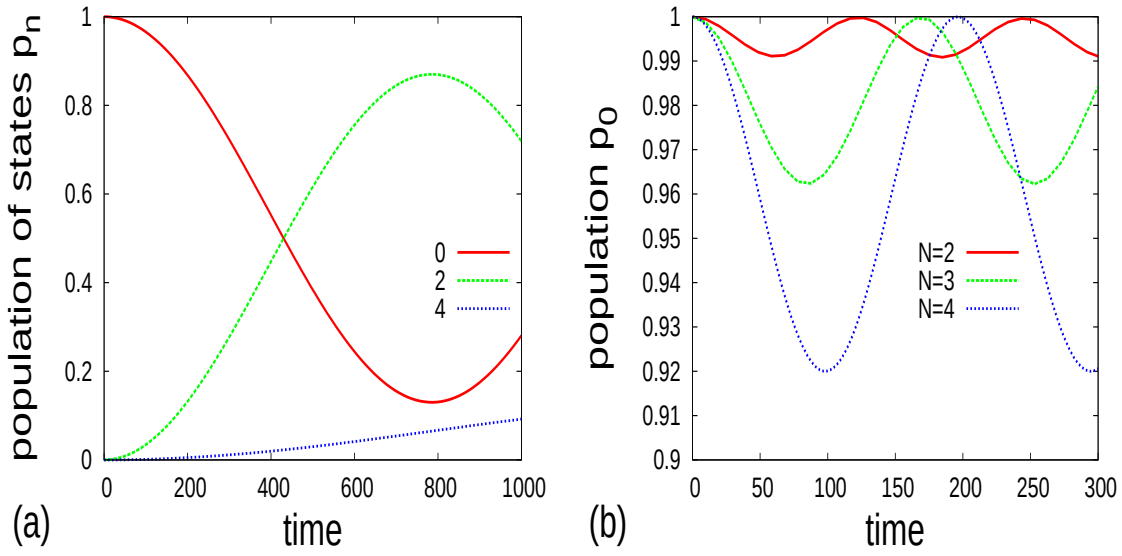


Figure 2.10: (a) population of instantaneous eigenstates for three atoms with $g_0 = 2.0$, $\Delta g = 0.05$ and $\omega = 0.9$. (b) Population of the instantaneous ground state for different particle numbers: $N = 2, 3, 4$ $g_0 = 0.0$ $\Delta g = 1.0$ and $\omega = 0.6$

particle number. Consequently a lower value of frequency is needed for larger atom number for the corresponding resonant excitation via driving of the interaction strength.

The above observation is important for modes of collective oscillation of the wavefunction, in analogy to the macroscopic collective oscillations [15, 1]. Many measurements in experiments are based on exciting collective modes, which are usually analyzed within the effective mean field descriptions [92]. The frequencies of these oscillations can be obtained with a high accuracy from the experimental data usually observing the size or the mean position of the condensate [24, 20], and represent a very important measure for identifying different interaction regimes. For example in 1D the TF limit, or the TG and Super-TG gas, possess a very characteristic ratio between the so-called dipole mode which is an oscillation of the center of mass of the condensate with the trap frequency $\omega_d$, and the breathing or first compression mode, where essentially the size of the condensate is oscillating with a frequency $\omega_b$. For the effectively non-interacting limits ($g = 0, \infty$) this ratio is $\omega_b/\omega_d = 2$ while for the Thomas Fermi limit it is $\omega_b/\omega_d = \sqrt{3} \approx 1.73$ [92]. These important theoretical results have been confirmed in the corresponding experiments [24, 20].

From the few body perspective which we examine here, the mode of oscillation that we excite by varying the scattering length, is of a compressional-breathing type. We demonstrate this in Fig. 2.11 where we show several snapshots of the one-body density for characteristic time moments. The excitation to the second state of the spectrum which corresponds to an excitation of the relative motion (and therefore to a broader wavefunction), possesses therefore the characteristics of a breathing mode. The characteristic frequency of such a mode, in the intermediate interaction regime could be compared with the mean field result for the TF regime. For non-interacting cases we confirm the ratio $\omega_b/\omega_t = 2$. The Thomas Fermi regime applies to large ensembles of atoms, and the analogy with a the finite system examined here can be at most indicative. Nevertheless in 1D systems we can take the minimum value of the energy gap which appears close to $g = 2.0$ as corresponding to the Thomas-Fermi regime (see also corresponding arguments in Chapter 2.1). In doing so, we can reveal finite size corrections for the breathing mode of the TF limit, starting with two atoms $\omega_b/\omega_t \approx 1.85$ and going to $\omega_b/\omega_t \approx 1.78$ for five

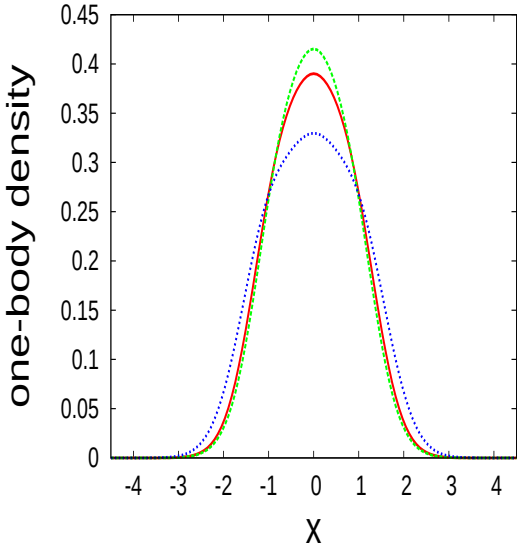


Figure 2.11: One body density for the case of three atoms as in Fig. 2.10 for several time snapshots.

atoms with a further tendency to decrease with increasing particle number. In the macroscopic limit $N \to \infty$ we should approach the mean field estimate $\omega_b/\omega_t = \sqrt{3} \approx 1.73$ [92].

This interrelation of the collective mode frequencies and their finite size deviations within the few-body spectrum are probably valuable for further studies on connecting, checking and reinterpreting mean field results in the light of the exact many-body spectrum and behaviour.

**Conclusive remarks**

We examined the effects of a periodically driven interaction strength on ultracold bosonic systems in a 1D harmonic trap which can be realized by a time modulation of magnetic fields utilizing Feshbach resonances or periodically changing the transversal confinement length in a waveguide via laser fields. Following our bottom-up approach we have first examined in detail the two-body case were all basic effects are present, demonstrated and analyzed. We have shown that the feature of near equidistant energy levels for arbitrary interaction strength for the relative motion of two atoms in a harmonic trap but also for the corresponding many-body spectrum for larger atom numbers has important consequences for the excitation dynamics. In particular, the energetical spacing yields resonant driving frequencies, which one can employ to excite particular states of bosonic relative motion. We underline that unlike other driven many-body systems, the variation of the interaction strength offers the possibility to design excitations of the relative motion of a certain species exclusively with a very high degree of controllability for certain regimes of the driving parameters. Approaching the resonant frequencies the atoms excite to the corresponding excited level of the relative motion which has been demonstrated here by calculating the occupation of instantaneous eigenstates. For strong driving amplitudes in the vicinity of the resonances the energy reaches out to very high values with several and successive excitations to energetically higher lying states of the spectrum. This multi-excitation process of acceleration is also analyzed via the properties of the Floquet spectrum. The initial interaction strength distorts the energy spectrum shifting the position of the resonances, while highly correlated initial states are quite insensitive with respect to the changes of the repulsive interaction. We have shown via our exact numerical calculations, that for any number of atoms there is a similar and for larger ensembles even more sensitive response to the driving of the

interaction strength leading to higher excitation amplitudes. Effects due to the finite size of the system, are also analyzed from the perspective of collective oscillation modes, and especially the analog to the macroscopic breathing mode is established, thereby discussing similarities and deviations from mean field approaches. Interesting outlooks are the exploration of different driving laws, including the possibility to alter between repulsive and attractive interactions or using different potential landscapes.

# Chapter 3

# Bosons in finite lattices

Right after the extensive studies of harmonically trapped systems, the interest of the cold-atom community focused on other kinds of potentials. The most popular and favorable potential landscape is the optical lattice which allows for the investigation of quantum phenomena occurring in different areas such as condensed matter physics or quantum simulators and information processing [2, 44]. In this Chapter we will examine stationary properties of few-boson systems in finite 1D lattices for different filling factors exploring the interplay between commensurability and correlation effects [42] (Chapter 3.1) and inter-band tunneling dynamics in a triple well [43] (Chapter 3.2). In Chapter 3.1 different filling factors will be investigated, focusing on effects beyond the standard single-band approach of the BHM. Apart from numerical calculations we will extend the CPWF to lattice geometries in order to cover strong-correlation on-site effects. In the second part (Chapter 3.2) we will analyze resonant tunneling mechanisms which appear for strong interactions in a 1D triple well potential, and can be explained via the stationary few-body spectrum, seen again from a bottom-up perspective.

## 3.1 Commensurability vs correlation

The flexible experimental toolbox of optical lattices enabled the investigation of specific models in a very controlable environment. The most prominent example is the Bose-Hubbard model (BHM) a very effective approach which will be described in the beginning of this chapter. The physics of this model which include a phase transition from a coherent superfluid (SF) to a Mott-insulator (MI) state with localized atoms in each lattice site [7] have been studied theoretically [44] and proposed for experimental realization in optical latices in [44]. The first seminal experiment on this system [7] has triggered a lot of research. Further highlights include quantum phases like Bose glass and Mott-shells, occurring for disordered, confined and incommensurate systems [93, 94, 95, 96, 97, 98, 99, 100, 101].

1D optical lattices are very special and appealing systems since they combine the physics in a lattice (phase transitions) with the special features of 1D [29, 42, 46, 73, 102, 103, 104, 105, 106]. An important phenomenon for strongly interacting systems is the so-called pinning transition where atoms close to the TG regime turn to a Mott insulator phase for a perturbatively deep lattice [46] also demonstrated experimentally in [47]. Localization, delocalization as well as lattice imperfection effects have been studied for small ensembles in Ref. [107] showing interesting analogies with macroscopic phases. In particular momentum distributions, pair correlations and energy spectra give insight to the MI-SF transition with increasing lattice depth or unveil the effect of an incommensurate filling, while a Bose-glass phase emerges when breaking the lattice symmetry. The effect of a higher filling factor and the subsequent on-site fragmentation of atoms in periodic 1D lattices has been explored in [45]. The authors investigate a commensurate

case with two atoms per site and distinguish between a phase of MI with unperturbed Wannier functions, and a second transition to a state with two fragmented orbitals on each site. In the first part of this Chapter 3.1 we aim to perform a complete numerically exact investigation for the whole range of interaction strengths from uncorrelated to fermionized bosons. Thus we go far beyond the BHM regime and concentrate on on-site effects and changes on the on-site localized functions. We examine via different observables both the localization mechanisms in the commensurate filling with one and two atoms per site for finite lattices and the on-site fragmentation of atoms for strong interactions, as well as various incommensurate cases.

In this section we will first introduce the 1D lattice model and discuss properties of the single-particle states within the tight-biding approximations and the Bose-Hubbard model. Then we will discuss properties of different filling factors commensurate and incommensurate via one and two-body densities, populations and fluctuations, one-body density matrices and natural orbitals. This extended study of few-body 1D systems in lattices extends the work that has been done with MCTDH in harmonic trap and double wells. In the very last part we will discuss an extension of the CPWF introduced for the harmonic trap in the previous Chapter 2.1 to cover lattice geometries.

### 3.1.1 Model

We are interested here in finite multi-well systems. These can be prepared experimentally e.g. by using more than one counter-propagating laser beams (standard optical lattice technique) and forming a superlattice of copies of small finite lattices, or from the beam waist which always produces an approximate harmonic confinement resulting in a concentration of the cloud density in the few central wells of the potential [2]. The effective 1D Hamiltonian reads:

$$H = -\frac{\hbar^2}{2M}\sum_{i}^{N}\frac{\partial^2}{\partial x_i^2} + \sum_{i}^{N} V_0 \sin^2(\kappa x_i) + g\sum_{i<j}\delta(x_i - x_j) \tag{3.1}$$

The potential is characterized by the depth $V_0$ and periodicity $d$ (distance between two successive minima) setting $\kappa = \pi/d$. In order to restrict the infinite potential to a finite number of sites $W$ and a length $L$, we impose hard-wall boundary conditions on appropriate position[1].

All the parameters are considered to be tunable almost at will in corresponding experiments, for example using Feshbach and confinement induced resonances for altering the interaction strength, as well as manipulating the intensity and angles between the laser beams to change the profile of the potential. The interaction strength $g$ is the main parameter and we will take representative values to cover the complete crossover to fermionization in all different cases of commensurability. We use a sufficiently large lattice depth[2] such that at least two single-particle bands lie energetically below the continuum for reasons we explain later on. The way we render our system finite via imposing hard-wall boundaries does not restrict the generality of our treatment and results. In particular, independently of the specific experimental implementation (using multi-color lattices and/or harmonic confinement [2]), finite systems exhibit intrinsic features which differ from infinite lattices (periodic boundary conditions); the confined traps result always in spatial inhomogeneities of the densities which are absent in the periodic case.

[1] In our numerical calculations, since we aim to different multi-well systems we chose for convenience to keep a standard grid and a standard length $L$ therefore the length unit was defined as $L_u = L/10$ and the energy unit as $\hbar^2/ML_u^2$ setting also $\hbar = M = 1$. This somewhat not standard choice of units was done only for numerical convenience, we keep here presenting the results as obtained with this scaling and presented in [42]. Since though the usual scaling is in units of the recoil energy $E_R = \frac{\hbar^2\kappa^2}{2M}$ and lattice constant $d$ we note that to transform in these units the relation $g' = \frac{g_{1D}}{dE_R} = \frac{2d}{L_u\pi^2}g$ holds.

[2] $V_0 = 7.0 - 20.0$ which is of the order of $4 - 20$ $E_R$ depending on $\kappa$

These inhomogeneities can be increased or manipulated if there is a harmonic confinement or a disordered surface. Although we are focusing here on the case of equal on site energies (our hard-wall boundaries let the potential unaffected in between), we observe a rich behaviour that captures the main effects of a finite confined system. All our numerically exact calculations are performed by the MCTDH method which is employed here for lattices (see appendix for a description) following the line of single double well potentials from previous studies [29]. In the following subsections we refer to the single-particle spectrum within the tight-binding approach and the Bose-Hubbard model for weak interactions. Both approximations are valid only in certain regimes which we address to explain a part of the observations. Covering the complete interaction crossover from $g = 0$ to $g \to \infty$ by MCTDH we are able to show the regimes of validity but also examine effects going beyond these models.

### 3.1.2 Single-particle states

A discussion of the single-particle states is necessary in order to understand the limit cases of non- and infinitely- interacting atoms (according to the Bose-Fermi map -see Chapter 1). Analytical expressions for the delocalised single-particle states, i.e. Bloch states, are available for periodic boundary conditions. For finite lattices, we use the tight-binding approximation assuming only a nearest-neighbor tunneling coupling term $J \propto -\int w_s(x) h_i w_{s+1}(x) dx$ between the sites $s$ and $s+1$ where $w_s(x)$ are the on-site localized Wannier states and $h_i = -\frac{\hbar^2}{2M}\frac{\partial^2}{\partial x^2} + V_0 \sin^2(\kappa x)$ the single-particle part of the lattice Hamiltonian Eq. 3.1. Within this approximation, valid for a relatively deep potential, we express the Bloch states in terms of Wannier functions. The single-particle Hamiltonian written in a matrix form using the localized states basis is:

$$\tilde{h}_i = \begin{pmatrix} \epsilon_1 & -J & 0 & .. \\ -J & \epsilon_2 & -J & .. \\ 0 & -J & \epsilon_3 & .. \\ .. & .. & .. & .. \end{pmatrix}$$

where $\epsilon_s$ ($s = 1, 2, .., W$) are the on-site energies, which in our case are equal ($\epsilon_1 = ... = \epsilon_W \equiv \epsilon$).

The hard-wall boundary conditions imply that there is no tunnel coupling between the first and the last lattice site as opposed to the periodic where there is a single coupling for all sites. The resulting eigenvalues are: $E_{q-1} = \epsilon - 2J\cos(\frac{q\pi}{W+1})$ ($q = 1, ..., W$), and the eigenfunctions read:

$$|\varphi_{q-1}\rangle = \sqrt{\frac{2}{W+1}} \sum_{s=1}^{W} \sin\left(\frac{sq\pi}{W+1}\right) |w_s\rangle \tag{3.2}$$

These lowest-band single-particle eigenstates are sketched in Fig. 3.1 for the triple well using the Gaussian approximation for the Wannier functions around the center of each well $\tilde{x}_s$ $\langle x|w_s\rangle = (\pi d^2)^{-1/4} e^{-(x-\tilde{x}_s)^2/2d^2}$: $|\varphi_0\rangle = \frac{1}{2}(|w_1\rangle + \sqrt{2}|w_2\rangle + |w_3\rangle)$, $|\varphi_1\rangle = \frac{1}{\sqrt{2}}(|w_1\rangle - |w_3\rangle)$, $|\varphi_2\rangle = \frac{1}{2}(|w_1\rangle - \sqrt{2}|w_2\rangle + |w_3\rangle)$, with corresponding energies $E_0 = \epsilon - \sqrt{2}J, E_1 = \epsilon, E_2 = \epsilon + \sqrt{2}J$. Note that for the ground state the middle well is occupied with a larger amplitude compared to the two outer ones. For the states of the excited bands the harmonic oscillator orbitals of higher order can serve as localized functions to a rather good approximation[3]. In a recent paper [94], the single-particle states of the lowest band for the case of a lattice with a superimposed parabolic trap were derived analytically within the tight-binding approximation.

[3]The computation of the eigenstates, done by numerical diagonalisation of the single-particle part $h_i$ of the Hamiltonian Eq. 3.1 (with $N = 1$) is in good agreement with this simple model $\tilde{h}_i$.

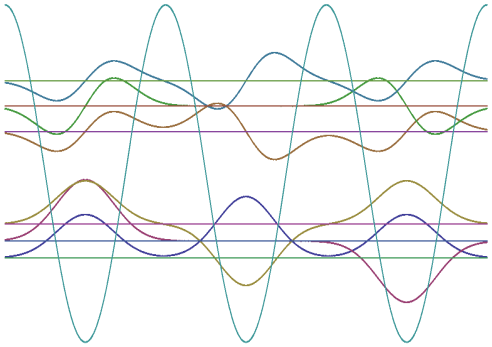

Figure 3.1: Sketch of the finite three-well lattice and the corresponding single-particle states for the first two bands.

### 3.1.3 Bose-Hubbard model

Bosons in optical lattices have bee mostly studied in the literature within the Bose-Hubbard model [44, 2], employing the tight-binding and lowest band approximation. Apart from the coupling term $J$ and the on-site energies $\epsilon_s$ introduced in $\tilde{h}_i$, there is additionally on-site interaction with strength $U$ which reads for a delta contact potential $U = g \int dx |w_s(x)|^4$:

$$\hat{H}_{BH} = -J \sum_{<s,s'>} \hat{a}_s^\dagger \hat{a}_{s'} + \frac{U}{2} \sum_s \hat{a}_s^\dagger \hat{a}_s^\dagger \hat{a}_s \hat{a}_s + \sum_s \epsilon_s \hat{a}_s^\dagger \hat{a}_s \tag{3.3}$$

where $< s, s' >$ indicates the sum over nearest neighbors. Both parameters $J$ and $U$ can be tuned by the lattice constants $V_0$ and $d$. Increasing for example the laser intensity, the lattice becomes deeper, and thus the ratio $U/J$ increases substantially leading to the MI phase in the commensurate case: the atoms save interaction energy by being localized in different wells and the tunneling to neighboring sites is strongly suppressed. The SF phase on the other hand, is characterized by phase coherence and delocalization of the atoms. Quantum phase transitions at zero temperature are triggered by quantum fluctuations, and in this sense, we can examine in our few-body ensembles signatures of the MI and SF phase. We use as a measure of localization, the local (on-site) particle number fluctuations:

$$\Delta {N_s}^2 = \langle {n_s}^2 \rangle - \langle n_s \rangle^2 = N[\rho_{2_s}(N-1) + \rho_{1_s}(1 - N\rho_{1_s})] \tag{3.4}$$

where $\rho_{1_s} = \int_s dx \rho(x)$ and $\rho_{2_s} = \int_s \int_s dx_1 dx_2 \rho(x_1, x_2)$ are the one- and two- body densities respectively, integrated over the lattice site $s$. The SF-MI transition is accompanied by decreasing and finally vanishing fluctuations $\Delta N_s$ as $U/J$ increases (corresponding in some sense to vanishing local compressibility in the MI phase [93]). Another sign of the transition is the loss of coherence because of the localization of the atoms in individual sites. This can be observed in the momentum distribution, where the visibility of the interference peaks in the coherent SF phase is reduced, ending up with a smoothened incoherent Gaussian-like profile in the MI regime [7]. Recent advances in experiments with single-site probing make it possible to exactly measure the structure of the density in the lattice, revealing mott cells of one two three and four atoms per cite [108].

For filling factors higher than one, $\nu \equiv \frac{N}{W} > 1$ and strong interactions it is necessary to go beyond the simple BHM, which assumes unperturbed Wannier orbitals and is restricted to the lowest band, one has to include higher band effects [107] to examine the fermionization and generally strong correlation effects. The Bose-Fermi map already indicates that the lowest band levels are not sufficient to accommodate a number of fermionized bosons larger than the number of wells. Let us briefly mention effective models relevant for the discussion of filling factors higher than one. A modulation of the Wannier functions to take into account on-site interaction effects has been proposed [107, 109, 110] or splitting into two orbitals into the same well [45]. Another recent few-body study suggests to optimize the BHM parameters such that they agree with the exact results specifically in the strongly interacting regime [111]. Besides this, the concept of extended fermionization valid in the extreme limit of BHM $U/J \to \infty$ under the assumption that the atoms occupy different layers of MI and SF character [112] gives a valuable picture for situations where an incommensurate fraction of atoms sits on a commensurate localized background. We need to emphasize that the following results are obtained by the numerically exact MCTDH method and we only refer to other models for explanation and comparison. Nevertheless in the end of this section we propose and test the extension of the CPWF to lattices as an alternative bottom-up approach to effects beyond Bose-Hubbard physics.

### 3.1.4 Commensurate filling factor $\nu = 1$

The SF-MI transition arises only for commensurate setups, since for incommensurate ones there is always a delocalised (SF) fraction of atoms. We will examine two cases of commensurate filling: $\nu \equiv \frac{N}{W} = 1$ and $\nu = 2$, the latter being particularly interesting for the study of on-site interaction effects with two atoms per site (see next subsection 3.1.5). The former case discussed here is important to understand the basic features of the system which also agree with the predictions of the BHM.

**The spatial distribution of the atoms** For the non-interacting ground state, the density of atoms is larger for the middle sites and decreases as we go to the outer ones, illustrated here for 6 wells and 6 atoms in Fig. 3.2(a) for $g = 0$. This occurs for setups with hard-wall boundary conditions but is generally characteristic of finite lattices (independent of the number of sites and atoms), since the kinetic energy term renders the middle wells energetically more favorable. We remark that the atoms reside all in the same single-particle ground state which has indeed the maximal density in the middle: $\rho_{1s} \propto |\sin\left(\frac{s\pi}{W+1}\right)|^2$ (see Eqs. 3.2, 3.4 and Fig. 3.1).

As the interaction strength increases (Fig. 3.2(a)), we observe a gradual redistribution of the density which leads to equal population of all sites. Let us explain this observation in terms of the BHM which predicts a simple localization process where each atom sits in one well to save interaction energy. In the Fock state representation $|N_1, N_2, ..., N_W\rangle$, where each basis vector is parametrized by the occupation numbers for each site, with increasing $U/J$, the vector which has no double occupation $|1, 1, 1, ...\rangle$ becomes the lowest eigenstate of the BHM Hamiltonian. As soon as the atoms localize (one per well), the increase of the interaction does not affect them anymore. In this fermionization limit their energy actually saturates to the fermionic value. Here $J$ is fixed (since there is a fixed depth $V_0 = 12.0$ corresponding to $6.2E_R$ with $d = 1.6$) and $U$ varies with $g$. In this special case $\nu = 1$ and in general for $\nu \leq 1$, the Bose-Fermi map does not hold only for the abstract state $\Psi_{\mathrm{TG}} \longleftrightarrow \Psi_{\mathrm{fer}}$ but also for the Wannier state [104, 105, 46]. In other words, the $U/J \to \infty$ limit of the BHM where each atoms sits in one well $|1, 1, 1, ...\rangle$, is here equivalent to the fermionization limit, where each atom occupies a single-particle level. Thus the BHM is valid in the case of $\nu = 1$ for the whole range of interactions. In Fig. 3.2(b) (inset) we plot the population of each well, $N\rho_{1_s}$, as a function of the interaction strength.

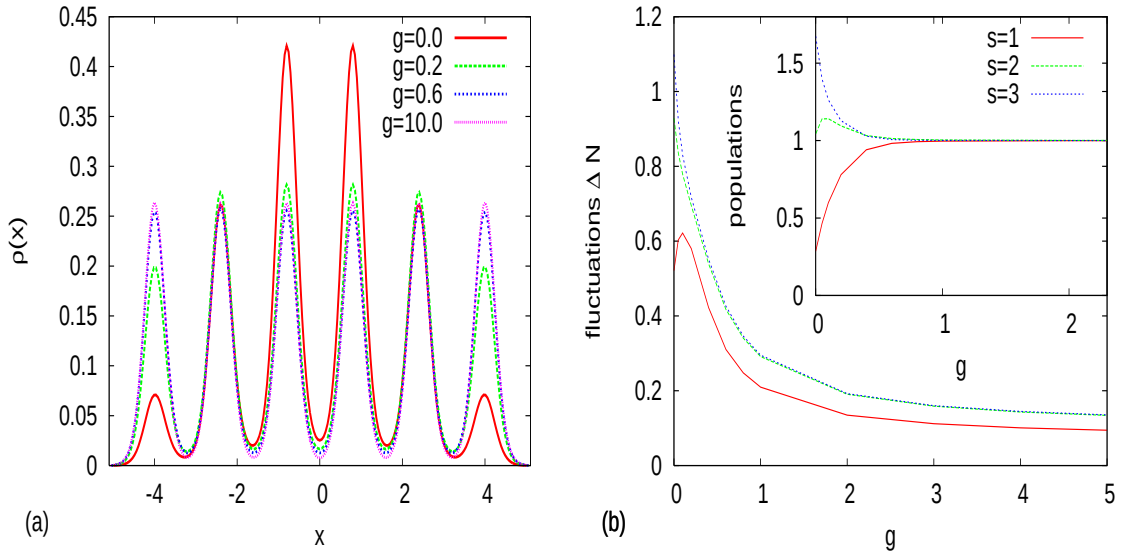


Figure 3.2: (a) One body-densities $\rho(x)$ for 6 wells and 6 atoms corresponding to different values of $g$: non interacting ($g = 0.0$), weakly interacting ($g = 0.2, 0.6$), Mott insulator-fermionization limit ($g = 10.0$). (b) Particle number fluctuations as $g$ increases: red, green and blue lines correspond to the left 3 wells $s = 1, 2, 3$ counting from the outermost one. (inset) On-site population as $g$ increases.

While for the outer ($s = 1$) and middle ($s = 3$) wells the population evolves monotonically to the final value, the intermediate wells (see $s = 2$) act as a 'carrier' of atoms and thus their population may exceed for some intermediate interaction strength ($g \approx 0.1$) their final one.

**Diminishing fluctuations as a sign of localization** The uniformisation of the population with increasing interaction strength is a pre-signature for the localization. A more accurate measure indicative for this mechanism, is the particle number fluctuations (Eq. 3.4) which decrease substantially as the interaction increases [Fig. 3.2(b)]. Of course, a lower $J$, corresponding to a deeper lattice, enhances the localization process. For a very deep lattice $U/J \to \infty$ we expect them to vanish completely, while in our case they saturate to a small value. The rather shallow depth of our lattice permits an occupation of the interwell space with a non-zero overlap between atoms sitting in neighboring sites. Including this area into the integrations of the one- and two-body density (Eq. 3.4) we end up with a small contribution to the fluctuations even in the strongly interacting limit. Note also that the middle wells ($s = 3$), which can 'lose' population with respect to both sides, keep on having larger fluctuations than the outer ones ($s = 1$).

In Fig. 3.2(b) we observe that the fluctuations converge to a constant value for $g \approx 3.0$. This convergence happens for values of $g$ significantly larger than those where the uniform distribution of the population is achieved ($g = 0.6$ Fig. 4.2(b) inset). Technically speaking, particle-hole excitations like $|2, 0, 1, ...\rangle$, $|0, 2, 1, ...\rangle$ contribute to the ground state vector for $g \approx 0.6$ resulting in an equal site distribution but without forming a localized state $|1, 1, .., 1\rangle$. Perfect localization occurs only when the latter vector is the eigenstate of the system suppressing all other contributions.

Let us point out here the effect of the hard wall in comparison with periodic boundary conditions. In our confined system for weak interactions, the Fock states with less occupation in the outer wells outweigh those with less occupation in the center and therefore we observe

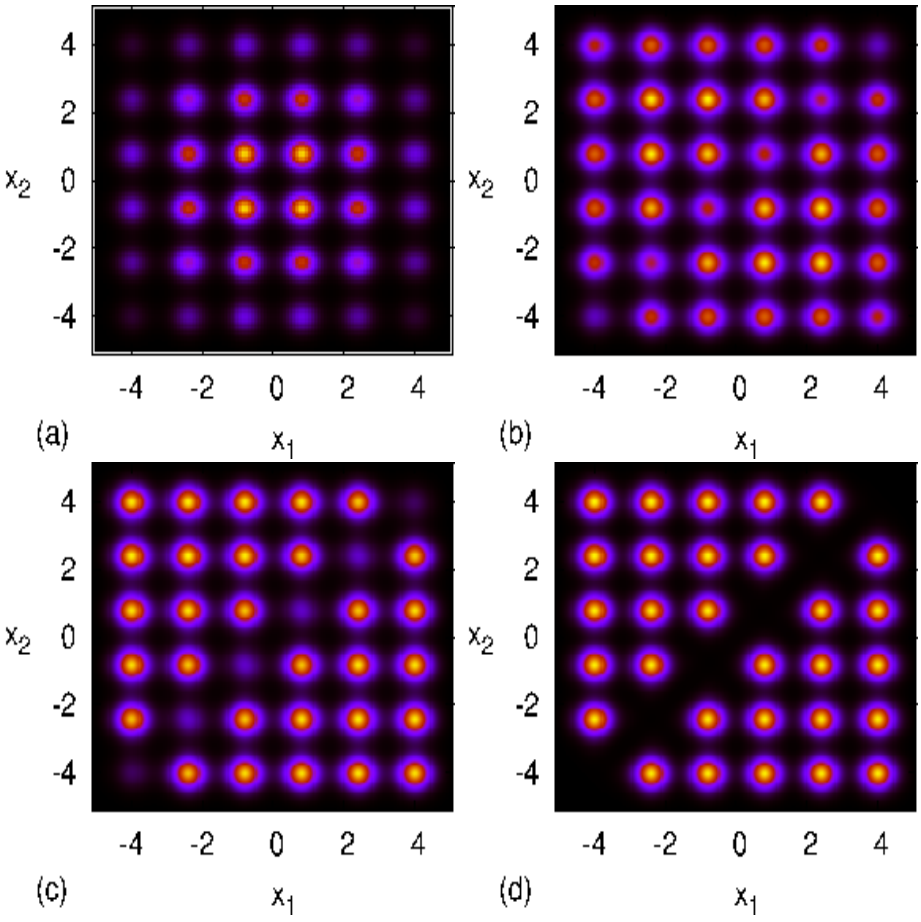


Figure 3.3: Two body-density $\rho_2(x_1, x_2)$ for 6 wells and 6 atoms. Shown are 4 values of the interaction strength (a) $g = 0.0$, (b) $g = 0.2$, (c) $g = 0.6$, (d) $g = 10.0$.

an imbalance of the sites population. In the case of periodic boundary conditions even the non-interacting state possesses a uniform population of the sites due to symmetry. Hence, what really happens in the latter case within the transition from weak to strong interactions, is only a reduction of fluctuations by going to the state $|1, 1, 1, ...\rangle$, and not a redistribution of the site populations as in our case.

**Two-body correlations** The two-body density $\rho_2(x_1, x_2)$ plotted in Fig. 3.3, gradually shows full depletion of the diagonal ($x_1 = x_2$) as the interaction increases[4]. . Starting from $g = 0$ and for increasing interactions ($g = 0.2$), the diagonal peaks indicating double occupation (especially the middle) fade out, while the off-diagonal ones are amplified. In the regime where equal distribution over the sites has been achieved ($g = 0.6$), the diagonal of the two body density has not yet been fully emptied, a sign that some double occupation is still present and thus a true localized state with unit filling is not yet reached (in accordance with the previous observations). For $g \to \infty$ the repulsive forces mimic the Pauli exclusion principle preventing two atoms from being at the same spot. As a result, if one atom sits in one well, any second one distributes itself equally over the other wells, but has zero probability to be in the same well.

**Non-local correlations** We will next cast light on the system from the perspective of the non-local properties specifically the off-diagonal kernel of the one-body density matrix $\rho_1(x, x') \equiv$

[4]The emptying of the diagonal of the pair-correlation function reminds the situation in the harmonic trap (see Chapter 2.1), and is a general two-body effect of the repulsion

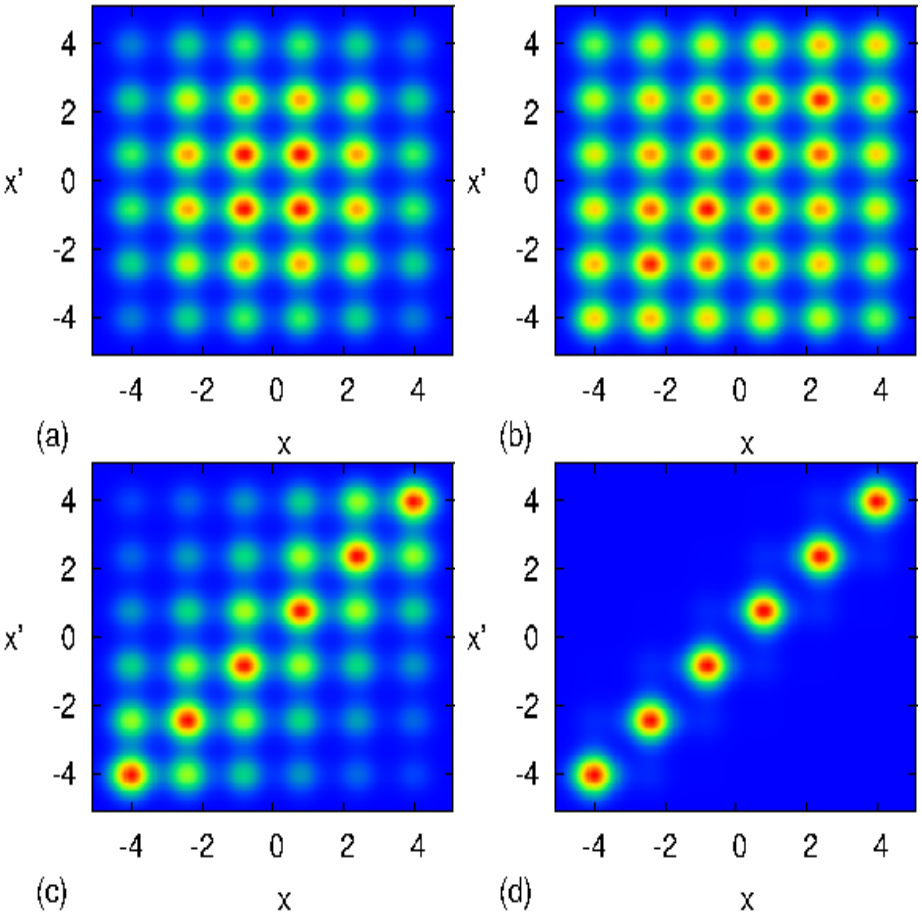


Figure 3.4: Off diagonal one-body density matrix $\rho_1(x, x')$ for 6 wells and 6 atoms for different the interaction strengths (a) $g = 0.0$, (b) $g = 0.2$, (c) $g = 0.6$, (d) $g = 10.0$.

$\langle x|\tilde{\rho}_1|x'\rangle$ and the momentum distribution. While the local properties in the TG-limit have exactly the fermionic profile, the bosonic permutation symmetry plays a significant role for the coherence properties (see also Chapter 1). The off-diagonal behaviour of $\rho_1(x, x')$ as $|x - x'| \to \infty$ is a measure of coherence [113]: it indicates non-vanishing off-diagonal long range order (ODLRO) in infinite homogeneous systems. In our finite setups though there can be no true ODLRO, so the term *coherence* refers here to the off-diagonal parts of $\rho_1(x, x')$ showing short and long range one-particle correlations.

For zero interactions (see Fig. 3.4 $g = 0.0$) we observe that the off-diagonal spots fade out for an increasing distance from the center as expected for a confined system. For weak interactions ($g = 0.2$), the off-diagonal contributions -especially the remote ones- become more pronounced, along with the outer wells on the diagonal. This is a common feature for finite setups, being accompanied by the initial density redistribution. The atoms redistribute all over the lattice such that they reduce the interaction energy, and as long as they stay in one orbital (see explanation later on), increase the correlations all over the space. As the interaction strength increases further ($g = 0.6$), the localization on discrete sites gradually destroys the ODLRO . However, some short range coherence persists as the distribution of the atoms becomes uniform ($g = 0.6$) and dies out for a stronger value of the interaction strength ($g = 10.0$). This matches with our previous observation, that the diminishing of the fluctuations and coherence in the MI phase does not necessarily coincide with the appearance of a uniform population.

**Momentum distribution** The off-diagonal part of the one-body density matrix is not an observable but it is indirectly accessible via time-of-flight measurements [2, 1], which yield the

momentum distribution $\tilde{\rho}(k)$:

$$\tilde{\rho}(k) = 2\pi\langle k|\rho_1|k\rangle = \int dx \int dx' e^{-ik(x-x')}\rho_1(x,x'). \tag{3.5}$$

The time-of-flight measurement is one of the first tools that optical-lattice experimentalists used [7, 2] switching of the light and letting the cloud fall and get absorbed. The wavefunctions at each lattice site expand and interfere with each other. The interference pattern reveals the momentum distribution and the degree of coherence of the system.

In Fig. 3.5(a) we observe that $\rho(k)$ exposes a rich pattern for $g = 0$ with Bragg peaks near the reciprocal lattice vector ($k = a^* = \frac{2\pi}{d}\ d = 1.6$) which is gradually smeared out as the interaction strength increases. The central peak corresponding to the ODLRO is high but gets even slightly higher for small interactions ($g = 0.05$), matching with our observation in $\rho_1(x,x')$ that the remote off-diagonal humps increase. In this SF coherent regime ($g = 0.0, 0.05, 0.2$) there occur also minor dips at the points $k_m = (m/W)a^*$, due to the suppression of standing waves with odd parity and wavelengths $\lambda_m = \frac{Wd}{m}$ ($m = 1, 2, ...$) resulting from the confinement, since the ground state possesses an even parity [107]. For $g = 0.6$ a value corresponding to uniform distribution in the density, the central peak is substantially lowered, which is a typical sign of coherence loss because of localization, but the lattice geometry fingerprints (side peaks) in the momentum profile do not vanish completely implying again imperfect localization. As the interaction increases further ($g = 10.0$), $\rho(k)$ goes to a smoothened Gaussian-like profile with complete destruction of the superfluid interference pattern and the visibility of the associated peaks [7, 107]. We end up with a 'MI-type' incoherent state.

**Fragmentation analysis via natural orbitals** The complete information in the one-body level is given by the spectral decomposition of $\tilde{\rho}_1 \equiv \sum_{l=0} n_l|\phi_l\rangle\langle\phi_l|$, where the relative populations $n_l$ serve as a measure of fragmentation into effective single-particle states $\phi_l$ (natural orbitals). In [114], a criterion for the a *non-fragmented* condensed state was introduced exactly by demanding the highest such occupation $n_0$ to be very close to one.

For zero interactions, all the atoms reside in the lowest (ground state) natural orbital (see Fig. 3.5(b) $g = 0.0$). Increasing the interaction they gradually fragment into the first $N = W = 6$ orbitals. Thus, in this case ($\nu = 1$) the effective description through the lowest-band single-particle states holds. The population of each orbital in the fermionization limit is not exactly $1/N$ as we would naively expect from a mapping to non-interacting single-particle states according to Girardeau's theorem (for fermions $n_l = 1/N$ for $l = 0, N-1$). This is because the natural orbitals are effectively modulated single-particle states originating from the spectral decomposition of $\tilde{\rho}_1$, and this modulation accounts for interaction effects. The lowest orbital $\phi_0$, for example (see Fig. 3.5(c)), is broadened for weak interactions ($g = 0.2$), following the evolution of the one-body density. The latter fact validates the use of the GPE mean-field treatment for weak interactions where all the atoms are assumed to reside in a single 'condensate orbital'. The modulation of this dominant orbital is responsible for the initial extension of the off-diagonal range in $\rho_1(x,x')$ and consequently leads to an increase of the central peak in $\rho(k)$ (see Fig. 3.5(a)). The fragmentation observed for higher interactions (see Fig. 3.5(b)), is beyond the regime of validity of the GPE, and due to the admixing of higher orbitals coherence is destroyed. This may be compared with the cases of the double well and the harmonic trap [29]: in the double well, the interaction immediately bridges the gap within the lowest-band doublet and thus destroys the coherence. Note that the ground state orbital in case of the double-well has already an equal distribution for the two wells and thus there is no dramatic flattening of the density due to the interactions as in the case of more wells examined here. In the harmonic trap there is an initial extension of the long-range order exactly for the same reason as here,

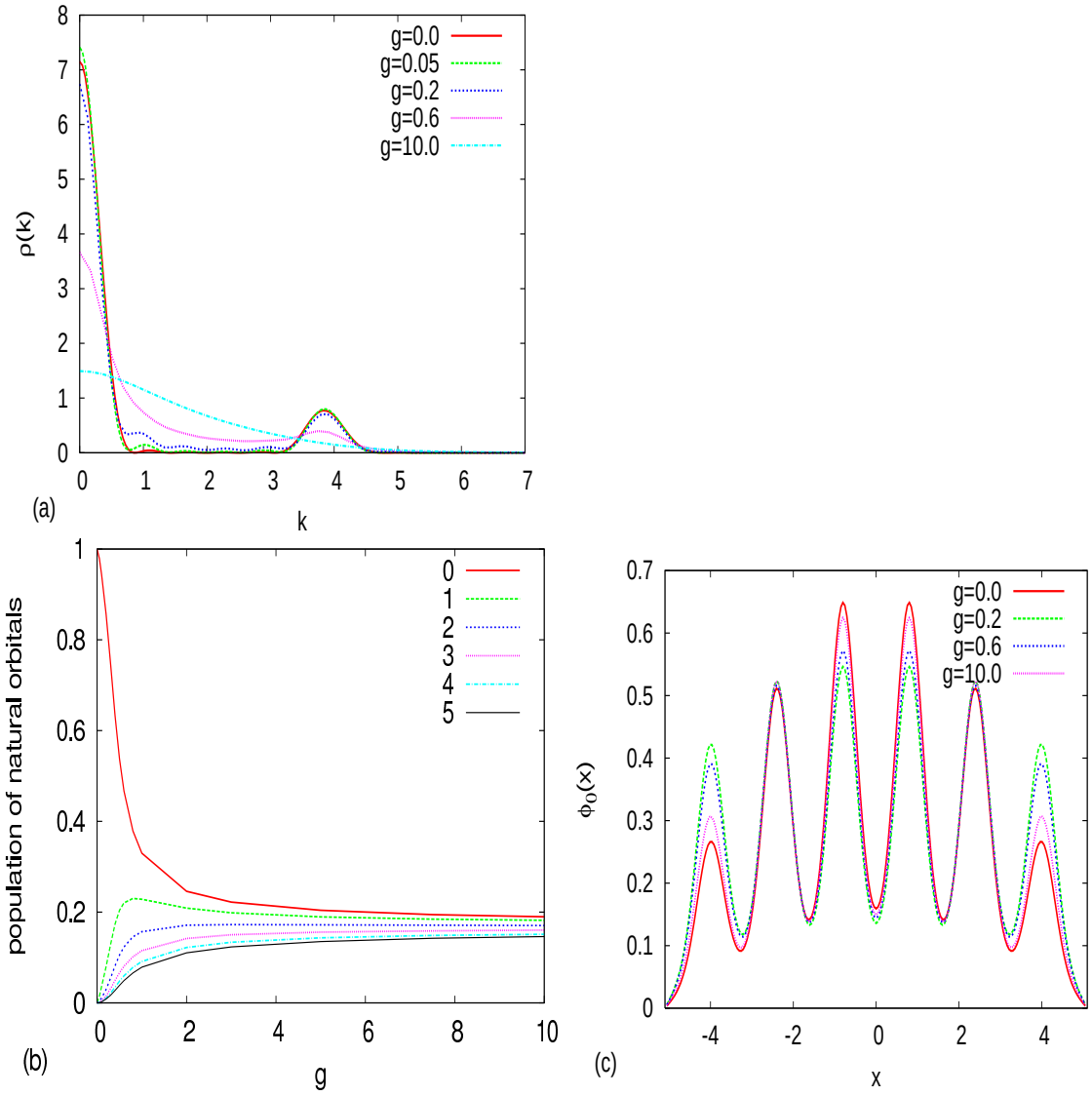


Figure 3.5: (a) Momentum distribution for 6 wells and 6 atoms. Shown are 5 different values of $g$: non interacting ($g = 0.0$), weakly interacting ($g = 0.05, 0.2, 0.6$), Mott insulator-fermionization limit ($g = 10.0$). (b) Population of the natural orbitals as a function of the interaction strength. (c) Profile of lowest natural orbital for several values of the interaction.

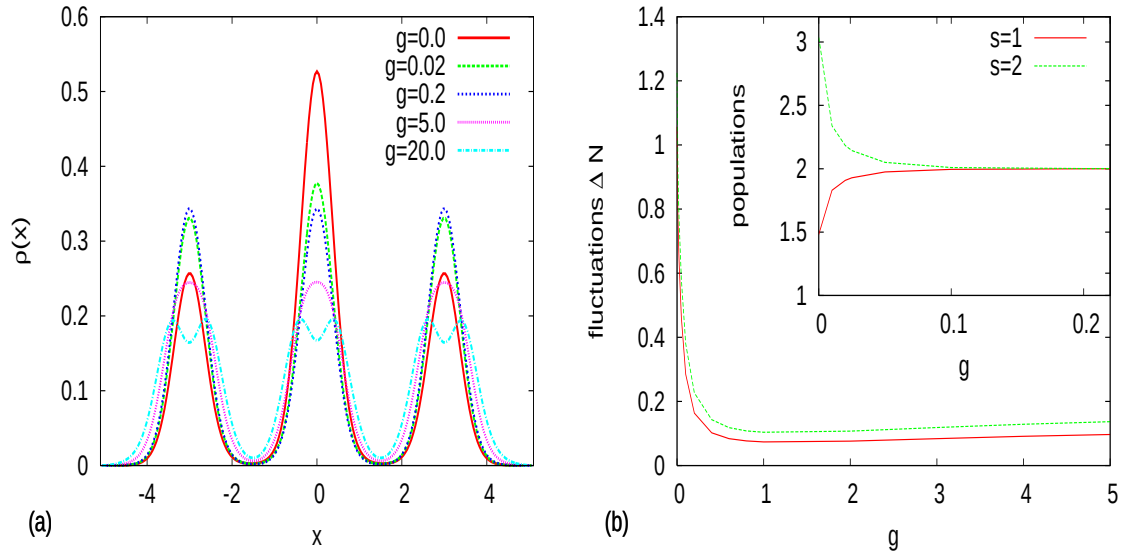


Figure 3.6: (a) One body-density $\rho(x)$ for 3 wells and 6 atoms. Shown are 5 different values of $g$: non interacting ($g = 0.0$), weakly interacting ($g = 0.02$, $g = 0.2$), and on-site fermionization crossover ($g = 5.0$, $g = 20.0$). (b) Particle number fluctuations as g increases for the left ($s = 1$) and the middle ($s = 2$) well. (inset) On-site populations.

i.e., the ground state orbital is broadened and holds the main population (the gap between the ground and the excited state is relatively large here). For very strong interactions (Fig. 3.5(c) $g = 10.0$), the profile of the orbitals tends to return to the non-interacting one indicating the validity of the Bose-Fermi map in the TG-limit.

### 3.1.5 Commensurate filling factor $\nu = 2$

The case of $\nu = 2$, is here examined for 6 atoms in 3 wells. This case is very important since we expect on-site interaction effects to be present because of the higher number density of atoms. These effects are on the focus of the extension of the CPWF that we will perform in the last part of this study. Essentially on-site effects are similar to harmonic trap effects (see Chapter 2.1) for strongly interacting bosons.

**Local densities** The one-body density $\rho(x)$ redistributes resulting to an equal population for all wells with increasing repulsion (see Fig. 3.6(a) $g = 0.2$). In terms of BHM, we have a formation of a 'Mott state' of 2 atoms per site residing in unaltered Wannier orbitals as the vector $|2, 2, 2, ...\rangle$ becomes eigenstate of the Hamiltonian for $U/J \to \infty$.

After this localization into pairs is achieved, on site interaction effects become apparent in $\rho(x)$ beyond BHM. In particular, there is a broadening of the one-body density in each well resulting from the increase of the on-site repulsion (Fig. 3.6(a) $g = 5.0$). For even stronger interactions, we observe the formation of two density maxima per site corresponding to the tendency for spatial separation (Fig. 3.6(a) $g = 20.0$). This on-site fermionization crossover is very similar to the single harmonic trap case discussed in the previous Chapter 2.1 and in this particular case of $\nu = 2$ the underlying system of two atoms in a trap [14] (see Chapter 1) shows similar patterns. This fact inspires our approach of these phenomena in terms of a generalization for lattices of the main proposal of this thesis, the CPWF (see subsection 3.1.8).

Similar patterns appear in the double well [115, 116, 117, 29] (the prototype finite lattice) and

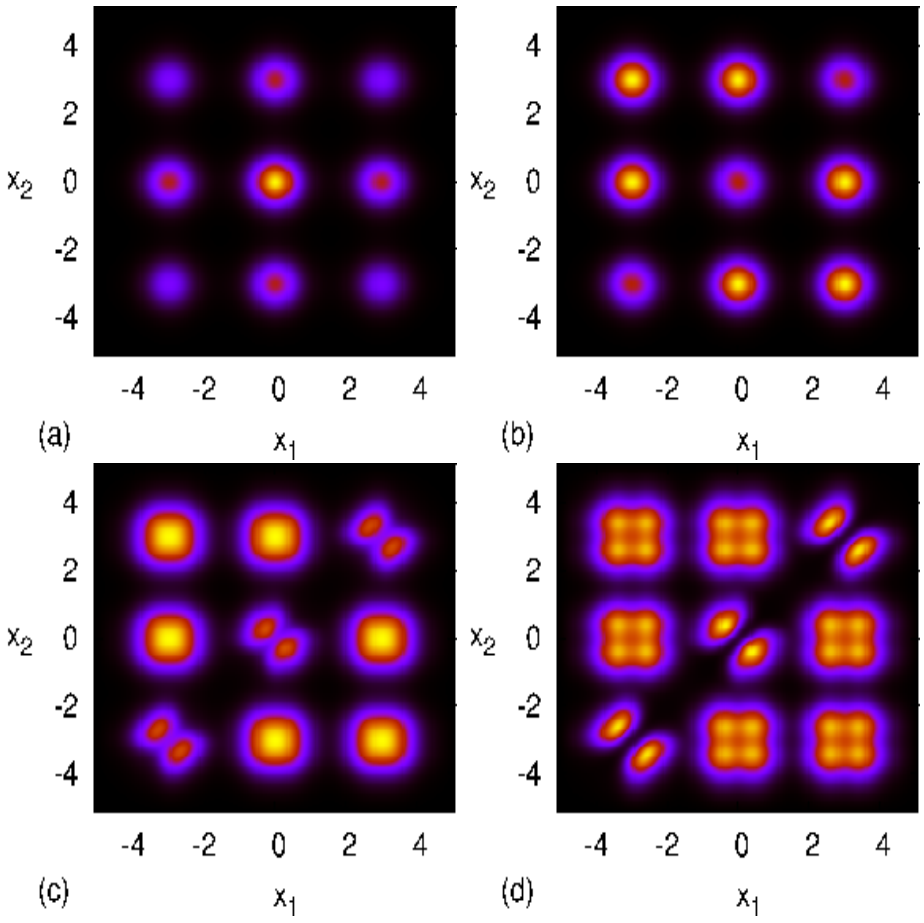


Figure 3.7: Two body-density $\rho_2(x_1, x_2)$ for 3 wells and 6 atoms for (a) $g = 0.0$, (b) $g = 0.2$, (c) $g = 5.0$, (d) $g = 20.0$.

1D lattices with periodic boundary conditions [45]. In the latter case the authors distinguish two phases: first the localization into pairs (BHM regime), and second fragmentation of each pair into two orbitals in the same well, which is consistent with our exact results. Another approach is the modulation of the Wannier localized-functions include on-site two-particle interaction effects [109]. It is important to note that the on site interaction effects appearing here, go beyond the validity of the BHM. This is because higher band contributions need to be taken into account[5]. In terms of the Bose-Fermi map, for $\nu = 2$ all the levels of the first two bands are occupied in the fermionization limit. The upper band (see Fig. 3.1) involves excited functions with one node per site. The combination of these functions with the lowest band ones, gives the observed wiggled fermionization profile with a local minimum in the middle of each well. The particle number fluctuations (Fig. 3.6(b)) together with the populations (Fig. 3.6(b) inset) illuminate the whole process: first the atoms distribute homogeneously ($g = 0.0 - 0.1$), then localize and the fluctuations tend to a low value ($g \approx 0.1 - 1.0$) as expected for commensurate filling in the MI phase, and finally each pair of atoms exhibits an individual on-site two-body crossover as described above.

In the two-body density $\rho_2(x_1, x_2)$ the diagonal contribution is reduced with increasing value of $g$ (see Fig. 3.7 $g = 0.2$). In fact the maxima on the diagonal acquire half the population of any off-diagonal one, which matches with the pair localization process leading to an equal population of all sites. For stronger interaction (see Fig. 3.7 $g = 5.0$) the formation of a correlation hole at $x_1 = x_2$ in the diagonal occurs. This is an inherent two-body effect of the on-site fermionization process which is smoothened out in the integrated one-body density (for the same interaction strengths maxima in $\rho(x)$ are not yet pronounced). The correlation hole is a significant characteristic of $\nu > 1$ filling factors in general, since it is impossible for the atoms to be in completely different wells (as they do in the $\nu = 1$ case- see above) and thus are obliged to minimize their overlap on the same site (diagonal). Nevertheless, we observe that the formation of the correlation hole begins after the localization of two atoms per well is established. Also visible in Fig. 3.7, is a broadening (for $g = 5.0$) and a fragmented pattern (for $g = 20.0$), which appear in the off-diagonal.

**Non-local properties** Regarding the non-local properties the main effects are similar to the case of $\nu = 1$. For the TG limit, $\rho_1(x, x')$ (Fig. 3.8 (a), $g = 20.0$) reflects the $N = 6$ maxima of its diagonal part $\rho_1(x, x) = \rho(x)$, while the off-diagonal shows slight short-range correlations because of the broadening of the on-site functions. In the momentum distribution the interference peaks (Bragg and central one) become lower already for the onset of interactions [ Fig. 3.8 (c)], ending up of course in a complete smoothening for strong interactions $g = 5.0, 20.0$. The TG profile ($g = 20.0$) differs from the localized (Mott) state ($g = 2.0$) in particular by the fact that the high momentum tails are more pronounced in the former case. Note that from $g = 2.0$ to $g = 5.0$ there is an increase of the $k = 0$ peak which can be attributed to the on-site broadening of the density (similar to the case of the harmonic trap, see [29]). The immediate lowering of the central peak for small interactions $g = 0.0, 0.02, 0.2$ is attributed to the deeper lattice that we use here compared to the case $\nu = 1$ in the previous subsection ($V_0 = 12.0 = 6.2E_R$ for $\nu = 1$ and $V_0 = 7.0 = 15.4E_R$ for $\nu = 2$ with $d = 3.3$). The fragmentation process is enhanced and thus the coherence is directly destroyed by admixing higher orbitals. Indeed, in a heuristic single-particle picture, the energy levels within one band

[5]In a different context an effective two-band model was introduced in ref [131]. In the course of the present research, a two band model (with the first two oscillator orbitals at each site) was also implemented and compared with the exact results. The agreement is qualitatively adequate, but a many-band approach is actually needed which make the calculation very tough. Therefore we have chosen as a better and more appropriate method in the context of this work, the modulation of the on-site function according to the CPWF. In a sense a multi-band approach is a try to catch the feature of the CPWF by an infinite expansion

come closer for a deeper lattice and thus the gap is bridged easily by the interactions. The instant approach of the populations of the contributing natural orbitals of the lowest band (see Fig. 3.8 (b) 0,1,2) accounts for this fact. Furthermore, the population of the natural orbitals goes in groups of $W$ reflecting the band structure. We have in principle contributing orbitals of the first 2 bands: orbitals 0-2 of the effective first band and 3-5 of the second band (being indistinguishable in Fig. 3.8 (c)). The first $W$ orbitals (0-2) corresponding to the lowest band have the dominant contribution and are modulated, following quite well the evolution of the one-body density, including the on site interaction effects (see eg. the lowest orbital profile in Fig. 3.8 (d)).

**General remarks and energy properties**

Let us generalize our findings before we move to the case of an incommensurate filling. The equal distribution of the density onto the lattice sites and the subsequent loss of fluctuations shown here, are also predicted by the BHM. These processes, which happen within the lowest band (and with Wannier states almost unaltered), are enhanced for a deeper lattice. On-site interaction effects occurring only for $\nu > 1$, i.e, density broadening and formation of maxima as well as correlation hole and fragmented patterns in the two-body density, only show up for strong interactions (beyond BHM) when a substantial population of atoms is well localized in one site. This fermionization crossover also applies to any integer filling factor, with the on-site phenomena involving $\nu = 2, 3, 4...$ atoms per well. The off-diagonal one-body correlations increase for increasing but weak interactions with the atoms dominantly occupying the first orbital which flattens initially. For stronger interactions the fragmentation of atoms destroys the coherence and the high visibility of the peaks in the momentum distribution is washed out to a smooth profile. For two atoms per site the high momentum tails show differences between the 'BHM insulator' and the Tonks limit.

A general comment about the behaviour of the energy is in order here. The ground state energy increases with $g$ and saturates for $g \to \infty$ to the corresponding fermionic one (see Chapter 1. One particular aspect of this crossover is the response of the energy when we switch on the interactions.. Close to $g = 0$ the slope for the energy is approximately

$$\frac{dE}{dg}\Big|_{g=0} = \frac{N(N-1)}{2} \int |\varphi_0(x)|^4 dx. \tag{3.6}$$

For hard-wall boundary conditions we know from Eq. 3.2 that with increasing the number of wells (the size of the system), the population in the center of the lattice also increases if we keep the filling factor constant. Thus one would expect that the repulsive interaction affects larger systems more strongly due to the existence of areas with higher density. On the other hand, the integral of the single-particle ground state wavefunction to the fourth power representing the interaction term in the Eq. 3.6 above, is lower for a potential with more wells as the delocalization of the state increases. The above effects cancel out resulting in an almost size-independent evolution of the ground state energy per atom as long as $N = W$ [see Fig. 3.9(a)]. Of course, for increasing filling factors interaction effects manifest more strongly in the evolution of the energy as the density plays the dominant role.

A second aspect is the energy gap between the ground and the first excited state. Let us point out that even without interactions, we have here an energy gap between the two states of the order of $J$ [see Fig. 3.9(b)]; a continuous band structure which results in a gapless spectrum in the SF regime arises only in the limit of an infinite lattice. Moreover, since the Bose-Fermi map holds also for excited states, we can compute exactly the gap in the fermionization ($g \to \infty$), which is of course the interband gap of the single-particle spectrum. In the BHM regime (see

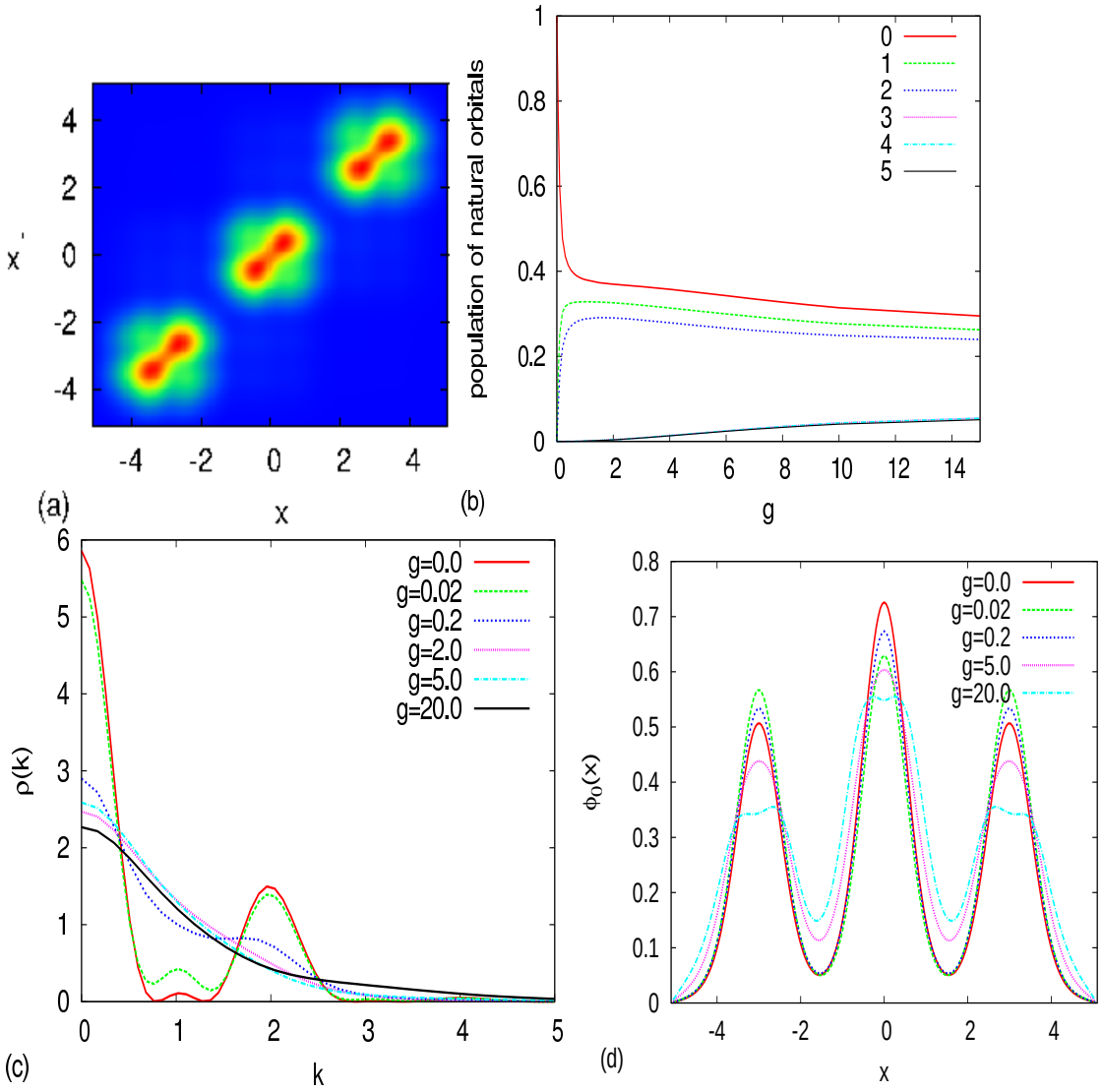


Figure 3.8: (a) One-body density matrix $\rho(x, x')$ for 3 wells and 6 atoms in the fermionization limit $g = 20.0$. (b) Population of the natural orbitals as a function of the interaction strength. (c) Momentum distribution: shown are 4 different values of $g$: non interacting ($g = 0.0$), weakly interacting ($g = 0.02, 0.2, 0.5$), on site fermionization crossover ($g = 5.0, 10.0$). (d) Profile of the lowest natural orbital for several values of the interaction.

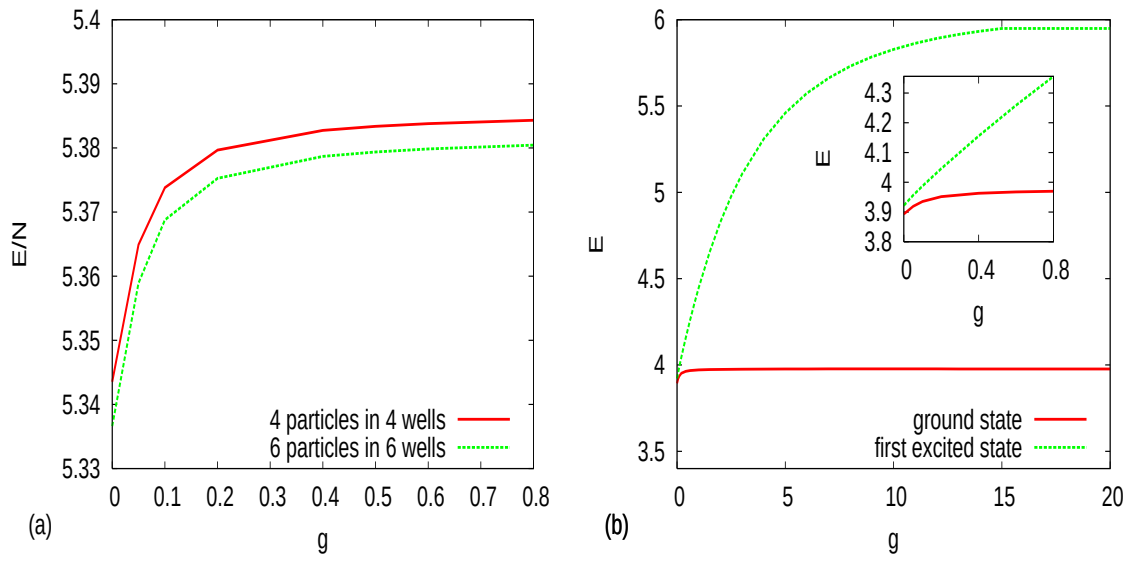


Figure 3.9: (a) Ground state energies per atom as the interaction increases for commensurate filling $\nu = 1$ for the cases 4 atoms in 4 wells and 6 atoms in 6 wells. (b) Two first eigenstates of the spectrum of 3 atoms in 3 wells as the interaction strength increases. (inset) weak interactions

Fig. 3.9(b) inset), the gap is of the order of $U$, but in general, as considered here, it is evolving continuously and occurs not as a sudden transition as it does in the macroscopic case [44, 7].

The last comment refers to the role of the kinetic energy, which is related to the parameter $J$ and this, in turn, to the lattice depth. We have already underlined its impact on the enhancement of localization and fragmentation for a lower $J$. In fact we performed all the calculations assuming a sufficiently deep lattice, such that at least two single-particle bands lie below the energy maxima of the barriers (see Fig. 3.1). This choice validates our argumentation in terms of the tight-binding approximation and also it ensures validity of the BHM for small interactions. In the other limit of a shallow lattice, a hydrodynamic approach in the framework of the sine-Gordon model has been employed [46] showing an arbitrarily small perturbative lattice potential is enough to result in an insulating phase for the TG gas with commensurate filling (see also the related experiment [47]). However, the latter discussion is based on the thermodynamic limit. For our system, if we have atoms delocalised above the barriers, then the on-site few-body effects smoothen out, and there is an interaction induced broadening leading to a filling of the space between the wells. Nevertheless, there is something important that we have to keep in mind for incommensurate filling $\nu > 1$ too (see subsection 3.1.7). As the total energy increases the atoms come energetically closer to the continuum (in other words occupy higher bands) where the barriers thin out and thus there is an enhanced penetration into the barrier (flattened on-site functions) which effectively results in larger fluctuations. A hint towards this effect is already evident in the case of $\nu = 2$ in the one body density [Fig. 3.6 (a)] where for strong interactions $g = 5.0, 20.0$ we see a slightly higher density in the inter-well space. Accordingly the fluctuations [Fig. 3.6 (b)] show a slope to slightly higher values .

### 3.1.6 Incommensurate filling factor $\nu < 1$

Incommensurate filling is more susceptible to the exact number of atoms compared to the number of wells, with one main feature: there is always a delocalised fraction of atoms which is crucial for the analysis of the observables. We consider essentially two cases of $\nu$ non-integer:

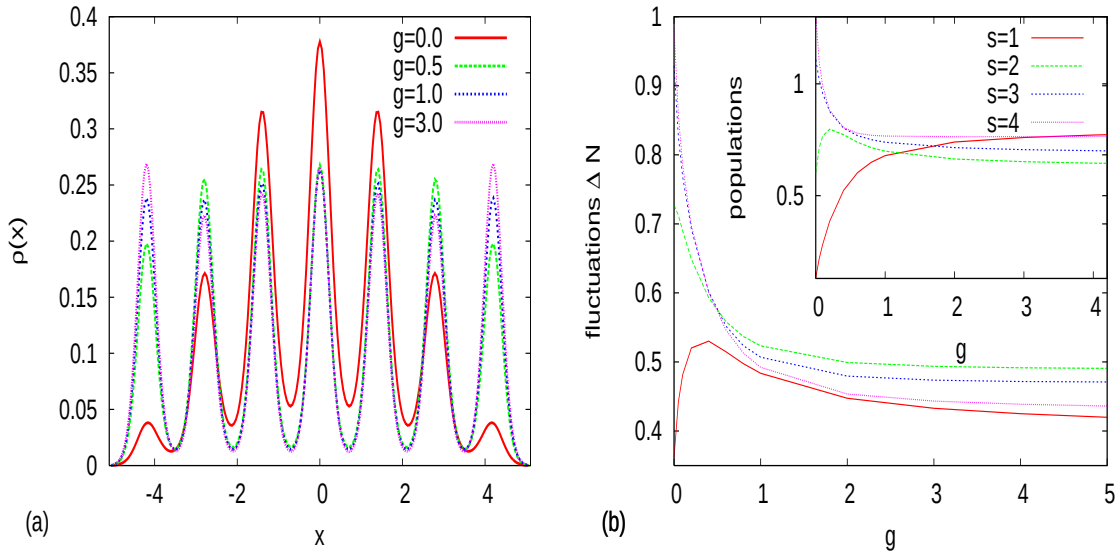


Figure 3.10: (a) One body-density for 7 wells and 5 atoms for different values of $g$: non interacting ($g = 0.0$), weakly interacting ($g = 0.5, g = 1.0$) and fermionized limit ($g = 3.0$). (b) Particle number fluctuations as g increases for the sites $s = 1, 2, 3, 4$.(inset) On-site population.

$\nu < 1$ where on-site interaction effects do not manifest due to low population and $\nu > 1$ (see next subsection) which for strong interactions can be interpreted as a fraction $N$ mod $W$ of extra delocalised atoms sitting on a commensurate background of localized atoms [112].

The main concern here is how the atoms distribute over the lattice as the repulsion increases. In the weak interaction regime, the repulsive forces drive the atoms away from the highly populated center of the potential, (see for example 5 atoms in 7 wells in Fig. 3.10 (a) for $g = 0.5,\ 1.0$). In this case the one-particle density does not tend to an equal site occupation (as in the commensurate cases), but stays even for strong interactions asymmetric ($g = 3.0$). The exact number of atoms $N$ and wells $W$ determines the fermionized distribution of the density:

$$\rho(x)_{\text{Fermi}} \propto \sum_{s}^{W} \sum_{q}^{N} |\sin\left(\frac{sq\pi}{W+1}\right)|^2 |w_s(x)|^2 \tag{3.7}$$

where $q$ includes only lowest-band states since $N < W$. Hence, the BHM is valid for the whole range of interactions. We can understand the final profile also in a hole-excitation picture where starting from the the Mott-insulator in the commensurate case $N = W$ we annihilate $W - N$ atoms $\Psi = \sum_{\alpha=1}^{N-W} a_\alpha |\text{MI}_{N=W}\rangle$. While in the case of commensurate filling $\nu = 1$ the addition of $N = W$ coefficients in Eq. 3.7 leads to equal site occupation, here we can have imbalances and oscillations of the density depending on how many orbitals contribute according to the numbers $W$ and $N$ [Fig. 3.10 (a) $g = 3.0$, Fig. 3.10 (b) inset]. Triggered by the interaction, the 'transfer' of atoms from the middle of the potential to the outer positions passes through the intermediate wells which gain and lose population (Fig. 3.10(b) inset $s = 2$). The number fluctuations in Fig. 3.10 (b) saturate to a rather high value because of the incommensurate filling $\nu < 1$ which allows only delocalised phases. The fluctuations are greater in the wells with less population corresponding to 'holes' (Fig. 3.10 (b) compare $s = 2, 3$ with $s = 1, 4$).

A main difference between commensurate and incommensurate filling is that in the latter case the 'coherence', or better the off-diagonal part of the one body density matrix $\rho_1(x, x')$, cannot vanish completely since the atoms remain in fact delocalised. The remaining one-body correlations in the fermionization limit (Fig. 3.11 (a) $g = 20.0$) are concentrated mostly close

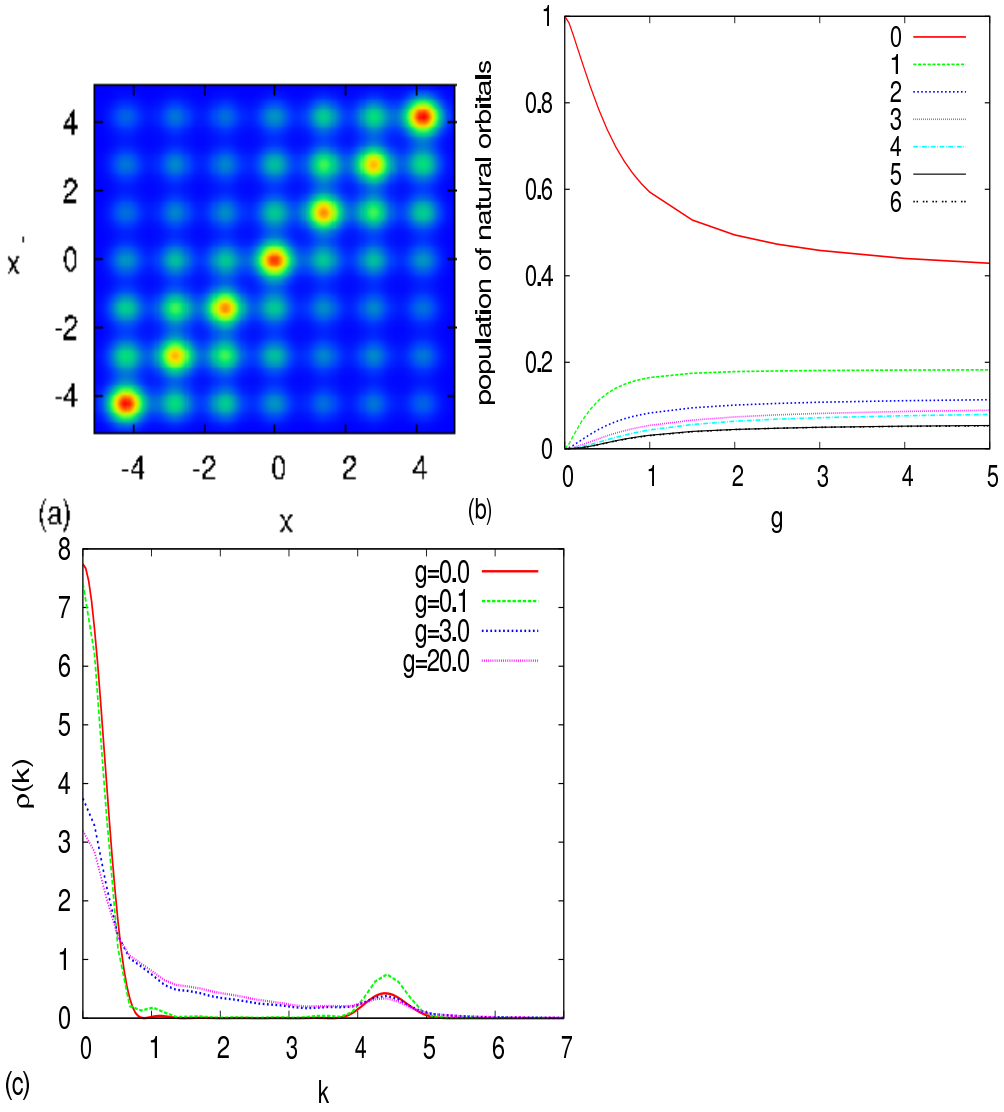


Figure 3.11: (a) $\rho_1(x, x')$ for 7 wells and 5 atoms in the fermionization limit. (b) Population of the natural orbitals as a function of $g$. (c) Momentum distribution for different values of $g$: non interacting ($g = 0.0$), weakly interacting ($g = 0.1$), fermionization limit ($g = 3.0, 20.0$).

to the diagonal, i.e., between neighboring lattice sites, although some amplitude is still visible for next to nearest neighbor sites. It is interesting though that this short range coherence is not equally distributed on all close to the diagonal spots. For example, in the case of 5 atoms in 7 wells, there is a quite well localized atom in the central site as the vanishing off-diagonal terms in the center of Fig. 3.11 (a) indicate. The distribution of short-range correlations is again related to the commensurability of the setup, and can be understood in the following way: divide the real space of the multi-well potential into N equal intervals and put each atom in the middle of one interval; then those which lie closer to the middle of a site are also better localized than those who lie close to the inter-well barriers affecting the one-body correlations accordingly, i.e., when there is more localization the correlations die out.

The attempted localization of the atoms as the repulsion increases distorts to some extent the interference pattern in the momentum distribution (Fig. 3.11 (b)). In particular the central peak is lowered due to the partial loss of coherence but the peaked structure is not fully smeared out (Fig. 3.11 (b) $g = 3.0, 20.0$). The initial increase of coherence for weak interactions is manifested

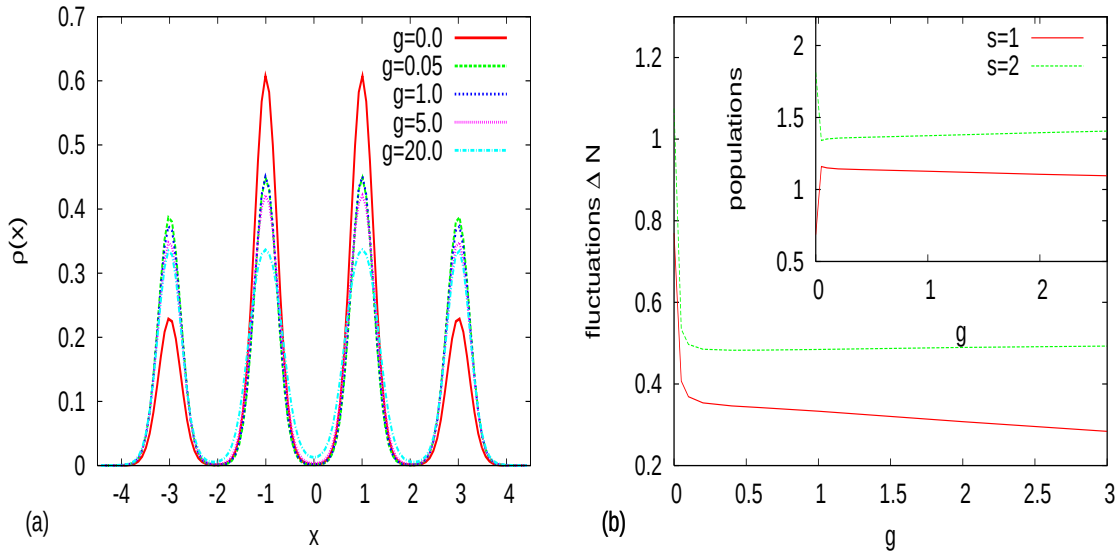


Figure 3.12: (a) One body-density for 5 atoms and 4 wells. Shown are 4 different values of $g$: non interacting ($g = 0.0$), weakly interacting ($g = 0.05, 1.0, 5.0$), fermionization limit ($g = 20.0$). (b) Particle number fluctuations as $g$ increases for the sites $s = 1, 2$. (inset) On-site populations.

by the increase of the height of the Bragg peaks ($g = 0.1$). These characteristic peaks remain also prominent in the case of fermionization, i.e., the delocalization persists. We do not observe an increase of the central peak of the momentum for low interactions as in the case of $\nu = 1$, even though we use a rather shallow lattice $V_0 = 10.0 = 4.1E_R$ with $d = 1.42$). Although the first natural orbital is broadened and dominant [Fig. 3.11 (c)], the density of 'condensed' atoms $\frac{n_0 N}{W}$ is not as high in this case of incommensurate filling $\nu < 1$ as for the case $\nu = 1$ and this explains the instant lowering of the $k = 0$ peak. As expected $W$ natural orbitals contribute substantially (see Fig. 3.11 (c)) as for $\nu = 1$, but the contribution of each orbital here, differs throughout the fermionization crossover.

### 3.1.7 Incommensurate filling factor $\nu > 1$

The incommensurate filling $\nu > 1$ case has a very rich behavior since it combines localization, delocalization as well as on-site interaction effects. It is instructive to keep in mind the properties of the corresponding $\nu^< = \frac{N \mathrm{mod} W}{W}$ filling case, which refers only to the 'extra' incommensurate fraction of $N \mathrm{mod} W$ atoms, thereby pointing out similarities and differences which allow to identify the effect of the commensurate background'[6].

#### One extra atom on a unit filling background

We begin with the simplest case of one extra atom added to the unit filling (here 5 atoms in 4 wells). For weak interactions the $g = 0$ nonuniform occupation of sites tends to become uniform [Fig. 3.12(a) $g = 0.05$]. For a slightly higher interaction strength though, there is an interesting revival of the tendency to predominantly occupy in the middle wells (compare Fig. 3.12(a) $g = 0.05$ and $g = 1.0$). To understand this, we need to go beyond the lowest band and BHM analysis (since $\nu > 1$) and consider contributions of higher bands. The higher band states possess a similar distribution with respect to the different wells as the lowest band (see $c_{s,k}$ Eq. 3.2).

[6]For all the following cases the length unit is $L/9$ and $d = 2.2$ (four wells). The lattice depth is chosen $V_0 = 20.0 = 19.6E_R$ such that the atoms are confined energetically below the continuum.

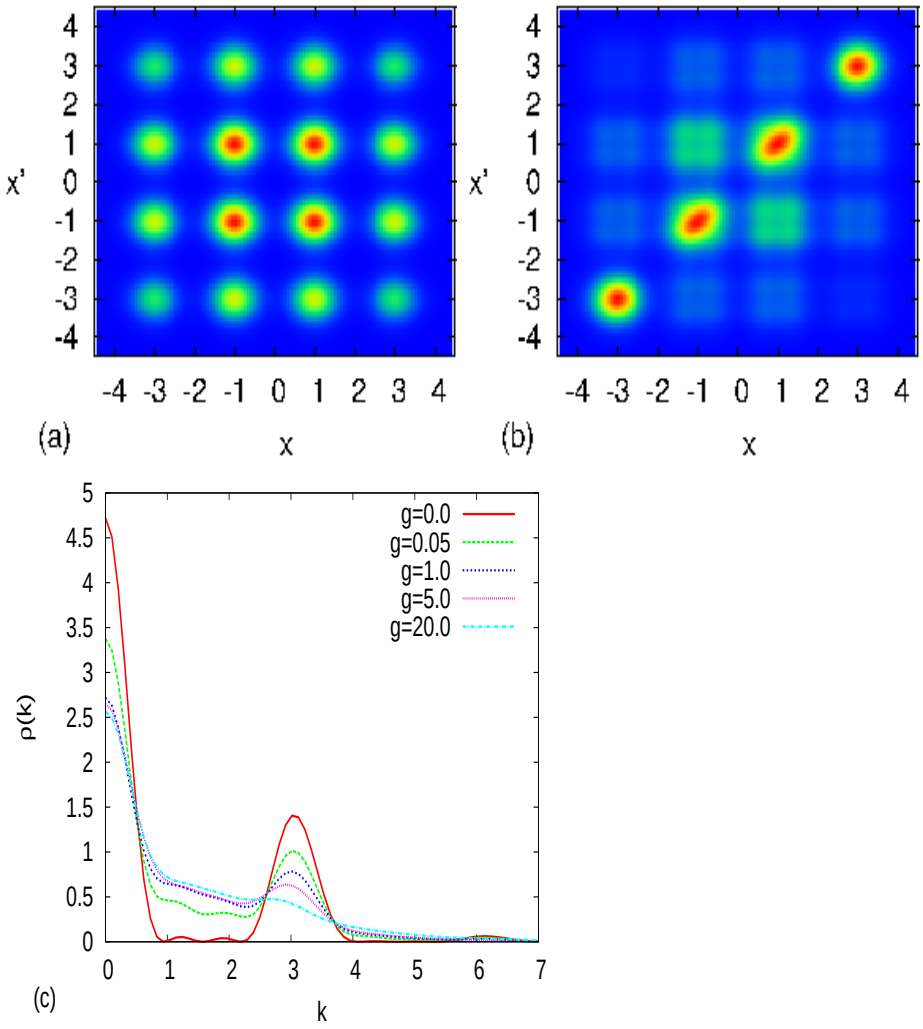


Figure 3.13: (a) One-body density matrix $\rho(x, x')$ for 5 atoms in 4 wells in the non-interacting $g = 0.0$ and (b) in the TG limit $g = 20.0$. (c) Momentum distribution for different values of $g$

Thus the energetically lowest level of the excited band, which has a dominant population in the middle (see eg. Fig. 3.1 for the triple well), when contributing, results in repopulation of the center. Additionally as the interaction increases, the total energy of the atoms becomes higher and thus they approach energetically the top of the barriers of the potential close to the continuum (see also the case $\nu = 2$). This enforces the hopping term since higher bands with larger coupling $J^1 > J^0$ contribute (compare intra-band splittings in Fig. 3.1) and as a consequence the kinetic energy term redirects the atoms to the center. This intuitive picture of contributions from higher energy states that we have drawn here for the repopulation of the middle, is also consistent with the treatment of the Tonks limit via the Bose-Fermi map, i.e., if bosons are thought as non-interacting fermions. According to the theorem, the extra atom lies exactly on the energetically lowest single-particle level of the excited band, which possesses also higher contributions in the middle, while the other atoms completely occupy the lowest band states forming a MI background of one atom localized per well. This results in a slight broadening especially of the central peaks of the one-body density (Fig. 3.12(a) $g = 20.0$), a standard on-site interaction effect for $\nu > 1$, which we encountered also in the previous section for $\nu = 2$. Let us note that the situation is quite different for a sufficiently shallow lattice not considered here: the extra atom would go closer or even above the barriers and thus would fill the inter-well space, distributing smoothly over the potential and resulting in strongly reduced two-body on-site effects [29]. A reference model to understand incommensurate filling $\nu > 1$, in qualitative agreement with our results, was given in [112]: the atoms occupy different horizontal 'layers', each one on top of the other, all having commensurate MI states and only the highest one being incommensurate (with $N \mathrm{mod} W$ atoms) and delocalised.

In the evolution of the populations with increasing $g$ we can verify the density variation in the center wells (see Fig. 3.12(b) inset). In the strongly interacting regime, the populations remain quite similar due to the background of localized atoms and they differ only because of the non-uniform distribution of the extra atom in the first level of the excited band. The particle-number fluctuations (Fig. 3.12(b)) remain quite large, since the extra delocalised atom does not allow for a perfect insulator phase. Nevertheless they are substantially diminished compared to the corresponding $\nu^< = 1/4$ single-particle case because of the localization of the background. The middle wells ($s = 2$) have larger particle-number fluctuations than the outer ($s = 1$), since the latter can 'lose or gain' population only from one side. The two-body density shown in Fig. 3.12 (c),(d) for the non-interacting and the fermionization limit, acquires a correlation hole in the diagonal, which is an inherent two-body effect for $\nu > 1$, integrated out in the one-body density. The effect is more prominent in the central diagonal peaks because of the higher population there. The off-diagonal maxima corresponding to the center wells show a slight broadening due to repulsion.

The non-local properties confirm the incomplete localization in this case. In the one body density matrix $\rho_1(x, x')$ the remaining coherence in the strongly interacting limit (Fig. 3.13 (b)), is concentrated close to the diagonal . Due to the localized background the long range off-diagonal terms almost disappear, compared to the $\nu^< = 1/4$ case of a single particle (Fig. 3.13 (a)). The off-diagonal humps, which are mainly visible in the center, reflect a widened pattern (Fig. 3.13 (b)). In general, as long as the population of the wells increases, the on-site interaction effects become more evident. In the momentum distribution (Fig. 3.13(c)) the central peak and the Bragg peaks are from very weak interactions ($g = 0.05, 1.0$) lowered because of the large depth of the potential used in this case ($V_0 = 20.0 = 19.6 E_R$). Small peaks still persist, revealing incomplete localization due to the extra atom (Fig. 3.13(c) for $g = 20.0$).

### A repulsive pair of atoms on a localized background

**One-body densities** Choosing the number of atoms and wells at will, one encounters many different incommensurate cases and corresponding effects. We focus here on the case of incommensurate filling with two extra atoms, which exhibits a distinct behaviour: the extra pair of atoms feels the interaction with the background atoms, additionally to the intra-pair repulsive forces. From the above discussion (sec IV. B.1), we recall tendencies to first equalize and then repopulate the center wells with increasing $g$. Indeed this happens also in the low-interaction regime for the case of 6 atoms in 4 wells examined here (see Fig. 3.14(a) $g = 0.1, 1.0$, Fig. 3.14(c)). It even results in a broadening of the central peaks and wiggles in the one-body density for higher interaction strengths (Fig. 3.14(a) $g = 10.0, 30.0$). To realize the peculiarity of this effect one has to consider the fermionization limit which exhibits only a slight broadening but no wiggles at all; the atoms are rather distributed uniformly in accordance to the Bose-Fermi map (Fig. 3.14(a) and Fig. 3.14 (b) for $g = 100.0$) which predicts equal contribution from the two first levels of the excited band. However, for strong but finite interactions the extra atoms concentrate more in the center resulting in an effectively higher local filling $\nu_{s=2,3} \approx 2$; only for $g > 30$ the repulsion is strong enough to drive the bosons to the outer wells.

In Fig. 3.14(c) we observe that for weak to intermediate interactions ($g \approx 0.05 - 0.8$), the populations and the fluctuations are almost constant. Beyond this regime (close to $g = 0.8$), the population of the center wells ($s = 2$) increases and approaches the value for two atoms in these sites $\nu_{s=2,3} \approx 2$, while the fluctuations are again strongly reduced. This can be understood as a localization behaviour ('Mott-like phase') in a central 'domain' of the potential in analogy with similar situations appearing for an optical lattice with a superimposed *harmonic* confinement [93, 94, 95, 96, 98, 99, 118, 119, 120]. In the latter case, the harmonic potential increases the on-site energy as we go to the outer wells and thus sets an 'energetic obstacle' for the atoms to occupy them. Therefore, they prefer to localize in the center and form Mott domains (or shells), possibly surrounded by a superfluid layer of delocalised atoms. As an illustration of this effect in our few-body setup, we present the case of 5 atoms in a 1D lattice with a superimposed harmonic trap (Fig. 3.14(a) inset). For strong interactions ($g = 30.0$ here) we have exactly two atoms in each middle well and one atom divided into the two outer wells surrounding the 'Mott-shell'. We underline that our numerically exact method which goes beyond BHM brings a new light on the strongly interacting regime including the on-site interaction effects; here we point out the formation of wiggles in the one-body density inside the 'Mott-shell' of two atoms per site. For our initial setup though there is no harmonic confinement and thus no 'energetic obstacles' between the wells; nevertheless the hard-wall boundary conditions on the edges, make it preferable for the atoms to be in the center. We can thus comment that the finite size itself makes it possible for qualitatively different spatial regions to occur in incommensurate 1D lattices. For stronger interactions, the fluctuations increase again (Fig. 3.14 (b)) as the atoms occupy higher energy levels and delocalize further. The fermionization comes with equal population $\frac{N}{W} = 1.5$ atoms per well (Fig. 3.14 (b) inset).

Similar phenomena of course can occur for other cases of incommensurate filling $\nu > 1$. The case of two extra atoms is representative, but let us stress that the exact number of wells and atoms is important for the possible effects. For example, in the case of 5 atoms in 3 wells (Fig. 3.14 (d)), the repulsively interacting extra pair of atoms is prohibited from occupying the middle well, since it would require a very undesirable triple occupation of a single site with strongly repulsive atoms. Thus the revival of occupation in the center is avoided, and each of the two extra atoms is mostly located in one outer well, indicated by the corresponding wiggles of the one-body density.

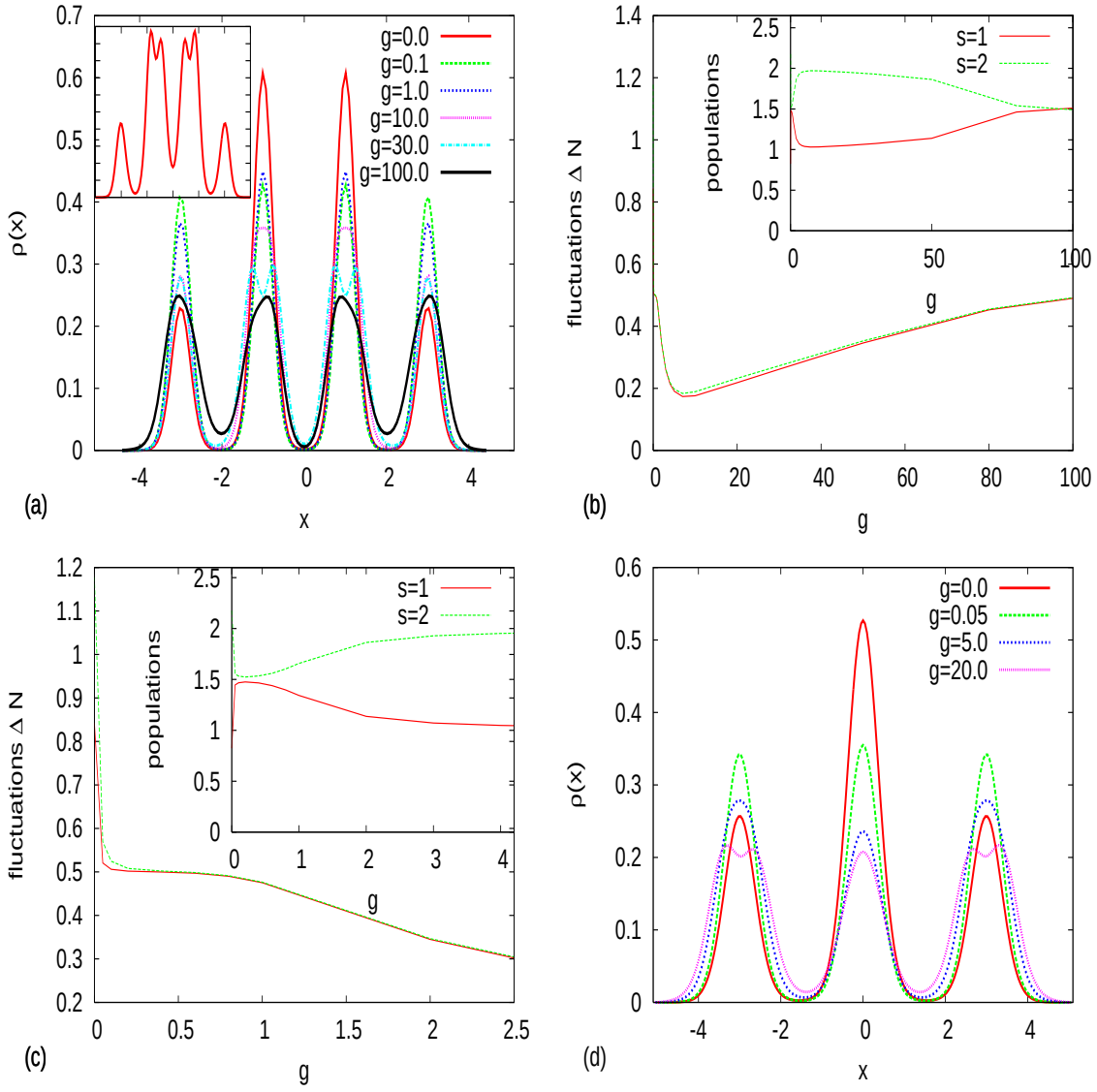


Figure 3.14: (a) One body-density for 6 atoms and 4 wells for different values of $g$: non interacting ($g = 0.0$), weakly interacting ($g = 0.1, 1.0$), strongly interacting ($g = 10.0, 30.0$) and fermionization limit ($g = 10.0$). (inset) The case of a superimposed harmonic trap with strong interactions $g = 30.0$ for 5 atoms. (b) Particle number fluctuations as a function of $g$ for $s = 1, 2$. (inset) On-site populations. (c) Same plot for the weak interaction regime. (d) One-body density for 5 atoms in 3 wells for $g = 0.0, 0.05, 5.0, 20.0$.

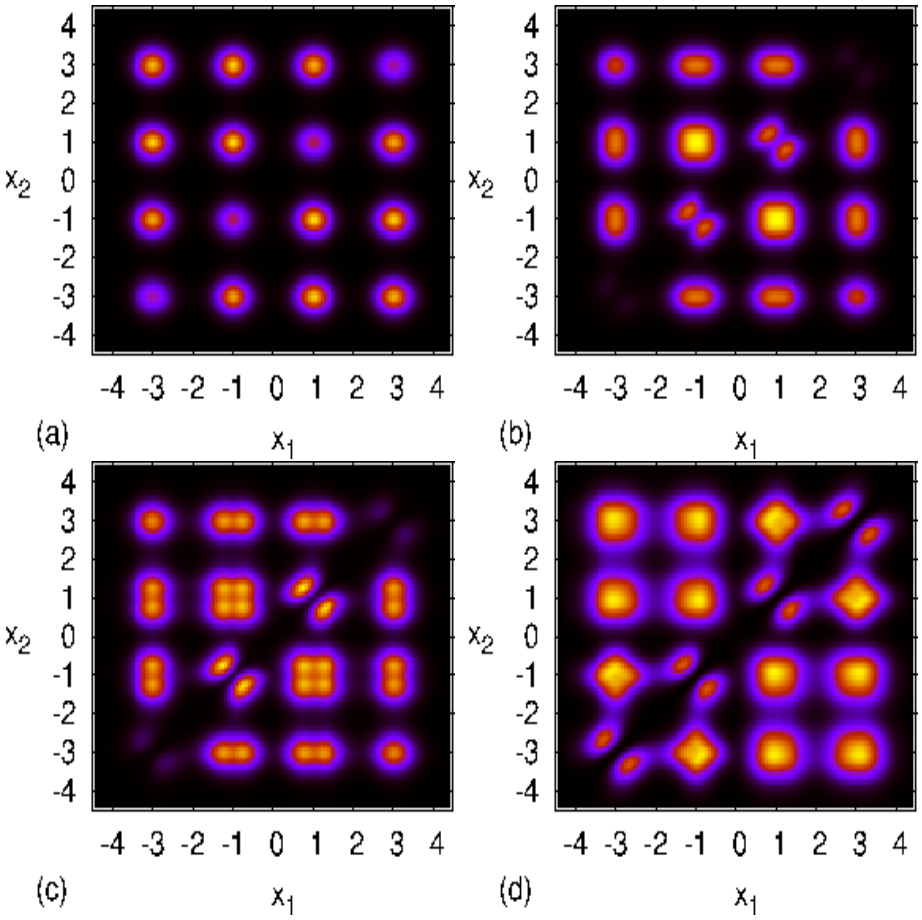


Figure 3.15: Two body-density $\rho_2(x_1, x_2)$ for 6 atoms and 4 wells for (a) $g = 0.1$, (b) $g = 10.0$, (c) $g = 30.0$, (d) $g = 100.0$.

**Two-body densities** We analyze now the case of 6 atoms in 4 wells from a two-body perspective. For weak interactions, the off-diagonal peaks of $\rho_2(x_1, x_2)$ become more pronounced than the diagonal contribution (Fig. 3.15 $g = 0.1$). For stronger interactions ($g = 10.0$) they reconcentrate in the center, the correlation hole is starting to be formed. The off-diagonal humps start to broaden in the middle and acquire fragmented patterns while the correlation hole becomes more evident ($g = 30.0$). In the fermionization limit ($g = 100.0$) the distribution on the diagonal becomes equal for all sites, and the off-diagonal contributions lose their fragmented pattern. As a last comment for the comparison of the crossover seen in the one- and two-body density, we observe that the formation of correlation hole in the diagonal of the two body-density (Fig. 3.15 $g = 10.0$) corresponds to a widening of the corresponding one-body density peaks (Fig. 3.14(a) $g = 10.0$), while the appearance of wiggles (Fig. 3.14(a) $g = 30.0$) is connected with the fragmented patterns in the corresponding off-diagonal humps of the two-body density (Fig. 3.15 $g = 30.0$).

An interesting effect occurs in this case for the one-body density matrix $\rho_1(x, x')$. The remaining coherence in the strongly interacting limit is only concentrated in the left and the right part of the space (diagonal squares in Fig. 3.16 (a),(b)). This indicates that the two extra atoms, tend to localize with respect to each other since the off-diagonal squares of this plot are completely depleted; the left is completely uncorrelated with the right part of the space. However, the extra atoms remain coherent with the background of localized atoms in the place where each of them is localized (left and right). Apparent is the formation of wiggles in the center of the diagonal for $g = 30.0$ (Fig. 3.16(a)) along with the formation of fragmented

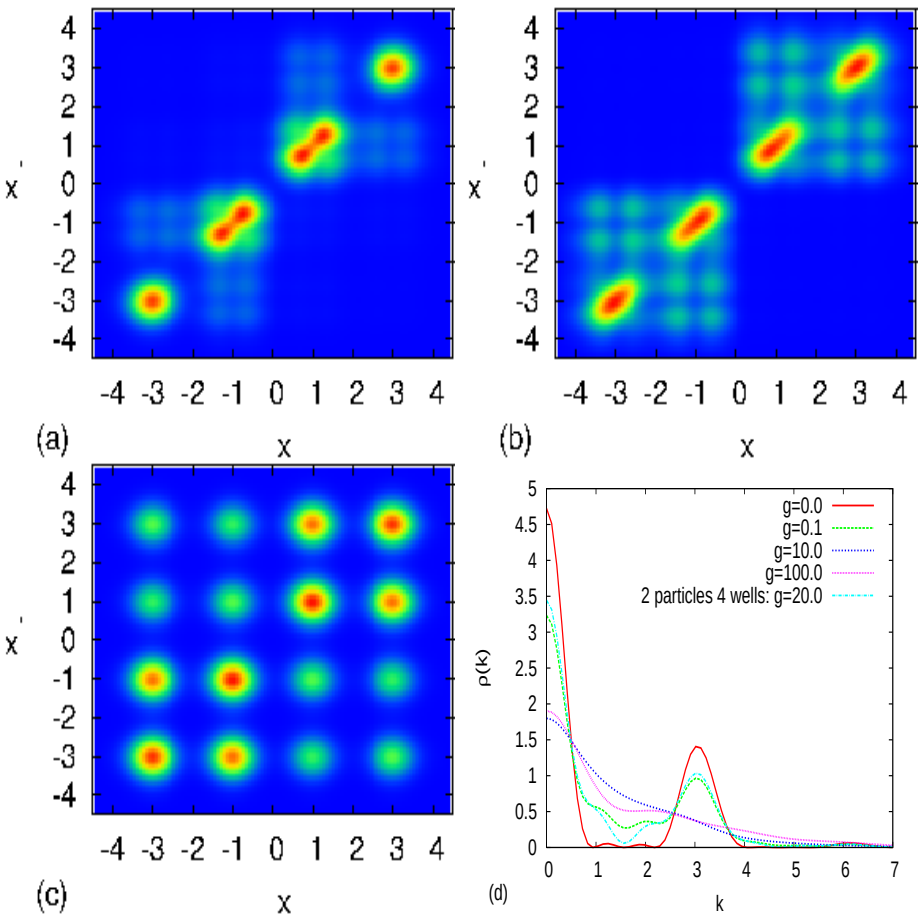


Figure 3.16: One-body density matrix $\rho(x, x')$ for 6 atoms in 4 wells (a) $g = 30.0$, (b) $g = 100$. and (c) 2 atoms in 4 wells fermionization limit $g = 20.0$. (d) Momentum distribution for 6 atoms in 4 wells for different values of $g$: non interacting ($g = 0.0$), weak interacting ($g = 0.005, 0.1, 2.0$), strong interactions ($g = 10.0, 30.0$) and TG limit ($g = 100.0$) which is compared with the TG limit of 2 atoms in 4 wells.

patterns in the remaining off-diagonal contribution. For the fermionization limit (Fig. 3.16(b) $g = 100.0$) these wiggles are smeared out to an equally broadened profile, while there is a very strongly fragmented pattern in the populated off-diagonal spots. It is worth comparing this to the fermionization limit with the corresponding $\nu^< = 2/4$ case, 2 atoms in 4 wells (Fig. 3.16 (c)). The coherence between left and right part of the potential is present in the latter case (off-diagonal squares retain contribution), which means that one atom mainly localized in the left part does penetrate into the right part. Contrarily, the background of localized atoms in the case of 6 atoms in 4 wells, prevents each of the excited extra atoms from intruding into the side where the other one sits.

The localization of the extra atoms in the two middle wells for strong interactions leads to an almost smoothened profile of the momentum distribution (Fig. 3.16(d) $g = 10.0$). As we go to the fermionization limit ($g = 100.0$), the central peak becomes a little higher, and the profile is somewhat distorted again because of the delocalization of the extra atoms. Of course the corresponding $\nu^< = 2/4$ case (Fig. 3.16(d) 2 atoms in 4 wells) is much less smoothened, since the delocalization is not hindered by any localized background.

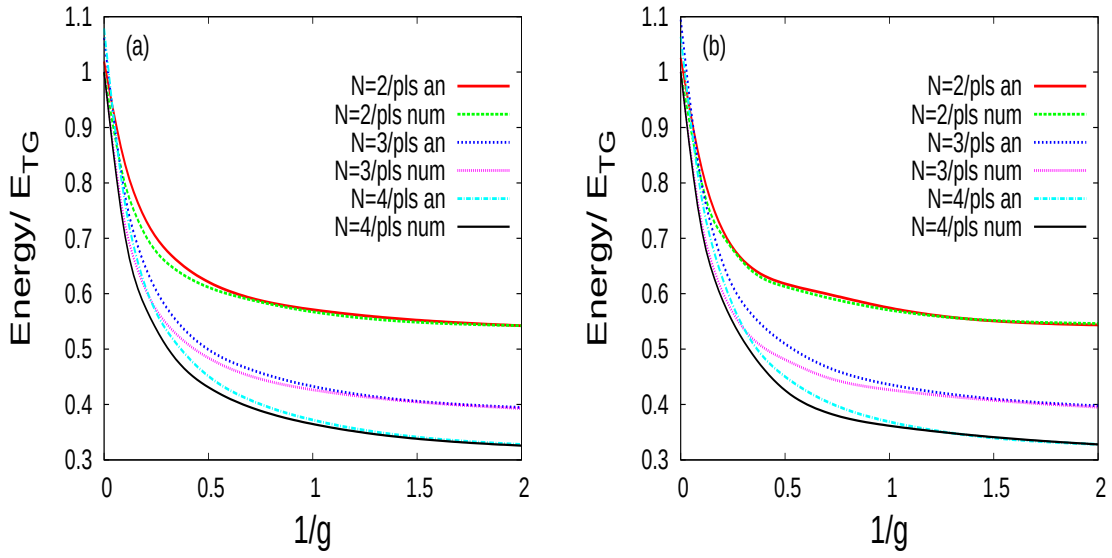


Figure 3.17: Ground state energies divided by the corresponding values of the Tonks-Girardeau (TG) limit for (a) a double and (b) a triple well as a function of the inverse interaction strength. Several cases with respect to the number of atoms per lattice site (pls) are shown, comparing numerical and analytical results.

### 3.1.8 Correlated-pair wavefunction approach

We have explored in the previous subsections few-body systems in lattice potentials. The most important finding are the on-site effects beyond the single-band BHM. Here we approach these effects via an explicit wave-function inspired from the CPWF proposed in Chapter 2.1 for the harmonic trap. The calculations for this part have been done with the Quantum Monte Carlo method (see Appendix A on computational methods). Our aim is therefore to write a Jastrow-type function as done for the harmonic trap (see Eq. 2.3) for the finite lattice potential, and check its accuracy compared with DMC calculations for the energy. Our proposal here is in the spirit of the CPWF to use for the two-body part of the trial function the exact solution two-body in a single trap (see Chapter 1). For the single-particle part we use localized Wannier functions of Gaussian profile to capture the arrangement of the atoms in the lattice, which are distorted by the hypergeometric functions inspired from the two-body problem in the trap to describe pair-correlation and on-site effects. A Variational Monte Carlo (VMC) approach allowing for one or two variational parameters has been also employed without substantial differences with respect to the evaluation of the energy compared to our parameter-free Ansatz. To overcome any restrictions of using a certain trial function, we perform a diffusion Monte-Carlo (DMC) simulation which provides us with the numerically-exact energy of the system with which we compare (see also Chapter 2.1). In a second step we demonstrate on-site features for several observables (one-body density, pair- correlation functions) captured from our analytical trial function.

We will examine here only double and triple well potentials with different commensurate filling factors[7]. The extension of the CPWF will be done keeping the two-body part (which is the core idea) but using a different SPP part for the case of a deep finite optical lattice. In the case of a perturbative lattice one could take the same approach or probably slightly

[7]The construction of these finite multi-well traps is similar to the one used previously (see Eq. 3.1) imposing hard-wall boundary conditions. Particularly here we use an optical lattice profile of the form $V_0 \sin^2\left(\frac{\pi x_i}{2\alpha} + \phi\right)$.

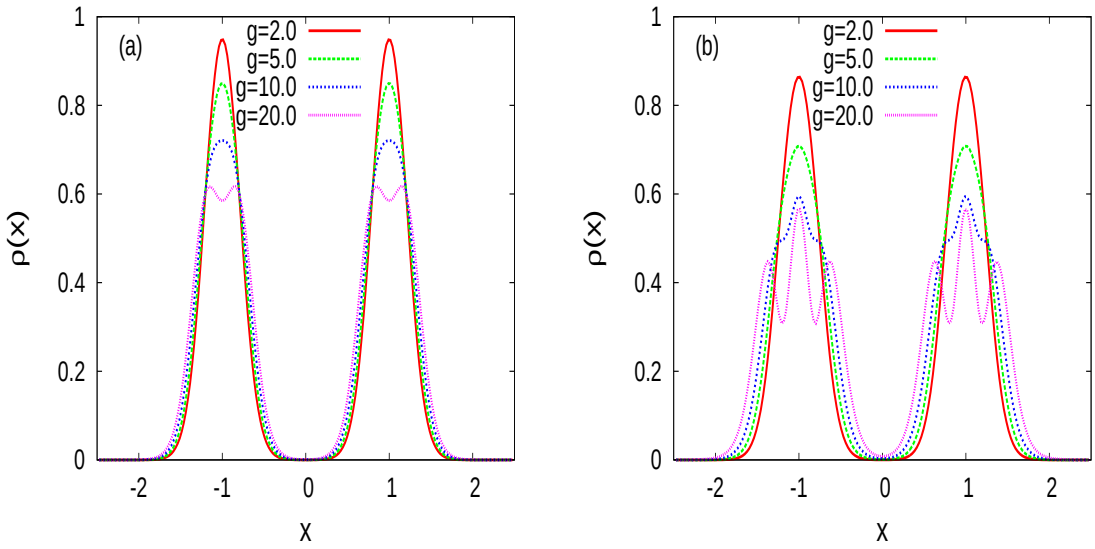


Figure 3.18: One body densities for (a) four and (b) six bosons in the double well for several interaction strengths covering the crossover from weak to strong couplings.

(Eq. 2.3) modified by an inverse lattice term for the SPP like $1-\gamma\sin^2(\pi x_i/2+\phi)$. But for a deep lattice $V_0 > 4(E_R)$ a radical change of the SPP should be employed in terms of the tight-binding model which is valid for this case, since next to next-neighbor tunneling is at least one order of magnitude smaller than nearest-neighbor tunneling. In a general sense one can write an expansion of Gaussian functions (as an approximation to the localized Wannier functions) localized at the position $x_j$ of each lattice site $j$:

$$\psi_{SPP}\left(x_i\right)=\sum_j f_j e^{-\beta(x-x_j)^2} \tag{3.9}$$

The parameter $\beta$ is related to the effective confinement frequency of each well (considered as a harmonic oscillator), and in our case can be set to $\beta=\sqrt{V_0}$. The coefficients $f_j$ are actually dependent on the interaction between the atoms, and can be in the general case derived from a Bose-Hubbard model calculation. In general for weak interaction strengths the atoms tend to be more in the center of the potential (for harmonic or hard-wall confinement), while increasing the interaction strength leads us to the Mott-insulator phase where the atoms are essentially equally populating all wells as we have seen in the previous results (or forming wedding-cake structures of several Mott shells) [44, 2]. In the case of an optical lattice plus a parabolic confinement the tight-binding model for the single-particle problem has been solved in [94] by means of Mathieu

---

The rescaled 1D Hamiltonian reads:

$$H_{\text{lat}}=-\frac{1}{2}\sum_{i=1}^{N}\frac{\partial^2}{\partial x_i^2}+\sum_{i=1}^{N}V_0\sin^2\left(\frac{\pi x_i}{2}+\phi\right)+g\sum_{i<j}\delta\left(x_{ij}\right) \tag{3.8}$$

where the lengths are scaled by the lattice constant $\alpha$ and the energies by the recoil energy $E_R=\frac{\hbar^2}{m\alpha^2}$. We further confine this infinite lattice system to a finite region $L\in[-5/2,5/2]$ (with $\phi=\pi/2$) and $L\in[-7/2,7/2]$ (with $\phi=0$) imposing hard-wall boundary conditions at the edges, such that two and three lattice sites are isolated, respectively. The Hamiltonian is characterized by two parameters: the rescaled interaction strength $g=\frac{g_{1D}}{E_R\alpha}$ and the potential depth $V_0$ (in units of $E_R$). We will consider here rather deep lattices ($V_0=40$) such that the on-site effects can be demonstrated and also a tight-binding approximation with well-localized Gaussian functions at each well which we will introduce next can be considered a good approach.

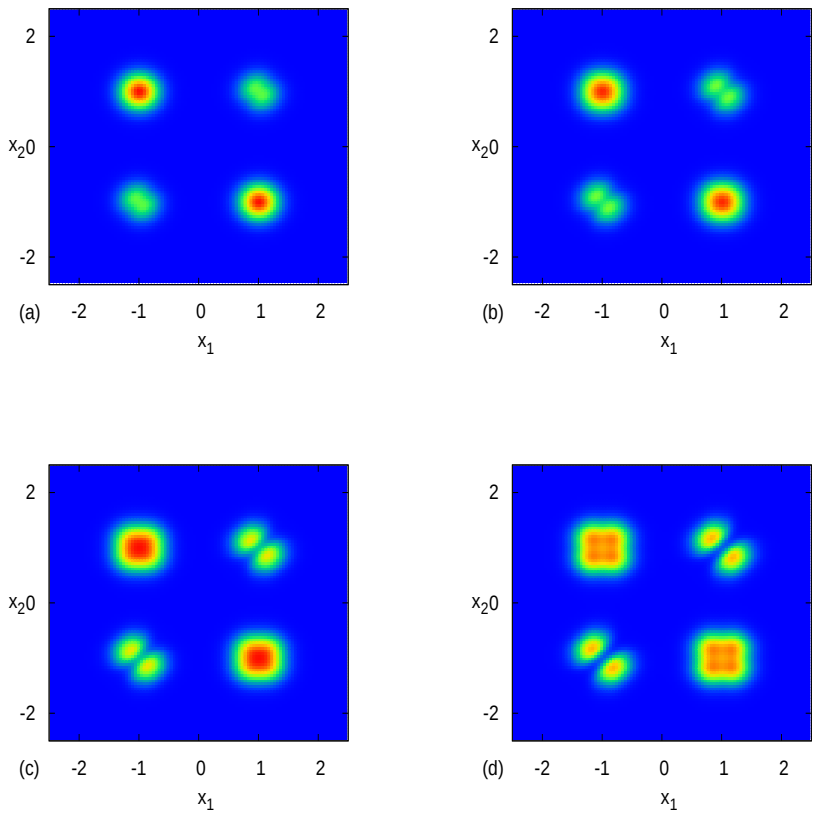


Figure 3.19: Two-body density for 4 atoms in the double well for (a) $g = 2.0$ (b) $g = 5.0$ (c) $g = 10.0$ (d) $g = 20.0$

functions which offer the coefficients for a localized functions expansion. We note here that this can be also considered as a parameter free Ansatz for the SPP provided that we use the form of Eq. 3.9 with a fixed $\beta = \sqrt{V_0}$[8]. Yet this will not cover the full range from weak to strong interactions since the distribution of weights will change with increasing interaction strength as we have seen above. We take a detour from this issue by focusing on interaction effects that appear on-site like those shown above [42] and not on the redistribution of the atoms from the superfluid to the Mott insulator state. We will examine here cases with equal population in each lattice site or obtain this equal distribution for a perturbatively weak interaction strength. We will therefore use equal coefficients ($f_j = 1$ for all $j$) in the expansion Eq. (3.9) constructing thus a direct generalization of our Ansatz for lattices (for periodic lattices this choice is actually the only reasonable). A similar approach based on the two-body solution [14] (see Chapter 1) was performed in [109].

Results from the generalization of the CPWF to finite lattice systems using the corresponding

[8] According to [94] $f_j$ are the Fourier coefficients of the Mathieu function $ce\,(x,-q)$: $f_j = \frac{1}{\pi}\int ce\,(x,-q)\cos(2jx)\,dx$. The parameter $q = \frac{8J}{\omega^2}$ where:

$$J = -\int w(x_j)\left(-\frac{1}{2}\frac{d^2}{dx^2} + V_0\sin^2(\pi x/2)\right)w(x_{j-1}) \tag{3.10}$$

characterizes the system, where $w(x)$ are the localized Wannier functions for each well . If Gaussian profile functions are used for w(x) like in Eq. 3.9 one obtains

$$q(V_0) = -\sqrt{8\pi}V_0^{1/4}e^{-2\sqrt{V_0}}\left[\left(3\sqrt{V_0}-1\right) + e^{-\frac{\pi^2}{8\sqrt{V_0}}}\sqrt{V_0}\right]. \tag{3.11}$$

.

single-particle part (Eq. 3.9) are compared in the following with DMC calculations for the energy. We consider here cases that are also relevant for cold-atom experiments, i.e., two to four atoms per lattice site [2]. In Fig. 3.17 the curves obtained from the Ansatz and the DMC are presented with respect to the same variables as in Fig. 2.2 for the double [Fig. 3.17 (a)] and the triple [Fig. 3.17 (b)] well potentials. The agreement between the trial-function and the DMC energy is very good for the case of two atoms per site both for the double and the triple well potentials. This is to be expected since the CPWF is actually the exact one in the case of a harmonic trap for two atoms (see Chapters 1, and 2.1) [14, 25]. However for three and four atoms per lattice site the deviations start to be substantial at intermediate interaction strength ($g \approx 1$) and become even stronger as we approach the resonance (see Fig. 3.17). The reason for these deviations lies in the nature of multi-well potentials. As long as the atoms stay in low energy states, which is the case for weak interactions the harmonic approach of each lattice site remains a good approximation. However, as the interaction strength increases and the atoms come energetically closer to the threshold of the barriers of the potential, each lattice site becomes more and more anharmonic, as well as the tunneling coupling to the neighboring lattice sites increases. This breaks the validity of a harmonic approach and produces deviations of the Ansatz which still though works qualitatively and as we will see next captures important properties of the on-site behaviour beyond the weak coupling and the Bose-Hubbard regime. Another important difference compared to the case of the harmonic trap is that here the fermionization limit ($g \to \infty$) is not reproduced exactly by the Ansatz, due to the anharmonicity explained above. Therefore one of the major advantages that our Ansatz proposed in Chapter 2.1 [25] possesses in the harmonic trap, namely reproducing the exact behaviour in the two limiting cases (non- and infinitely interacting ensemble) is missing here. Yet the predictions of the Ansatz are slightly better if one treats the parameter $\beta$ variationally (VMC calculations show a correction up to $1-2\%$ in the error), but certainly there is space for improvement combining probably Bose-Hubbard and exact solutions for the particular profile of the multi-well potential in the trial function.

In Fig. 3.18 the one-body density for the cases (a) four and (b) six atoms in the double well is shown. We observe that the main on-site effects from the previous results are capture from the CPWF Ansatz here: the density at each well becomes broader (see $g = 2.0, 5.0$) acquires a small plateau ($g = 10.0$) and finally develops a number of maxima corresponding to the number of atoms localized per site. In Fig. 3.19 the two-body density or pair-correlation function of 4 atoms in the double well is plotted. For weak interactions [$g = 2.0$ Fig. 3.19 (a)] we have only 4 distinct peaks due to the double well potential and as the interaction strength increases [$g = 5.0$ Fig. 3.19 (b)] the diagonal $x_1 = x_2$ tends to deplete (as seen also in the results above). For stronger interactions [$g = 10.0$ Fig. 3.19 (c)] even the off-diagonal peaks broaden while close to fermionization [$g = 20.0$ Fig. 3.19 (d)] there are additional peaks appearing at the off-diagonal spots.

**Conclusive remarks**

We have performed in this part (Chapter 3.1) a numerically exact investigation (via MCTDH) of few-boson systems in finite 1D lattices for varying strength of the repulsive interactions and extended our analytical approach in terms of CPWF to capture on-site effects on lattice geometries. In the unit filling case, we have shown the evolution from a non-interacting state with a maximum of the density in the center well to an equal site distribution and a simultaneous decrease of the fluctuations; these effects are in accordance with the predictions of the BHM, following the SF - MI transition from a delocalised to a localized state. Beyond that, for higher commensurate filling, on-site interaction effects like broadening and wiggles in the one-body density as well as correlation hole and fragmented patterns in the two body density occur especially

in the strongly repulsive limit approaching fermionization. To capture these effects analytically with a bottom-up approach we have performed a generalization of the CPWF approach for lattices and tested it via Quantum Monte Carlo calculations. Concerning non-local properties, the coherence loss due to the interaction is reflected in the reduced off-diagonal contribution in the one-body density matrix and the smoothening of the peaked pattern in the momentum distribution. The high-momentum tails show a difference between the Mott-insulator within the Bose-Hubbard model with unperturbed Wannier functions and the Tonks limit with two fermionized atoms per site. Interestingly, there is a slight increase of long-range correlations on the onset of interactions with the atoms remaining mostly in one orbital which broadens. The fragmentation into different natural orbitals for strong interactions reflects the band structure of the lattice. The effect of a deeper lattice on enhancing and accelerating these processes was pointed out. For incommensurate filling we have shown that the density distributes inhomogeneously depending on the number of atoms and wells, and partially delocalised incoherent states are formed. In particular for filling factor greater than one, the degree of localization of these extra atoms depends on the interaction strength, the presence of the background atoms as well as the specific conditions of the setup. For finite systems, it can vary locally, leading to spatial variations for the observables, in analogy with the insulating and superfluid domains which appear in the case of an additional harmonic confinement.

Our study suggests many promising routes for further investigations, like spatially inhomogeneous lattices, particularly the case of an external harmonic trap and disorder with arbitrary energy offsets between the wells. A combination of the BHM with modified Wannier localized functions inspired from the CPWF or multi-band approaches could probably provide a more accurate and insightful bottom-up approach on lattice potentials in 1D also for many-body systems. The extension of this idea to fermions or mixtures (see next Chapter 4.1) and the improvement of it to describe more accurately the full crossover may represent a valuable input to relevant experimental studies [60, 61].

## 3.2 Interband tunneling dynamics in a triple well

Another very important application of multi-well systems is the study of tunneling phenomena this fundamental quantum dynamics mechanism. Many studies both theoretical and experimental [49, 50] concentrate on mean-field tunneling mechanims. Theoretical investigations for 1D systems with MCTDH have demonstrated beyond-mean field effects [51, 52] in the crossover from correlated tunneling to fermionization effective single-particle behaviour [40]. In this part we will show beyond mean-field and single-band mechanisms of resonant tunneling in a triple well few body system. Our treatment relies on generalized number states which include multi-band structures and inter-band tunneling mechanisms. We will see that the underlying few-body spectrum in a single site (related to the 'two to many' perspective in the harmonic trap in Chapter 2.1) supports certain resonances and corresponding single- two- and in general few-body correlated tunneling in the strongly interacting regime.

The double well is the simplest case of a multi-well potential, and a plethora of phenomena have been observed and analyzed in great detail for this system [29, 115, 117, 121, 122, 123]. Loaded with a Bose-Einstein Condensate (BEC), the double well manifests itself as a bosonic analogue of the superconducting Josephson junction [18, 51]. In the low-interaction regime, the coherent phase coupling of the BEC in neighboring wells dominates the tunneling properties, and gives rise to population transfer such as Rabi oscillations and $\pi$-mode oscillations [124], while in the somewhat stronger-interaction regime, the nonlinearity introduced by the interaction dominates, and the BEC can become self-trapped [18]. On the other hand, for few-body systems, the microscopic counterpart of BECs, the tunneling between two neighboring wells also takes

place in a correlated manner, exhibiting pair tunneling in the low- to intermediate-interaction regime [50, 40], and turning to self-trapping for stronger interactions [40, 49], which indicates the intrinsic correlation between micro- and macro-ensembles of ultracold atoms. The generalization from double well to multi-well systems can provide a bottom-up understanding of mechanisms operating in the infinite optical lattice.

A straightforward natural extension of the double well is the 1D triple well. In the triple well, ultracold atoms also show correlated tunneling and self-trapping in the lower- and stronger interaction regime, respectively [125], and present at the same time novel properties such as stationary tunneling, in which the loss of coherence between bosons leads to a steady state [126]. Reference [126] provides an extensive study of the long-time evolution of the dynamical properties of micro- and macro-ensembles of bosons in the triple well. All these studies may generalize the phenomena in the double well to the optical lattices, and bridge the gap between the micro- and macro-systems, as we can see the triple well as a prototype of optical lattices. Moreover, similarly to the analogue of the double well to the Josephson junction, the triple well is the minimal system which can model the source-gate-drain junction, and draws lots of attention from the perspective of atomtronics. A variety of proposals to achieve controllable atom transport based on the triple well have been presented [127].

A widely used approximation in the study of cold atoms is the single-band approximation, which ignores the higher band contribution. This single-band approximation, working successfully in the low interaction regime, finds difficulties in the strong interaction regime, where the strong correlation between bosons suppresses the coherence, and consequently leads to phenomena such as the fragmentation of bosonic ensembles, fragmented pair tunneling and eventually breaking up of the tunneling pairs in the Tonks-Girardeau regime [50, 128]. Efforts have been done to extend the studies to the strong-interaction regime, by explicitly taking into account the higher band contributions. It has been shown that higher band effects can give rise to effective many-body interactions [129, 130], and can modify the Bloch oscillation [131] as well as Mott transition [45, 132].

In this part the stationary properties discussed before provide the basis to explore dynamics in a lattice system. We study the tunneling of a small ensemble of strongly repulsive bosons in a 1D triple-well potential. The usual treatment within the single-band approximation suggests suppression of tunneling in the strong interaction regime. However, we show that several windows of enhanced tunneling are opened in this regime. This enhanced tunneling results from higher band contributions, and has the character of interband tunneling. It can give rise to various tunneling processes, such as single-boson tunneling and two-boson correlated tunneling of the ensemble of bosons, and is robust against deformations of the triple well potential and could be used to transport cold atoms in a controllable way. We introduce a basis of generalized number states including all contributing bands to explain in a bottom-up manner the resonant tunneling mechanisms.

### 3.2.1 Setup and generalized number-state Representation

We explore the correlated quantum dynamics of a few-boson system confined to a 1D triple well depicted in Fig. 3.20(a). The bosons are initially loaded in one well with a certain interaction strength (which is obviously not a stationary state) and then we let the system evolve dynamically. The model Hamiltonian is given by Eq. 3.1 as before and the triple well is confined by hard wall boundaries[9]. The potential depth is large enough such that each well confines three

[9]We rescale here Eq. 3.1 in units of the recoil energy $E_R = \hbar^2\kappa^2/2M$, while the space and time are given in the unit of $\kappa^{-1}$ and $\hbar/E_R$, respectively. This amounts to setting $\hbar = M = \kappa = 1$. The coupling of the interaction potential now reads $g = g_{1D}M/\hbar^2\kappa$. We we apply hard-wall boundary conditions at $x = \pm 3\pi/2\kappa$. Experimentally the triple well potential can be realized, e.g., by a bichromatic optical lattice, formed by laser beams of different

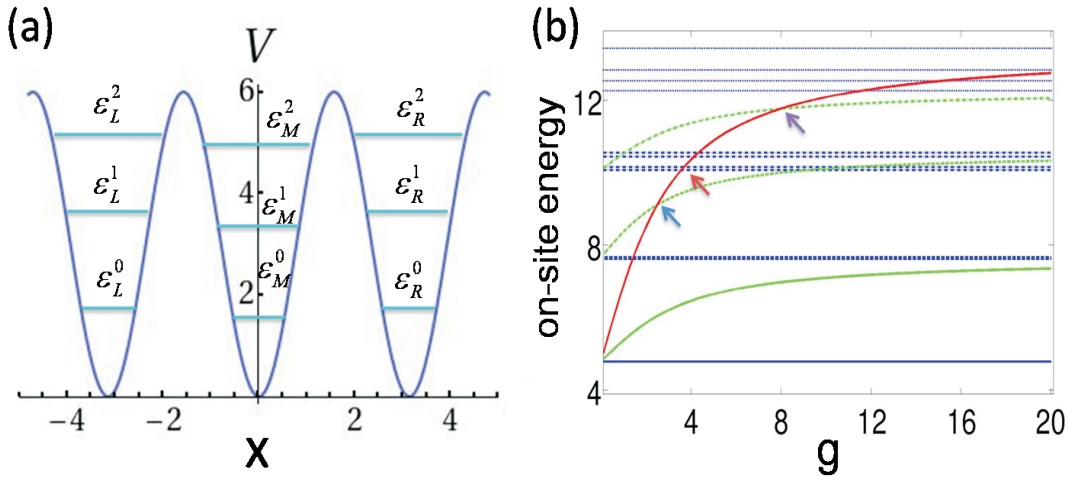


Figure 3.20: (a) Sketch of the triple well potential as well as the first three Wannier levels in each well. (b) Response of the on-site energy of different number states to the interaction strength. The red line gives the response of the triple modes, and the blue and green lines provide the response of the single modes and pair modes, respectively. number states belonging to different bands are denoted by different line types: solid - ground band, dashed - first excited band, dash-dotted - second excited band, dotted - third excited band. Arrows indicate the resonance points of the triple mode with various modes.

localized single-particle Wannier states: the ground, first excited and second excited Wannier states. As a result of the hard wall boundary conditions, the on-site energy of the Wannier states in the left and right well $\varepsilon^i_{L/R}$ is slightly larger than that of the Wannier states of the same energetic level in the middle well $\varepsilon^i_M$ ($i \in [0,2]$), as shown in Fig. 3.20(a).

We approach the dynamics of this system by a number-state representation including the contribution of different bands. This representation is closely related to the bottom-up approach and the energies of on-site configurations that we have approached previously by the CPWF (see Chapters 2.1, 3.1). In this sense it follows the bottom line of the present thesis for the approach of many-body effects via the two-body underlying system. The wavefunction of the bosons can be expanded in a series of generalized number states which encode the distribution of all the bosons among the three individual wells and the degree of excitation (in upper bands):

$$|\Psi\rangle = \sum_{\boldsymbol{N},i} C^i_{\boldsymbol{N}} |N_L, N_M, N_R\rangle_i. \tag{3.12}$$

The summation runs over all possible configurations $\boldsymbol{N} = (N_L, N_M, N_R)$, where $N_L$, $N_M$ and $N_R$ are the number of bosons localized in the left, middle and right well, respectively, with $N_L + N_M + N_R = N$.The summation runs also over the index $i$ which labels the excitations for a given configuration $\boldsymbol{N} = (N_L, N_M, N_R)$ according to their energetical order. In the spirit of the BHM the interaction takes place only for bosons siting in the same well.

The spatial representation of these generalized number states reads:

$$\langle \mathbf{x}|N_L, N_M, N_R\rangle_i = S\phi^i_{\boldsymbol{N}}(\mathbf{x} - \mathbf{r}_{\boldsymbol{N}}) \tag{3.13}$$

frequency, or a harmonic trap superimposing an optical lattice [2]. The results and findings presented here are to a large extent independent of the exact form the triple well potential and the boundary conditions.

where $S$ refers to the symmetrization operator among all the bosons, and $\mathbf{x} = (x_1, ..., x_N)$ is a vector containing the positions of all particles. $\phi^i_{\boldsymbol{N}}(\mathbf{x} - \mathbf{r}_{\boldsymbol{N}})$ is a function with multiple centers $\mathbf{r}_{\boldsymbol{N}} = (\underbrace{r_L, ..., r_L}_{N_L}, \underbrace{r_M, ..., r_M}_{N_M}, \underbrace{r_R, ..., r_R}_{N_R})$ where $\{r_L = -\pi, r_M = 0, r_R = \pi\}$ label the minimum positions of the three wells. The function $\phi^i_{\boldsymbol{N}}(\mathbf{x} - \mathbf{r}_{\boldsymbol{N}})$ possess non-zero values only in the interval $\mathbf{x} - \mathbf{r}_{\boldsymbol{N}} \in [-\pi/2, \pi/2]$ accounting for strong localization in each well (it is a very localized version of the Wannier functions). This wavefunction $\phi^i_{\boldsymbol{N}}$ satisfies the following eigenvalue problem:

$$\left[\sum_{j=1}^{N} -\frac{\hbar^2}{2M}\partial^2_{x_j} + \sum_{j=1}^{N} W(x_j) + V_I(\mathbf{x})\right] \phi^i_{\boldsymbol{N}}(\mathbf{x}) = e^i_{\boldsymbol{N}} \phi^i_{\boldsymbol{N}}(\mathbf{x}), \tag{3.14}$$

where $W(x) = V_0 sin^2(x)$ with hard wall boundary conditions at $x = \pm\pi/2$ such that the confinement is limited to a single site, and $e^i_{\boldsymbol{N}}$ is the *ith* eigenenergy. The potential $V_I(\mathbf{x})$ contains interactions only among bosons that belong to the same well eg. interactions only for the $N_L$ bosons among themselves and correspondingly for the $N_R$ and $N_L$ atoms.

The most important feature here is the response of the energies $e^i_{\boldsymbol{N}}$ to the interaction strength. As the interaction strength rises from zero to infinity, the wavefunctions of the number states change from the non-interacting form to the fermionized one [29, 25, 42], in which bosons with strong repulsive interaction in 1D avoid spatial overlap. Correspondingly, the on-site energy increases from the sum of the (non-interacting) single-particle (Wannier) energies and saturates to the corresponding value of non-interacting fermions. Tunneling dynamics appear when between these two limiting cases, the energy difference of two number states becomes much smaller than the effective coupling between them. For instance, the on-site energy of number states with lower excitation $i$, but higher degree of localization of the bosons can cross that of other number states at a particular interaction strength, resulting in an enhanced tunneling between the corresponding number states. As such tunneling directly results from the contributions of excited number states, from higher bands of the system, we refer to this enhanced tunneling as "interband" tunneling.

Let us briefly provide a comparison of the number states introduced here and in other works focusing on higher band effects. In previous works [129, 130, 131], the wavefunction is expanded with respect to the number states of non-interacting bosons, and the interaction potential is treated as a perturbation to these states. This means that these number states are just products of non-interacting single-particle Wannier functions. The perturbative treatment of the interaction potential limits such an expansion to the low-interaction regime. In our case the generation of number states intrinsically treats the interaction and the confinement potential, *i.e.*, $V_I(\mathbf{x})$ and $W(x)$ in Eq. 3.14, in an inseparable manner, so that it becomes valid in the complete interaction regime, and uncovers the interplay between the interaction potential and the confinement potential.

### 3.2.2 Mechanisms of interband tunneling

Interband tunneling is a general phenomenon insensitive to the total number of bosons, given all the bosons are well localized in the individual wells. The minimal system to unravel this phenomenon is that of three repulsively interacting bosons in the triple well. Therefore to illustrate the whole process and make clear the previously introduced concept of generalized number states we will focus on this particular example. The number states of this system can be divided into three categories: the "single mode" $\{|1,1,1\rangle_i\}$, implying that all the bosons are localized in different wells, the "pair mode" $\{|2,1,0\rangle_i, |2,0,1\rangle_i, |1,2,0\rangle_i, |0,2,1\rangle_i, |1,0,2\rangle_i, |0,1,2\rangle_i\}$, refer-

ring to that two bosons are localized in the same well, and the "triple mode" $\{|3,0,0\rangle_i, |0,3,0\rangle_i, |0,0,3\rangle_i\}$, which refers to all the bosons residing in the same site.

The three categories of number states show a different response to the increase of the interaction strength, as schematically shown in Fig. 3.20(b). For the single modes (blue lines), the on-site energy is barely affected by the interaction strength and remains constant in the complete interaction regime. It corresponds to the summation of the on-site energy of single-boson Wannier states in each well, *i.e.*, $e^i_{|1,1,1\rangle} = \varepsilon^l_L + \varepsilon^m_M + \varepsilon^n_R$, where the configuration $(l,m,n)$ depends on the degree of energetic excitation $i$. This mode is the simplest one but the generalization of such Mott-like $|1,1,1>$ configurations to possible occupation of on-site excited levels (or bands) is very important for the analysis performed here[10]. The energy crossover from weak to strong interaction for the pair-modes (green lines in Fig. 3.20(b)) reminds a lot the case of two-atoms in a harmonic trap [14]. Indeed for this single-site which is approached here as a sinus-lattice potential with hard-wall boundaries the difference with the fundamental case in the parabolic trap is only quantitative. In a sense this case and the other many-body modes can be approached by the generalization of the CPWF that lies on the core of the present thesis (Chapter 2.1,3.1) or some other effective treatment[11]. The on-site energy of the pair modes always coincides with that of the corresponding single modes in the non-interacting regime, and saturates to the next upper band of the single modes in the TG limit. For the triple modes, the on-site energy saturates to the third upper band of the single modes, and crosses several energy levels of single and pair modes in the intermediate regime (see for example the crossings indicated by arrows in Fig. 3.20(b)). These crossings are essentially the underling mechanism of interband tunneling. When the on-site energy of the triple modes crosses that of the single and pair modes of different energy levels, resonant tunneling processes take place, while away from these resonant regimes, the tunneling will be suppressed, and self-trapping is prominent. In general, windows of enhanced tunneling open on top of the self-trapping, due to the resonant coupling of number states belonging to different bands. It is worth mentioning here that if we consider only single band approximation, i.e. only number states with $i = 0$ the interband tunneling cannot occur and be analyzed.

In the following we provide several examples of the interband tunneling process by numerically exact quantum dynamical studies: The simulations are performed by applying the MCTDH method and the concept of generalized number states is used for the interpretation of our results.

### 3.2.3 Single-boson tunneling

We demonstrate the single-boson interband tunneling process for three bosons initially localized in the same well of a triple well. Let's concentrate first on the case where all atoms are loaded in the left (or equivalently rightmost) well, i.e. , the initial state is of the form $|3,0,0\rangle_0$ (triple mode). The single-band model predicts self-trapping of all the bosons in the initial well when the interaction strength is large enough. Fig. 3.21 shows the oscillation of the population in each well for different interaction strengths. As shown in Fig. 3.21(a), for the interaction strength $g = 0.1$, all the bosons remain essentially trapped in the left well, and tunneling is strongly suppressed. This indicates that the bosons become self-trapped due to the repulsive

[10]The on-site energy spectrum of the number states shown in Fig. 3.20(b), illustrates the "band-like" structure of the number states. In the figure, the "energy gap" between "bands" is to a good approximation the on-site energy difference of Wannier states of adjacent energy levels, while the energy splitting within a "band" results from the on-site energy difference of the Wannier states in the outer and middle well, *i.e.*, $\varepsilon^l_{L/R} - \varepsilon^l_M$.

[11]This holds for the energetically lower pair or triple mode, while for the corresponding excited (or higher band) modes of the generalized number state representation (eg. the upper green lines of Fig. 3.20(b)) an excited-state Ansatz is necessary.

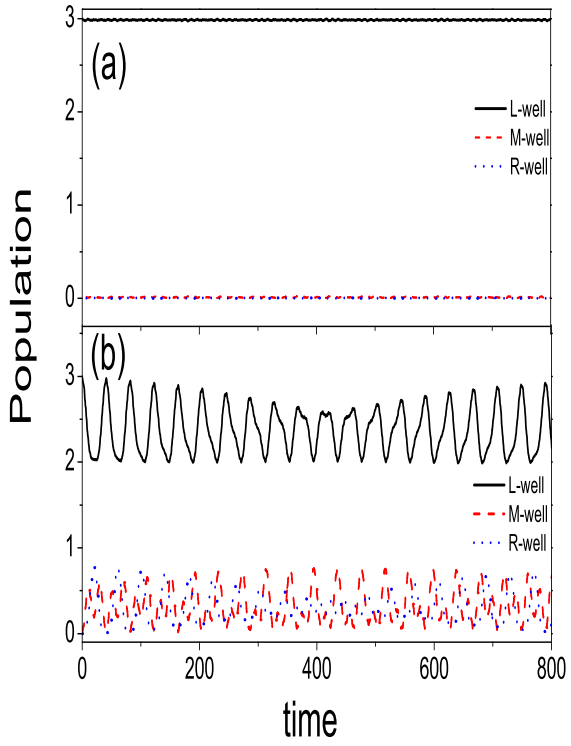


Figure 3.21: The population oscillations of three bosons in the triple well initially localized in the left well for (a) $g = 0.1$ and (b) $g = 3.26$. The emergence of enhanced tunneling windows (b) on top of the suppressed-tunneling background (a) is demonstrated

interaction. In Fig. 3.21(b), however, for $g = 3.26$, where the single-band model predicts even stronger self-trapping than that of $g = 0.1$, we observe the enhanced tunneling. The population in the left well oscillates between three and two, and that of the middle and right well oscillates between zero and one approximately. This implies that a single boson tunnels to the middle and right well with the other two bosons remaining localized in the left well.

To clarify the mechanism underlying the enhanced tunneling in Fig. 3.21(b), we monitor the contribution from different number states, $|_i\langle N_L, N_M, N_R|\Psi(t)\rangle|^2$, as a function of time. Here the number states $|N_L, N_M, N_R\rangle_i$ are computed numerically utilizing improved relaxation within MCTDH, and then $|\Psi(t)\rangle$ is projected onto them at different times[12]. As shown in Fig. 3.22 only the states $|3,0,0\rangle_0$ (initial state), $|2,1,0\rangle_1$ and $|2,0,1\rangle_1$ possess a significant contribution in the course of the tunneling process. $|2,1,0\rangle_1$ and $|2,0,1\rangle_1$ refer to states where two bosons localize in the two-boson ground state of the left well while one is in the first excited Wannier state of the middle and right well, respectively. In this way a boson hops to the first excited Wannier state of the middle and right well during the tunneling process, and the tunneling is indeed a single-boson tunneling. This tunneling mechanism corresponds therefore to the first crossing of the triple mode $|3,0,0\rangle_0$ with the first excited pair mode $|2,1,0\rangle_1$ which is indicated by the (light-blue) arrow in Fig. 3.21(b).

Besides the number states occupation, the tunneling process can also be demonstrated by the one-body density evolution. Fig. 3.23(a) shows the one-body density at different time instants of the tunneling process. The density profiles offer additional evidences of the excitation into different bands throughout the time evolution. At $t = 0$ the density profile is roughly a Gaussian localized in the left well, and this corresponds to the initial state $|3,0,0\rangle_0$. As time evolves, the density profile populates the middle and right well, and instead of the typical single-particle

[12]It is of course challenging to perform a better approximation for these states analytically by means of the CPWF or another approach to predict also the position of the resonance.

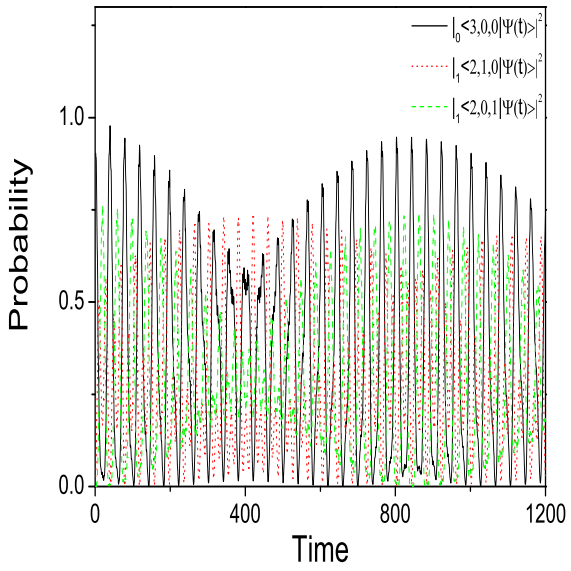


Figure 3.22: Probability of number states for the tunneling process shown in figure 2(b), for the states $|3,0,0\rangle_0$, $|2,1,0\rangle_1$ and $|2,0,1\rangle_1$, among which the tunneling mainly takes place. For this value of $g$, these three number states are in resonance, as marked by the blue arrow in figure 1(b).

ground-state (Gaussian-like) profile, the density in the middle and right well shows a nodal structure, which is typical for a single boson in the first excited on-site state, thereby verifying the contribution of the states $|2,1,0\rangle_1$ and $|2,0,1\rangle_1$ to which we referred above. A schematic picture of this tunneling process is shown in Fig. 3.23(b), where a single boson initially localized in the left well tunnels among all the three wells, and the other two bosons remain localized in the left well. When the boson tunnels to the middle and right well, it actually occupies the first-excited on-site level in the corresponding well.

An alternative single-boson tunneling mechanism appears when all bosons are initially trapped in the middle well, i.e in the state $|0,3,0\rangle_0$ and the interaction strength is very strong ($g = 9.85$) such that the boson tunnels to even higher Wannier states. This time the population in the middle well oscillates approximately in the interval $[2,3]$, while the population in the left and right well oscillates approximately within $[0,0.5]$, as shown in Fig. 3.24(a). This indicates that a boson in the middle well tunnels to left and right well with the same probability. Fig. 3.24(b) confirms this tunneling behavior with the probability evolution of the number states with $|0,3,0\rangle_0$, $|1,2,0\rangle_3$ and $|0,2,1\rangle_3$ sharing the major contribution. $|1,2,0\rangle_3$ and $|0,2,1\rangle_3$ refer to the states of two bosons in the middle well with the third one in the second excited Wannier state of the left and right well respectively, and this indicates that the bosonic tunneling to the left and right well hops to the second excited on-site state. This interband tunneling mechanism corresponds to the (purple) arrow in Fig. 3.21(b), where the triple mode $|0,3,0\rangle_0$ meets the second excited pair mode $|1,2,0\rangle_3$.

In the one-body density [Fig. 3.25(a)] we see initially all bosons trapped in the middle well. The deviation of this profile from a Gaussian indicates the strong on-site interaction which leads to patterns similar to this of the harmonic trap (see also Chapters 2.1, 3.1 [29, 25, 26]. At later times, where a single boson tunnels to the left and right well, where two nodes (in each site) appear demonstrating the occupation of the second excited on-site energy levels in both wells. We also illustrate this tunneling process in Fig. 3.25(b) showing that the bosons tunnel between

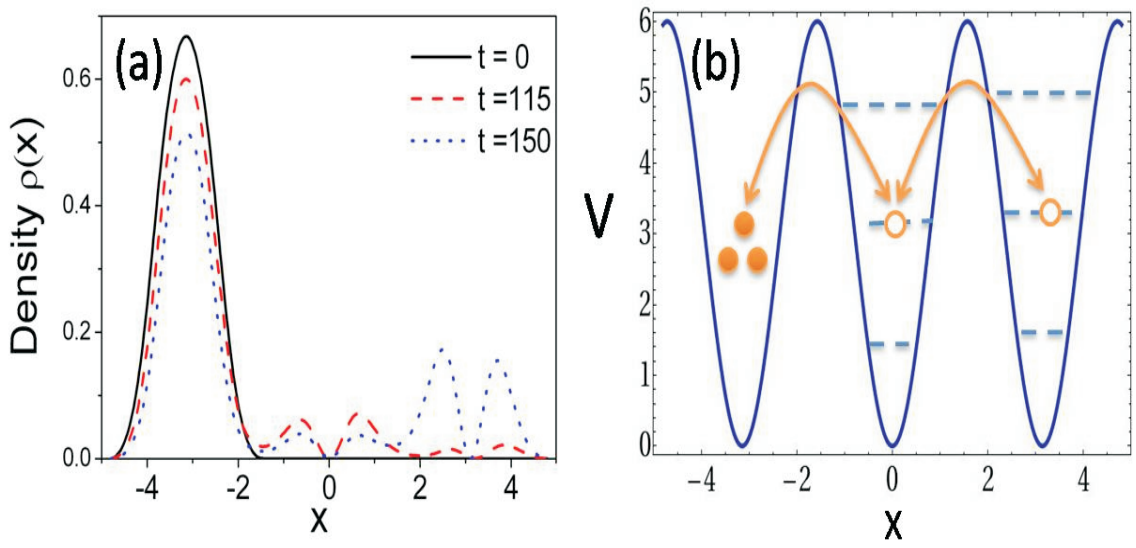


Figure 3.23: (a) The one-body density at various time instants. Initially all bosons are localized in the left well (black line), then one boson tunnels to the middle well (red line), and to the right well (blue line). The nodal structure in the middle and right well demonstrates that the boson in the middle and right well are in the first excited Wannier level. (b) Visualization of the tunneling process: in the tunneling process a boson tunnels forth and back between the left, middle and right well, with the other two bosons remaining in the left well. The dashed lines in the middle and right well illustrate the Wannier energy levels as in figure 1(a). The parameters are the same as in Fig. 3.21(b) and Fig. 3.22.

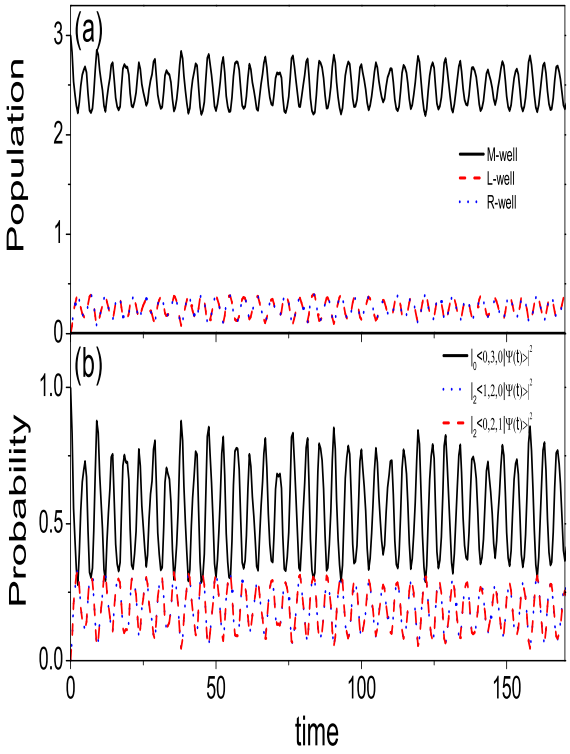


Figure 3.24: (a) The population oscillation of three bosons in the triple well, for the interaction strength $g = 9.85$. The three bosons are initially localized in the middle well. (b) Time-dependence of the occupation of $|0,3,0\rangle_0$, $|1,2,0\rangle_3$ and $|0,2,1\rangle_3$. As the system tunnels to the cat state $|1,2,0\rangle_3 + |0,2,1\rangle_3$, one boson tunnels to the left and right well with the same probability, which gives rise to the coincidence of the population in the left and right well and that of the two number states $|1,2,0\rangle_3$,$|0,2,1\rangle_3$, as shown in (a) and (b), respectively.

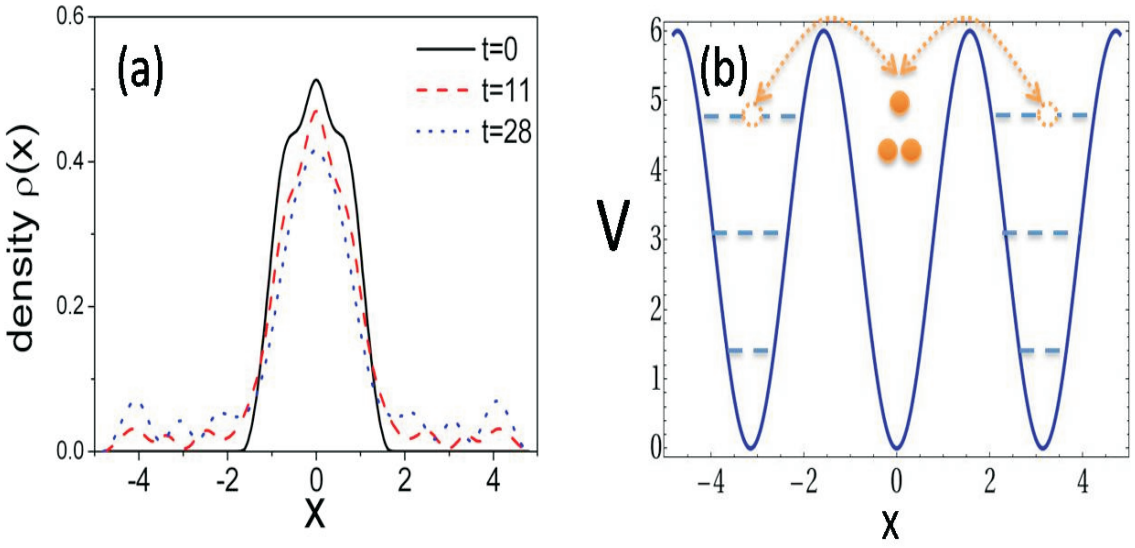


Figure 3.25: (a) The one-body density at various time instants for the tunneling process in Fig. 3.24. All bosons are initially localized in the middle well (black line), then one boson tunnels to the left and right well with the same probability (red and blue lines). The nodal structure in the left and right well indicates the occupation of the second excited Wannier states in both wells . (b) Visualization of the tunneling process: in the tunneling process a boson tunnels from the middle well to the outer wells. The dashed lines in the left and right well illustrate the Wannier energy levels.

the initial state $|0,3,0\rangle_0$, and the cat state $|1,2,0\rangle_3 + |0,2,1\rangle_3$[13].

Up to this point we have demonstrated that tunneling emerging from a state of three bosons localized in the same well can be enhanced by the resonant coupling to number states relating to higher bands, and this resonant coupling gives rise to interband tunneling, in which a single boson tunnels to different excited Wannier states of different wells. The above-mentioned interband tunneling mechanism may also interplay with the external confinement to achieve a tunable tunneling not only to a certain band but also to a certain well. A slight tilt potential $V_{tilt} = 0.1 \cdot x$ can be applied to the triple well, which detunes $|2,1,0\rangle_1$, $|2,0,1\rangle_1$, and now $|3,0,0\rangle_0$ gets into resonance with $|2,1,0\rangle_1$ and $|2,0,1\rangle_1$ separately at different interaction strengths. Consequently a boson can selectively tunnel to the middle or right well at different interaction strengths. For instance, $|3,0,0\rangle_0$ gets into resonance only with $|2,1,0\rangle_1$ at the particular interaction strength $g = 3.0$, and consequently a single boson tunnels only to the middle well as shown in Fig. 3.26. In experiments, the main difference of various realizations of the triple well potential is represented by the shift of the on-site energy of each well. The interband tunneling under tilt potential demonstrates that such tunneling is robust against the on-site energy shift, and consequently robust against deformations of the triple well potential from the ideal sine-square form. Earlier works also suggest that the tilt potential can be used to transport bosons in multi-well trap both dynamically [133] and adiabatically [127]. We point out that the interplay between the interaction potential and tilt potential can realize a specific transport of bosons not only into particular wells but also to particular on-site states (of excited bands) in corresponding wells.

[13]The states $|1,2,0\rangle_3$ and $|0,2,1\rangle_3$ have the same coupling to $|0,3,0\rangle_0$, and during tunneling no relative phase arises between these two states.

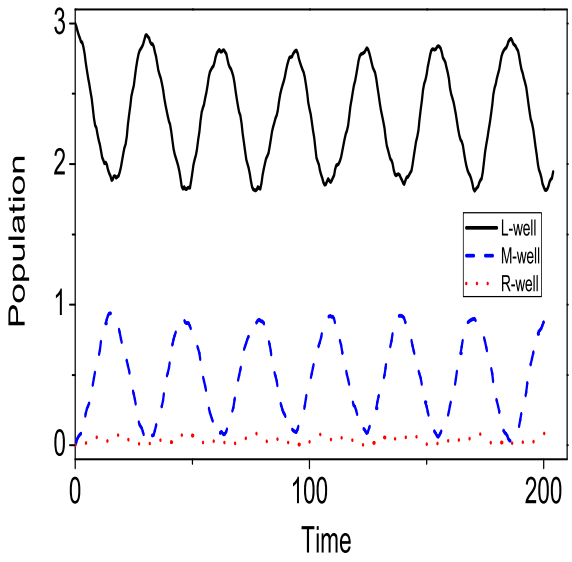


Figure 3.26: Applying a tilt potential $V_{tilt}(x) = 0.1 \cdot x$, the tunneling of three bosons is shown with the initial condition that all bosons reside in the left well, for $g = 3.0$. The population in the left, middle and right well is provided. One boson exclusively tunnels to the middle well.

### 3.2.4 Two-boson correlated tunneling and beyond

An interesting phenomenon in case of a double well is pair tunneling [50, 40], for which two repulsively interacting bosons tunnel as a pair forth and back. Pair tunneling arises since number states corresponding to bosonic pairs in each well are resonant with each other, and detuned from all other states. Pair tunneling is a special case of correlated tunneling, in which atoms do not tunnel independently. When higher bands come into play, various types of correlated tunneling occur and can be addressed by simply tuning the on-site energy of the initial state into resonance with the desired state.

As an example, we demonstrate numerically a correlated tunneling process, in which two of the three bosons initially localized in the middle well simultaneously tunnel to the left and right well, respectively. We take as the initial state $|0,3,0\rangle_0$ for $g = 5.8$, where $|0,3,0\rangle_0$ is resonant with $|1,1,1\rangle_6$. The latter excited single mode refers to the configuration of a single boson located at the ground state of the middle well while the other two are in the first excited level of the left and right well. From the population oscillation shown in Fig. 3.27(a), we see that the occupation of the middle well oscillates within the interval $[1,3]$, and each occupation of the left and right well oscillates within $[0,1]$. This indicates that two bosons initially localized in the middle well propagate in a correlated manner to the left and right well in the course of the tunneling process. From the time evolution of the probability of number states, shown in Fig. 3.27(b), we find that the tunneling mainly takes place between $|0,3,0\rangle_0$ and $|1,1,1\rangle_6$, with a minor intermediate contribution from $|1,2,0\rangle_1$ and $|0,2,1\rangle_1$. According to the configuration $|1,1,1\rangle_6$, this means that during the tunneling two of the three bosons initially localized in the middle well tunnel to the first excited Wannier states of the left and right well simultaneously. The nodal pattern of the density profile in the left and right well in Fig. 3.28(a) confirms the occupation of the first excited on-site states in these wells. Fig. 3.28(b) is a schematic plot of such a tunneling process which corresponds to the (blue) arrow in Fig. 3.21(b) where the triple mode $|0,3,0\rangle_0$ crosses the sixth excited single mode $|1,1,1\rangle_6$.

Correlated tunneling refers to the notion of tunneling of interacting atoms that don not move independently, in comparison with the independent tunneling of free atoms. In the single

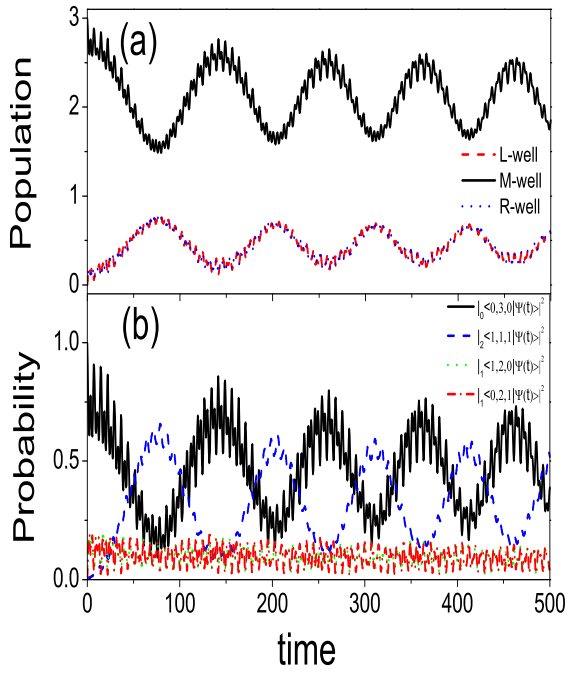


Figure 3.27: Tunneling of three bosons initially localized in the middle well for $g = 5.8$. (a) Population oscillation of the left well (red line), the middle well (black line), and the right well (blue line). The plots of the population in the left and right well practically lies on top of each other, indicating the correlated property of the two bosons tunneling to these wells. (b) Time occupation probability of the states $|0,3,0\rangle_0$, $|1,1,1\rangle_6$, $|1,2,0\rangle_1$ and $|0,2,1\rangle_1$.

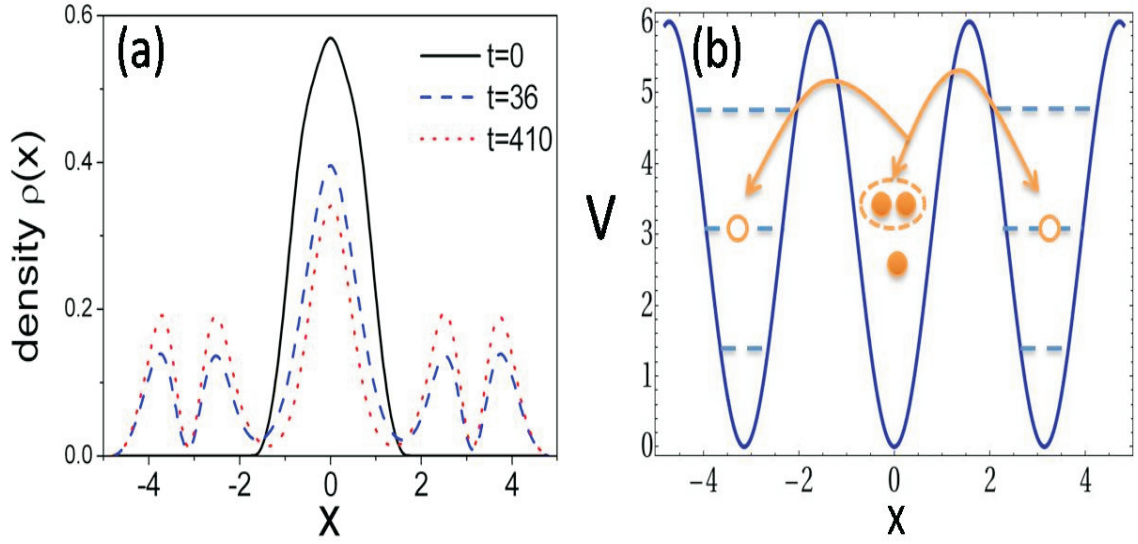


Figure 3.28: (a) One-body density at different times for the tunneling as in Fig. 3.27. Initially all the three bosons are localized in the middle well (black line), and gradually two of them tunnel to the left and right well (red and blue lines). (b) illustration of such tunneling process.

band approximation it is impossible to tune arbitrary number states into resonance via a change of the interaction strength, which is due to the different on-site energy dependence of number states on the interaction strength. This, however, becomes possible when we take into account higher bands, and in principle tunneling between arbitrary spatial and energetic configurations is achievable. As an example, we have shown here the correlated tunneling of two bosons initially in the middle well simultaneously to the left and right well.

Such interband tunneling mechanisms can be straightforwardly extended to larger systems containing more bosons. We take four bosons in the triple well for instance. In such a system, there are four different categories of number states. In addition to the single mode, pair mode and triple mode, there exists the "quadruple modes" of $\{|4,0,0\rangle_i, |0,4,0\rangle_i, |0,0,4\rangle_i\}$, referring to four bosons in the same well. We can further separate the pair mode into two categories: the "double-pair modes", such as $|2,2,0\rangle_i$, referring to the case that the four bosons are divided into two pairs and each of the pairs occupies a different well, and the "single-pair mode", containing a pair and two separate bosons, such as $|1,2,1\rangle_i$. Now in this system, besides the single-boson tunneling and two-boson correlated tunneling in the three-boson case, we can even realize correlated tunneling of pairs, by tuning the number states $|0,4,0\rangle_0$ and $|2,0,2\rangle_1$ into resonance, for instance. Therefore our bottom-up approach with the generalized number states, provide an intuitive explanation but also a detection tool of inter-band tunneling mechanisms, which break in certain strong-interaction regimes the self-trapping of the atoms.

**Conclusive remarks**

We have demonstrated in this part (Chapter 3.2 that in a system consisting of a small ensemble of bosons confined in a 1D triple well, several windows of enhanced tunneling are opened in the strong interaction regime, where in general the background of suppressed tunneling dominates. When the initial state resonantly couples to different excited number states, various tunneling processes can be realized, which manifests itself as a potential tool for controllable dynamical transport of bosons. As an example, we demonstrated the single-boson tunneling to the first and second excited on-site states, and the two-boson correlated tunneling. In this way, tunneling between arbitrary spatial and energetic configurations of bosons in a multi-well trap are in principle achievable just by tuning the interaction strength, and as a consequence controllable dynamical transport of bosons to specific wells and specific in-well energy levels becomes possible. To understand the interband tunneling, we introduced a basis of generalized number states, which treat the interaction in a non-perturbative way such that these are valid even in the strong-interaction regime (and are only meaningful and defined for large $V_0$). The bottom-up approach with these number states was done here in a numerical manner, but the core of the explanation is strongly related to the approaches we have performed in the previous Chapters 2.1, 3.1 via the CPWF and the 'two to many' bottom line. We also notice that similar efforts have been put forward to provide an analytical description in the strong interaction regime [132, 130, 129]. The interband tunneling we discuss here can be straightforwardly generalized to multi-well systems with more atoms while mixed or fermionic ensembles may show additional interband tunneling effects. This also opens the doorway to an interpretation and controllable preparation of the general non-equilibrium quantum dynamics in multi-well system.

# Chapter 4

# Fermions in a harmonic trap

In this Chapter we turn our attention to fermionic systems, which have different statistics than the bosonic ones that we have considered so far. In a sense fermionic physics are richer already due to the mere fact that there is an additional degree of freedom namely the spin, or the pseudospin. In the first part (Chapter 4.1) we explore two-component fermi-mixtures numerically via MCTDH and analytically via a generalization of the CPWF. In the second part (Chapter 4.2) we compare our results with recent experimental data for the case of an impurity in a few-body Fermi sea.

## 4.1 Two-component Fermi mixture

Degenerate Fermi gases have been prepared in low temperatures [54] exposing impressive features like superfluidity [134] according to the Bardeen-Cooper-Schrieffer (BCS) pair theory [135]. Two-component Fermi-mixtures prepared usually in two hyperfine states or with different atomic species are in the core of research for novel phases [3]. Ensembles with imbalanced component populations [136] can lead to the coexistence of normal and superfluid phases [137] or to a more complex phase with a spatially varying gap [138]. For extreme polarizations (population imbalances) polaronic physics for attractive [57] and repulsive impurity atoms [58] have been recently examined. An open debate in the field is the observation of itinerant ferromagnetism induced by interactions [55]. Fermionic physics in 1D may prove to be even richer in phenomenology as the first experiments in confinement-induced molecules [139] and spin-imbalanced Fermi gases [140] indicate. On theoretical side there have been already several studies on the corresponding polaronic physics [141, 142, 144, 143, 145], TG and super-TG gases specifically their pairing properties and dynamics [65].

In this part, we explore in particular a few-fermion mixture consisting of two distinguishable components which are repulsively interacting and confined in a 1D harmonic trap. Different scenarios of population imbalance ranging from the completely imbalanced case where the physics of a single impurity in the Fermi-sea is discussed to the partially imbalanced and equal population configurations are investigated. For the numerical calculations we use for first time in such systems the MCTDH method, used only for few-boson systems so far in this thesis and in the literature [29, 41, 40]. Apart from numerical calculations we generalize our Ansatz the CPWF proposed in the previous Chapters for bosons to mixtures. From weak to strong coupling between the components the energies the densities and the correlation properties of 1D systems change vastly with an upper limit set by fermionization where for infinite repulsion all fermions can be mapped to identical ones (see Chapter 1. The numerical and analytical treatments are in good agreement with respect to the description of this crossover. The case of an impurity atom showing reach behaviour of the evolution of the energy and density as we approach

fermionization both for the impurity atom and the majority ones is a case of particular interest: in recent experiments [63, 60, 61] exact populations of majority atoms have been prepared with high fidelity and their energy has been measured, and will be compared (in Chapter 4.2 with the results obtained here. Our work is also in close connection with other theoretical treatments of two-component fermi gases which share also the viewpoint of this thesis 'from to to many' [146].

### 4.1.1 System

The system consists of a two component Fermi gas with the two species prepared e.g. in the two lowest hyperfine states ( for $^6$Li $|F = 1/2, m_F = \pm 1/2 >$ see ref. [60, 61]) confined in a pure 1D harmonic oscillator potential. We have to stress here that the two components are distinguishable, therefore we may speak of a pseudospin degree of freedom (in this particular example the nuclear spin) that distinguishes the two 'species'[1]. . The atomic species are therefore the same, but only atoms with exactly the same hyperfine state are indistinguishable, i.e. atoms that belong to the same component (like atoms) and are subject to fermi statistics. Due to antisymmetry s-wave interactions between identical fermions (same hyperfine state) are not possible, while p-wave interactions are negligible. Therefore the important interaction parameter here, is the interaction strength that between atoms belonging to different components (unlike atoms). Still this has to take into account the quasi-1D nature of the confining potential and the resulting confinement induced resonances [13]. The effective 1D interaction strength is then the same as that for bosons Eq. 1.37. Again this inter-species (or inter-component) interaction strength can be regarded as tunable over a very large range from zero to infinitely repulsive. The effective rescaled 1D Hamiltonian is then similar to that of the bosons in the harmonic trap that we have studied in the first Chapter 1 Eq. 2.1:

$$H = -\frac{1}{2}\sum_{i=1}^{N}\frac{\partial^2}{\partial x_i^2} + \frac{1}{2}\sum_{i=1}^{N} x_i^2 + g\sum_{i\leq N_M<j\leq N}\delta(x_i - x_j) \tag{4.1}$$

with the difference that the interaction term applies to unlike atoms. The total number of atoms is $N$ and $N_M$ is number of like atoms which has the larger population in the trap. We remain therefore with a single parameter $g$, the rescaled coupling strength between the $N_M$ majority fermions and the $N_m = N - N_M$ minority fermions. We will examine next the following cases

- a single impurity for the completely imbalanced configurations 2:1, 3:1, 4:1
- a balanced population 2:2
- a partially imbalanced population 3:2

the notation being $N_M$:$N_m$. We restrict ourselves to these few-body scenarios which are relevant to the experiment [60, 61] (the first case is already realized experimentally [63]) and for which we can obtain reliable accurate numerical results with the MCTDH method (see Appendix A Computational Methods). In most cases these are sufficient to reveal the mechanisms present also for larger $N$. Next we present the generalization of the CPWF for this case.

### 4.1.2 Ansatz: generalization of correlated-pair wavefunction

We may start here with the special balanced case of two atoms (1:1) which allows for an exact solution not only in 1D but also in higher dimensions as we have seen in Chapter 1 [14]. We

[1]We will call atoms belonging to different components 'unlike atoms' and those which belong to the same component 'like atoms' as it is common in the literature [146]

should underline here that this case concerns two distinguishable atoms and it coincides with the case of two interacting bosons. It can be nevertheless studied also with two atoms of fermionic species (eg. $^6$Li) but in different hyperfine states which are as we stated above distinguishable. This system has been prepared experimentally very recently in Ref. [61] and the energy was measured with a very good accuracy and agreement with the theoretical analytical curves of Ref. [14] via tunneling rates after opening the harmonic trap from one side (more about this experiment in the next section). Extending this study to higher particle numbers from the theoretical side is the basic scope of the present section. The important starting point here, is that the nature of the interaction effects between unlike atoms is exactly the same as that for bosons. This is the connecting line between this last Chapter 4 on trapped fermions and Chapter 2.1 for trapped bosons. This fact allows us to use again the known two-body solution (see Chapter 1) which corresponds here to the 1:1 case also for constructing a many-body wave-function in the spirit of CPWF for the general $N_M : N_m$ case.

There are also a lot of other similarities with the bosonic case (Chapter 2.1) in the trap enhancing the introduction of a CPWF for the fermionic case. The most important point is the Hamiltonian can also in this case be separated into a center-of-mass and relative motion part the latter being the complex one resisting an analytical solution. The substantial difference in the case of fermions is that like atoms should be put on the levels of the Fermi ladder to put it in a simple way. The identical fermions of each component should be represented by an antisymmetric function. We have seen already in Chapter 1 that the Slatter determinant for the trapped fermionic system can be also written in form of products of pairs (Jastrow-type function). This is the way the bosonic function for the TG case was written in Eq. 1.12 after the application of the Bose-Fermi map. The absolute value appearing in the TG function to symmetrize it (according to the bosonic permutation symmetry) is here not needed, in fact it should be absent such that the function becomes antisymmetric for exchange of identical fermions.

Concretely, the generalization of the CPWF we propose here for the relative motion reads then:

$$\Psi_{\mathrm{cp}} = \prod_{i\leq N_M<j}^{P} D_\mu(\beta r_{ij}) \prod_{i<j\leq N_M}^{P_M} D_1(\beta x_{ij}) \prod_{N_M<i<j}^{P_m} D_1(\beta x_{ij}) \tag{4.2}$$

(up to a normalization constant which we neglect here), where $P$ is the number of distinct pairs of unlike atoms, $P_M$ and $P_m$ are the number of pairs of majority and minority like atoms respectively. The pinning of identical fermions belonging to the same component on the corresponding Fermi-ladder is done by choosing $\mu = 1$ as a parameter for the PCFs and $x_i j = x_i - x_j$ as their argument (see the two last terms of Eq. 4.2) which corresponds to the energetically lowest orbital of the fermionic relative motion: $D_1(x) = \sqrt{2}xe^{-x^2/4}$. Therefore the part of the total wavefunction which refers to identical fermions is the correct non-interacting ground state resulting from the Slatter Determinant: $\Psi_{id} = \prod_i e^{-x_i^2/2} \prod_{i<j}(x_i - x_j)$ with all $x_i$'s and $x_j$'s being exclusively coordinates belonging to like fermions. For the interacting pairs in the wavefunction the parameter $\mu$ of the PCF (see first term of Eq. 4.2) which depends on the interaction strength $g$ should be determined. This can be done exploiting the Bethe condition $2\beta D'_{ij}(0) = gD_{ij}(0)$ which is imposed for each pair of unlike atoms at $r_{ij} = 0$ exactly as in the case of bosons (see Chapter 2.1). The resulting transcendental Eq. 1.19 is solved for $\mu$, selecting the solution in the interval $\mu \in [0, 1]$ which corresponds to the ground state.

A key feature of the CPWF as we have seen also in Chapter 2.1, is that it reproduces the exact analytically known solutions in the limits $g = 0$ and $g \to \infty$, for any $N$ by choosing $\beta = \sqrt{\frac{2}{N}}$. In these limits, $\mu$ equals 0 and 1, respectively and the total wavefunction takes the

following form

$$\Psi_{g=0} = e^{-\sum_{i=1}^{N} x_i^2/2} \prod_{i<j\leq N_M}^{P_M} r_{ij} \prod_{N_M<i<j}^{P_m} r_{ij} \tag{4.3}$$

for the non-interacting and

$$\Psi_{g\to\infty} = e^{-\sum_{i=1}^{N} x_i^2/2} \prod_{i\leq N_M<j}^{P} |r_{ij}| \prod_{i<j\leq N_M}^{P_M} r_{ij} \prod_{N_M<i<j}^{P_m} r_{ij} \tag{4.4}$$

for the infinitely strong repulsion limit [65] which are the exact solutions in both cases. Of course the CPWF is also exact for arbitrary $g$ for the case $N = 2$ (with $\beta = 1$) [14] since indeed our general Ansatz is inspired by this two atom case [14, 25].

Using the CPWF as trial function one can treat $\beta$ as a variational parameter for given values of $g$ and $N$. One may also decouple the full wavefunction not to a center-of-mass/ relative motion frame, but to a single-particle and two-body part in a Jastrow form as we have done in Chapter 2.1 for the bosons. Then it can be used for Monte Carlo simulations also inserting more variational parameters (at least one for each part). Generalizations of this function can also be extended to other cases like bosonic mixtures or even fermion-boson mixtures or to many component mixtures. One should take $\mu = 1$ for identical fermions and a $\mu \in [0, 1]$ for interacting pairs (bosonic or distinguishable) according to Eq. 1.19. Yet one has to keep in mind that in case of more than two species and for the situation that only a subset of the coupling strengths are infinite the above Ansatz may not be exact. For example for a mixture of bosons, the unlike ones may be interacting and the like atoms non-interacting does not constitute a TG gas. Consequently the cases of a single species bosons and two species fermions are the most natural ones for which this Ansatz should have its best performance. Applications to other cases or even other potentials or higher dimensions are left as an open possible research field.

A first illustration of the behaviour of the CPWF is given for the case 2:1 in Fig. 4.1 (b) for weak and (c) for strong interaction strength, where contour plots of the probability density are shown. On the manifolds $\mathcal{M}_{ij} = \{(x_1, ...x_i, ..., x_j, ..., x_N) \in \mathbb{R}^N | x_i = x_j\}$ where the identical atoms meet (here the plane $x_1 = x_2$) the probability density possesses already for weak interactions [Fig. 4.1 (b)] a low probability, while stronger interactions between the non-identical atoms [see Fig. 4.1(c)] reduce the values of the density also on the other two planes ($x_1 = x_3$, $x_2 = x_3$). This is a main intuitive picture that the CPWF captures, treating each fermionic pair –being interacting or not – correctly at its contact point, where the wavefunction should tend to vanish as we increase the coupling strength from weak to strong interactions. In the next section the accuracy of this approach with respect to the energy is tested by comparison with corresponding numerical results for all cases examined in this work. The specific behaviour of the densities will be addressed in the sections thereafter.

### 4.1.3 Accuracy of the Ansatz

The energy of the interacting ensemble is a first observable that can be measured experimentally for example by RF-spectroscopy (see e.g. Refs. [57, 58, 63]) or by determining tunneling rates [61]. We compare here the numerical MCTDH results to the calculations using the CPWF and consequently obtain information on the validity and accuracy of the CPWF in the same way we did in Chapter 2.1.

In Fig. 4.1 we also show the energies obtained from calculating the expectation value of the Hamiltonian operator using the CPWF [Eq. (4.2)]. The accuracy of the Ansatz is very good especially for weak and very strong interactions, yet there are deviations from the numerical results in particular for intermediate coupling strengths, especially for larger particle numbers

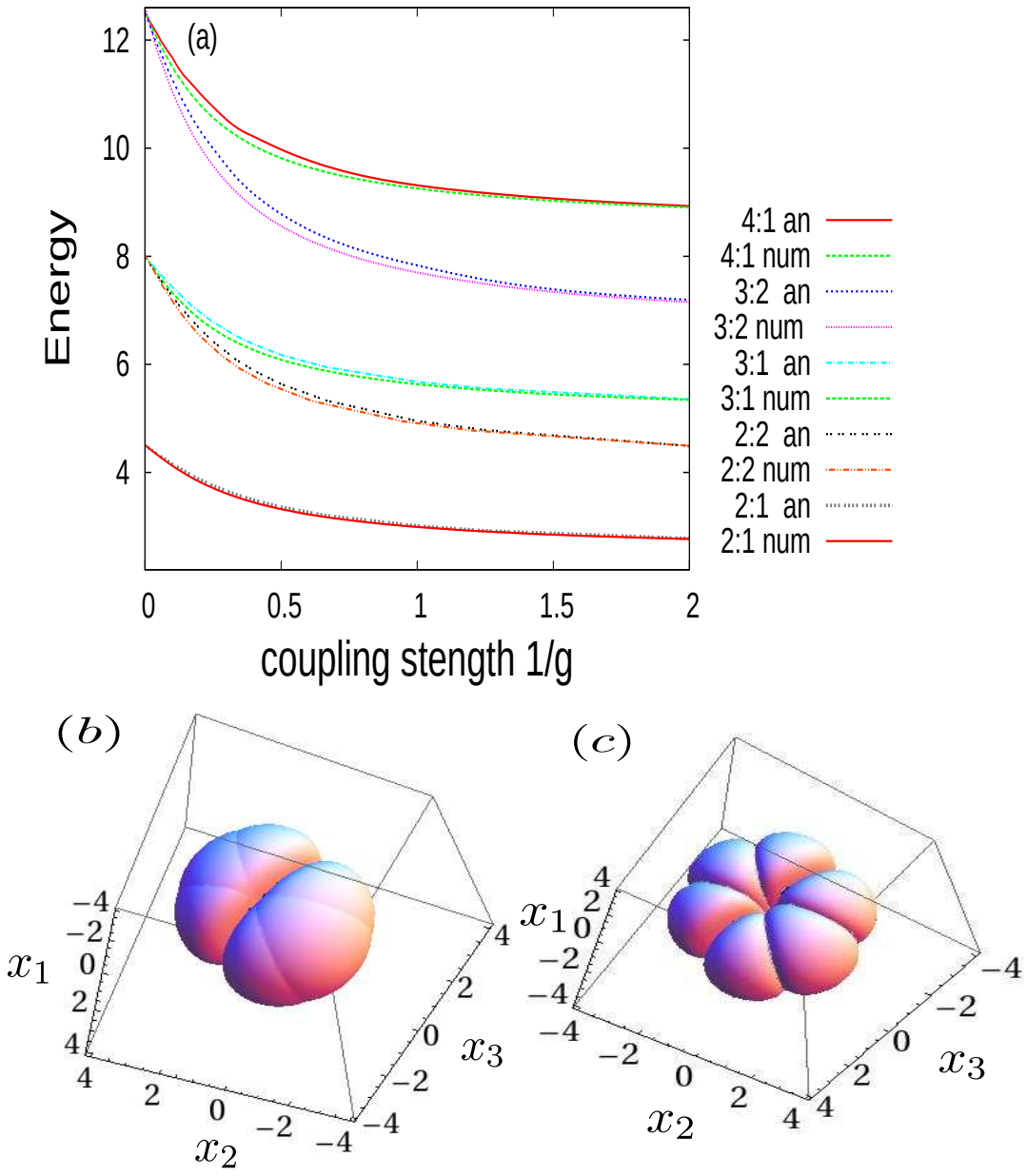


Figure 4.1: (a) Energy as a function of the inverse interaction strength $1/g$ for all cases examined in this work (impurity 2:1, 3:1, 4:1, balanced 2:2, imbalanced 3:2). For each case the lower line corresponds to the numerical results employing MCTDH and the line slightly above to the energy computed from the Ansatz CPWF Eq. 4.2. Contour plots of the density distribution $|\Psi(x_1, x_2, x_3)|^2 = 0.01$ for the configuration 2:1 using the CPWF for a weak (b) $g = 0.5$ and a strong (c) $g = 5.0$ interaction strength.

(see e.g. the curves for the configuration 2:1 in comparison with 4:1). It is to be expected that the CPWF works good close to the two exactly known limiting cases since it reproduces them [see Eqs. (4.3) and (4.4)]. The deviation for larger numbers of atoms is due to the two-body nature of the function which does not take into account higher correlations. Nevertheless a relative error of 2-3% can be achieved also by taking variational trial functions with a single variational parameter. Admittedly the accuracy of this CPWF is not as strong as it was for the bosonic case (see Chapter 2.1) which may also be attributed to the face that the CPWF here includes the non-interacting like pare of atoms in a unperturbed form. Still obviously these pairs are also affected indirectly from the inter-species interaction, and it can be that this is not optimally taken into account with the present form of the CPWF. Introducing variational parameters all over may improve the performance, but this is left to further research, which may get also better insight on the nature of this indirect correlation of the fermions (with respect to their the short- and long-range behavior).

Concerning the physical behavior, the energy increases as the coupling strength gets larger (Fig. 4.1), but not with the same slope for all configurations. The range of the energies is bounded by the non-interacting values (for the configurations 2:1, 2:2, 3:1, 3:2 and 4:1 it is 2.5, 4, 5, 6.5 and 8.5 respectively) and the value at fermionization which is $E_{g\to\infty} = N^2/2$. This means that e.g. the partially imbalanced case 3:2 or the equal population one 2:2 increase stronger than the corresponding impurity cases 4:1 and 3:1 since more interacting pairs of atoms are included in the ensemble. On the other hand if we consider only the impurity cases, then the gain of energy per majority atom (compared to the corresponding non-interacting state) at a finite value of the interaction strength is larger for a smaller number of atoms. This means that by adding majority fermionic atoms the energy gain per atom decreases since the majority atoms lie higher and higher in energy, such that they almost do not feel the impurity fermion at the bottom. Yet when the interaction becomes very large the impurity affects all atoms and at fermionization the energy gain is for all cases equal to $E_{g\to\infty} - E_{g=0} = N^2/2 - N_M^2/2 - 1/2 = N_M$. Further features of the behaviour of the physics of the impurity in the finite Fermi-sea confined in a harmonic trap, a case also related to the experiment [63] will be illustrated in the next section. A relevant question in this context is the connection between many-body polaronic physics in the continuum (see eg. Refs. [141, 142, 56, 57, 58]) and the few-body behaviour of an impurity in the harmonic trap.

### 4.1.4 An impurity atom in a sea of majority fermions

In this section we focus on the impurity physics in 1D and analyze the corresponding probability densities. Major progress in recent experiments [108] have extended towards probing the density distribution on a single atom or a single site level. As demonstrated in Figs. 4.2 and 4.3 for the configurations 2:1 and 3:1 respectively, the probability density shows a vast change for both the majority atoms and the single minority one. In the same Figures we show also the one-body density obtained by the CPWF (Eq. 4.2).

We focus first on Fig. 4.2 (a-d) which shows the evolution of the one-body density of the impurity from weak ($g = 0.5, 2.5$) to stronger interactions ($g = 5.0, 20.0$). For weak interactions [$g = 0.5$ Fig. 4.2 (a)] the impurity density is very close to the ground state orbital of the harmonic trap (Gaussian profile). As the interaction increases [$g = 2.5$ Fig. 4.2 (b)] the density becomes broader and the peak lowers, which is a typical effect of repulsive interaction also in the case of bosons (see also Chapter 2.1) [25, 29]. Still one may expect that in the case of fermions this single impurity atom would be even more confined and pinned in the middle of the trap due to the repulsive interaction with the surrounding majority atoms. However the opposite effect is observed: the density is stretched to cover a larger space in the trap and becomes delocalised. For even higher interaction strengths [$g = 5.0$ Fig. 4.2 (c)] it even tends to acquire

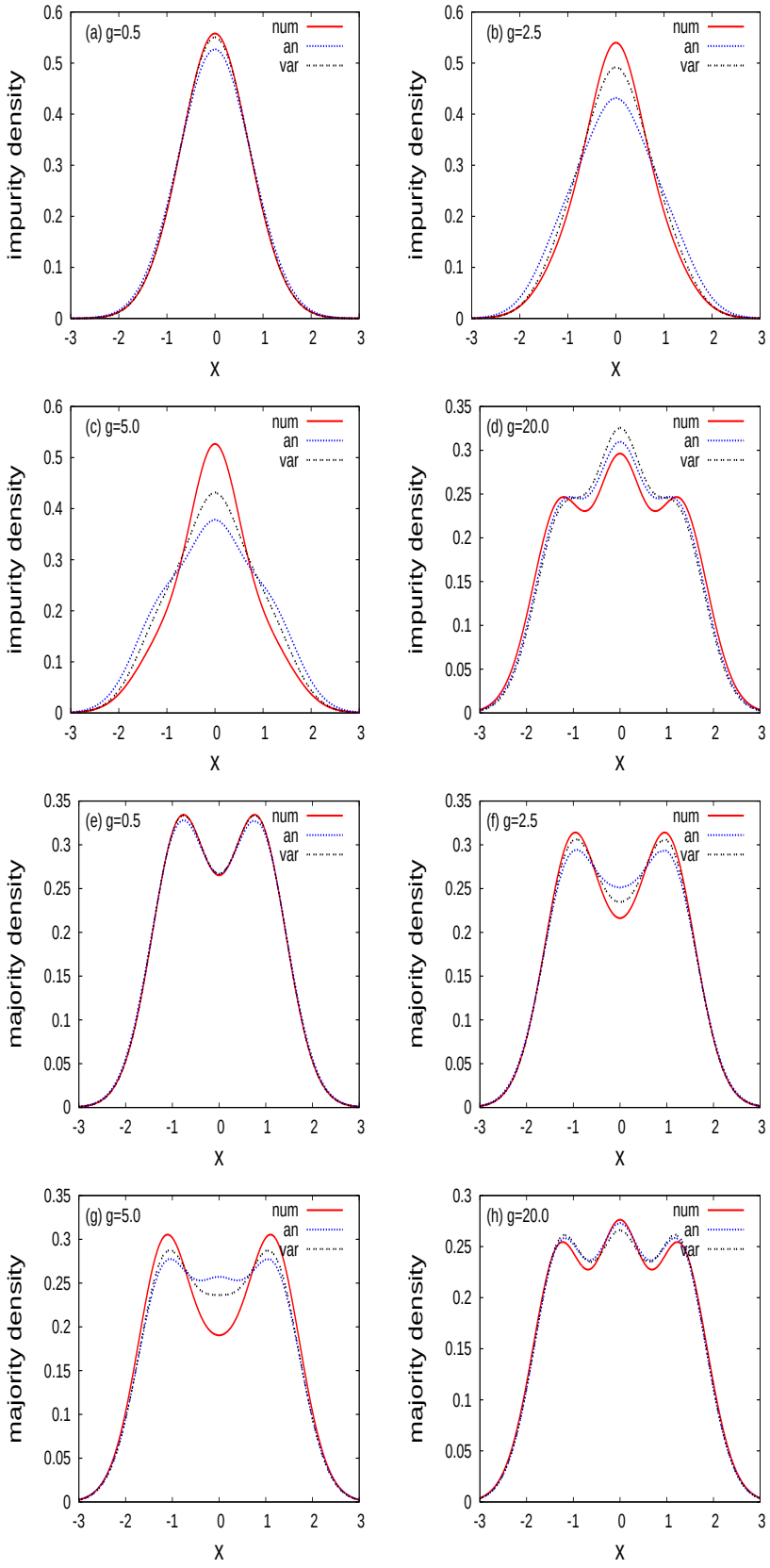


Figure 4.2: One body densities of (a-d) the impurity and (e-h) majority fermions for the 2:1 case with varying interaction strength $g$ using the numerical (MCTDH) approach, and the analytical (CPWF) and variational Ansatz.

side lobes. More spectacularly for very strong interactions, the density of the impurity acquires three distinct maxima, an effect which is very evident in few-body fermionization profiles also for bosons (see also Chapter 2.1) [65, 25, 29]. The number of maxima is equal to the total number of atoms in the trap and according to Girardeau's theorem [65] the local properties like densities should be exactly the same for a fermionized ensemble and for the corresponding ensemble of $N$ identical fermions. This vast change of the density of the impurity atom as we follow the crossover from weak interactions to fermionization also for the case of the 3:1 configuration is shown in Fig. 4.3 (a-d).

The impurity is strongly affected by the repulsion with the majority atoms, which in turn are also strongly influenced by the single minority atom. Their densities for the case 2:1 depicted on Fig. 4.2 (e-h) possess at weak interactions [$g = 0.5$ Fig. 4.2 (e)] two maxima (corresponding to a two identical-fermion ground-state profile) which are pushed to outwards as the repulsion increases [$g = 2.5$ Fig. 4.2 (f), remember that the corresponding impurity density becomes more delocalized in Fig. 4.2 (a),(b)] and start to acquire a plateau and finally an additional peak in the middle for very strong coupling [$g = 5.0, 20.0$ Fig. 4.2 (g),(h)]. A similar behaviour is observed also for the case 3:1 where the middle peak for weak interactions is slightly broadened pushing the outer maxima outwards [$g = 0.5, 2.5, 5.0$ Fig. 4.3 (e),(f),(g)] and finally is turned to two peaks reaching the fermionization profile for strong coupling [$g = 20.0$ Fig. 4.3 (h)]. The impurity fermion affects therefore the density profile of the majority atoms equally strong, leading to the extreme infinitely repulsive limit where it becomes effectively indistinguishable from the majority fermions (strictly only for the local properties, of course).

An issue that is worth noting here is that the very strong change in the density profile (where more distinct peaks appear) is happening rather abruptly for a very high interaction strength. The latter distinguishes the case of few fermions from that of few bosons which acquire substantial peaks already for intermediate interactions (see Chapter 2.1 and [25]). In other words, this is a characteristic behaviour of two-composite few fermion systems, which becomes interesting in the very strong correlation regime, being the important regime of 1D physics. This regime is difficult to access both for the experiment (one has to approach very closely to the $g \to \infty$ resonance, and simultaneously avoid losses to the molecular side [63]) and for numerical calculations since a lot of basis functions have to be included, rendering the treatment of a resulting huge Hilbert space very difficult. The application and convergence of MCTDH for such strong interactions is a very subtle issue, and has been tested extensively in this work, leading to the reliable results for the cases presented, which we also compare with the corresponding CPWF (which naturally provides the correct profile for infinite repulsion, thus not running into the aforementioned difficulties).

The accuracy of CPWF to describe the evolution of the densities of the impurity or the majority atoms is very good close to the two, the non-interacting and fermionization, limits as expected and describes the crossover qualitatively very well. Yet at intermediate interactions, the CPWF densities tend to be broader and acquire minor additional peaks compared to the numerical results [see Figs. 4.2, 4.3 (b),(c),(f),(g)]. This is in accordance with behaviour of the corresponding energies, i.e., the fact that the analytical CPWF energies lie above the numerical ones in the intermediate interaction regime [see Fig. 4.1(a)]. For the 2:1 case we present also the densities obtained by a variational treatment of the parameter $\beta$ (minimization of the energy using the CPWF $\Psi_{cp}$ as a trial function). We observe in Fig. 4.2 that the variational treatment of the CPWF represents a significant improvement over the fixed $\beta$ CPWF case: the corresponding densities get closer to the numerical ones. Further improvements of the Ansatz to capture the exact quantitative behaviour may include more variational parameters or a different construction as discussed above. Yet we may emphasize that the correct qualitative behaviour is captured by the explicit function $\Psi_{cp}$. A similar good agreement exists for the next two cases

of partial and complete balance of populations that we present in the next section.

### 4.1.5 Equal populations and partial imbalance

In the following we analyze the density profiles of two cases which exhibit a different crossover to fermionization than the impurity physics discussed above: equal populations and partial imbalance. Since the Ansatz of the CPWF possesses a similar accuracy as already depicted in Fig. 4.1 (a) we will concentrate here on the physical effects for these cases and present only the numerically obtained densities in Fig. 4.4.

Fig. 4.4 (a) shows the one-body density profiles for different interaction strengths for the case of equal populations (2:2). Note that the two hyperfine states possess exactly the same profile features in this completely balanced case. The two initial peaks for weak $g = 0.5$ get broadened and flattened ($g = 2.0$) and start already for intermediate $g = 5.0$ to acquire side peaks, resulting in 4 distinct peaks for a strong coupling $g = 15$ according to the fermionization theorem. The crossover is here much smoother than in the case of the impurity (reminiscent of the bosonic case [25, 29]) with each peak (corresponding to a pair) spiting to two. The behaviour for equal populations can be also generalized to higher particle numbers, and we expect no substantial differences which we have checked for the few body case of 3:3 where the 3 initial peaks evolve to 6 again due to 'repulsive pair splitting'.

Another very interesting scenario is that of a partially imbalanced population, which we illustrate here for the case 3:2 in Fig. 4.4 (b) and (c) showing the density profiles with increasing coupling strengths for the minority and the majority atoms, respectively. The two minority atoms possess 2 lobes for weak interactions $g = 0.5$ which are slightly pushed outwards in the trap for intermediate interactions $g = 5.0, 10$ forming a small plateau in the middle. Only for a strong coupling $g = 14$ a third maxima rises in the middle of the potential and some outermost side wings are forming, which result to two additional peaks at $g = 16$. We see again here a rather abrupt and interesting behaviour for strong interactions very close to the resonance, like in the case of the impurity fermion. The majority atoms [Fig. 4.4 (c)] also hold the three-lobe profile for intermediate interactions ($g = 0.5, 5.0, 10$), while from the plateaus forming between the peaks two additional peaks emerge near $g = 14.0$ resulting in a profile with five maxima close to the resonance. Inspecting Fig. 4.4 (b) and (c) the two peaks of the minority density ($g = 10$) which are located at the positions of the two plateaus of the majority density seem to represent a rather stable configuration for the repulsive particles. Still the tendency to fermionize in order to avoid each other as much as possible breaks this configuration giving rise to the additional peaks.

The above mechanisms of the crossover to fermionization are present also in ensembles with larger number of atoms, yet they are more prominent and illustrative for few-atom systems. The connection between these mechanisms and the many-body phases like BCS and FFLO, is an open research pathway.

**Conclusive remarks** Exact numerical calculations (MCTDH) and the analytical approach the correlated-pair wavefunction CPWF have been employed to explore the properties of few-fermion two-component mixtures in an 1D harmonic trap. The CPWF was here generalized to cover the case of mixtures, is shown to be in a very good agreement (for the energies and the densities) with the numerical results of MCTDH (used here for the first time for the few-fermion case). Three general cases were examined: (a) an impurity in a sea of majority fermions, where we have observed a strong variation of the density with an increasing strength of the repulsive interaction both for the impurity atom and the majority ones, (b) an equal population case for which the behaviour is smoother with two peaks arising in the place of one as the coupling

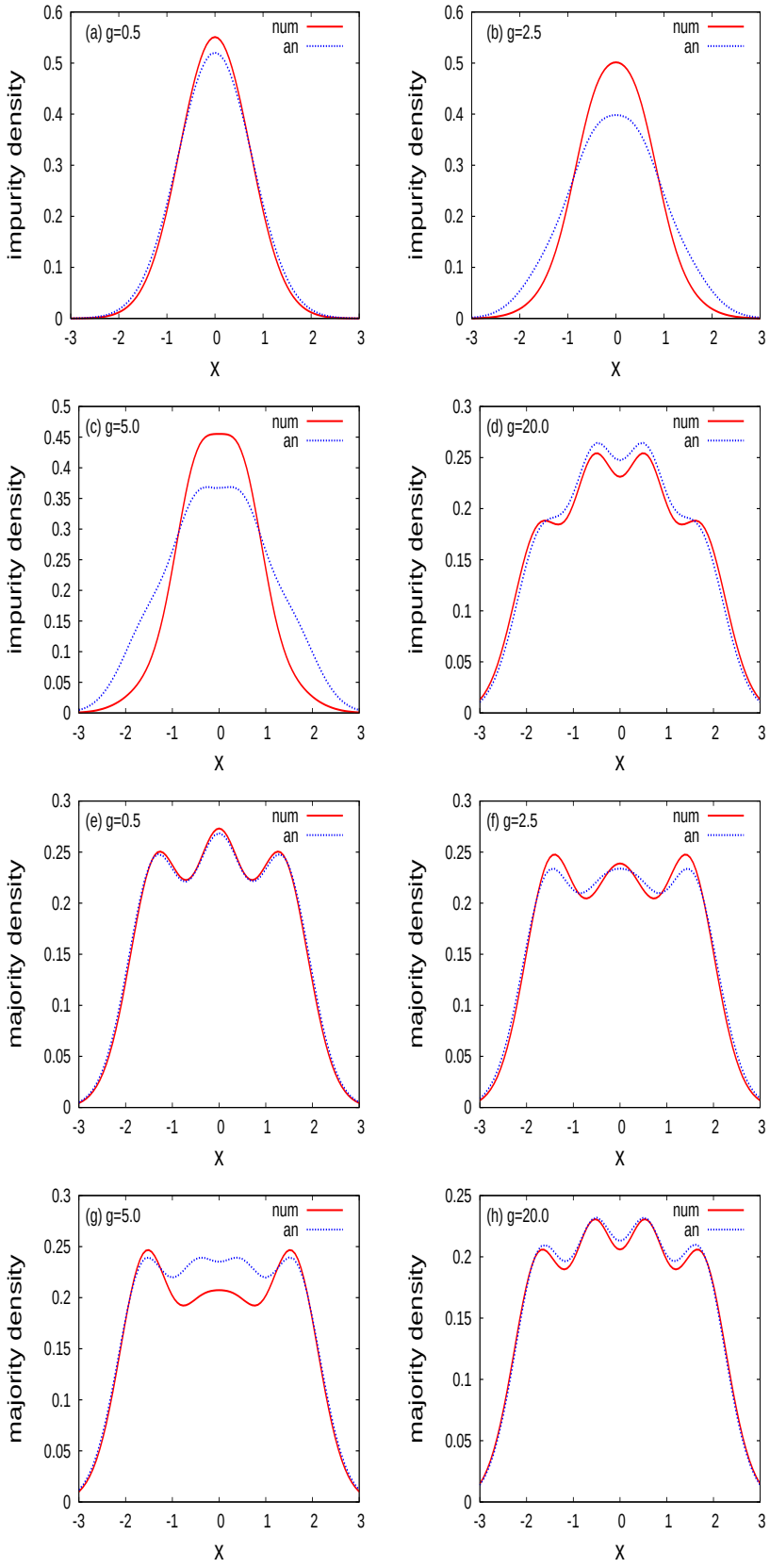


Figure 4.3: One body densities of (a-d) the impurity and (e-h) majority fermions for the 3:1 case with varying interaction strength $g$ using the numerical (MCTDH) approach, and the analytical (CPWF) Ansatz.

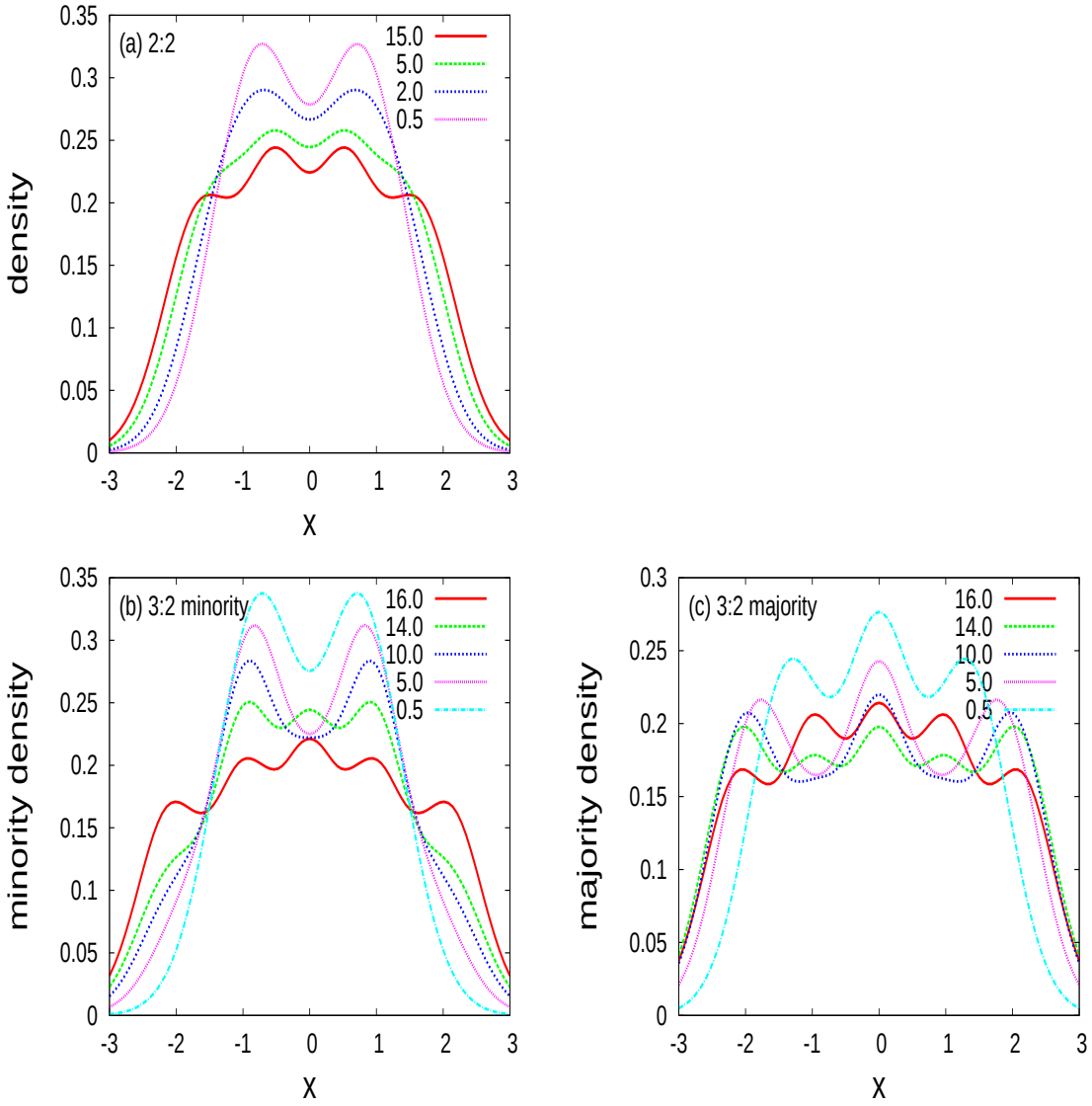


Figure 4.4: one body densities for the case (a) 2:2 (the densities for the two components are identical) and for the case 3:2 for the (b) minority and (c) majority fermions.

strength increases for each pair of atoms and (c) a partially imbalanced case where very close to the resonance additional peaks arise on top of the plateaus in the density.

Most of these theoretical considerations are also studied in a very controllable manner in experiments of few fermion systems with a deterministically preparable atom number [63, 60, 61] which we will report in the next part of this Chapter. The generalization of our Ansatz for the CPWF to mixtures is open to further improvements and applications which were initiated and sketched here, as well as to the extraction of other observables unraveling mechanisms and physical properties characterizing few-body systems in connection with and analogue to the corresponding many-body physics.

## 4.2 Application to the experiment

Our present study is close connection to the experimental work in preparation [63], which has achieved the deterministic loading with a specific number of fermions of their quasi-1D trap with a very high fidelity [60, 61] and accurately controlled imbalance of population. The state-of-the art of these experiments, allows for a study of specific configurations of populations of different hyperfine states like those which we have discussed above: highly imbalanced with one impurity atom surrounded by several (1-5) majority atoms, as well as a balanced or partially imbalanced ensemble. The first efforts of this group have concentrated on preparing deterministically the number of fermions in the trap [60] with an innovative trick: they open partially the trap from the one side by a constant magnetic field and the fermions that are energetically above the barrier tunnel completely out, letting only a part of the Fermi Ladder occupied. Of course this trick is specific for fermions, which occupy high states due to the Fermi pressure (or Pauli exclusion principle). With this innovative mechanism they were also able to measure energies, firstly of two distinguishable atoms [61], the most important underlying theory for the present thesis (see Chapter 1), and confirm the theoretical curves of ref. [14]. To determine the energy after preparing the two atoms, and tuning their interaction to a certain strength via Feshbach and confinement-induced resonances, they opened the trap once again, and measured the tunneling time for one atom to leave the trap. The higher energetically the atoms are due to stronger interaction, the faster they leave the trap. The connection of this tunneling rates with the energy has provided a measurement of the lowest repulsive and super-repulsive state of Ref. [14] for the 1D case. Extending their study to larger number of atoms, and probing the transition 'from two to few' (or 'from few to many') is the next step of these experiments which nicely meets the concept of the present theoretical thesis.

**System** The first idea and current research focus of these experiments after the realization of the two atom (1:1) case, is to add majority atoms 'one-by-one' in the fermi see around the impurity and measure the energy via radio-frequency spectroscopy. This preparation of the fermi see follows the exactly opposite pathway to the standard method of loading impurities in a fermi see, to study impurity or polaronic physics. The aim is to probe the transition to the thermodynamic limit $N_M \to \infty$ step by step or better 'atom by atom'. The system is consisted of a two component Fermi gas ($^6$Li) with the two species prepared in the two lowest hyperfine states [60, 61]. The trap is in a good approximation harmonic and quasi-1D since the ratio between the longitudinal over the transversal trap frequency is $\omega_\parallel/\omega_\perp \approx 1/10$. After preparing a few-body equal population system, the trap is opened from the one side only for atoms belonging to one hyperfine state, leaving only one atom of this component in the trap playing the role of the impurity (while the majority atoms remain trapped) and thus the configurations 1:1, 2:1, 3:1, 4:1 and 5:1 are obtained. The system is described by the same pure 1D Hamiltonian Eq. 4.1 but we have to underline that the scaling is somewhat different

taking the reduced-mass $\mu$ instead of the atom mass $m$ in the relevant length $a_{\parallel} \equiv \sqrt{\frac{\hbar}{\mu\omega_{\parallel}}}$ and energy scale $\hbar\omega_{\parallel}$ to be in accordance with the experimental units. Therefore also the interaction strength $g$ values considered below should be multiplied with $\sqrt{2}$ to transform to the old units.

### 4.2.1 Energy

Two values of the interaction strength a weak $g = 0.26$ and a stronger one $g = 2.009$ are measured on the repulsive side of the resonance for all configurations. The experimental data for the energy gain per majority atom due to the interaction $\Delta E = E(g) - E(g = 0)$ are shown in Fig. 4.5 (a) for both interaction strengths and for all configurations $N_{maj} = 1, ..., 5$ while Fig. 4.5 (b) and (c) focus on weak and strong interactions respectively. Predictions of numerical calculations in a pure 1D harmonic trap with MCTDH (see section above) plotted in the same figures show a very good agreement with the experiment. We have seen in the previous section that the CPWF deviates slightly (2-3%) from the numerical results, therefore also from the experimental. Therefore only numerical exact calculations are shown here for simplicity, and in order to keep the focus on the experimental results. These results demonstrate that for higher interaction strength $g = 2.009$ we have higher gain of energy, while for increasing number of majority atom the energy gain per atom becomes lower and vanishes as $N_{maj} \to \infty$ since the energy gain is finite for finite $g$ and distributes to more and more atoms. The higher value that the energy gain can reach is at the TG-limit $g \to \infty$ $\Delta E \to N_{maj}$ which can be understood as a crossover of the non-identical impurity atom to become 'identical' due to the interaction (see Chapter 4.1 and Chapter 1). Since the impurity lying for $g = 0$ on the single-particle ground state of the harmonic trap it has to jump $N_{maj}$ states to reach the Fermi energy (the highest occupied state for the system of $N$ identical fermions).

One of the main purposes of the experiment is to reach the thermodynamic limit of $N_{maj} \to \infty$. Our methods focusing mainly on few body physics are not capable to make claims on this limit. One approach that has been tried is to use the theoretical results obtained in the continuum (without trapping potential) in the seminal paper of McGuire [141]. This paper uses a Bethe-Ansatz approach like in the Lieb-Liniger model (see Chapter 1) to calculate the wavefunction in the continuum for an impurity atom in the Fermi-see. In the limit of $N_{maj} \to \infty$ with $\gamma = g\sqrt{2}/k_F$ constant[2], McGuire obtained the following formula for the energy gain

$$\Delta E = \frac{k_F^2}{\pi}(\gamma/2 + \tan^{-1}(\gamma/2) - (\gamma/2)^2 \left(\frac{\pi}{2} - \tan^{-1}(\gamma/2)\right) \tag{4.5}$$

where $k_F$ denotes the Fermi momentum of $N_{maj}$ atoms which in the case without trap is $(N_{maj} - 1)\pi/L$ with $L$ being the size of the system. This has been shown be in good agreement in 1D systems with other standard theoretical approaches for polaronic physics in the continuum like the particle-hole excitations [142]. Here we will use this formula adapted to the case of the harmonic trap. The energy gain at fermionization is in the case of the the continuum and for $N_{maj} \to \infty$ approximately $\Delta E = E_F = \frac{k_F^2}{2}$. The corresponding energy gain for the harmonic trap is as we have seen $\Delta E = N_{maj}$ (which is a factor 1/2 lower than the Fermi energy which we omit). Therefore we set $k_F = \sqrt{2N_{maj}}$. Then we can plot the results as a function of $\gamma$ according to the formula Eq. 4.5. In Fig. 4.6 we show the experimental data together with McGuire's curve and numerical calculations for finite number of atoms. All curves and experimental data for finite $N_{maj}$ lie between the exact solution for 2 atoms [14] and the $N_{maj} \to \infty$ formula Eq. 4.5. This implies that the latter formula resulting from considerations in the continuum sets an upper limit for the energy gain. An important observation here is that 6-7 atoms are enough

[2]The $\sqrt{2}$ factor appears here again to adapt McGuire's scaling to the experimental one

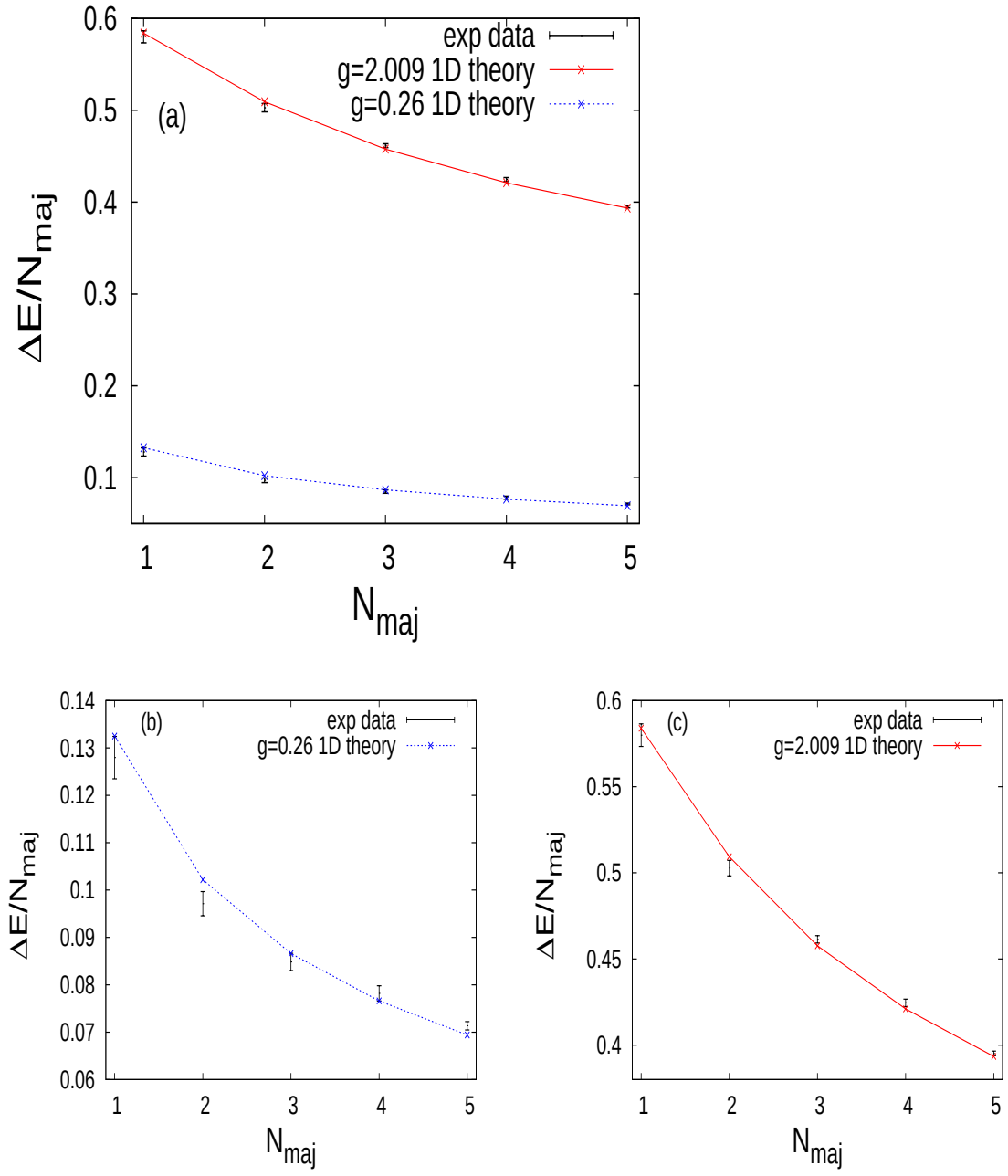


Figure 4.5: (a) Energy gain $\Delta E$ due to the interaction over the number of majority atoms $N_{maj}$ plotted for two different interaction strengths a weak (b) $g = 0.26$ and a stronger one (c) $g = 2.009$.

to capture the physics of the impurity in the 1D trap as both calculations and measurements demonstrate. Adding more majority atoms in the trap lying in excited single-particle states, does not affect the impurity a lot, while in the continuum the majority atoms lie energetically closer and therefore have a larger impact on the impurity. This is observed also in the context of 3D polaron physics where the impurity attracts or repels (as in our case) a few surrounding majority atoms [57, 58]. These results provide a first evidence to the direction of understanding many-body phenomena, via a few body system. In this case experiment and theory go hand in hand, trying to give an answer to very fundamental questions like what is the underlying physics of many-body systems or 'how many is many?'.

### 4.2.2 Impurity tunneling

We have given already the picture of the impurity atom shifted energetically up in the Fermi sea of the majority atoms due to the interaction. While the previous measurement has shown the 'collective' total effect on the energy gain, here we aim to understand the impurity atom itself on its way from the bottom of the trap at $g = 0$ to higher energy levels as $g \to \infty$. The measurement performed here is similar the one described in Ref. [61], where the potential is opened from the one side and one atom is left to tunnel out. The barrier is set to a different hight for each interaction strength, in order to let only one (majority or minority) atom to tunnel out (after a certain holding time), and then a measurement is performed to probe weather the impurity atom has tunneled out or one of the majority atoms. The impurity tunneling is an event which is expected to be rather seldom, since most majority atoms lie on higher energy levels close to the top of the trap and therefore have larger probability to pass the barrier. The experimental results together with theoretical predictions for the tunneling probability of the impurity over the total one-particle tunneling probability are shown in Fig. 4.7. We observe that the impurity does tunnel out only for rather high interactions because it is shifted energetically closer to the edge of the Fermi sea, and therefore close to the top of the barrier.

The theoretical approach to the evaluate the probability of one-particle tunneling and particularly of impurity tunneling relies on a projection of the many-body state onto non-interacting many-body configurations. We denote by 211 in the first two places the energy levels that the majority atoms occupy (in this example first excited and ground state), and in the last place the corresponding level for the impurity (here ground state). The latter configuration is also the starting point at $g = 0$, and the only possible configuration for the atoms (the corresponding antisymmetric configuration 121 is also included on the same time). In this configuration and since the barrier should lie close to the second non-interacting level to let only one atom to tunnel out, we assume that this atom will be always from the majority, since it lies energetically certainly above the impurity. As the interaction strength increases, configurations which have the same total symmetry such as 213 (but not 212) gain population (as a part of the projection coefficients of the many-body state), thereby increasing the probability of minority tunneling since in some of them like 213 or 215 the impurity atom sits energetically above the majority ones on the top. The most important such configurations for the one-particle tunneling are: 211 / 312, 321, 213, 411 / 422, 215, 521, 512 (separated with '/' are levels with different total energy) and from those only 213 and 215 lead to tunneling of the minority. Note here that we have excluded the possibility of two-particle tunneling, i.e., all the states like 413 or 323 which have two atoms above the second energy level. Yet, in this particular measurement one has also to take into account that atoms lying on level 2 may tunnel which is very important due to the increase of majority tunneling from the always highly populated state 211. For this we have used a fitting function of the possibility of one atom tunneling from the second level (within a certain holding time) and the hight of the barrier (this possibility is rather high only for low interactions and low barriers). The theoretical predictions take into account all the

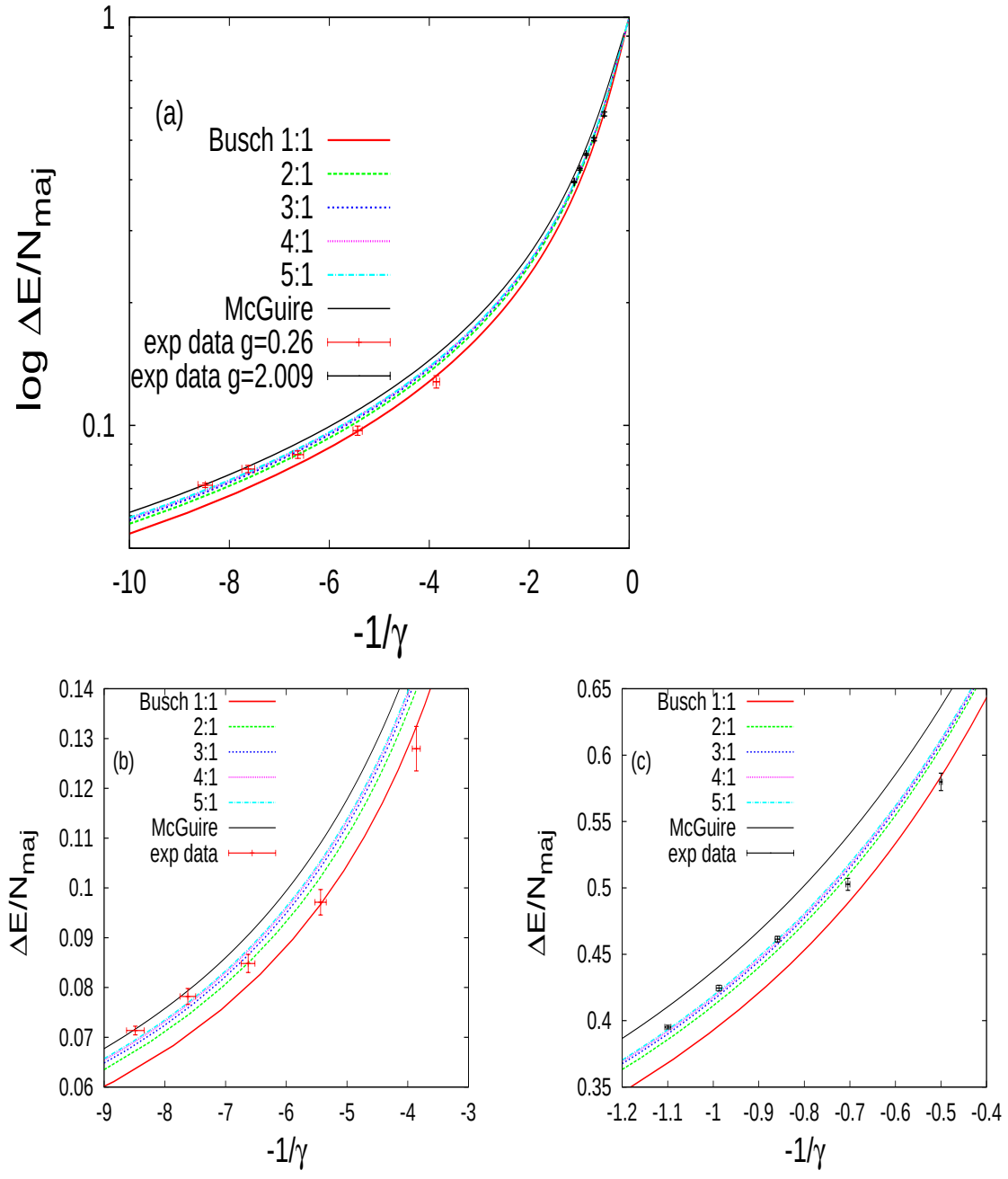


Figure 4.6: (a)Energy gain $\Delta E$ due to the interaction over the number of majority atoms $N_{maj}$ plotted as a function of $-1/\gamma = -\sqrt{N}/g$. Focus on the points for weak (b) $g = 0.26$ and a strong (c) $g = 2.009$ interaction strength.

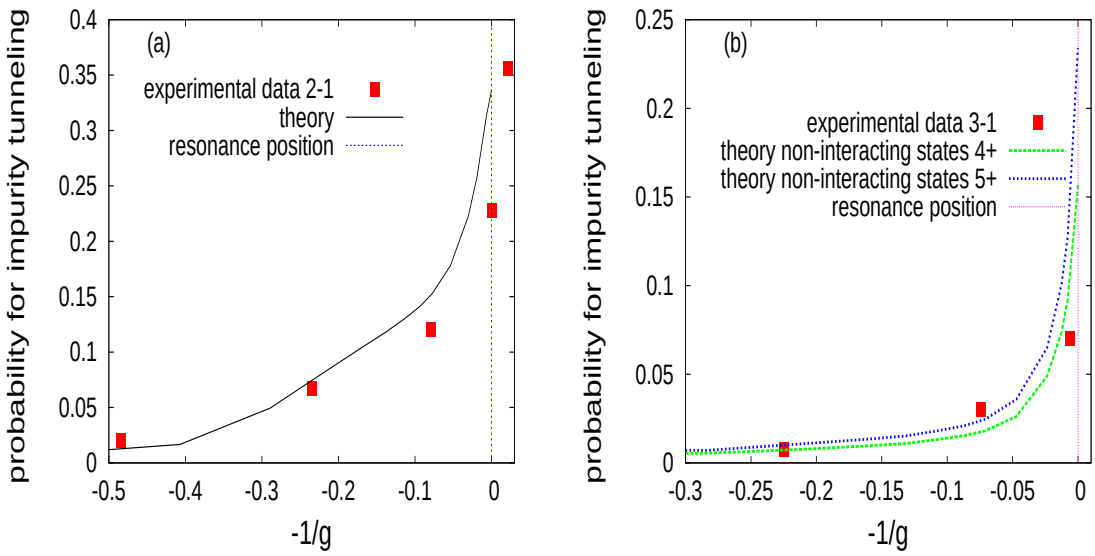


Figure 4.7: (a) $N_{maj} = 2$ and (b) $N_{maj} = 3$ probability of impurity tunneling as a function of $-1/g$

aforementioned states and divide those who give probability of impurity tunneling by all others [P= prob(impurity tunnel)/prob(1-atom tunnel)]. The agreement with the experimental data, demonstrate exactly this behaviour of the impurity which pushes its way up to the top. At fermionization of the impurity, although the atoms are not identical fermions (see also Chapter 1), the probability of minority tunneling reaches approximately 1/3 since all atoms have the same possibility to occupy the highest level.

For the configuration 3-1 the problem is more involved since for the non-interacting ground state 3211 the impurity sits energetically very low at the bottom and therefore is very difficult for it to tunnel. Moreover, the state 3214 is excluded due to symmetry reasons and the only rather highly populated state from which the impurity can tunnel alone is 3215. Additionally the barrier is set rather close the third level where the majority atoms have a lather large probability to tunnel. The involved states here are (the last number denotes always the energy level which the impurity occupies): 3211/ 3213, 4212, 4313, 5211 / 3215, 4214, 4313, 4322, 5213, 5312, 5321, 5411, 6311, 7211. We take two theoretical curves one including only states which have one atom on level 5, and one which has all possibilities with one or two atoms on level 4 and above. Both still reveal an increasing probability of minority tunneling approaching the TG limit, while the latter case shows always a lower probability like the experimental data, since it contains more lower lying states. For the impurity tunneling is also taken 50% from the 4214 state which results from the mechanism shown in [61] where one of the two atoms tunnels out and the energy of the other drops after the tunneling process.

### Conclusive remarks

This very innovative method of probing features of exclusively one (impurity) atom belonging to a highly correlated many-body ensemble, may give very important insights to other polarized systems, in connection to very exciting questions eg. for the physics of itinerant ferromagnetism [55]. Here the physics of an impurity in an 'atom by atom' constructed 1D Fermi sea have been studied, with important implications on the corresponding many-body physics. The system is studied both experimentally and theoretically with very good agreement. The experiment has prepared and probed an 1D highly imbalanced system of a few fermions with one impurity and

a deterministically determined number of majority atoms (up to 5). With the RF spectroscopy measurements the total energy of the highly polarized 1D system has been obtained with a very good accuracy, while the one-atom tunneling measurement can probe the energy shift of the impurity exclusively, since one can still distinguish between the different components even reaching the fermionization limit.

# Chapter 5

# Conclusions and outlook

Conclusive remarks and perspectives have been included in each section of the present thesis. In this Chapter we will only summarize the very basic aspects and provide a more general outlook.

All one-dimensional systems studied in this thesis are investigated numerically or analytically by a bottom-up approach. The basic proposal of this work, the correlated-pair wavefunction, is inspired from the solution of two-body problem in a harmonic trap. Generalizing the function describing the two-atom problem to approach the crossover from weak to strong repulsive interactions of the trapped many-body system of bosons (Chapter 2.1) or two-component fermions (Chapter 4.1) we were able to capture qualitatively but also quantitatively main features of observables like energies and densities. A basic feature and inspiration for our approach have been –apart from the two-body case – the exact solutions for the infinitely repulsive limit (Tonks-Girardeau gas) which our function reproduces and for the crossover in the homogeneous case [all analyzed in Chapter 1]. In the trapped case, since there is no exact solution that covers the whole crossover, we compare observables like the energy and the density obtained by our Ansatz, the correlated-pair wavefunction, with numerical calculations via the Multi-Configurational Time-Dependent Hartree method and Quantum Monte Carlo (Appendix A) showing a very good qualitative and quantitative agreement.

Apart from this approach we analyze in detail effects appearing for strong interactions beyond the single band Bose-Hubbard model for one-dimensional finite lattices (Chapter 3.1). We discuss different classes of commensurability and localization mechanisms, and uncover strong correlation effects for large filling factors and strong interactions, like on-site broadening and peaks in the density and correlation-holes in the pair-correlation function. Particularly incommensurate setups make it possible for an inhomogeneous distribution of the density and correlation properties. A detailed study has been also performed for the fermionic two-component mixture in Chapter 4.1 for various population imbalances. Especially the case of a single impurity in a few body Fermi sea, shows a very special behaviour in the one-dimensional case, with strong correlation effects between the impurity atom and the surrounding ones. Our results for this case have been also compared with recent experimental measurements (Chapter 4.2) showing a very good agreement.

Not only stationary but also dynamical properties have been studied in this thesis. The resonant mechanisms of excitation and acceleration in a harmonic trap with driven interaction strength have been analyzed via a bottom-up approach stemming out from the two-body energy and Floquet spectrum and the corresponding properties of the stationary many-body spectrum (Chapter 2.2). In a different context, resonant tunneling mechanisms which brake the self-trapping in the strongly interacting regime have been unveiled with few atoms in a triple well (Chapter 3.2). The bottom-up approach here is based on generalized number states which take into account the on-site interaction and its effect on the many-body energy. The mechanisms

of inter-band tunneling going beyond the single-band approach make it possible to control and design the transfer of a specific number of atoms (single- and two- atom processes have been shown) to a particular excited state (or band).

In all systems tackled here we have concluded that our bottom-up approach can shed new light to extensively studied phenomena, but also to uncover novel effects which appear in strongly correlated many-body systems. The questions and further research options that pop up from these investigations are twofold. On the one hand, this study can be extended to other systems, setups and phenomena. Most directly one may explore other potential landscapes, possibly with higher dimensionality (2D and 3D) or mixed dimensions, or different configurations of mixed systems (eg. Fermi-Bose or Bose-Bose mixtures). Another possibility is to change the nature of the interaction, eg. taking dipolar forces changing drastically the two-body properties which are the basis of the bottom-up approach proposed here. The 'two-to-many' perspective has to be extended to really large ensembles of atoms in order to approach the thermodynamic limit and possibly address the question 'how many is many?'. On the other hand, a further deepening in the fundamental systems discussed here, possible developments, improvements and analysis of the properties of the correlated-pair wavefunction bottom-up approach as well as the examination of other observables can provide more insight to the many-body physics from a two-body perspective. We may conclude that 'more is indeed different' but the knowledge we gain from the 'single pair' and its correlation properties is very insightful for the many-body system.

# Appendix A

# Computational methods

Treating time-dependent or independent quantum systems with many interacting degrees of freedom, i.e. solving the corresponding Schrödinger equation, is a computationally very demanding problem. In the standard approaches the many-body wavefunction for a highly-correlated ensemble should be represented in terms of an enormous basis of single-particle functions, rendering the Hilbert space very huge. Unavoidably all methods for ab initio numerical calculations employ a truncation of the Hilbert space, in the best case still able to represent the main features of the function, and to reduce the computational effort meanwhile assuring the convergence of the process[1]. The most natural and direct of all methods is of course the exact diagonalization, which is nothing but the most standard approach of quantum mechanics, for any Hamiltonian system. The Hamiltonian operator $H$ is expressed as a set of matrix elements $H_{kl} =< k|H|l >$ where $|k >, |l >$ are elements of the orthonormal basis which can be choosen according to the particular features of the problem (truncated of course to render the algorithm feasible). Computational schemes then allow to diagonalize this matrix and obtain the corresponding eigenstates and eigenvalues. The many-body nature of the problem is represented in the basis vectors typically by number states which are usually a superposition of single-particle states, each one assigned to a certain degree-of-freedom. A highly correlated system requires a lot of such uncorrelated basis states to be adequately treated, rendering the standard computational methods inoperative. Yet there is a workaround which helps the reduction of the necessary basis vectors, if they are variationally optimized. A relatively smaller non-fixed single-particle basis, subject to a variational principle, is likely to represent the correlated state more effectively and render the corresponding code feasible. In general terms this procedure is also a part of the method we resorted to in the largest part of the present thesis, the Multi-Configurational Time-Dependent Hartree (MCTDH) which we explain in details in the first Section A.1 of this Appendix. The straight-forward exact diagonalization is only used selectively in certain cases of small ensembles (2-4 atoms) to cross-check the MCTDH results. MCTDH is also an inherently time-dependent code (wave-packet propagation), very efficient for driven systems (see

[1] Another possibility is of course to reduce the complexity of the problem itself, by proposing a simplified model which is equally rich and captures the physical properties of the system (e.g. the GPE or the BHM see Chapter 3.1). The procedure of consecutive simplifications and modeling of the natural reality is probably the strongest tradition in physics, and in fact the usual method it employs to approach a problem. For instance the models and systems studied in this thesis are all simplifications of the real scattering and interaction processes happening even in this highly isolated, ideally controlled quantum world of experimental ultracold atom realizations [5]. The mere fact that we consider purely one-dimensional confining potentials in zero temperature is already a strong approximation. Therefore the purpose here is to tackle the problem without any further simplifications, as the Hamiltonians studied in this thesis describe it (and this is thought and proved to be accurate enough for many experimental realizations). The way out of the complexity proposed here are the analytical functions to describe the highly-correlated many-body ensemble inspired from the relatively simpler and more intuitive two-body problem.

eg. Chapter 2.2) as well as time-evolution of wave-packets (see e.g. Chapter 3.2) and therefore ideal for the purposes of the present thesis. Other popular methods also very efficient for highly-correlated low-dimensional systems include the Density-Martix Renormalization group [28] and Quantum Monte Carlo (QMC) citeastra. The latter method, with a different philosophy from the others, combining variational and diffusion Monte-Carlo, has been also used complementary in this thesis for stationary problems to cover larger numbers of particles, and will be exposed in the second Section A.2 of this Appendix. Apart from these state-of-the-art methods, there is a whole tradition in cold-atom physics based on mean-field approaches such as the celebrated GPE, the Bogoliubov theory extended also to multi-orbital mean field providing explanations to several phenomena within there range of validity (typically weak interactions). Although at certain points we will resort to benchmark results obtained by the latter methods, our treatment of highly-correlated systems takes a detour of mean-field approaches in general, trying to move the standard single-particle picture to a single-pair one with the correlated-pair functions as a building stone. In the following sections we will then only refer in detail to the two numerical methods used within these thesis MCTDH ( Section 6.1) and QMC (Section 6.2).

## A.1 Multi-configurational time-dependent Hartree

The MCTDH method [39] is the computational tool which is applied in all systems discussed in this thesis, providing also all observable quantities which are shown and compared with other approaches. MCTDH is in principle a wave-packet propagation method, very efficient for higher dimensional problems and correlated systems, typically for molecular and nuclear applications (usually with non-identical particles). It has been proven to be reliable also systems with few cold bosons first with respect to their static properties in harmonic trap and double well [29] as well as corresponding dynamics [40]. Extensions to bosonic mixtures either of different mass, or different hyperfine state have been performed [29, 40, 41]. In the present thesis some of these calculations are repeated and refined (concerning mainly the harmonic trap for bosons) while the application of MCTDH is extended to mixtures of fermions (Chapter 4.1) and explicitly time-dependent (driven) systems (Chapter 2.2). In other works, MCTDH has been extended also to treat already by the construction of the corresponding Ansatz bosonic (MCTDHB) [147] or fermionic systems (MCTDHF) [148] as well as multi-layer schemes (ML-MCTDH). In this thesis we have resorted to the initial Heidelberg MCTDH package [149] implemented for distinguishable particles and enforce the correct (anti)symmetry by the corresponding choice of the coefficients of the MCTDH expansion as it was done in previous few body studies [29, 40, 41]. All methodological details around MCTDH and its extensions are explained extensively in corresponding textbooks and reviews of the pioneering scientists [39]. Here we will essentially summarize the main ideas, with a focus on the treatment of indistinguishable atomic systems and particular relevant tricks and considerations that have been employed within the present thesis.

### A.1.1 The main idea

Within MCTDH, the time-dependent Schrödinger equation

$$\begin{cases} i\dot{\Psi} = H\Psi \\ \Psi(Q,0) = \Psi_0(Q) \end{cases} \tag{A.1}$$

is treated as an initial-value problem by an expansion in terms of direct (or Hartree)products $\Phi_J$:

$$\Psi(Q,t) \;=\; \sum_J A_J(t)\Phi_J(Q,t)$$

$$\equiv \sum_{j_1=1}^{n_1} \dots \sum_{j_f=1}^{n_f} A_{j_1 \dots j_f}(t) \prod_{k=1}^{f} \varphi_{j_\kappa}^{(k)}(x_k, t), \tag{A.2}$$

using a convenient multi-index notation for the configurations, $J = (j_1 \dots j_f)$, where $f = N$ denotes the number of degrees of freedom and $Q \equiv (x_1, \dots, x_f)^T$. The single-particle functions $\varphi_{j_\kappa}^{(\kappa)}$ are in turn represented in a fixed, primitive basis implemented on a grid. For indistinguishable particles as in our case, the single-particle functions for each degree of freedom $\kappa = 1, \dots, N$ are of course identical in both type and number ($\varphi_{j_\kappa}$, with $j_\kappa \leq n$).

The principle idea of MCTDH is to treat both the coefficients $A_J$ and the Hartree products $\Phi_J$ in the above expansion variationally at every time step (therefore both of them are time-dependent). Using the Dirac-Frenkel variational principle, one derives equations of motion for both $A_J, \Phi_J$:

$$i\dot{A}_J = \sum_L \langle \Phi_J | H | \Phi_L \rangle A_L \tag{A.3}$$

$$i\dot{\varphi}^\kappa = \left(1 - P^k\right) \left(\rho^k\right)^{-1} \langle H \rangle^k \varphi^k \tag{A.4}$$

where $P^\kappa = \sum_{j=1}^{n_k} |{\varphi_j}^k\rangle\langle{\varphi_j}^k|$ is the projection operator on the orthogonal complement of the single-particle basis functions, $\rho_{jl}^k = \langle {\varphi_j}^k | \hat{\rho}_1^k | {\varphi_l}^k \rangle$ is the reduced one-body density matrix and $\langle H \rangle_{jl}^k = \langle \Psi_j^k | \hat{\rho}_1^k | \Psi_l^k \rangle$ is the mean-field Hamiltonian on the basis of functions ${\Psi_j}^k = \langle \varphi_j^k | \Psi \rangle$ (the k-th degree of freedom has been integrated out).

The advantage here is that the basis $\{\Phi_J(\cdot, t)\}$ is variationally optimal at each time $t$, allowing us to keep it fairly small. Exactly for this reason MCTDH is ideally designed to solve time-dependent Hamiltonians like driven and in general time-dependent and highly-correlated systems. The correct permutation symmetry can be enforced by symmetrizing the coefficients $A_J$ using (anti)symmetric superpositions of Hartree products for (fermions) bosons [2]. In the state-of-the art versions of MCTDH the permutation symmetry is by construction imposed to the Ansatz (permanents or Slatter determinants) for bosons [147] (MCTDHB) or fermions [148] (MCTDHF), while for mixtures one may use different layers of single-particle products in a multi-layer scheme (ML-MCTDH).

### A.1.2 Calculating stationary states and dynamics

Although the code is in principle designed for wave-packet dynamics, the calculation of stationary states is also incorporated, among other reasons to make an initial state preparation possible. The Heidelberg MCTDH package [149] includes the so-called relaxation method which provides the lowest eigenstates of the system by propagating a wavefunction $\Psi_0$ (usually the many-body product of single-particle functions of the corresponding single-particle problem) by the non-unitary operator $e^{-H\tau}$ propagation in imaginary time. For reasonably large time of propagation $\tau \to \infty$, this automatically damps out any other contribution except that of the ground state where it relaxes

$$e^{-H\tau}\Psi_0 = \sum_J e^{-E_J\tau} |J\rangle\langle J|\Psi_0\rangle. \tag{A.5}$$

Also available in the code is the scheme of improved relaxation [150] where $\langle \Psi | H - E | \Psi \rangle$ is minimised with respect to both the coefficients $A_J$ and the configurations $\Phi_J$. The equations

[2] The ground state is automatically of bosonic character also for nonidentical atoms. Of course for identical-fermions antisymmetrization of the coefficients should be enforced.

of motion are solved iteratively, first for $A_J(t)$ (by diagonalisation of $\langle\Phi_J|H|\Phi_K\rangle$ with fixed $\Phi_J$) and then propagating $\Phi_J$ in imaginary time over a short period. The cycle will then be repeated. The latter method is used in the present work to calculate the eigenstates and the energy spectrum for all systems studied. The method is reliable and already used in previous works [29], but one has to take care for instabilities in intermediate and strong interaction strengths. An important trick is to use the function obtained for a certain interaction strength $g$ as an initial guess for a slightly increased $g$ in order to avoid large and unstable variations, especially for excited states which may lie close to other ones.

Another technical point is the effort of this method which scales exponentially with the number of degrees of freedom, $n^N$. As an illustration, using 15 single-particle functions and $N = 5$ identical bosons requires $7.6 \cdot 10^5$ configurations $J$. This fact restricts the number of atoms that can be treated via MCTDH depending of course on the strength of the correlation. In any case, it is possible to cover at least for the ground state up to $N = 6$ atoms with 10 orbitals in the whole crossover from weak to strong interactions (and fermionization in 1D). Still a finite number of even optimized orbitals are not sufficient to represent correlated many-body states. This inherent deficit of all methods using a truncated Hilbert space, can be healed in certain cases by repeating the same calculation with increasing number of orbitals, and thereby check weather the code has converged. This convergence check has been employed allover in the present thesis.

Recently useful workaround to this problem has been proposed in Ref. [151] and employed also here enhancing a lot the calculations of the ground state in 1D. The main idea is to take advantage of the fact that in 1D systems there is the exactly known limit of TG gas at interaction strength $g \to \infty$ (see Chapter 1). Therefore the upper limit of the ground state energy of the system, i.e. the energy at fermionization, can be calculated given that one knows the single particle spectrum (from exact calculations or analytical formulas); The energy obtained from any truncated Hilbert space method, will at some finite $g_0$ cross the fermionization energy. Only by using infinitely many orbitals one could avoid this fact. The proposal of the authors in Ref. [151] is to rescale the numerically used interaction strength parameter $g_n$ such as $g_0$ becomes the real fermionization limit. This can be done by the formula:

$$g = \frac{g_n}{1 - g_n/g_0} \tag{A.6}$$

which ensures that $g \to \infty$ when $g_n = g_0$. All higher values of the numerical coupling strength $g_n$ are skipped as unphysical. This trick has been in detailed explained and checked not only concerning the energy but also other observables like the one-body density (where another $g_0$ should be chosen according to the closeness of the function profile to the fermionized one), showing firstly a vast improvement of the agreement between numerical results and solutions of integrable systems in 1D (Lieb-Liniger and two atoms in harmonic trap, see Chapter 1). We have also resorted to this method for the calculations of ground state energy of bosons and fermions, and cross-checked results obtained also with different number of single-particle functions. This double-check of the numerical results, have been proven to be very important and efficient, since for example energies obtained with sufficiently enough orbitals (6-10) are in very good agreement if one additionally rescales the interaction strength $g$ according to the above. This in fact enhances also the numerical effort since lower number of single-particle functions can be used. However, we have explicitly used this trick only for energy calculations, since other observables like densities (with functional form) are difficult to judge with respect to their agreement with the fermionization profile. In fact other observables are generally not so sensitive to small changes of the interaction strength. Still this method is certainly important and valuable for truncated Hilbert space 1D calculations.

A further technical detail concerns the representation of the $\delta$-like profile of the interaction potential. We have used a potfit scheme already included in the package of MCTDH with a very narrow Gaussian profile

$$\delta(x) \approx \frac{1}{\sqrt{2\pi\sigma^2}} e^{-x^2/2\sigma^2} \tag{A.7}$$

choosing the effective width $\sigma = 0.02 - 0.05$ such that it is small enough to portray a contact interaction, but large enough to be sufficiently represented on the grid (typically of $0.01 - 0.03$ spacing). A cross check of certain cases using different $\sigma$ and grid spacings was also performed without substantial differences between different configurations. In general the griding affects the effort of the calculations but not so immense as the number of single-particle functions, and the workaround exposed previously in principle heals all numerical limitations.

On the other hand, the propagation in time of an initially prepared wave packet, should be done by a lower number of atoms (typically 2-4) such that one can use enough orbitals (around 20-40) to describe it correctly in a reasonable time and ensure convergence. MCTDH is very powerful especially at this type of calculation due to the optimization to the orbitals at each time step, making even long-time dynamical calculations for relatively weak correlations available. For driven systems which is the specialty of MCTDH one should take care to provide a lot of orbitals if the calculation is close to a resonance (see Chapter 2.2) and multiple excitation processes are expected. The time-evolution of the systems studied in this thesis, has been checked by repeating the same calculation with a larger number of orbitals and checking for short-and medium time convergence in the cases where this is possible. For an extension of this work to larger number of atoms one should employ the state-of-the-art methods specialized on bosons or fermions (MCTDHB or MCTDHF) while for mixtures a multi-layer scheme would enhance the calculations dividing the space to more and less correlated degrees of freedom.

For the calculation of the ground state of bosonic systems we have used also the Quantum Monte Carlo method, which we shortly explain next, performing thereby a crosscheck for few atoms with the MCTDH results and extending the calculations to more particles.

## A.2 Quantum Monte Carlo

The Quantum Monte Carlo (QMC) method, is one of the most popular in the field of cold atoms and not only. Based on a random process in the course of which some artificial particles called walkers are distributed in space (Markov chain) is ideal for large ensembles of atoms. It is very convenient for the treatment of second quantization Hamiltonians like the Bose-Hubbard model for extracting the properties of the system, but also for calculations explicitly on the configuration space, like those we perform here. There are several types of the method, the path-integral (based on the partition function to extract the observables), the Variational (VMC) and the Diffusion (DMC) Monte Carlo. The latter two are employed in this thesis for the calculation of the ground state of bosons in the harmonic trap and finite lattices. A standard tool of the DMC method is to use a so-called guiding (or sampling or trial) function which acts as a 'guide' to the walkers such that they tend to sample more the important regions of the configuration space. Especially for correlated many body problems there are explicitly correlated functions typically of Jastrow type optimized by a VMC calculation which have been employed in several works. Here we propose a modification of this guiding function, in particular of its two-body term according to our correlated-pair wavefunction, inspired for the two-atom problem in the trap. This function is not only used as a guiding here, but it is actually compared as a (variational) Ansatz with which we compare the final DMC results. Therefore we next present the main ideas of the method, with particular focus on the important role of the guiding function.

### A.2.1 Main ideas

The key idea of the QMC method, is the importance sampling which allows to distribute spatial configurations of the atoms such that the correspond to a physical probability distribution. The observables can then be obtained by estimators which are essentially the arithmetic average value. The idea is better illustrated in the scheme of Monte-Carlo integration. The integral over the configuration space of the function $f(x)$ [in the following $x$ denotes a vector containing the positions of the $N$ atoms) is usually done by a sample of equally spaced grid points $x_i$ with the estimator $I = \sum f(x_i)/N$. Monte-Carlo integrals first choose a sampling function $g(x)$ (normalized as a probability function) which should have the overall properties and shape of $f(x)$ such that the important regions of the configuration space are better covered. Then the Monte-Carlo estimator of the integral is $I_{MC} = \frac{1}{N}\sum \frac{f(x_i)}{g(x_i)}$.

The VMC technique is in particular the application of this method to the calculation of the expectation value of the energy. In the standard variational process, one chooses (or makes a good guess) a certain function $\psi_T(x)$ with one or more free (variational) parameters. Then one calculates for a certain set of the variational parameters the expectation value of the hamiltonian operator with the Monte-Carlo scheme choosing as probability distribution for the sampling points (or measure of the integral):

$$g(x) = \frac{|\psi_T(x)|^2}{\int |\psi_T(x)|^2 dx} \tag{A.8}$$

and as kernel of the integral the so-called local energy:

$$E_L(x) = \frac{H\psi_T}{\Psi_T}. \tag{A.9}$$

Then the variational energy $E_{var} = \int g(x)E(x)dx \geq E_0$ is here calculated as a sum $E_{var} = \sum E_L(x_i)/N$ over the $N$ sampling points $x_i$ chosen randomly according to the probability distribution function $g(x)$ and results to an upper limit for the true ground state energy $E_0$. To proceed for optimization of the trial function $\psi_T(x)$ one chooses other sets of variational parameters and tries to find the one which minimizes the energy. Obviously the whole process of variational optimization is severely dependent on weather the initial guess is a good one in the sense that it captures the main shape and properties of the function. Since this is not always the case, one may obtain an upper limit for the energy from a VMC calculation but then use the corresponding function as an educated guess for the DMC calculation which does not possess this restriction and converges to the numerically exact ground state.

The DMC method essentially also relies to an imaginary time propagation (or diffusion) such as MCTDH relaxation process. The idea of solving it is though different than that of MCTDH, and relies on stochastic processes which in the typical algorithms take the form of Markov chains. The Markov chains are well defined memoryless transitions from one state to another since they depend only on the state in the previous time step and not on states further in the past. A random walk (Markov chain) procedure is applied on the walkers that in our case represent spatial configurations of the atoms in the N-body space. We will explain next in brief how this is seen from the perspective of Green functions and how it is in fact applied algorithmically.

The aim of the DMC method is to solve the diffusion equation (Schrödinger in imaginary time) $\frac{\partial\psi(x,\tau)}{\partial\tau} = -H\psi$. In terms of the Greens function $G(x', x, \tau) = \langle xe^{-\tau\hat{H}}\rangle$ the solution can be written as $\psi(x', \tau) = \int G(x', x, \tau)\psi(x, 0)dx$. Performing a short time approximation one may neglect higher orders of $\mathcal{O}(\tau^3)$ and then split the exponential containing the Hamiltonian to kinetic $\hat{K}$ and potential term $\hat{V}$ as $e^{-\tau\hat{K}}e^{-\tau\hat{V}}$. Then for a small time step $\Delta\tau$ we obtain for

the Greens function

$$G(x', x, \Delta\tau) = \left(\frac{1}{2\pi\Delta\tau}\right)^{N/2} e^{-\frac{(x-x')^2}{2\Delta\tau}} e^{-\Delta\tau V(x')}. \tag{A.10}$$

This can also be seen as a transition probability (in terms of a Markov chain) from configuration $x$ to $x'$. To do so one should correspondingly impose the normalization of the Greens function multiplying with $e^{\Delta\tau E_R}$ which in other words means that we solve a new Hamiltonian $H' = K + V - E_R$. The reference energy $E_R$ is a shift of the energy such that the ground state is always set as zero, but exactly this $E_R$ converges to a value (or oscillates around it) which is the numerically exact ground state energy. The normalization of the Greens function is adequate condition to preserve the norm of the state itself but only in the case that the state is everywhere positive. This is the case for bosons, but not for fermions which suffer from the well-known sign problem of QMC calculations usually healed by the fixed node approach. Since in this thesis QMC is only applied to bosonic systems this problem will does not affect the calculations.

The essential feature of importance sampling is applied through the Ansatz of QMC which is mixed product of a guiding (or trial) function $\psi_G(x)$ and the wave-function $\psi(x.\tau)$ (unknown solution of the Hamiltonian $H'$) : $f(x, \tau) = \psi(x, \tau)\psi_G(x, \tau)$. This function satisfies the Fokker-Plank equation (derived from the diffusion):

$$\frac{\partial f(x,\tau)}{\partial \tau} = \frac{1}{2}\frac{\partial}{\partial x}\left(\frac{\partial}{\partial x} - F(x)\right) f(x,\tau) - (E_L(x) - E_R)\, f(x,\tau). \tag{A.11}$$

where $F(x) = 2\frac{\partial\psi_G(x)}{\psi_G(x)}$ is the so-called quantum force which then enters the short-time approximation of the Greens function via the effective the kinetic energy term $\hat{K} = \frac{1}{2}\frac{\partial}{\partial x}\left(\frac{\partial}{\partial x} - F(x)\right)$.

We can rewrite now the short-time approximation Greens function as product of two terms: $G(x', x, \Delta\tau) = G_D(x', x, \Delta\tau)G_B(x', x, \Delta\tau)$. The diffusion term:

$$G_D(x', x, \Delta\tau) = e^{-\frac{(x-x'+\Delta\tau F(x)/2)^2}{2\Delta\tau}} \tag{A.12}$$

which algorithmically is interpreted as a random step $x' = x + \Delta\tau F(x)/2 + \sqrt{\Delta\tau}\eta$ where $\eta$ is a random variable with Gaussian distribution. The appearance of the quantum force and therefore of the guiding function in this step is crucial and underlines the importance of an educated guess for $\psi_G$ which should guide optimally the random process. This random step has an acceptance rate according to the Markovian chain prescriptions:

$$p = \frac{G_D(x', x, \Delta\tau)\psi_G^2(x')}{G_D(x, x', \Delta\tau)\psi_G^2(x)} \tag{A.13}$$

(in case this quantity is greater than one the step is always accepted). If the step is accepted then the branching term of the Greens function

$$G_B(x', x, \Delta\tau) = e^{-\Delta\tau(E_L - E_R)} \tag{A.14}$$

is calculated and the walkers are reweighted accordingly multiplying each walker weight by $G_B$. Here we rather used and birth and death process for the walkers instead of reweighting. In this scheme the branching factor $G_B$ defines how may copies of new walkers (in the new positions) will be created, and if $q$ is very small the walker is killed. By this random walk process the walkers are guided to the positions where they minimize the total energy of the system, and this is the core idea of the DMC code.

### A.2.2 The guiding function

In all of the three algorithmic steps described in the previous section –the random walk step, the acceptance and the branching process– as well as for the initial guess to start the DMC calculation, the guiding (or trial) function plays a crucial role. Essentially it governs the whole stochastic process and the its outcomes, and therefore the choice one makes is essential. Furthermore the distribution we finally obtain after the DMC run $f(x_1, ..., x_N) = \psi_0(x_1, ..., x_N)\psi_G(x_1, ..., x_N)$ is also a mixed product containing not only the true many-body ground state $\psi_0$ but also the guiding function $\psi_G$. Therefore observables like densities should be treated accordingly. For all operators there $\hat{A}$ is the so-called pure estimator $\langle\hat{A}\rangle_p = \langle\psi_0|A|\psi_0\rangle$ (using the exact ground state) and the variational estimator $\langle\hat{A}\rangle_v = \langle\psi_G|A|\psi_G\rangle$ (using the trial or guiding function), but here one should use the mixed estimator which contains both functions:

$$\langle\hat{A}\rangle_m = \frac{\langle\psi_G|A|\psi_0\rangle}{\langle\psi_G|\psi_0\rangle} \tag{A.15}$$

For example the one-body density should be calculated as follows

$$\rho(x, x') = \int \psi_0(x, ..., x_N)\psi_G(x', ..., x_N)dx_2dx_N \tag{A.16}$$

$$= \int f(x_1, ..., x_N)\frac{\psi_G(x', ..., x_N)}{\psi_G(x, ..., x_N)}dx_2dx_N \tag{A.17}$$

where we use as a measure for the integral in the spirit of Monte-Carlo integration the quantity $\frac{\psi_G(x',...,x_N)}{\psi_G(x,...,x_N)}dx_2dx_N$ which is only dependent on the guiding function.

For the construction of an optimal guiding function, the particular features of the physical system are very important. Considering 1D interacting bosonic ensembles the standard approach is to make a product Ansatz containing a single-particle part, which mainly deals with the properties of the trapping potential and a two-body interaction part accounting for the pairwise short range collision properties:

$$\psi_G(x_1, ..., x_N) = \prod_{i=1}^{N}\psi_{SPP}(x_i)\prod_{i<j}\psi_{IP}(x_i - x_j) \tag{A.18}$$

The typical functions that are used for the single-particle part in the case of harmonic trap are Gaussian distributions $e^{-\beta x^2}$ where $\beta$ can be used as a variational parameter for the VMC calculation. For the interaction part almost all approaches use the trigonometric functions $\cos[k(|x_ij| - L/2)]$ which are in close connection with the solution of the problem in the continuum (LL-model see Chapter 1) with one variational parameter $L$, and $k$ determined from the boundary condition (or Bethe condition as it is often called –see Chapter. 1, 2.1). Our approach in the present thesis is to use for the interaction part the solution of the two-body problem in the trap the hypergeometric functions $U\left(-\frac{\nu}{2}, \frac{1}{2}, \frac{x_{ij}^2}{2}\right)$. The main advantage of this approach, apart from the conceptual one (using the exact two-body for the corresponding many-body case), is that there is no need for variational parameters on the first place, as it is the case for the parameter $L$ in the standard approach. Further discussion on these approach and its extension to finite lattices is left to the main part of the thesis (see Chapter 2.1). In this methodological Appendix our main intention was to illustrate the importance of choosing an appropriate guiding function for the QMC method.

# Appendix B

# Special Functions

> In the characters too, exactly as in the structure of the incidents, [the poet] ought always to seek what is either necessary or probable, so that it is either necessary or probable that a person of such-and-such a sort say or do things of the same sort, and it is either necessary or probable that this [incident] happen after that one. It is obvious that the solutions of plots too should come about as a result of the plot itself, and not from a contrivance, as in the Medea and in the passage about sailing home in the Iliad. A contrivance must be used for matters outside the drama—either previous events which are beyond human knowledge, or later ones that need to be foretold or announced. For we grant that the gods can see everything. There should be nothing improbable in the incidents; otherwise, it should be outside the tragedy, e.g., that in Sophocles' Oedipus.
>
> *Aristotle*, Poetics (1454 a33-b9) [on "*Deus ex machina*"]

Functions are mathematical objects or machines which serve a very specific purpose or "function": they associate (or transform) each input (from a set of inputs called arguments) with exactly one unique output. One can imagine and construct arbitrarily many such objects. Some of them though have become very popular since –due to their particular properties– they occur very frequently as solutions to basic mathematical problems and physical models. For their great contribution they are awarded with names. Some of them are build from basic operations (addition etc) and are categorized as elementary. Such are for example the algebraic functions (polynomials, roots, etc) and transcendental functions (exponential, hyperbolic, logarithm, periodic and trigonometric functions, etc). These constitute the basis for the vast majority of calculations and solutions of physical problems. There are, however, some more specialized objects, less well-known but still very useful for particular problems, appearing as a "*Deus ex machina*", when certain symmetries and relations exist in physical systems. It is then logical due to their special character, properties and use, to call them "special functions". We will name just a few which are of particular interest for problems that the present thesis tackles: the absolute value, the sign function, the Heaviside step and Dirac-delta function, the Gamma function, the Hermite polynomials, the (confluent) hypergeometric functions and the parabolic cylinder function. The rest of this mathematical appendix is devoted to a short –but elaborate enough for the purposes of this work– introduction to the properties and relations of these functions and acquaintance with their characteristics which are essential for the understanding of the present thesis. This appendix serves therefore the self-consistence of the text, but aims not to a complete and strict mathematical presentation of the special functions, which can be found in textbooks -"Bibles"of functional analyses such as [80]

## B.1 Absolute Value, step, sign and Dirac-delta function

The functions introduced in this subsection have a very simple definition which can be written in one line without mathematical complication. Yet, important properties and some peculiarities or singularities they have as well as the connection between them, is not self-evident. They are also connected with several aspects of the physical problems relevant to this thesis.

The absolute value has a different definition depending on the nature of input (or argument), particularly weather it is a real or a complex number. We are more interested in real numbers here, but it is much more than a side-remark to mention that the absolute value or modulus of a complex number has played a decisive role for the physical theory underlying this whole thesis namely Quantum theory. The wave-function which describes quantum particles is in the general case a complex number and only its absolute value square is a directly measurable quantity in the experiments according to the standard "orthodox"Copenhagen interpretation (Bohr, Heisenberg, etc).

For a real number input the absolute value gives the (positive) numerical value of the input without its sign. The blue line in Fig. B.1 shows the function $|x|$. Already the basic property of this function is of great importance for our purposes. Consider a function for two particles $f(x_1, x_2) = x_1 - x_2$. If now apply the permutation (exchange $x_1$ with $x_2$) we will get a minus sign $f(x_2, x_1) = -f(x_1, x_2)$ which means that $f(x_1, x_2)$ is of fermionic character. Now consider that we use the absolute value $\tilde{f}(x_1, x_2) = |x_1 - x_2|$. Now the permutation of two particles gives the same function because the sign plays no role now due to the absolute value. We have then $\tilde{f}(x_2, x_1) = \tilde{f}(x_1, x_2)$ which is a function of bosonic character. This simple fact plays a very important role for the construction of a many-body (bosonic) function out of pairs. Furthermore it shows probably an intuitive understanding of the absolute value as the distance from the origin or the distance between two numbers (or two points in configuration space, or two particles). This notion of distance which is better illustrated by the definition $|x| = \sqrt{x^2}$ which has its analog even for complex numbers $|z = x + iy| = \sqrt{x^2 + y^2}$.

The sign (signum) function has also a very simple definition: it gives +1 when the real number input is positive and -1 when it is negative (see also the illustration in Fig. B.1. As one guesses immediately it has a very close relation to the absolute value:

$$|x| = x\mathrm{sgn}(x) \tag{B.1}$$

What is so important about this relation? If $x \neq 0$ then we can write $\frac{|x|}{x} = \mathrm{sgn}(x)$ which is by the way the derivative of the absolute value. One can see also in Fig. B.1 that the absolute value has just a positive or negative constant slope, while it is ill defined at $x = 0$.

If one tries to go further with derivatives, will meet even more peculiar functions: the Heaviside step function $\Theta(x)$ and the Dirac (generalized) function $\delta(x)$. The Heaviside step function is a discontinuous function, zero for negative arguments and 1 for positive arguments, and a conventional value at 0 (usually 1/2). It is plotted in Fig. B.1 and one can show easily that $\mathrm{sgn}(x) = 2\Theta(x) - 1$. More important is that the step function is the integral of the probably most important function for the present thesis: the Dirac-delta function $\delta(x)$. We have that $\Theta(x) = \int_{-\infty}^{x} \delta(t)\,\mathrm{d}t$. Now we are ready to define the derivative of the sign function or the second derivative of the absolute value (for $x \neq 0$):

$$\frac{\mathrm{d}}{\mathrm{d}x}\frac{\mathrm{d}|x|}{\mathrm{d}x} = \frac{\mathrm{d}}{\mathrm{d}x}\frac{|x|}{x} = \frac{\mathrm{d}}{\mathrm{d}x}\mathrm{sgn}(x) = 2\frac{\mathrm{d}\Theta(x)}{\mathrm{d}x} = 2\delta(x) \tag{B.2}$$

So (two times) the Dirac $\delta$-function is the second derivative of the absolute value! This is probably not the way that Dirac has thought of it. The $\delta$-function is in general very difficult to think of (since it is not a function in the common sense but rather a distribution), but there is

certainly one way which is the more common but also probably the most wrong and misleading: to say that $\delta(0) = \infty$ and it is zero elsewhere. This picture comes from usual approaches of the $\delta$-function as a limit of a sequence of Gaussian (or other functions with peak at $x = 0$) when the width tends to zero. This is also the approach that numerical methods (also the ones used in this thesis) follow. The formal definition though is the following:

$$\int_{-\infty}^{\infty} \delta(x)\mathrm{d}x = 1. \tag{B.3}$$

You may allow now a comment on that. The $\delta$-function is the usual model for contact (or even short range) interactions (where the argument is the relative distance). From the common picture we referred to previously, it makes sense that the $\delta$-function has a local character, it acts only at the point of contact (in terms of our physical system). This is probably a good picture for classical physics when the contact interaction really affects the orbits of the particles only when they meat. In quantum physics it is not necessarily so. The probability distribution, the natural picture for a quantum particle, is not affected only locally at the meeting point from the action of the $\delta$-function. This is a very important fact for the considerations of the present thesis. In fact it lies on the core of it, especially for the quantum-mechanical aspect of the theoretical considerations. One should take seriously into account how the contact interaction modeled by a $\delta$-function acts, first to a single pair and then to the many-body system. Before we enter this discussion let us mention two more important properties of the Dirac $\delta$-function in connection to the absolute value. The argument of the $\delta$-function is sign-irrelevant like for the absolute value, i.e, we have $\delta(-x) = \delta(x)$. More general a scaling factor in the argument of the $\delta$-function can be easily extracted since $\int_{-\infty}^{\infty} \delta(\alpha x)\,\mathrm{d}x = \int_{-\infty}^{\infty} \delta(u)\,\frac{\mathrm{d}u}{|\alpha|} = \frac{1}{|\alpha|} \Rightarrow \delta(\alpha x) = \frac{\delta(x)}{|\alpha|}$.

We have introduced and illustrated properties and relations of the most basic special functions. We hope that the revising of these mathematical objects underlying and reconstructing properties from the point of view of the physical systems examined in these thesis, will help to the understanding of the physical problem itself, because these are decisive functions defining the problem and indicating paths to solve it. In the following we introduce more complicated special functions being solutions of important differential equations which are relevant here. The functions introduced up to know have more to do with symmetry considerations, boundary conditions and the interaction part of the problem, while in the next we will enter more the field of differential equations arising.

## B.2 Special functions for the parabolic trap

The functions introduced in this subsection are in close relation to each other and constitute solutions of similar differential equations. The most general form of the differential equation considered here is:

$$\frac{d^2 f}{dz^2} + \left(\tilde{a}\tilde{z}^2 + \tilde{b}z + \tilde{c}\right) f = 0. \tag{B.4}$$

By completing the square and renormalizing $z$ one obtains two distinct standard forms called Weber equations (1869, Heidelberg):

$$\frac{d^2 f}{dx^2} + \left[-\frac{1}{4}x^2 + E(\equiv \nu + 1/2)\right] f = 0 \tag{B.5}$$

and

$$\frac{d^2 f}{dx^2} + \left(\frac{1}{4}x^2 + E\right) f = 0. \tag{B.6}$$

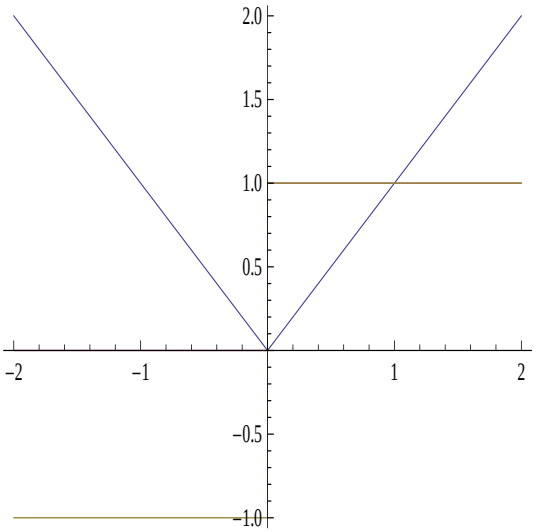


Figure B.1: Illustration of basic special functions

For anyone who has has been engaged in quantum physics, these equations should ring a bell. Most textbooks of quantum physics after setting up the postulates of quantum mechanics, set out to solve particular systems, and specifically eigenvalue problems stemming up from the (time-independent) Schrödinger equation [$\hat{H}\psi = E\psi$ or in configuration space $-\frac{\hbar}{2m}\frac{d^2\psi(x)}{dx^2} + V(x)\psi(x) = E\psi(x)$. There are not many that are solvable. Apart from free space (and all possible boundary conditions, from periodic to infinite and finite square wells) where only the kinetic energy operator $-\frac{\hbar}{2m}\frac{d^2}{dx^2}$ is present, there is one form of potential that has attracted a lot of interest: the parabolic or harmonic trap $V(x) \propto x^2$. This is not without reason: any arbitrary potential can be approximated as a harmonic potential at the vicinity of a stable equilibrium point. This means that in principle it can be a good model for many systems.

From this perceptive Eq. B.5 is not just another differential equation but probably one of the most important in quantum physics. It occurs even in problems where it is not obvious, like the famous Landau-Zener problem, swap in a two-level system. Before we set out to examine in particular the solutions of Eq. B.5 let us note that if any of the functions $f(E,x)$,$f(E,-x)$,$f(-E,ix)$ ,$f(-E,-ix)$ is a solution of Eq. B.5 or Eq. B.6, then all are solutions of either Eq. B.5 or Eq. B.6. In general $x$ and $E$ can take complex values but we constrain ourselves here to real solutions of real equations which can be given independently for Eq. B.5 and Eq. B.6.

We focus now on Eq. B.5. Let us also use the following notation for the constant $E = \nu + \frac{1}{2}$, which makes directly the link to an effective quantum number $\nu$ like the one of the harmonic oscillator. The most direct solution of the Weber equation is called parabolic cylinder function $D_\nu(x)$ [often also denoted $U(\alpha, x)$ where $\alpha = -\nu - 1/2 = -E$]. In most textbooks introduce them via their relation with confluent hypergeometric functions[1] which are solutions of the (Kummer's) differential equation

$$xy'' + (b - x)y' - ay = 0. \tag{B.7}$$

The confluent hypergeometric function of first kind ${}_1F_1(a, b, x)$ or Kummer's function [also

[1]These are special cases of the genus hypergeometric functions, solution of the Euler's hypergeometric differential equation

denoted $M(a,b,x)$] is given by:

$$ {}_1F_1(a;b;x) = \sum_{k=0}^{\infty} \frac{(a)^k}{(b)^k k!} x^k, \tag{B.8} $$

where $(a)^k = x(x+1)\cdots(x-k+1) = \frac{\Gamma(x+k)}{\Gamma(x)}$ is the Pochammer Symbol or rising factorial[2].

.

Using this function one can write down odd and even solutions of Eq. B.5:

$$ f_1(\nu;x) = e^{-\frac{x^2}{4}} F_1\left(-\frac{\nu}{2}, \frac{1}{2}, \frac{x^2}{2}\right) \quad \text{(even)} \tag{B.9} $$

$$ f_2(\nu;x) = x e^{-\frac{x^2}{4}} F_1\left(-\frac{\nu}{2} + \frac{1}{2}, \frac{3}{2}, \frac{x^2}{2}\right) \quad \text{(odd)} \tag{B.10} $$

Now the parabolic cylinder function can be written as

$$ D_\nu(x) = \frac{1}{\sqrt{\pi}} 2^{\frac{\nu}{2}} \left[\cos(-\frac{\nu\pi}{2})\Gamma(\frac{1+\nu}{2})\, f_1(\nu,x) - \sqrt{2}\sin(-\frac{\nu\pi}{2})\Gamma(1+\frac{\nu}{2})\, f_2(\nu,x)\right] \tag{B.11} $$

The confluent hypergeometric function of second kind $U(a,b,x)$ or Tricomi's function [also denoted $\Psi(a,b,x)$] is another solution[3] of Kummer's differential equation B.7:

$$ U(a,b,x) = \frac{\Gamma(1-b)}{\Gamma(a-b+1)} {}_1F_1(a,b,x) + \frac{\Gamma(b-1)}{\Gamma(a)} x^{1-b} {}_1F_1(a-b+1, 2-b, x). \tag{B.12} $$

and the parabolic cylinder function is written in these terms:

$$ D_\nu(x) = 2^{\frac{\nu}{2}} e^{-\frac{x^2}{4}} \frac{(-ix)^{\frac{1}{4}}(ix)^{\frac{1}{4}}}{\sqrt{x}} U(-\frac{\nu}{2}, \frac{1}{2}, \frac{x^2}{2}), \tag{B.13} $$

which for the case which interests us here $x > 0$ reads:

$$ D_\nu(x) = 2^{\frac{\nu}{2}} e^{-\frac{x^2}{4}} U(-\frac{\nu}{2}, \frac{1}{2}, \frac{x^2}{2}), \tag{B.14} $$

This is the most useful expression of the parabolic cylinder function for our purposes. We usually take $D_\nu(|x|)$ which means that we are interested only in the right half plane where the function does not diverge thanks to the exponential term in Eq. B.14. But before we abandon the purely mathematical world, and turn to physics, i.e., to boundary conditions of specific problems, which will help us to see these abstract objects from a specific point of view, we state a pair of properties of $D_\nu(x)$. First its recurrence relations and derivatives which make it a solution of the Weber equation Eq. B.5:

$$ D_{\nu+1}(x) - x D_\nu(x) + \nu D_{\nu-1}(z) = 0 \tag{B.17} $$

[2]Here we have also the appearance of the Gamma function $\Gamma(x) = (x-1)!$, one important property of which is: $\Gamma(1+x) = x\Gamma(x)$.

[3]The confluent hypergeometric functions are also connected to the Whittaker functions

$$ M(\kappa,m,x) = e^{-\frac{x}{2}} x^{m+\frac{1}{2}} {}_1F_1(m-\kappa+\frac{1}{2}, 1+2m; x) \tag{B.15} $$

$$ W(\kappa,m,x) = e^{-\frac{x}{2}} x^{m+\frac{1}{2}} U(m-\kappa+\frac{1}{2}, 1+2m; x) \tag{B.16} $$

which are solutions to the equation $\frac{d^2w}{dx^2} + \left(-\frac{1}{4} + \frac{\kappa}{x} + \frac{1/4-m^2}{x^2}\right) w = 0$. To Whittaker we owe the notation $D_\nu(x)$ for the parabolic cylinder functions

$$D_\nu^{'}(x) = -\frac{x}{2}D_\nu(x) + \nu D_{\nu-1}(x) = \frac{x}{2}D_\nu(x) - \nu D_{\nu+1}(x). \tag{B.18}$$

$$\begin{aligned} D_\nu^{''}(x) &= \frac{x^2}{4}D_\nu(x) + \frac{1}{2}D_\nu(x) - xD_{\nu+1}(x) + D_{\nu+2}(x) && \text{(B.19)} \\ &= \frac{x^2}{4}D_\nu(x) - (\nu + \frac{1}{2})D_\nu(x) && \text{(B.20)} \end{aligned}$$

The last equation B.20 which follows from Eqs.B.17 and B.19, is nothing but the Weber differential equation Eq. B.5. Other useful properties of $D_\nu(x)$ is its value and its derivative at $x = 0$:

$$D_\nu(0) = \frac{2^{\frac{\nu}{2}}\sqrt{\pi}}{\Gamma\left(\frac{1-\nu}{2}\right)} \tag{B.21}$$

$$D'_\nu(0) = \left.\frac{dD(x)}{dx}\right|_{x=0} = \frac{2^{\frac{1+\nu}{2}}\sqrt{\pi}}{\Gamma\left(-\frac{\nu}{2}\right)} \tag{B.22}$$

Also the integrals:

$$\int_{-\infty}^{\infty} D_m(x)D_n(x)dx = n!\sqrt{(}2\pi)\delta_{mn}, \tag{B.23}$$

where $\delta_{mn}$ is the Kronecker delta [orthogonality], and

$$\int_0^{\infty} (D_\nu(x))^2 dx = \pi^{\frac{1}{2}}2^{-\frac{3}{2}}\frac{\phi_0(\frac{1-\nu}{2}) - \phi_0(-\frac{\nu}{2})}{\Gamma(-\nu)} \tag{B.24}$$

where $\phi_0(x)$ is the polygamma function.

Last but not least, the impressive fact that for $\nu = n = 0, 1, ...$ we have a special relation to what every physicist would expect from the experience with the harmonic oscillator: the Hermite polynomials:

$$U\left(-\frac{n}{2}, \frac{1}{2}, \frac{x^2}{2}\right) = 2^{-n}H_n\left(\frac{x}{\sqrt{2}}\right) \tag{B.25}$$

$$D_n(x) = 2^{-\frac{n}{2}}e^{-\frac{x^2}{4}}H_n\left(\frac{x}{\sqrt{2}}\right) \tag{B.26}$$

$H_n(x)$ are the Hermite polynomials, the usual ones participating in the solution of the harmonic oscillator $\psi_n(x) = \frac{\mathrm{e}^{-\frac{x^2}{2}}H_n(x)}{\sqrt{2^n n!\sqrt{\pi}}} = \frac{(-1)^n \mathrm{e}^{-\frac{x^2}{2}}\frac{d^n}{dx^n}\mathrm{e}^{-x^2}}{\sqrt{2^n n!\sqrt{\pi}}}$. With all these in hand we are ready to enter the world of physics.

**Acknowledgements**

This thesis is a collective work as every other. Many people have contributed either with ideas and scientific help or with their support and encouragement. The author is particularly thankful to all these people who are mentioned or not here and have made this work possible.

It was a great pleasure to be engaged from my supervisor Peter to the fascinating field of cold atoms. Peter provided me a great scientific environment and all the means to carry out this work. He was always available and open to new ideas, and had the most substantial contribution to my projects with his invaluable remarks, ideas and advices.

At this place I have also the opportunity to thank my teacher in Greece, Fotis, to whom I owe a whole period of my life. Without his unquestionable goodness, substantial scientific help, advice and encouragement, I would have never been able to carry through my studies and PhD. In his name I also want to thank from the bottom of my heart all official and unofficial teachers that I had in my life, in all different subjects.

I had the great luck to meet in Heidelberg a man who I admire for his way of life and his mind not only in physics but in general. Christian is a friend that I would like to have forever. I will never forget the nice and difficult moments, especially when his daughter our beloved Elina was born and he insisted to correct my paper in the clinic.

Panos my friend and closest colleague stood by me in all difficult moments, and our endless discussions between chess games and analysis were invaluable. He and my other colleagues in the group, my office and research mates Anika, Sascha, Lushuai, Budha and Alexander, Christoph, Alexandra, Panagiotis, Bernd, Emmerich, Sven, Jan and Martina, Nicolas, Mathias, Andrea, Markus, Florian and Michael and the two brilliant students that I worked with, Rüdiger and Michael made my life in the office and out of it much brighter. I am also thankful to all my students in the exercise groups and seminars that I gave, from whom I learned a lot. The scientists I have met in conferences and elsewhere and have inspired my thoughts and research are innumerable, to mention only a few: Dieter Meyer, a wise sientist always open to advice me particularly concerning the basic algorithm I used in this thesis which is his creation, Lincoln Carr, Thomas Gasenzer, Ofir Alon, Alexej Streltsov, Lenz Cederbaum, and their students Kaspar and Axel, Oriol Vendrell, Panos Kevrekidis, Rosario Paredes, Markus Oberthaler and Sandro Wimberger and his students Ghazal and Patrick in Heidelberg, Henning Moritz, Ludwig Mathey and Juliette Simonet in Hamburg but also Alekos Karanikas and Dimitris Frantzeskakis who I met again there, Doerte Blume and Wolfgang Schleich in Bad Honnef, Hans-Christoph Nägerl and Elmar Haller in Innsbruck, Grigori Astrakharchik, Bruno Diaj, Jordi Boronat, Artur Polls, and Marcej Lewenstein in Barcelona and their students Om and Marina, Jacob Sherson in Denmark, Philipp Schneider and Simon Sala in Dresden in Hannover and in Stuttgart.

My favorite poet K.P Kavafis writes 'This city will always pursue you', and indeed my most exciting scientific cooperation happened to be in Heidelberg, the city where I started my PhD, with Selim Jochim and his experimental group, Andre Wenz, Gerhard Zürn and Thomas Lompe. It is not only the long and instructive discussions that I had with them and from which I learned a lot, but also the great atmosphere and hospitality they created every time I was there.

In Heidelberg, I have met a lot of people who made this city my second hometown. I would like to thank at this place the city of Heidelberg, because 'the city is the people' as Thucydides wrote. In my first steps, I got naturally in touch mainly with people speaking the same language, but it was a great luck that we had much more in common. Marios with his unstoppable appetite for physics, music, traveling and parties, with most unforgettable moment the 'last tango in Heidelberg'. Alexandros with his passionate character, an invaluable companion in my first steps in the world of science during my diploma thesis. The unpredictable girls with whom we spend a lot of nice afternoons ending up to evenings full of singing, laughing and moving

moments, my beloved Efi, Nina and Aliki. In this first period I had also the luck to get in touch with the German society mainly through my invaluable colleagues Anika and Bernd, who were very open and helpful to all of us. Matthis, the physicist and musician, was my first cello partner in the nice music afternoons in Physikalisches Institute. Sascha, the person whose work and advices in the beginning of my PhD, provided the starting point and greatest inspiration, is one of the most brilliant physicists I got to know. In this unforgeable period I had the luck to share my apartment with Nicola and Tobias, the best mates I could ever imagine, and to share my life with Evangelia, who coped with and supported me in all my doubts and difficulties. In Hamburg I had the luck to meet great people Kay, Svenja, Stefania, Phillip, Rosa, Vasil, Ekrem and Jil in my apartment, Stefania and Doris in the theater-German course and many others. The other friends I made in Heidelberg Monika, Ersin, Heike, Giorgos, Maria, Iliana, Dimitris, Nikos and others made my visits there unforgetable. In my hometown Athens I left also a lot of friends and relatives who are very important for me, and were always there when I found the way back home: Niki, Andreas, Yiannis in Voula and Yiannis in Pireus, Fotis, Maro, Angelos, Orestis, Emilia, Nikoletta, Kostas, Minas, Yiannis, Michalis, Giorgos, Vangelis, Margarita, my piano teacher Rubina my chess and music theory teacher Nikos and my english teacher Ada and all those who fight for a better life for justice and dignity, in the birthplace of democracy against those who steal them.

The most important people behind this thesis and for whom there are no words that I can write, to whom all this work, all this time, all these thoughts are dedicated are the members of my family, my siblings Asimina and Michalis, my parents Paola and Stelios, my grandma Margarita and my dear Caroline. I hope they know that without their existence and love nothing would be possible. I hope they know wherever they are and they go, wherever I am, close or far away, they will be always present in my heart, I will always love them.

# Bibliography


[1] C. J. Pethick and H. Smith, *Bose-Einstein condensation in dilute gases* (Cambridge University Press, 2008); L. Pitaevskii and S. Stringari, *Bose-Einstein Condensation* (Oxford University Press, 2003); F. Dalfovo, S. Giorgini, L. P. Pitaevskii and S. Stringari, Rev. Mod. Phys. **71**, 463 (1999); A. J. Leggett, Rev. Mod. Phys. **73**, 307 (2001).

[2] I. Bloch, J. Dalibard and W. Zwerger, Rev. Mod. Phys. **80**, 885 (2008); M. Lewenstein, A. Sanpera, V. Ahufinger, B. Damski, A. Sen and U. Send, Adv. Phys. **56**, 243 (2007). M. Lewenstein, A. Sanpera and V. Ahufinger, *Ultracold Atoms in Optical Lattices: Simulating quantum many-body systems* (Oxford University Press, 2012); K. Bongs and K. Sengstock, Rep. Prog. Phys. **67**, 907 (2004); D. C. McKay and B. DeMarco, Rep. Prog. Phys. **74**, 054401 (2011).

[3] S. Giorgini, L. P. Pitaevskii and S. Stringari, Rev. Mod. Phys. **80**, 1215 (2008).

[4] M. A. Cazalilla, R. Citro, T. Giamarchi, E. Orignac and M. Rigol, Rev. Mod. Phys. **83**, 1405 (2011); A. Imambekov, T. L. Schmidt and L. I. Glazman, Rev. Mod. Phys. **84**, 1253–1306 (2012); T. Giamarchi, *Quantum Physics in One Dimension* (Oxford University Press, 2003); E. H. Lieb, R. Seiringer, J. Yngvanson, Commun. Math. Phys. **244**, 347 (2004); E. B. Kolomeisky and J. P. Straley, Rev. Mod. Phys. **68**, 175 (1996);

[5] C. Chin, R. Grimm, P. Julienne and E. Tiesinga, Rev. Mod. Phys. **82**, 1225 (2010); M. G. Moore, T. Bergeman and M. Olshanii, Phys. IV France **116**, 69 (2004); V. A. Yurovski, M. Olhanii, D. S. Weiss, Adv. At. Mol. Opt. Phys. **55**, 61 (2008).

[6] M. H. Anderson , J. R. Ensher, M. R. Matthews, C. E. Wieman and E. A. Cornell, Science **269**, 198 (1995); C. C. Bradley, C. A. Sackett, J. J. Tollett and R. G. Hulet, Phys. Rev. Lett. **75**, 1687 (1995); K. B. Davis, M.-O. Mewes, M. R. Andrews, N. J. van Druten, D. S. Durfee, D. M. Kurn and W. Ketterle, Phys. Rev. Lett. **75**, 3969 (1995).

[7] M. Greiner, O. Mandel, T. Esslinger, T. W. Hänsch, and I. Bloch, Nature **415**, 39 (2002).

[8] O. Morsch and M. Oberthaler, Rev. Mod. Phys. **78**, 179 (2006); A. Polkovnikov, K. Sengupta, A. Silva and M. Vengalattore, Rev. Mod. Phys. **83**, 863 (2011).

[9] D. Blume, Rep. Prog. Phys. **75**, 046401 (2012); D. C. Mattis, Rev. Mod. Phys. **58**, 361 (1986).

[10] L. P. Pitaevskii, Zh. Eksp. Teor. Fiz. **40**, 646 (1961) [Sov. Phys. JETP **13**, 451 (1961)].

[11] M. Girardeau, J. Math. Phys. **1**, 516 (1960).

[12] E. H. Lieb and W. Liniger, Phys. Rev. **130**, 1605 (1963).

[13] M. Olshanii, Phys. Rev. Lett. **81**, 938 (1998).

[14] T. Busch, B.-G. Englert, K. Rzażewski and M. Wilkens, Found. Phys. **28**, 549 (1998).

[15] D. S. Jin, J. R. Ensher, M. R. Matthews, C. E. Wieman, and E. A. Cornell, Phys. Rev. Lett. **77**, 420 (1996); M.-O. Mewes, M. R. Andrews, N. J. van Druten, D. M. Kurn, D. S. Durfee, C. G. Townsend, and W. Ketterle, Phys. Rev. Lett. **77**, 988 (1996).

[16] S. Burger, K. Bongs, S. Dettmer, W. Ertmer, K. Sengstock, A. Sanpera, G. V. Shlyapnikov and M. Lewenstein, Phys. Rev. Lett. **83**, 5198 (1999); J. Denschlag, J. E. Simsarian, D. L. Feder, C. W. Clark, L. A. Collins, J. Cubizolles, L. Deng, E. W. Hagley, K. Helmerson, W. P. Reinhardt, S. L. Rolston, B. I. Schneider and W. D. Phillips, Science **287**, 97 (2000); L. Khaykovich, F. Schreck, G. Ferrari, T. Bourdel, J. Cubizolles, L. D. Carr, Y. Castin and C. Salomon, Science **296**, 1290 (2002); G. B. Partridge, K. E. Strecker, R. I. Kamar, M. W. Jack and R. G. Hulet, Phys. Rev. Lett. **95**, 020404 (2005).

[17] M. R. Matthews, B. P. Anderson, P. C. Haljan, D. S. Hall, C. E. Wieman and E. A. Cornell, Phys. Rev. Lett. **83**, 2498 (1999); K. W. Madison, F. Chevy, W. Wohlleben, and J. Dalibard, Phys. Rev. Lett. **84**, 806 (2000); J. R. Abo-Shaeer, C. Raman, J. M. Vogels and W. Ketterle, Science **292**, 476 (2001).

[18] F. S. Cataliotti, S. Burger, C. Fort, P. Maddaloni, F. Minardi, A. Trombettoni, A. Smerzi and M. Inguscio, Science **293**, 843 (2001); M. Albiez, R. Gati, J. Fölling, S. Hunsmann, M. Cristiani and M. K. Oberthaler, Phys. Rev. Lett. **95**, 010402 (2005); R. Gati, M. Albiez, J. Fölling, B. Hemmerling and M. Oberthaler, Appl. Phys. B **82**, 207 (2006); G. J. Milburn, J. Corney, E. M. Wright and D. F. Walls, Phys. Rev. A **55**, 4318 (1997).

[19] T. Kinoshita, T. Wenger and D. S. Weiss, Science **305**, 1125 (2004); B. Paredes, A. Widera, V. Murg, O. Mandel, S. Fölling, I. Cirac, G. V. Shlyapnikov, T. W. Hänsch and I. Bloch, Nature **429**, 277 (2004).

[20] E. Haller, M. Gustavsson, M. J. Mark, J. G. Danzl, R. Hart, G. Pupillo and H.-C. Nägerl, Science **325**, 1224 (2009).

[21] H. A. Bethe, Z. Phys. **71**, 205 (1931).

[22] V. Dunjko, V. Lorent and M. Olshanii, Phys. Rev. Lett. **86**, 5413 (2001). G. E. Astrakharchik, Phys. Rev. A **72** 063620 (2005).

[23] V. Efimov, Phys. Lett. B **33**, 563 (1970); T. Kraemer, M. Mark, P. Waldburger, J. G. Danzl, C. Chin, B. Engeser, A. D. Lange, K. Pilch, A. Jaakkola, H.-C. Nägerl and R. Grimm, Nature **440**, 315 (2006); S. Knoop, F. Ferlaino, M. Mark, M. Berninger, H. Schöbel, H.-C. Nägerl and R. Grimm, Nature Physics **5**, 227 (2007); M. Zaccanti, B. Deissler, C. D'Errico, M. Fattori, M. Jona-Lasinio, S. Müller, G. Roati, M. Inguscio and G. Modugno, Nature Physics **5**, 586 (2009).

[24] H. Moritz, T. Stöferle, M. Köhl and T. Esslinger, Phys. Rev. Lett. **91**, 250402 (2003).

[25] I. Brouzos and P. Schmelcher, Phys. Rev. Lett. **108**, 045301 (2012).

[26] F. Deuretzbacher, K. Bongs, K. Sengstock and D. Pfannkuche, Phys. Rev. A **75**, 013614 (2007).

[27] D. Blume Phys. Rev. A **66**, 053613 (2002), G. E. Astrakharchik and S. Giorgini, Phys. Rev. A **66**, 053614 (2002); G. E. Astrakharchik, D. Blume, S. Giorgini and B. E. Granger, Phys. Rev. Lett. **92**, 030402 (2004); ibid, J. Phys. B **37**, 205 (2004); G. E. Astrakharchik,

J. Boronat, I. L. Kurbakov, Y. E. Lozovik and F. Mazzanti, Phys. Rev. A **81**, 013612 (2010).

[28] B. Schmidt and M. Fleischhauer, Phys. Rev. A **75**, 021601 (2007).

[29] S. Zöllner, H.-D. Meyer, and P. Schmelcher, Phys. Rev. A **74**, 053612 (2006); ibid, Phys. Rev. A **74**, 063611 (2006); ibid, Physical Review A **75**, 043608 (2007).

[30] I. Brouzos and P. Schmelcher, Phys. Rev. A **85**, 033635 (2012).

[31] H.-J. Stöckmann, *Quantum Chaos* (Cambridge University Press, 1999).

[32] E. A. Donley, N. R. Claussen, S. T. Thompson and C. E. Wieman C E, Nature **417**, 529 (2002).

[33] S. E. Pollack, D. Dries, R. G. Hulet, K. M. F. Magalhaes, E. A. L. Henn, E. R. F. Ramos, M. A. Caracanhas and V. S. Bagnato, Phys. Rev. A **81**, 053627 (2010).

[34] P. G. Kevrekidis, G. Theocharis, D. J. Frantzeskakis, and B. A. Malomed, Phys. Rev. Lett. **90**, 230401 (2003).

[35] H. Lignier, C. Sias, D. Ciampini, Y. Singh, A. Zenesini, O. Morsch and E. Arimondo, Phys. Rev. Lett. **99**, 220403 (2007).

[36] A. Zenesini, C. Sias, H. Lignier, Y. P. Singh, D. Ciampini, O. Morsch, R. Manella, E. Arimondo, A. Tomadin and S. Wimberger, New J. Phys. **10**, 053038 (2008).

[37] A. Eckardt, M. Holthaus, H. Lignier, A. Zenesini, D. Ciampini, O. Morsch and E. Arimondo, Phys. Rev. A **79**, 013611 (2009).

[38] C. Sias, H. Lignier, Y. P. Singh, A. Zenesini, D. Ciampini, O. Morsch and E. Arimondo, Phys. Rev. Lett. **100**, 040404 (2008).

[39] H.-D. Meyer, G. A. Worth and F. Gatti, *Multidimensional Quantum Dynamics: MCTDH Theory and Applications*, (Wiley-VCH, Weinheim, 2009); H. D. Meyer, U. Manthe and L. S. Cederbaum, Chem. Phys. Lett. **165**, 73 (1990); M. H. Beck, A. Jäckle, G. A. Worth and H. D. Meyer, Phys. Rep. **324**, 1 (2000).

[40] S. Zöllner, H. D. Meyer and P. Schmelcher, Phys. Rev. Lett. **100**, 040401 (2008); ibid, Phys. Rev. A **78**, 013621 (2008); B. Chatterjee, I. Brouzos, S. Zöllner and P. Schmelcher, Phys. Rev. A **82**, 043619 (2010).

[41] S. Zöllner, H. D. Meyer, and P. Schmelcher, Phys. Rev. A **78**, 013629 (2008); B. Chatterjee, I. Brouzos, L. Cao and P. Schmelcher, Phys. Rev. A **85**, 013611 (2012); A. C. Pflanzer, S. Zöllner and P. Schmelcher, Phys. Rev. A **81**, 023612 (2010); ibid J. Phys. B **42**, 231002 (2009); L. Cao, I. Brouzos, B. Chatterjee and P. Schmelcher, New J. Phys. **14**, 093011 (2012).

[42] I. Brouzos, S. Zöllner and P. Schmelcher, Phys. Rev. A **81**, 053613 (2010).

[43] L. Cao, I. Brouzos, S. Zöllner and P. Schmelcher, New J. Phys. **13**, 033032 (2011).

[44] D. Jaksch and P. Zoller, Annals of Physics **315**, 52 (2005); D. Jaksch, C. Bruder, J. I. Cirac, C. W. Gardiner and P. Zoller, Phys. Rev. Lett. **81**, 3108 (1998); M. P. A. Fisher, P. B. Weichman, G. Grinstein and D. S. Fisher, Phys. Rev. B **40**, 546 (1989).

[45] O. E. Alon, A. I. Streltsov and L. S. Cederbaum, Phys. Rev. Lett. **95**, 030405 (2005).

[46] H. P. Büchler, G. Blatter and W. Zwerger, Phys. Rev. Lett. **90**, 130401 (2003).

[47] E. Haller, R. Hart, M. J. Mark, J. G. Danzl, L. Reichsöllner, M. Gustavsson, M. Dalmonte, G. Pupillo, H.-C. Nägerl, Nature (London) **466**, 597 (2010).

[48] I. Brouzos and P. Schmelcher, to appear in J. Phys. B.

[49] T. Anker, M. Albiez, R. Gati, S. Hunsmann, B. Eiermann, A. Trombettoni and M. K. Oberthaler, Phys. Rev. Lett. **94**, 020403 (2005).

[50] K. Winkler, G. Thalhammer, F. Lang , R. Grimm, J. H. Denschlag, A. J. Daley, A. Kantian, H. P. Büchler and P. Zoller, Nature **441**, 853 (2006).

[51] K. Sakmann, A. I. Streltsov, O. E. Alon and L. S. Cederbaum, Phys. Rev. Lett. **103**, 220601 (2010).

[52] A. I. Streltsov, K. Sakmann, O. E. Alon and L. S. Cederbaum, Phys. Rev. A **83**, 043604 (2011).

[53] I. Brouzos and P. Schmelcher, arXiv:1209.2891 (submitted to PRA).

[54] B. DeMarco and D. S. Jin, Science **285**, 1703 (1999); B. DeMarco, S. B. Papp and D. S. Jin, Phys. Rev. Lett. **86**, 5409 (2001); A. G. Truscott, K. E. Strecker, W. I. McAlexander, G. B. Partridge and R. G. Hulet, Science **291**, 2570 (2000); F. Schreck, G. Ferrari, K. L. Corwin, J. Cubizolles, L. Khaykovich, M.-O. Mewes and C. Salomon, Phys. Rev. A **64**, 011402 (2001).

[55] G. B. Jo, Y. R. Lee, J. H. Choi, C. A. Christensen, T. H. Kim, J. H. Thywissen, D. E. Pritchard and W. Ketterle, Science **325**, 1521 (2009).

[56] F. Chevy and C. Mora, Rep. Prog. Phys. **73**, 112401 (2010).

[57] A. Schirotzek, C-H Wu, A. Sommer and M. W. Zwierlein, Phys. Rev. Lett. **102**, 230402 (2009).

[58] C. Kohstall, M. Zaccanti, M. Jag, A. Trenkwalder, P. Massignan, G. M. Bruun, F. Schreck and R. Grimm, Nature **485**, 615–618 (2012).

[59] P. Massignan and G. M. Bruun, Eur. Phys. J. D **65**, 83 (2011).

[60] F. Serwane, G. Zürn, T. Lompe, T. B. Ottenstein, A. N. Wenz and S. Jochim, Science **332**, 6027 (2011).

[61] G. Zürn, F. Serwane, T. Lompe, A. N. Wenz, M. G. Ries, J. E. Bohn and S. Jochim, Phys. Rev. Lett. **108**, 075303 (2012).

[62] Z. Idziazek and T. Calarco, Phys. Rev. A **74**, 022712 (2006).

[63] A. Wenz et. al, in preparation.

[64] P.W. Anderson, Science **177**, 393–396 (1972).

[65] M. Girardeau, Phys. Rev. A **82**, 011607 (2010); ibid, Phys. Rev. A **83**, 011601 (2011); ibid, Phys. Rev. Lett. **102**, 245303 (2009); ibid Phys. Rev. Lett. **97**, 210401 (2006); M. D. Girardeau and A. Minguzzi Phys. Rev. Lett. **96**, 080404 (2006); ibid Phys. Rev. Lett. **99**, 230402 (2007); M. D. Girardeau and E. M. Wright, Phys. Rev. Lett. **95**, 010406 (2005); A. Minguzzi and M. D. Girardeau, Phys. Rev. A **73**, 063614 (2006); F. Deuretzbacher, K. Fredenhagen, D. Becker, K. Bongs, K. Sengstock and D. Pfannkuche, Phys. Rev. Lett. **100**, 160405 (2008); M. D. Girardeau and M. Olshanii, Phys. Rev. A **70**, 023608 (2004);

[66] Y. Hao et al, Y. Zhang, J. Q. Liang and S. Chen, Phys. Rev. A **73**, 063617 (2006).

[67] R. Jastrow, Phys. Rev. **98,** 1479 (1955).

[68] M. D. Girardeau, E. M. Wright and J. M. Triscari, Phys. Rev. A **63**, 033601 (2001); V. I. Yukalov and M. D. Girardeau, Laser Phys. Lett. **2**, 375 (2005); G. J. Lapeyre, M. D. Girardeau and E. M. Wright, Phys. Rev. A **66**, 023606 (2002); M. D. Girardeau and E. M. Wright, Phys. Rev. Lett **87**, 050403 (2001); M. D. Girardeau and G.E. Astrakharchik, Phys. Rev. A **81**, 061601 (2010).

[69] S. Franke-Arnold, S. Barnett, G. Huyet and C. Sailliot, Europ. Phys. J. D **22**, 373 (2003).

[70] R. B. Laughlin, Phys. Rev. Lett. **50**, 1395 (1983).

[71] G. E. Astrakharchik and S. Giorgini, Phys. Rev. A **68** 031602(R) (2003); ibid J. Phys. B **39** (2006).

[72] H. G. Vaidya and C. A. Tracy, Phys. Rev. Lett. **42**, 3 (1979); A. Minguzzi, P. Vignolo and M. P. Tosi, Phys. Lett. A **294**, 222 (2002).

[73] M. Rigol and A. Muramatsu, Phys. Rev. A **72**, 013604 (2005).

[74] K. K. Das, M. D. Girardeau and E. M. Wright, Phys. Rev. Lett. **89**, 170404 (2002).

[75] E. H. Lieb, R. Seiringer and J. Yngvason, Phys. Rev. Lett. **91**, 150401 (2003).

[76] D. S. Petrov, G. V. Shlyapnikov and J. T. M. Walraven, Phys. Rev. Lett. **85**, 3745 (2000).

[77] D. M. Gangardt and G. V. Shlyapnikov, Phys. Rev. Lett. **90**, 010401 (2003).

[78] E. B. Kolomeisky, T. J. Newman, J. P. Straley and X. Qi, Phys. Rev. Lett. **85**, 1146 (2000).

[79] T. Haugset and H. Haugerud, Phys. Rev. A **57**, 3809 (1998).

[80] M. Abramowitz and I. A. Stegun, *Handbook of Mathematical Functions* (Dover, New York, 1972).

[81] P. G. Kevrekidis, V. V. Konotop, A. Rodrigues and D. J. Frantzeskakis, J. Phys. B **38**, 1173 (2005).

[82] S. K. Adhikari, Phys. Rev. A **66**, 013611 (2002).

[83] E. R. F. Ramos, E. A. L. Henn, J. A. Seman, M. A. Caracanhas, K. M. F. Magalhaes, K. Helmerson, V. I. Yukalov and V. S. Bagnato, Phys. Rev. A **78**, 063412 (2008).

[84] I. Vidanović, A. Balaž, H. Al-Jibbouri and A. Pelster, Phys. Rev. A **84**, 013618 (2011).

[85] J. Gong, L. Morales-Molina and P. Hänggi, Phys. Rev. Lett. **103**, 133002 (2009).

[86] J. F. Bertelsen and K. Mølmer, Phys. Rev. A **73**, 013811 (2006).

[87] B. Borca, D. Blume and C. H. Greene, New J. Phys. **5** 111 (2003).

[88] M. Colome-Tatche and D. S. Petrov, Phys. Rev. Lett. **106**, 125302 (2011).

[89] Y. Kagan, E. L. Surkov and G. V. Shlyapnikov, Phys. Rev. A **54**, 1753 (1996)

[90] V. Gritsev, P. Barmettler and E. Demler, New J. Phys. **12**, 113005 (2010).

[91] T. P. Billam and S. A. Gardiner, Phys. Rev. A **80**, 023414 (2009).

[92] S. Stringari, Phys. Rev. Lett. **77**, 2360 (1996).

[93] G. G. Batrouni, V. Rousseau, R. T. Scalettar, M. Rigol, A. Muramatsu, P. J. H. Denteneer and M. Troyer, Phys. Rev. Lett. **89**, 117203 (2002).

[94] A. M. Rey, G. Pupillo, C. W. Clark and C. J. Williams, Phys. Rev. A **72**, 033616 (2005).

[95] G. K. Campbell, J. Mun, M. Boyd, P. Medley, A. E. Leanhardt, L. G. Marcassa, D. E. Pritchard and W. Ketterle, Science **313**, 649 (2006).

[96] B. Damski, J. Zakrzewski, L. Santos, P. Zoller and M. Lewenstein, Phys. Rev. Lett. **91**, 080403 (2003).

[97] V. A. Kashurnikov, N. V. Prokofev and B. V. Svistunov, Phys. Rev. A **66**, 031601(R) (2002).

[98] D.-S. Lühmann, K. Bongs and D. Pfannkuche, J. Phys. B **42**, 145305 (2009).

[99] M. Rigol, G. G. Batrouni, V. G. Rousseau and R. T. Scalettar, Phys. Rev. A **79**, 053605 (2009).

[100] P. Sengupta, M. Rigol, G. G. Batrouni, P. J. H. Denteneer and R. T. Scalettar, Phys. Rev. Lett. **95**, 220402 (2005).

[101] S. Wessel, F. Alet, M. Troyer and G. G. Batrouni Phys. Rev. A **70**, 053615 (2004).

[102] Y. Lin and B. Wu, Phys. Rev. A **75**, 023613 (2007).

[103] B.-B. Wei, S.-J. Gu and H.-Q. Lin, Phys. Rev. A **79**, 063627 (2009).

[104] M. A. Cazalilla, Phys. Rev. A **70**, 041604(R) (2004).

[105] M. A. Cazalilla and A. F. Ho, Phys. Rev. Lett. **91**, 150403 (2003).

[106] H. C. Jiang, Z. Y. Weng and T. Xiang, Phys. Rev. B **76**, 224515 (2007).

[107] D.-S. Lühmann, K. Bongs, K. Sengstock and D. Pfannkuche, Phys. Rev. A **77**, 023620 (2008).

[108] W. S. Bakr, A. Peng, M. E. Tai, R. Ma, J. Simon, J. Gillen, S. Foelling, L. Pollet and M. Greiner, Science **329**, 547 (2010); M. Karski, L. Förster, J.M. Choi, W. Alt, A. Widera, and D. Meschede, Phys. Rev. Lett. **102**, 053001 (2009).

[109] K. R. A. Hazzard and E. J. Mueller, Phys. Rev. A **81**, 033404 (2010).

[110] J. Li, Y. Yu. A. M. Dudarev and Q. Niu, New J. Phys. **8**, 034610 (2006).

[111] P.-I. Schneider, S. Grishkevich and A. Saenz, Phys. Rev. A **80**, 013404 (2009).

[112] G. Pupillo, A. M. Rey, C. J. Williams and C. W. Clark, New J. Phys. **8**, 161 (2006).

[113] C. N. Yang, Rev. Mod. Phys. **34**, 694 (1962).

[114] O. Penrose and L. Onsager, Phys. Rev. **104**, 576 (1956).

[115] D. S. Murphy, J. F. McCann, J. Goold and T. Busch, Phys. Rev. A **76**, 053616 (2007).

[116] X. Yin, Y. Hao, S. Chen and Y. Zhang, Phys. Rev. A **78**, 013604 (2008).

[117] E. J. Mueller, T.-L. Ho, M. Ueda and G. Baym, Phys. Rev. A **74**, 033612 (2006).

[118] F. Gerbier, S. Fölling, A. Widera, O. Mandel and I. Bloch, Phys. Rev. Lett. **96**, 090401 (2006).

[119] G. Roux, T. Barthel, I. P. McCulloch, C. Kollath, U. Schollwock and T. Giamarchi, Phys. Rev. A **78**, 023628 (2008).

[120] R. T. Scalettar, G. G. Batrouni and G. T. Zimanyi, Phys. Rev. Lett. **66**, 3144 (1991).

[121] T. Busch and G. Huyet, J. Phys. B **36**, 2553 (2003).

[122] R. W. Spekkens and J. E. Sipe, Phys. Rev. A **59**, 3868 (1999).

[123] D. Masiello, S. B. McKagan and W. P. Reinhardt, Phys. Rev. A **72**, 063624 (2005).

[124] A. Smerzi, S. Fantoni, S. Giovanazzi and S. R. Shenoy, Phys. Rev. Lett. **79** 4950 (1997); S. Raghavan, A. Smerzi, S. Fantoni and S. R. Shenoy, Phys. Rev. A **59** 620 (1999).

[125] B. Liu, L. Fu, S.-P. Yang and J. Liu, Phys. Rev. A **75**, 033601 (2007).

[126] R. Paredes, Phys. Rev. A **73**, 033616 (2006); ibid Laser Physics **16**, 1714 (2006); R. Paredes and E. Neri J. Phys. B **42**, 035301 (2009)

[127] P. Schlagheck, F. Malet, J. C. Cremon and S. M. Reimann, New J. Phys. **12**, 065020 (2010); J. A. Stickney, D. Z. Anderson and A. A. Zozuly, Phys. Rev. A **75**, 013608 (2007); A. Benseny, S. Fernández-Vidal, J. Baguda, R. Corbalan, A. Picon, L. Roso L, G. Birkl and J. Mompart Phys.Rev. A **82**, 013604 (2010).

[128] J-Q. Liang, J-L. Liu, W-D. Li and Z-J. Li, Phys. Rev. A **79**, 033617 (2009).

[129] P.R. Johnson, E. Tiesinga, J.V. Porto and C.J. Williams, New J. Phys. **11**, 093022 (2009).

[130] S. Will, T. Best, U. Schneider, L. Hackermuller, D.S. Lühmann and I. Bloch, Nature **465**, 197 (2010).

[131] P. Plötz, J. Madronero and S. Wimberger, J. Phys. B **43**, 08100 (2010).

[132] O. Dutta, A. Eckardt, P. Hauke, B. Malomed and M. Lewenstein, New J. Phys. **13**, 023019 (2011).

[133] D. R. Dounas-Frazer, A. M. Hermundstad and L. D. Carr, Phys. Rev. Lett. **99**, 200402 (2007); L. D. Carr, D. R. Dounas-Frazer and M. A. Garcia-March, Europhys. Lett. **90**, 10005 (2010).

[134] C. Chin, M. Bartenstein, A. Altmeyer, S. Riedl, S. Jochim, J. Hecker Denschlag and R. Grimm, Science **305**, 1128 (2004).

[135] J. Bardeen, L. N. Cooper and J. R. Schrieffer, Phys. Rev. **108**, 1175 (1957).

[136] M. W. Zwierlein, C. H. Schunck, A. Schirotzek and W. Ketterle, Science **311**, 492 (2006); G. B. Partridge, W. Li, R. I. Kamar, Y. Liao and R. G. Hulet, Science **311**, 503 (2006).

[137] P. F. Bedaque, H. Caldas, and G. Rupak, Phys. Rev. Lett. **91**, 247002 (2003).

[138] A. I. Larkin and Yu. N. Ovchinnikov, Zh. Eksp. Teor. Fiz. **47**, 1136 (1964) [Sov. Phys.-JETP **20**, 762(1965)]. P. Fulde and R. A. Ferrell, Phys. Rev. **135**, A550 (1964).

[139] H. Moritz, T. Stöferle, K. Günter, M. Köhl and T. Esslinger, Phys. Rev. Lett. **94**, 210401 (2005).

[140] Y. Liao, A. S. C. Rittner, T. Paprotta, W. Li, G. B. Partridge, R. G. Hulet, S. K. Baur, E. J. Mueller, Nature **467**, 567 (2010).

[141] J. B. McGuire, J. Math. Phys. **6**, 432 (1965).

[142] S. Giraud and R. Comberscot, Phys. Rev. A **79**, 043615 (2009).

[143] M. J. Leskinen, O. H. T. Nummi, F. Massel and P. Törmä, New J. Phys. **12**, 073044 (2010).

[144] A. Lamacraft, Phys. Rev. Lett. **101**, 225301 (2008).

[145] X. W. Guan, Frontiers of Physics **7**, 8-15 (2012).

[146] S. Tan, Annals of Physics **323** 2952, 2971 (2008); ibid Phys. Rev. Lett. **107**, 145302 (2011); M. Cazalilla, Int. J. Mod. Phys. B **25**, 329 (2011); X.-J. Liu, H. Hu and P. D. Drummond, Phys. Rev. A **82**, 023619 (2010); ibid, Phys. Rev. B **82**, 054524 (2010); D. Blume, Physics **3**, 74 (2010); S. E. Gharashi, K. M. Daily and D. Blume, Phys. Rev. A **86**, 042702 (2012); J. von Stecher, C. H. Greene, and D. Blume, Phys. Rev. A. **76**, 053613 (2007); ibid, Phys. Rev. A. **77**, 043619 (2008); D. Blume, J. von Stecher and C. H. Greene, Phys. Rev. Lett. **99**, 233201 (2007); ibid, Phys. Rev. A. **77**, 033627 (2008).

[147] O. E. Alon, A. I. Streltsov and L. S. Cederbaum, Phys. Rev. A **77**, 033613 (2008); A. I. Streltsov, O. E. Alon and L. S. Cederbaum, Phys. Rev. Lett. **99**, 030402 (2007).

[148] J. Zanghellini, M. Kitzler, C. Fabian, T. Brabec and A. Scrinzi, Laser Physics **13** 1064 (2003); T. Kato and H. Kono Chem. Phys. Lett. **392**, 533 (2004); M. Nest, T. Klamroth, and P. Saalfrank, J. Chem. Phys. **122**, 12402 (2005).

[149] G. A. Worth, M. H. Beck, A. Jäckle, and H.-D. Meyer, The MCTDH Package, Version 8.4 (2007). See http://mctdh.uni-hd.de.

[150] H.-D. Meyer and G. A. Worth, Theor. Chem. Acc. **109**, 251 (2003).

[151] T. Ernst, D. W. Hallwood, J. Gulliksen, H. D. Meyer, J. Brand, Phys. Rev. A **84**, 023623 (2011).